

High-resolution NMR structure and functional studies of the oligomerization domain of PsIAA4, an auxin-inducible transcriptional repressor from pea (*Pisum sativum*)

Dissertation

To obtain the Doctoral Degree in Natural Sciences (Dr. rer. nat.)

Submitted to

The Faculty of Natural Sciences I (Biological Science)
Martin Luther University Halle-Wittenberg (MLU), Germany



Dinesh Dhurvas Chandrasekaran

Born on 27.07.1985 in Pondicherry, India

Halle (Saale), Germany | September 2015

Reviewers (Gutachter)

- (1) **Prof. Dr. Steffen Abel** (Leibniz Institute of Plant Biochemistry and MLU)
- (2) **Prof. Dr. Jochen Balbach** (MLU)
- (3) **Prof. Dr. Wolfgang Dröge-Laser** (Julius-Maximilians-Universität Würzburg)

Date of defense (Datum der öffentlichen Verteidigung): 21.12.2015

Dedicated to my beloved parents, sister & friends...

"I begin with an idea, and then it becomes something else ..."

-Pablo Picasso

ABBREVIATIONS

At	<i>Arabidopsis thaliana</i>
AA	Amino Acid
ABP1	Auxin Binding Protein 1
AD	Activation Domain
AFB	Auxin signaling F-Box protein
APS	Ammonium persulfate
ARF	Auxin Response Factor
ARIA	Ambiguous Restraints for Iterative Assignment software
AUC	Analytical Ultra Centrifuge
AUX/IAA	Auxin/Indole-3-acetic acid (IAA)-inducible protein
<i>AuxRE</i>	Auxin Response DNA Elements
BMRB	Biological Magnetic Resonance Bank
CD	Circular Dichroism
CryoEM	Cryo Electron Microscopy
CSI	Chemical Shift Index
CSP	Chemical Shift Perturbations
CTD	C-Terminal Domain
CV	Column Volume
DBD	Deoxyribo Nucleic Acid (DNA) Binding Domain
DD	Dimerization Domain
DTT	Dithiothreitol
<i>E. coli</i>	<i>Escherichia coli</i>
EAR	Ethylene-responsive element binding factor associated Amphiphilic Repression
EDTA	Ethylenediaminetetraacetic acid
FL	Full-Length
FPLC	Fast Protein Liquid Chromatography
GOI	Gene Of Interest
HADDOCK	High Ambiguity Driven biomolecular DOCKing
HDAC	Histone DeAcetylase Complexes
HEPES	4-(2-hydroxyethyl)-1-piperazineethanesulfonic acid
HSQC	Heteronuclear Single Quantum Coherence
IMAC	Immobilized Metal Affinity Chromatography
InsP6	Inositol Hexakisphosphate
IPTG	Isopropyl β -D-thiogalactopyranoside
ITC	Isothermal Titration Calorimetry
JA	Jasmonic Acid
K_D	Equilibrium dissociation constant
L-Trp	L-tryptophan
LRR	Leucine-Rich Repeats
LTR2	LaTeral Rootless 2
MRE	Mean Residual Ellipticity
MSA	Multiple Sequence Alignment
MWCO	Molecular Weight Cut-Off
NMR	Nuclear Magnetic Resonance spectroscopy
NOESY	Nuclear Overhauser Effect Spectroscopy

o/n	overnight
OPCA	Octicosapeptide repeat, p40phox, Cdc24p, Atypical PKC motif
PAGE	Polyacrylamide Gel Electrophoresis
PB1	Phox/Bem1p domain
PBS	Phosphate-Buffered Saline
PCR	Polymerase Chain Reaction
PDB	Protein Data Bank
Pfu	<i>Pyrococcus furiosus</i>
POI	Protein Of Interest
ppm	parts per million
Ps	<i>Pisum sativum</i>
RE	Restriction Endonucleases
RHH	Ribbon-Helix-Helix
RT	Room Temperature
SAUR	Small Auxin Upregulated RNA
SCF	S-Phase Kinase Associated Protein 1-Cullin-F-box Protein complex
SDM	Site-Directed Mutagenesis
SDS	Sodium dodecyl sulfate
SKP2A	S-Phase Kinase Associated Protein 2A
ssDNA	single stranded DNA
TALOS	Torsion Angle Likelihood Obtained from Shift and sequence similarity
Taq	<i>Thermus aquaticus</i>
TBS	Tris-Buffered Saline
TCEP	Tris(2-carboxyethyl)phosphine
TEMED	Tetramethylethylenediamine
TF	Transcription Factor
TIR1	Transport Inhibitor Response 1
TOCSY	TOTAL Correlation Spectroscopy
TPD	TOGGLE Switch Domain
TPL	TOGGLE Switch co-repressor protein
TRIS-HCl	Tris(hydroxymethyl)aminomethane hydrochloride
TROSY	Transverse Relaxation-Optimized Spectroscopy
Ub	Ubiquitin
UV	UltraViolet
vs	versus
w/o	without
WT	Wild-Type
WB	Western Blot
X-Gal	5-bromo-4-chloro-3-indolyl- β -D-galactopyranoside
Y2H	Yeast Two-Hybrid assays
ΔG	Overall free energy
ΔH	Enthalpy
ΔS	Entropy

TABLE OF CONTENTS

ABBREVIATIONS.....	4
SUMMARY	14
1 INTRODUCTION.....	15
1.1 Historical perspective	15
1.2 Nuclear auxin action	16
1.2.1 The phytohormone auxin.....	21
1.2.2 SCF ^{TIR1/AFB} receptor proteins	24
1.2.2.1 TIR1/AFBs domain architecture.....	24
1.2.2.2 Structural insights of auxin perception by co-receptor complexes	24
1.2.3 AUXIN RESPONSE FACTORS	29
1.2.3.1 ARF domain architecture.....	29
1.2.3.2 Structural insights of ARF DBD recognition of auxin-responsive DNA elements.....	29
1.2.4 AUXIN/IAA-INDUCIBLE Proteins	32
1.2.4.1 AUX/IAA domain architecture.....	34
1.2.4.2 Structural insights into the TPL/TPR co-repressor interaction with AUX/IAA DI	34
1.2.4.3 Structural insights into the AUX/IAA DII and its conformational changes.....	35
1.2.4.4 Structural insights into the C-terminal DIII/IV of AUX/IAAs and ARFs	36
1.2.5 AUX/IAA:ARF interaction using the CTD	39
2 HYPOTHESIS AND OBJECTIVES.....	42
3 MATERIALS AND METHODS	43
3.1 MATERIALS.....	43
3.1.1 Bacterial and yeast strains	43
3.1.2 Bacterial and yeast plasmids.....	43
3.1.3 Culture media, buffers and solutions	44
3.1.3.1 Media	44
3.1.3.2 DNA electrophoresis buffers and solutions	45

3.1.3.3	Protein electrophoresis buffers and solutions	45
3.1.3.4	Western blotting buffers and solutions	46
3.1.3.5	Protein purification buffers	46
3.1.3.6	Yeast transformation buffers and solutions.....	47
3.1.4	FPLC column materials	47
3.1.5	DNA and protein markers.....	47
3.1.6	Enzymes	48
3.1.7	Miscellaneous	48
3.1.8	Molecular biology kits.....	48
3.1.9	Instruments	49
3.1.10	Computational software and servers	50
3.2	METHODS	51
3.2.1	Molecular biological techniques.....	51
3.2.1.1	Plasmid isolation.....	51
3.2.1.2	Agarose gel electrophoresis	51
3.2.1.3	Quantification of nucleic acids	51
3.2.1.4	Polymerase chain reaction	51
3.2.1.5	Site-directed mutagenesis	52
3.2.1.6	Gateway® directional TOPO cloning.....	54
3.2.1.7	Chemically competent cells preparation	54
3.2.1.8	Bacterial heat-shock transformation	55
3.2.1.9	DNA sequencing.....	55
3.2.1.10	Recombinant protein expression and optimization	55
3.2.1.11	Protein purification	56
3.2.1.12	Dialysis	56
3.2.1.13	Polyacrylamide gel electrophoresis	57
3.2.1.14	Protein PAGE gel staining.....	58
3.2.1.15	Western Blotting.....	58

3.2.1.16	Immunostaining	59
3.2.1.17	Quantification of proteins	59
3.2.2	Biophysical Techniques.....	60
3.2.2.1	Circular Dichroism spectroscopy.....	60
3.2.2.2	Analytical ultracentrifugation	60
3.2.2.3	Isothermal Titration Calorimetry	61
3.2.2.4	NMR spectroscopy	61
3.2.2.5	NMR titration and interface mapping	66
3.2.3	Yeast-two hybrid assays	67
3.2.3.1	LiAc yeast transformation.....	67
3.2.3.2	Protein-protein interaction assays	67
3.2.3.3	Preparation of yeast protein extract	67
3.2.4	<i>In silico</i> analyses.....	68
3.2.4.1	Sequence analyses.....	68
3.2.4.2	Structural analyses	68
3.2.4.3	Protein-protein docking	68
4	RESULTS.....	69
4.1	Structural characterization of PsIAA4 C-terminal domains	69
4.1.1	Recombinant protein expression and purification of PsIAA4 DIII/IV	69
4.1.2	Structural analyses of the PsIAA4 DIII/IV	70
4.1.2.1	CD spectroscopy showed that PsIAA4 DIII/IV contains mixed secondary structures	70
4.1.2.2	PsIAA4 DIII/IV is monomeric in a high salt or an acidic buffer system	71
4.1.2.3	¹ H NMR spectral analysis confirmed that the PsIAA4 DIII/IV is folded	72
4.1.3	Three-dimensional structure determination of the PsIAA4 DIII/IV	73
4.1.3.1	NMR based sequential backbone assignment and secondary structure prediction	74
4.1.3.2	NMR based analyses revealed the boundaries of PsIAA4 DIII/IV structured regions	76
4.1.3.3	Solution structure of the PsIAA4 oligomerization domain	78

4.2	Functional studies of the PsIAA4 DIII/IV	82
4.2.1	Structural comparison confirms the presence of PB1 fold in the PsIAA4 DIII/IV	83
4.2.2	Mutations of typeI/II conserved residues disturb the PsIAA4 PB1 surface charges.....	84
4.2.3	PsIAA4 FL mutations abolish homotypic interaction <i>in vivo</i>	85
4.2.4	Mutations suppress homotypic interaction at neutral pH.....	87
4.2.5	NMR based pH scanning and sequential backbone assignment of the PsIAA4 PB1 ^{BM3} variant	89
4.2.6	Mapping the acidic interface of the PsIAA4 PB1 dimer	91
4.2.7	Thermodynamic analysis of PsIAA4 PB1 homo-dimerization by ITC	93
4.3	<i>In silico</i> analyses	94
4.3.1	Sequence comparison of PsIAA4 PB1 with AtAUX/IAA and AtARF PB1s.....	94
4.3.2	Comparison of PsIAA4 PB1 with AtAUX/IAA and AtARF PB1 structures	96
4.3.3	Data-driven homodimer docking of PsIAA4 PB1	98
4.3.4	Comparison of homodimer interfaces of PsIAA4 and AtARF5 PB1	100
5	DISCUSSION	103
5.1	Structural comparison of AUX/IAA and ARF PB1 domains.....	104
5.2	Comparison of AUX/IAA and ARF homo- and heterotypic interactions	105
5.3	Comparison of interaction interfaces of AtAUX/IAA and AtARF PB1s.....	107
5.4	AUX/IAA and ARF PB1 domain interacts with other proteins	110
6	CONCLUSION.....	112
7	APPENDICES	113
7.1	Selection of an AUX/IAA protein for the structure-function studies	113
7.2	Large scale purification of selected IAAs.....	114
7.3	CD spectral comparison of AtAUX/IAA1 DIII and PsIAA4 DIII/IV	115
7.4	Sequence information of the WT PsIAA4 DIII/IV fusion protein	115
7.5	The high salt analyses of the PsIAA4 DIII/IV at neutral pH.....	117
7.6	Sequential walk on 3D HNCA strips of the PsIAA4 DIII/IV	118
7.7	Sequence information for PsIAA4 PB1 double and triple mutants	130

7.8	Expression analyses of PsIAA4 PB1 variants	131
7.9	NMR based pH scanning of the PsIAA4 PB1 ^{BM3} at a low pH	131
7.10	Y2H controls	136
7.11	PsIAA4 ^{D100N} and PsIAA4 ^{E181A} mutational studies	136
7.12	Cloning and <i>in vitro</i> analysis of the non-canonical AtAUX/IAA33.....	137
7.12.1	Traditional Cloning of AtAUX/IAA33	137
7.12.2	Protein over-expression and AUC analysis of the AtAUX/IAA33	139
BIBLIOGRAPHY.....		140
CURRICULUM VITAE		152
PUBLICATIONS.....		153
DECLARATIONS.....		156
ACKNOWLEDGEMENTS		157

INDEX OF FIGURES

Figure 1: Various auxin responses in plants.....	16
Figure 2: Domain architecture of the core components of nuclear auxin action	17
Figure 3: Timeline of nuclear auxin response model	19
Figure 4: Chemical structures of natural and synthetic auxins and of anti-auxins	22
Figure 5: Auxin perception by TIR1-ASK1:auxin:AUX/IAA7 degron co-receptor complex.....	25
Figure 6: ARF DBD as "molecular calipers" bound to <i>AuxRE</i> DNA elements.....	30
Figure 7: TOPLESS related protein homotetramer binding to AtAUX/IAA DI	34
Figure 8: Structure of ubiquitin and Ub-like fold containing proteins, and PB1 domain classification.....	37
Figure 9: AUX/IAA:ARF interaction and co-expression networks.....	40
Figure 10: Schematic illustration of sequential walk with HNCA strips plot.....	64
Figure 11: Purified PsIAA4 DIII/IV using IMAC.....	70
Figure 12: Far-UV CD spectrum of the PsIAA4 DIII/IV	71
Figure 13: Sedimentation equilibrium analysis of the PsIAA4 DIII/IV	72
Figure 14: 1D NMR spectrum of the PsIAA4 DIII/IV at low pH	73
Figure 15: 2D HSQC spectral overlay of the PsIAA4 DIII/IV at low pH	74
Figure 16: ¹³ C strip-plot of 3D HNCACB (C α and C β) of PsIAA4 DIII/IV	75
Figure 17: Complete sequential backbone assignment of the PsIAA4 DIII/IV	76
Figure 18: NMR based steady-state hNOE data revealed the flexible regions of PsIAA4 DIII/IV.....	77
Figure 19: CSI plot of the PsIAA4 DIII/IV displays the C α chemical shift differences	77
Figure 20: NMR structure of the PsIAA4 DIII/IV	78
Figure 21: PsIAA4 DIII/IV illustrating twisted β -sheet grasping the α 1 helix.....	79
Figure 22: The bar diagram of NOE data of the PsIAA4 DIII/IV	80
Figure 23: The Ramachandran plot analysis of the PsIAA4 DIII/IV	80
Figure 24: Conserved basic and acidic patch residues of PsIAA4 DIII/IV are highlighted in the MSA	82
Figure 25: NMR structure highlighting basic and acidic patch residues	83
Figure 26: Structural alignment between PB1 domains of NBR1 and PsIAA4	84
Figure 27: Electrostatic charged surfaces of the WT and mutant PsIAA4 PB1	85

Figure 28: Y2H assays confirm type I/II PB1-mediated homotypic interaction of the PsIAA4 FL.....	86
Figure 29: Protein purification of PsIAA4 PB1 double and triple mutants	87
Figure 30: Sedimentation equilibrium analysis of PsIAA4 PB1 double and triple mutants.....	88
Figure 31: NMR-based pH scanning of the PsIAA4 PB1 ^{BM3} mutant protein.....	90
Figure 32: Sequential backbone assignment of 2D HSQC-TROSY spectrum of the PsIAA4 PB1 ^{BM3} mutant.....	90
Figure 33: Acidic dimer interface analysis of the PsIAA4 PB1 mutant	91
Figure 34: NMR based interface mapping of the PsIAA4 PB1	92
Figure 35: Thermodynamic analysis of the PsIAA4 PB1 homodimerization	93
Figure 36: MSA of the PB1 domains of PsIAA4, AtAUX/IAA and AtARFs.....	95
Figure 37: Structural alignment of AUX/IAA and ARF PB1 domains	96
Figure 38: Comparison of PsIAA4 and AtAUX/IAA17 PB1 domains surface electrostatics	98
Figure 39: PsIAA4 PB1 HADDOCK dimer model and interface analysis	99
Figure 40: The MSA of PsIAA4 PB1 and, selected AtAUX/IAA and ARF PB1 domains.....	100
Figure 41: Interaction surfaces of the PsIAA4 and AtARF5 PB1 homodimers	101
Figure 42: The current model of nuclear auxin response core module.....	103
Figure 43: AUX/IAAs and ARFs core and family-specific residues at the basic interface.....	108
Figure 44: AUX/IAAs and ARFs core and family-specific residues at the acidic interface	109
Appendices	
Figure A1: Expression and purification analyses of selected AUX/IAAs.....	113
Figure A2: Large scale batch purification and optimization of AUX/IAAs.....	114
Figure A3: CD spectra of AtAUX/IAA1 DIII and PsIAA4 DIII/IV	115
Figure A4: Comparison of sedimentation analysis of the PsIAA4 DIII/IV.....	117
Figure A5: ¹³ C strip-plot of the 3D HNCA (Cα) from PsIAA4 DIII/IV.....	118
Figure A6: PsIAA4 PB1 mutant protein expression analysis.....	131
Figure A7: Low pH HSQC spectral overlay of WT PsIAA4 PB1 and PsIAA4 PB1 ^{BM3}	131
Figure A8: Sequential backbone assignment of bound PsIAA4 PB1 ^{BM3} and PsIAA4 PB1 ^{AM3}	132
Figure A9: Controls for Y2H assays of homotypic PsIAA4 interaction	136
Figure A10: Y2H analysis of PsIAA4 ^{D100N} and PsIAA4 ^{E181A} mutants.....	136
Figure A11: Protein expression and AUC analysis of AtAUX/IAA33	139

INDEX OF TABLES

Table 1: List of available 3D structures involved in nuclear auxin action	21
Table 2: Currently available protein structures related to auxin homeostasis	23
Table 3: List of currently available PB1 domain structures	38
Table 4: Genotype and details of bacterial and yeast strains	43
Table 5: List of bacterial and yeast plasmids.....	43
Table 6: List of instruments.....	49
Table 7: List of software and servers.....	50
Table 8: List of oligonucleotides used for SDM of the PsIAA4.....	53
Table 9: Oligonucleotides used for Gateway® cloning.....	54
Table 10: List of primary and secondary antibodies.....	59
Table 11: NMR structure constraints and refinement statistics for PsIAA4 DIII/IV	81
Table 12: Interface statistics for PsIAA4 PB1 and AtARF5 PB1	102
Appendices	
Table A1: The residue number and a three-letter AA code of the PsIAA4 DIII/IV	116
Table A2: Total amino acid composition of the PsIAA4 DIII/IV	116
Table A3: TALOS+ torsion angle restraints.....	119
Table A4: All amino acid residues and its side-chain atoms	122
Table A5: Complete assignment of the wild-type PsIAA4 PB1 domain (AA 86-189).....	123
Table A6: Sequential backbone assignment of the PsIAA4 PB1 ^{BM3}	133
Table A7: CSP calculated from free/unbound and bound spectra.....	135
Table A8: Oligonucleotides used for the traditional AtAUX/IAA33 cloning	137

SUMMARY

The plant hormone auxin (IAA), is a versatile small molecule that is essential during the entire plant life cycle and regulates numerous growth and development processes, mainly via hierarchical control of gene expression. Two main classes of transcription regulators involved in primary auxin response are the AUXIN/IAA-inducible (AUX/IAA) transcriptional repressors and the AUXIN RESPONSE FACTOR (ARF) transcription factors. Early auxin-induced *AUX/IAA* genes encode short-lived nuclear proteins with four sequential domains that are conserved at amino-acid level (DI-IV). DI recruits the transcriptional co-repressors TOPLESS, DII displays a degron motif (GWPPV motif) responsible for protein turnover and the C-terminal DIII and IV are structured regions present in both AUX/IAA and ARF proteins, mediating physical homo- and heterotypic interactions. DIII was initially predicted to adopt a $\beta\alpha\alpha$ -fold similar to prokaryotic DNA-binding Ribbon-Helix-Helix (RHH) TFs. Structure prediction and evolutionary studies of ARF and AUX/IAA suggested the presence of a similar structural domain in the C-terminal region of both proteins, which has emerged from an ancient Phox and Bem1p (PB1) protein-protein interaction domain.

In this research work, the NMR structure of wild-type PsIAA4 C-terminal domains (DIII/IV) from pea (*Pisum sativum*) was solved, which was a pioneering model for exploring AUX/IAA function in auxin action. The highly aggregating behavior of AUX/IAA proteins was resolved by protonation of acidic charged residues using a very low pH buffer condition (pH 2.5). Subsequent biophysical studies confirmed that the protein sample was folded, monomeric and not in a molten globule state at low pH. The calculated 3D structure of PsIAA4 DIII/IV adopts a globular ubiquitin-like β -grasp/ $\beta\beta\alpha$ fold with homologies to PB1 domain, which is a versatile domain conserved across all organisms. *In vivo* mutational analyses in yeast, along with NMR-based interface mapping and thermodynamic studies revealed that PsIAA4 possess two distinct surface patches of oppositely charged amino acid residues, mediating front-to-back multimerization mainly via electrostatic interactions. *In silico* docking studies further provided insights into the interaction interface between PsIAA4 PB1 dimers. Therefore, these structure-function studies of PsIAA4 PB1 along with a comparative analysis of very recently available PB1 structures of AtAUX/IAA17, AtARF5 and AtARF7 provide a framework for unraveling molecular determinants that confer specificity to complex interactions between AUX/IAA and ARF transcriptional regulators in auxin response networks.

1 INTRODUCTION

Plants are sessile, living creatures that grow continuously throughout their life-cycle and adjust their morphology in response to endogenous and external environmental factors, leading to their high architectural plasticity (Jaillais and Chory, 2010; Rymen and Sugimoto, 2012; Rigal et al., 2014; Wang et al., 2015b). Plant hormones (or phytohormones) are important signaling molecules that regulate every aspect in plant growth and development, from embryogenesis to senescence (Bishopp et al., 2006). Several classes of structurally unrelated phytohormones derived from various metabolic pathways are present in plants. They include the classical auxins (IAA), abscisic acid (ABA), cytokinins (CK), gibberellins (GA) and ethylene (C₂H₄), and the more recently discovered brassinosteroids (BR), jasmonates (JA), nitric oxide (NO), salicylic acid (SA), stringolactones (SL), and karrikins (KAR) (Santner et al., 2009). In addition, plants also use several peptides as hormonal signals (Lindsey et al., 2002; Jun et al., 2008; Matsubayashi, 2011). Auxin is a crucial phytohormone associated with an extraordinarily wide variety of plant growth, development and defense mechanisms, and acts as a versatile regulator by integrating with multiple plant hormones (Fig. 1) (Jaillais and Chory, 2010; Sauer et al., 2013). Tremendous advances in the last two decades resulted in the identification of the phytohormone receptors and their key signaling components (Kumari and van der Hoorn, 2011; Shan et al., 2012).

1.1 Historical perspective

In the late 19th century, Theophil Ciesielski first postulated the presence of a ‘transmitted influence’ in plants root tip, which governs gravitropism (Ciesielski, 1871). Charles Darwin studied phototropism of canary grass coleoptiles and hypothesized the existence of a mobile growth promoting substance (Darwin and Darwin, 1880). Julius von Sachs, Martinus Beijerinck, Julius Wiesner and several others have also made pioneering contributions to the fundamentals for today’s advance in modern plant physiology (Pennazio, 2002; Tivendale and Cohen, 2015). Frits Warmolt Went conducted extensive auxin-related experimental works, which paved the way for chemists, Hermann Dolk, Jan Haagen-Smit, Fritz Kögl and Kenneth Thimann to isolate, characterize and name the growth promoting compound as auxins. The term ‘auxin’ was derived from the Greek word *αυξεν* (*Auxein* - “to expand” or “to grow”) and was coined by Fritz Kögl and Jan Haagen-Smit (Kögl and Smit, 1931). Indole-3-acetic acid (IAA or auxin), a tryptophan-related small molecule was the first hormone identified and

crucial in various growth and developmental processes, for example apical dominance, shoot elongation, embryo patterning, response to biotic and abiotic external cues etc. (Fig. 1) (Mockaitis and Estelle, 2008; Zhao, 2010; Rymen and Sugimoto, 2012; Kazan, 2013). IAA is the principal auxin produced by plants and synthesized by several soil microbes (Huang et al., 2014; Tivendale et al., 2014; Wang et al., 2014; Yue et al., 2014).

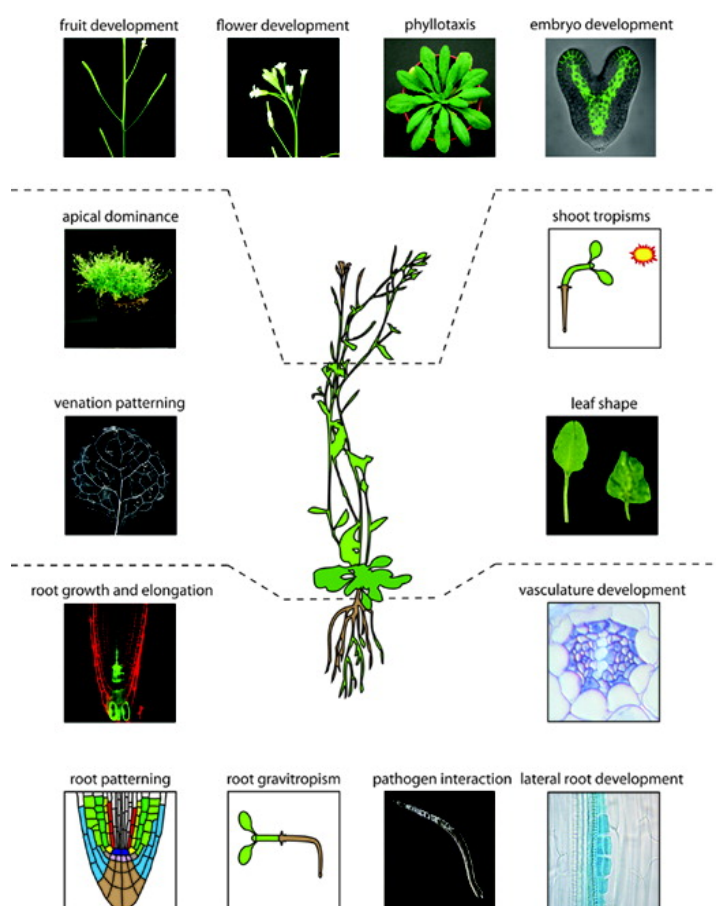


Figure 1: Various auxin responses in plants

The phytohormone auxin regulates virtually every aspect of growth and developmental stages throughout the lifespan of a plant (model plant *Arabidopsis thaliana*), namely embryo development, flower and fruit development, phyllotaxis, apical dominance, root and shoot tropisms, leaf shape, venation patterning, root growth and elongation, root patterning, vascular development, lateral root development and pathogen interaction. Adapted from (De Rybel et al., 2009).

1.2 Nuclear auxin action

Auxin taken up by the cell, diffuses into the cell nucleus and rapidly triggers the expression of primary auxin response genes within 2-30 min (Abel and Theologis, 1996; Grones and Friml,

2015a). The auxin signaling pathway is surprisingly short and direct as suggested by the kinetics of primary gene activation (Abel and Theologis, 1996). Various *Arabidopsis* genetics and molecular biology studies have enabled the identification of the core components of the nuclear auxin response circuit, and biochemical analyses uncovered the mode of nuclear auxin action (Chapman and Estelle, 2009). Advances in molecular genetics have also revealed that transcriptional regulation is critical for auxin response in plants (Kato et al., 2015). During the past few years, advances in the field of structural biology have allowed us to better understand the nuclear auxin action in a molecular perspective, from nuclear auxin perception to transcriptional regulation through AUX/IAA and ARF proteins (Table 1).

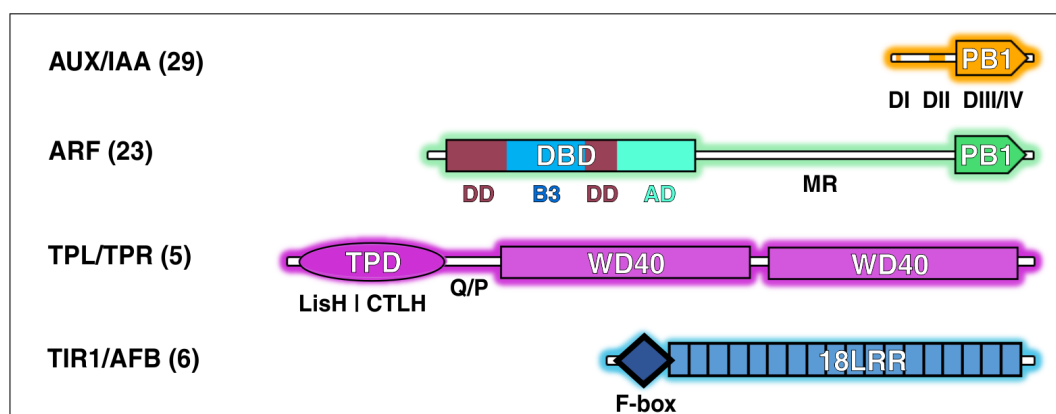


Figure 2: Domain architecture of the core components of nuclear auxin action

Consensus domain structure of AUX/IAA repressors, ARF activators/repressors, TPL/TPR co-repressors, and TIR1/AFB F-box receptor proteins. Depicted are the four conserved domains I-IV (DI-DIV) of AUX/IAAs, which share the C-terminal PB1 domain with ARF proteins (DIII/IV). A variable middle region (MR) separates the ARF PB1 domain and the N-terminal DNA-binding domain (DBD), which consists of a plant-specific B3-type (B3), a dimerization (DD), and an ancillary (AD) subdomain. TPL/TPR proteins share an N-terminal tetramerization domain, named TOPLESS (TPD) domain consisting of two motifs (LisH and CTLH), which is separated by a glutamine and proline-rich spacer from C-terminal WD40 repeat β -propeller domains. TIR1/AFB proteins possess the F-box domain, followed by 18 leucine-rich repeat (LRR) motifs.

In *Arabidopsis thaliana*, the first model species of higher land plants (embryophytes), the core components of the nuclear auxin response apparatus are encoded by 29 *AUX/IAAs*, 23 *ARFs*, 6 *TRANSPORT INHIBITOR RESPONSE 1/AUXIN SIGNALING F-BOX PROTEIN 1-5* (*TIR1/AFBs*) and 5 *TOPLESS/TPL-RELATED* (*TPL/TPR*) genes (Fig. 2) (Wang and Estelle, 2014).

When auxin levels are low, members of the AUX/IAA family of transcriptional repressors interact with ARF transcription factors bound to the auxin-responsive promoter DNA elements (*AuxREs*) and repress its transcriptional activity (Kim et al., 1997; Guilfoyle and Hagen, 2007; Vernoux et al., 2011). ARF proteins bind to a canonical TGTCTC-type *AuxRE* motif usually found as multiple repeats in the majority of auxin response genes promoter and regulate auxin-mediated transcriptional responses (Ulmasov et al., 1995; Ulmasov et al., 1997b; Guilfoyle et al., 1998). AUX/IAA DI (D/E-L-X-L-X-L motif) binds to TPL/TPR (Tup1/Groucho/TLE-like) co-repressors (Szemenyei et al., 2008; Ke et al., 2015). TPL/TPR proteins actively recruit HISTONE DEACETYLASE COMPLEXES (HDAC) and associated chromatin modifying enzymes through their two C-terminal WD40 domains (Long et al., 2006; Szemenyei et al., 2008; Kagale and Rozwadowski, 2011; Causier et al., 2012a). Chromatin deacetylation results in the silencing of ARF target genes. Target gene silencing by TPL/TPR proteins could also be passive by sequestering ARF proteins away from their target promoters (Farcot et al., 2015).

A rise in auxin concentration is registered by auxin-promoted assembly of co-receptor complexes that are composed of an F-box protein (TIR1/AFB1-5) subunit of the nuclear S-PHASE KINASE ASSOCIATED PROTEIN 1-CULLIN-F-BOX PROTEIN (SCF)-type E3 ubiquitin ligases ($SCF^{TIR1/AFB}$) and an AUX/IAA member (Tan et al., 2007; Calderon-Villalobos et al., 2010; Wang and Estelle, 2014). The ternary TIR1-AFB:auxin:AUX/IAA complexes enable polyubiquitylation of AUX/IAA repressors and subsequent 26S proteasome-dependent degradation (Gray et al., 2001; Tan et al., 2007). Thus, auxin initiated AUX/IAA degradation relieves ARF repression, that triggers the expression of early auxin-response genes and coordinates the numerous processes through hierarchical control of gene expression (Chapman and Estelle, 2009; Salehin et al., 2015). Early auxin response genes include e.g., *GRETCHEN HAGEN 3 (GH3)*, *SMALL AUXIN-UPREGULATED RNA (SAUR)*, and *AUX/IAAs*. (Abel and Theologis, 1996; Hagen and Guilfoyle, 2002). AUX/IAA proteins are often products of early auxin genes that establishes a robust negative feedback loops (Fig. 3) (Reed, 2001).

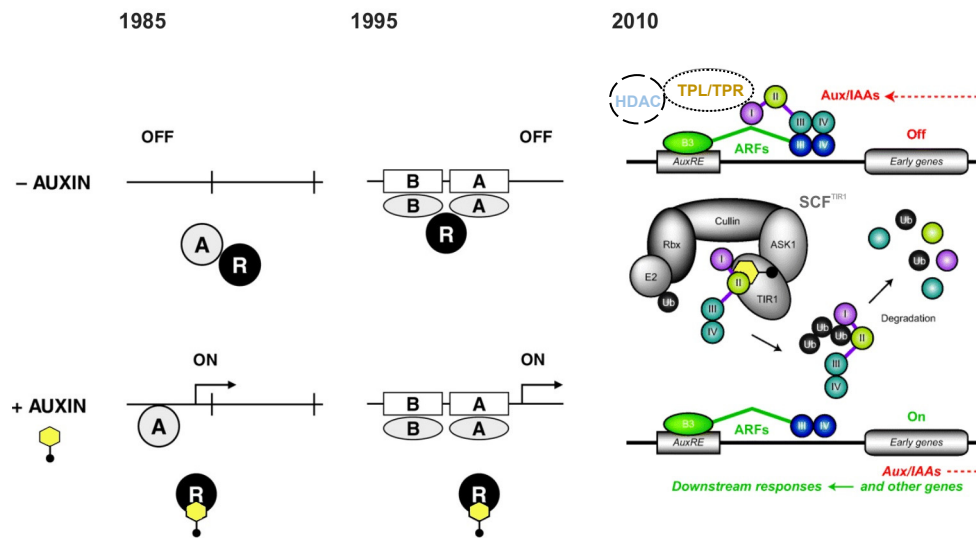


Figure 3: Timeline of nuclear auxin response model

Progression of nuclear auxin action models at low and high auxin scenarios (since 1985-2010). The left model (1985) was proposed initially based on the pioneering research in Prof. Athanasios Theologis's laboratory (Theologis et al., 1985; Theologis, 1986), suggesting control of primary genes by short-lived protein repressors (R) that inhibit the transcriptional activation (A). The middle model (1995) was refined after analyzing the auxin responsive region of *PsIAA4/5* promoter, identified two domains (A and B). Domain A contains typical auxin-response DNA elements (*AuxREs*) (Ballas et al., 1993) and both domains interact with ARF transcription factors (Ulmasov et al., 1997a). The right model (2010) displays the various contributions from different laboratories, including the identification of the TIR1 auxin receptor (Dharmasiri et al., 2005a; Kepinski and Leyser, 2005) and its structural auxin perception mechanism (Tan et al., 2007). The AUX/IAA family members repress ARF function via heterodimerization through shared C-terminal domains (III and IV) and they contain N-terminal domain I and II for co-repressor (TPL/TPR) interaction and the degron signal for degradation, respectively. TPL/TPRs recruiting HDAC and associated chromatin-modifying enzymes, resulting in a transcriptionally inactive chromatin state. The transcription of primary genes is induced by ARF activators, which bind to *AuxRE* promoter elements of early auxin genes via a B3-type, plant-specific, N-terminal DNA-binding domain. Auxin further stimulates AUX/IAA protein degradation by the ubiquitin/proteasome pathway, which leads to derepression of primary genes. Because AUX/IAA genes are a class of early genes, the interaction of both transcription factor families, establishes negative feedback loops that often result in transient auxin responses. The SCF^{TIR1} E3 ubiquitin protein ligase is essential for auxin sensing in the regulation of gene expression. The complex consists of a CULLIN-RBX and TIR1, an F-box LRR protein that is attached to the CULLIN scaffold by the ASK1 adapter. Auxin mediates recruitment of AUX/IAA repressor to SCF^{TIR1/AFB} complexes. Subsequent polyubiquitinylation triggers AUX/IAA protein destruction by the 26S proteasome, which is thought to release ARF factors and promote transcription. Adapted and modified from (Abel, 2007; Abel and Theologis, 2010).

AUX/IAA, ARF and TIR1/AFB protein homologs are present in lower plants, such as bryophytes (*Physcomitrella patens*) and lycophytes (*Sellaginella moellendorffii*) but absent in

chlorophytes (algae) (Lau et al., 2009; Paponov et al., 2009; De Smet et al., 2011; Finet and Jaillais, 2012). A minimal auxin response circuit with a single member of four central protein families is sufficient to reconstitute *AuxRE*-dependent activation of reporter genes in yeast (Pierre-Jerome et al., 2014). In marchantiophytes (*Marchantia polymorpha*), it was recently shown that they contain the simplest natural auxin response system with single orthologs of TIR1, AUX/IAA, TPL and three ARFs, which is critical for its morphogenesis throughout its life-cycle (Flores-Sandoval et al., 2015; Kato et al., 2015).

Diversification of the auxin sensing machinery is believed to specify the multitude of responses to the hormone. For each family, the developmental regulation of cell type-specific *mRNA* expression at multiple levels, the cellular control of protein abundance and activity, and the functional diversification of protein domains provide a vast repertoire for combinatorial interactions between the core components (Overvoorde et al., 2005; Parry et al., 2009; Rademacher et al., 2011). The imaginable complexity is likely necessary to appropriately interpret the context-specific information of auxin distribution profiles in a field of cells, which may range from steep maxima to distinct minima (Brunoud et al., 2012; Bargmann et al., 2013). Such complex auxin gradients are often modified by internal and external cues and have been implicated in the nonlinear regulation of numerous auxin-mediated processes relevant to the adaptation of plant form and function. Differential expression of *AUX/IAA* multigene family members seem to be significant for tuning auxin responses because *AUX/IAA*s notably determine the affinities of the co-receptor pairs for auxin and its structural analogs (Calderon-Villalobos et al., 2012; Lee et al., 2014). A broad range of auxin concentration can be differentially sensed by the numerous TIR1/AFB:*AUX/IAA* co-receptor combinations, which result in different *AUX/IAA* degradation rates (Calderon-Villalobos et al., 2012; Havens et al., 2012; Lee et al., 2014; Shimizu-Mitao and Kakimoto, 2014). The *AUX/IAA* repressors engage in sophisticated *AUX/IAA*:ARF interaction networks (Krogan et al., 2014). Finally, ARF-dependent selection of downstream target genes is thought to confer specificity to the countless auxin responses (Fig. 1) (Guilfoyle and Hagen, 2007).

Recent high-resolution structure-function studies provide an impetus for elucidating the intricate interactions between the core components of the nuclear auxin response module. The 3D structures involved in the nuclear auxin action are summarized and discussed in Table 1.

Table 1: List of available 3D structures involved in nuclear auxin action

Macromolecule name	PDB ID	Fold	Molecular function	Reference
TIR1-ASK1:auxin: AtAUX/IAA7 degron- co-receptor complex	2P1M, 2P1N, 2P1O, 2P1P, 2P1Q	F-box/LRR (TIR1) and POZ (ASK1)	Protein-protein and protein-ligand interaction, Auxin perception	(Tan et al., 2007)
TIR1:small-molecule agonist and antagonists interaction	3C6N, 3C6O, 3C6P	F-box/LRR (TIR1)	Protein-ligand interaction, auxin agonist and antagonist design	(Hayashi et al., 2008)
ARF DNA-binding domain (ARF DBD)- AtARF1 DBD and AtARF5 DBD, apo and bound to <i>AuxRE</i> (ER7)	4LDU, 4LDV, 4LDW, 4LDX, 4LDY	B3, Tudor (AD) and Taco (DD)	DNA-protein interaction, transcription regulation	(Boer et al., 2014)
TOPELESS (TPL/TPR)- OsTPR2 N-terminal TPD domain:AtIAA1 DI and AtIAA10 DI	5C7F, 5C7E	Novel tetrameric fold and zinc finger (TPD)	Protein-protein interaction, co-repression	(Ke et al., 2015)
AUXIN RESPONSE FACTOR (ARF)- AtARF7 CTD and AtARF7 CTD	4CHK, 4NJ6	Ub-like β -grasp (PB1)	Protein-protein interaction, activation/repression	(Nanao et al., 2014; Korasick et al., 2014)
AUXIN-IAA-inducible (AUX/IAA)- PsIAA4 CTD and AtAUX/IAA17 CTD	2M1M, 2MUK	Ub-like β -grasp (PB1)	Protein-protein interaction, repression	(Dinesh et al., 2015; Han et al., 2014)

1.2.1 The phytohormone auxin

IAA is the natural form of this phytohormone which is synthesized from L-tryptophan (L-Trp) (Tivendale et al., 2014). Recent discoveries have led to the identification of several genes involved in tryptophan-dependent auxin biosynthesis (Zhao, 2010; Tivendale et al., 2014), but not much is known about the tryptophan-independent biosynthesis pathways (Wright et al.,

1991; Di et al., 2015b; Wang et al., 2015a). TRYPTOPHAN AMINOTRANSFERASE OF ARABIDOPSIS 1 (TAA1) was the only structurally characterized enzyme involved in main auxin biosynthesis, which converts L-Trp to indole-3-pyruvic acid (IPyA) (Table 2) (Tao et al., 2008). Other three major natural auxins include 4-chloroindole-3-acetic acid (4-Cl-IAA), which is more active than IAA and found only in legumes (Porter and Thimann, 1965; Reinecke, 1999; Lam et al., 2015). Auxins with weak activity are phenylacetic acid (PAA), which is found in higher levels in many plants but shows distinct characteristics when compared to IAA (Korasick et al., 2013; Sugawara et al., 2015), and indole-3-butyric acid (IBA), an inactive auxin precursor (Enders and Strader, 2015).

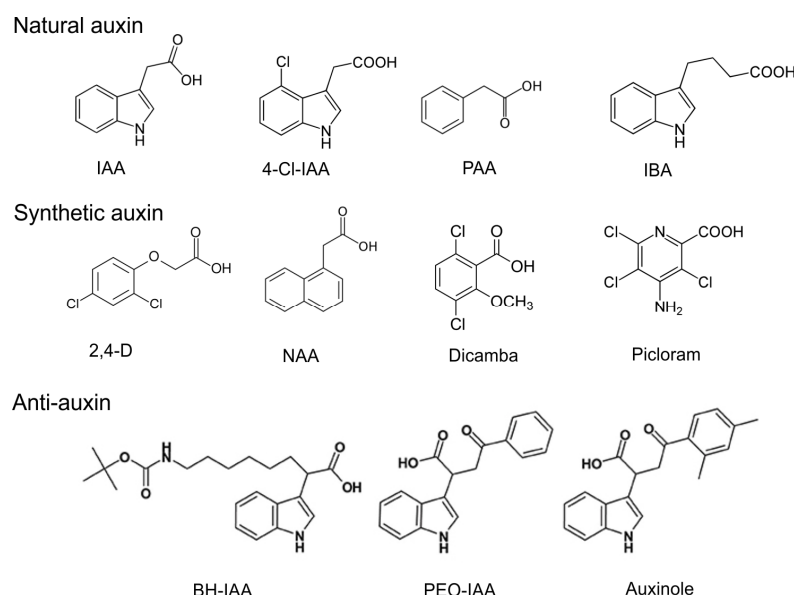


Figure 4: Chemical structures of natural and synthetic auxins, and of anti-auxins

Natural auxins: Indole-3-acetic acid (IAA), 4-chloroindole-3-acetic acid (4-Cl-IAA), phenylacetic acid (PAA) and inactive auxin precursors indole-3-butyric acid (IBA). Synthetic auxins: 2,4-dichlorophenoxyacetic acid (2,4-D) and naphthalene acetic acid (NAA), 3,6-dichloro-2-methoxybenzoic acid (dicamba) and 4-amino-3,5,6-trichloro-2-pyridinecarboxylic acid (picloram). Anti-auxins: tert-butoxycarbonylaminoethyl-IAA (BH-IAA), α -(phenylethyl-2-oxo)-IAA (PEO-IAA) and α -(2,4-dimethylphenylethyl-2-oxo)-IAA (auxinole) (Rigal et al., 2014).

The discovery of synthetic auxins has given the advantage over the rapidly degraded and light sensitive natural auxins to use them more efficiently for laboratories and agricultural application as growth regulators and herbicides (Ljung, 2013; Salehin et al., 2015). Synthetic

auxins include 2,4-dichlorophenoxyacetic acid (2,4-D), 3,6-dichloro-2-methoxybenzoic acid (dicamba), 4-amino-3,5,6-trichloro-2-pyridinecarboxylic acid (picloram), etc. (Fig. 4) (Santner et al., 2009; Enders and Strader, 2015). Since the discovery of the auxin perception mechanism (Tan et al., 2007), rational structure-based anti-auxins or antagonists were generated, i.e., tert-butoxycarbonylaminoethyl-IAA (BH-IAA), α -(phenylethyl-2-oxo)-IAA (PEO-IAA) and α -(2,4-dimethylphenylethyl-2-oxo)-IAA (auxinole) (Hayashi et al., 2008; Hayashi et al., 2012). Auxin homeostasis is maintained through auxin biosynthesis, modification and transport (Korasick et al., 2013; Sugawara et al., 2015). In plants, IAA usually forms conjugates, either ester-linked (to sugar or myo-inositol) or amide-linked (to amino acid or peptide) through the GH3 family of amidosynthases for storage or degradation (Table 2) (Hobbie, 1998; Westfall et al., 2013; Zažímalová et al., 2014). Auxin-conjugating GH3-1 amidosynthase from *Vitis vinifera* is structurally characterized (Table 2) (Peat et al., 2012). Active IAA is released from IAA-amino acid conjugates through different classes of hydrolases. IAA-LEU RESISTANCE1-LIKE 2 (ILL2) is the only hydrolase which is structurally characterized (Table 2) (Levin et al., 2007; Bitto et al., 2009).

Table 2: Currently available protein structures related to auxin homeostasis

Macromolecule name	PDB ID	Family	Biological function	Reference
L-TRYPTOPHAN AMINOTRANSFERASE 1 (TAA1)	3BWN, 3BWO	Alliinase family	Auxin biosynthesis	(Tao et al., 2008)
GRETCHEN HAGEN 3 (GH3)	4B2G	ANL superfamily	Auxin conjugation	(Peat et al., 2012)
IAA-AMINO ACID RESITANCE1-LIKE 2 (ILL2)	1XMB, 2Q43	M20 peptidase family	Auxin metabolism	(Levin et al., 2007; Bitto et al., 2009)

Currently, four major auxin transporters (importers and exporters) have been studied in *Arabidopsis* i.e., PIN-FORMED (PIN), PIN-LIKE (PILS), AUXIN TRANSPORTER PROTEIN 1 (AUX1) and AUX1-like (AUX1/LAX), and P-GLYCOPROTEINS (PGP) of the ATP-BINDING CASSETTE (ABC) transporters (Grones and Friml, 2015a).

1.2.2 SCF^{TIR1/AFB} receptor proteins

Auxin sequesters AUX/IAA repressors to SCF^{TIR1/AFB} complexes like a ‘molecular glue’. Auxin perception triggers the destruction of AUX/IAA repressors, and its degradation rates largely determine the rates of ARF-dependent gene activation (Pierre-Jerome et al., 2014). TIR1/AFBs are the bona fide nuclear auxin receptors (Gray et al., 2001; Dharmasiri et al., 2003; Dharmasiri et al., 2005a; Kepinski and Leyser, 2005; Parry et al., 2009). Six TIR1/AFB F-box proteins containing 18 LRR domains (Fig. 2) are encoded in *Arabidopsis thaliana*, which act as a substrate recognition component that is a part of the SCF-type E3 ubiquitin ligase complex (Gagne et al., 2002; Calderon-Villalobos et al., 2010). The *tir1-1* mutant was isolated based on its resistance to inhibitors of auxin transport and showed auxin resistance with mild auxin-related phenotype (Ruegger et al., 1998). It was the first characterized plant F-box LRR containing protein (Calderon-Villalobos et al., 2010). Auxin regulates AUX/IAA degradation through the SCF^{TIR1} complex by an AUX/IAA degron (DII) interaction with TIR1 (Gray et al., 2001; Zenser et al., 2001). AUX/IAAs are polyubiquitylated and subsequently degraded by the 26S proteasome system (Hobbie and Estelle, 1994; Gray et al., 1999; dos Santos Maraschin et al., 2009; Vierstra, 2009).

1.2.2.1 TIR1/AFBs domain architecture

TIR1 and AFB1-5 proteins share similar domain structure, consisting of an N-terminus F-box domain, followed by an 18 LRR repeat domain (Fig. 2). The F-box domain helps TIR1 to bind to the SKP1 (ASK1) adaptor protein. LRR domains are potential protein-protein interaction domains that confer substrate specificity (AUX/IAA repressor). AFB4 and AFB5 proteins alone contain an additional N-terminal extension of unknown function (Calderon-Villalobos et al., 2010).

1.2.2.2 Structural insights of auxin perception by co-receptor complexes

The co-crystal structure of *Arabidopsis* TIR1-ASK1 with the degron peptide (DII) of the AtAUX/IAA7 repressor along with auxin (IAA), revealed the molecular mechanism of auxin perception (Fig. 5) (Tan et al., 2007). The TIR1-ASK1 complex resembles a mushroom, where TIR1 contains an N-terminal F-box domain (~40 AA), forming three-helix bundle bound to the C-terminal helices of ASK1 (stem). The C-terminal region of TIR1 comprises of 18 LRR forming a twisted horseshoe shaped solenoid-like structure (cap) with a single

binding pocket (Calderon-Villalobos et al., 2010; Salehin et al., 2015). Auxin acts as a ‘molecular glue’ filling a polar gap in the bottom of the AUX/IAA-recruiting pocket positioned on the LRR domain of TIR1 to create a continuous hydrophobic protein interaction surface, without creating an allosteric switch or profound conformational change (Abel, 2007; Tan et al., 2007; Calderon-Villalobos et al., 2010; Salehin et al., 2015). Experimental data indicate that at least some AUX/IAA repressors are polyubiquitylated by SCF^{TIR1} (Maraschin Fdos et al., 2009; Gilkerson et al., 2015) and degraded by the 26S proteasome (Gray et al., 2001; Ramos et al., 2001), which likely applies to all DII-containing AUX/IAAs. The half-life of AUX/IAA varies widely from a few minutes to hours even though they contain a similar DII degon motifs (e.g., AtAUX/IAA17, 5-10 min and AtAUX/IAA28, 80 min) (Dreher et al., 2006b). But AUX/IAA31 with a degenerated DII has half-life of >20 h. AtAUX/IAAs without canonical DII (AtAUX/IAA20, 30, 33, and 34) have an increased half-life and insensitivity to auxin (Sato and Yamamoto, 2008; Calderon-Villalobos et al., 2010). The coiled AUX/IAA degon peptide of 13 AAs (conserved DII) seals the hydrophobic pocket by packing its core GWPPV motif against the indolyl moiety of the hormone, which is believed to remain trapped until AUX/IAA ubiquitylation and destruction ensues (Calderon-Villalobos et al., 2010).

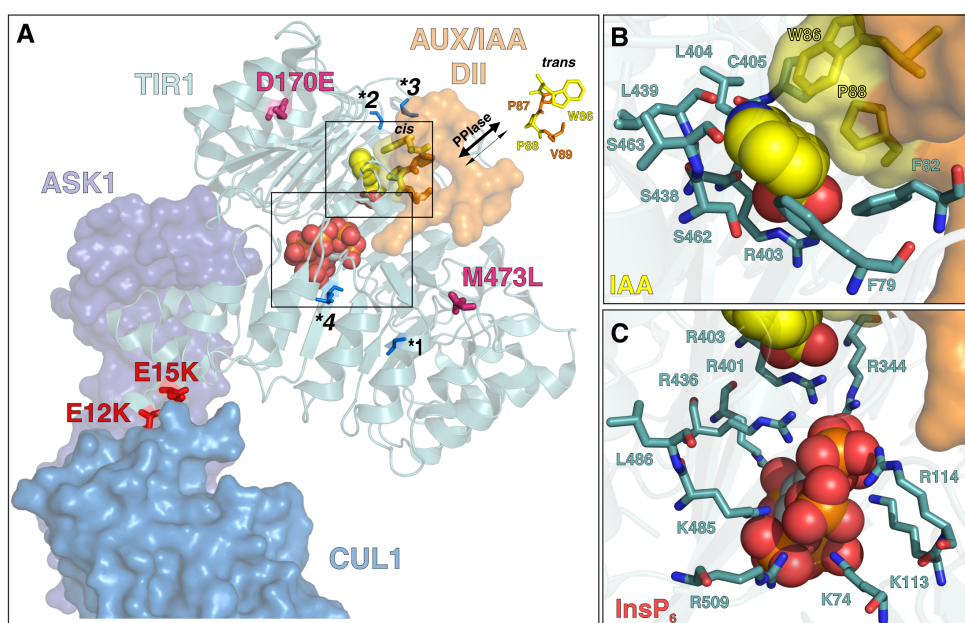


Figure 5: Auxin perception by TIR1-ASK1:auxin:AUX/IAA7 degon co-receptor complex

(A) Structural model of the substrate recognition wing of the SCF^{TIR1} E3 ubiquitin-protein ligase co-receptor complex. Shown are the ASK1-TIR1:auxin:AUX/IAA7 DII co-receptor

complex (PDB ID: 2P1Q) together with the N-terminal part of human CUL1 (PDB ID: 1LDJ). Auxin (IAA, yellow space-filling presentation) occupies a pocket on the top surface of the TIR1-LRR domain. An InsP₆ co-factor (red spheres) is positioned in the center of the solenoid fold. The coiled degron peptide (pale orange space filling) covers the pocket and places its conserved GWPPV fold (sticks) on top of the auxin indole ring. Auxin binding extends the hydrophobic interaction surface of TIR1 and thus facilitates AUX/IAA docking without substantial conformational changes. Two mutations on the TIR1-LRR surface, D170E and M473L (bright pink sticks), increase the affinity for AUX/IAAs (Yu et al., 2013), whereas other mutations (blue sticks) abrogate TIR1 function: *1 (*tir1-1*: G147D), *2 (*tir1-2*: G441D), *3 (*tir1-6*: P409S), and *4 (*tir1-7*: L112Q). Mutations (E12K, E15K) that disrupt TIR1 and CUL1 interaction (red sticks) lead to auxin insensitivity (Yu et al., 2015b). The *cis*-conformation of the first proline residue in the GWPPV motif is necessary for maintaining the coiled binding conformation of the degron peptide, which is facilitated by a cyclophilin-type peptidyl-prolyl *cis/trans* isomerase (PPIase) (Jing et al., 2015). The two boxes frame the auxin-binding pocket and the InsP₆ binding site, which are enlarged in panel B and C, respectively. (B) A close-up view of the spatial arrangement of the TIR1 auxin binding pocket, which illustrates the hydrophobic stacking (yellow) between the indole ring of auxin (center space-filled molecule, a carboxylate group in red) and the GWPPV motif of the coiled degron, with its critical residues (W86 and P88) shown in stick representation. (C) A close-up view of the spatial arrangement of the InsP₆ binding site (center space-filled molecule in red). The InsP₆ co-factor anchors the auxin compound (upper space-filled molecule) via salt bridges (R344, R401) between one of its phosphate groups and the carboxylate function of IAA.

Thus, auxin perception promotes the assembly of TIR1/AFB:auxin:AUX/IAA co-receptor complexes, which displays a wide range of auxin binding affinities *in vitro* ($K_D \sim 10 \text{ nM} - 1 \mu\text{M}$) (Calderon-Villalobos et al., 2012). Inositol hexakisphosphate (InsP₆) was found below the auxin-binding pocket, acting as a structural co-factor. Moreover, the promiscuous auxin binding pocket guided in designing novel agonist or antagonist molecules, modulating protein-protein interaction (Table 1) (Hayashi et al., 2008; Hayashi et al., 2012). TIR1 mutational studies have shown that residues outside binding pocket, D170E and M473L increase AUX/IAA affinity (Fig. 5) (Yu et al., 2013). Additionally, auxin sensitivities of AUX/IAA depend on AUX/IAA:TIR1/AFB co-receptor pair (Shimizu-Mitao and Kakimoto, 2014). Different AUX/IAA:TIR1 co-receptor complexes showed varying affinities to auxin e.g., TIR1:AUX/IAA7, K_D 10-15 nM and TIR1:AUX/IAA12, K_D 250-300 nM (Calderon-Villalobos et al., 2012). Therefore, diverse auxin co-receptor pairs are necessary to respond to a wide range of auxin levels, and describe how auxin controls various growth and developmental processes in plants (Lee et al., 2014; Salehin et al., 2015). Thus, the repertoire of various co-receptor combinations provides the molecular basis for the wide range of dynamic auxin responses.

A similar ‘molecular glue’ mechanism was reported for plant JA perception through the co-crystal structure of COI1-ASK1:JA-Ile:JAZ co-receptor complex (Sheard et al., 2010; Perez and Goossens, 2013). Recently, another example of ‘molecular glue’ model was also discovered in humans for Ikaros and Aiolos degradation facilitated by Lenalidomide/Thalidomide drug molecules (Chamberlain et al., 2014; Fischer et al., 2014).

Regulation of auxin co-receptor formation

AUX/IAA half-lives, which vary widely from 6-80 min (Abel et al., 1994; Ramos et al., 2001; Dreher et al., 2006; Gilkerson et al., 2015), are determined by TIR1/AFB identity and abundance as well as by intrinsic properties of AUX/IAA proteins (Vernoux et al., 2011; Calderon-Villalobos et al., 2012; Havens et al., 2012; Yu et al., 2013; Wang and Estelle, 2014; Moss et al., 2015). Genetic evidence suggests that TIR1 and AFB2 are the major nuclear auxin receptors in *Arabidopsis* promoting auxin response (Dharmasiri et al., 2005b; Parry et al., 2009). Synthetic approaches in yeast provided direct evidence that the two F-box proteins confer rapid auxin-induced degradation of degron-harboring AUX/IAAs, whereas the remaining four AFBs do not affect degradation rates, although they interact with AUX/IAAs in the presence of auxin (Vernoux et al., 2011; Calderon-Villalobos et al., 2012; Havens et al., 2012; Shimizu-Mitao and Kakimoto, 2014). Recently, E12K and E15K mutations in TIR1 F-box domain abrogated binding to CULLIN1 (CUL1), affecting SCF complex assembly and TIR1 stability (Yu et al., 2015). Therefore, a co-crystal structure of SCF^{TIR1}:AUX/IAA FL co-receptor complex with all components will disclose more structural insights (Salehin et al., 2015).

Additionally, auxin perception and signaling is also regulated by various small molecules (Di et al., 2015a). A recent study showed that inositol heptakisphosphate (InsP₇) binds more efficiently to the JA-Ile co-receptor than the less anionic InsP₆ and InsP₅ polyphosphates, and that the binding pocket may even accommodate a single InsP₈ molecule (Laha et al., 2015). Therefore, InsP_x small molecules add yet another layer to hormone response regulation (Sheard et al., 2010), which has to be further investigated in detail to understand its effect on auxin co-receptor assembly.

In the last few years, it has been shown that regions outside degron motif in AUX/IAA are also responsible for its increased affinity to TIR1, creating complexity and degradation

dynamics that modulate the auxin response (Calderon-Villalobos et al., 2012; Havens et al., 2012; Lee et al., 2014; Pierre-Jerome et al., 2014; Guseman et al., 2015). Indeed, dissection of the broader, variable DII context of AUX/IAAs with different half-lives identified several degron-flanking ‘rate motifs’ that differentially affect auxin-dependent co-receptor assembly and AUX/IAA turnover (Moss et al., 2015). The uncoupling of AUX/IAA binding to SCF^{TIR1} from AUX/IAA degradation points to regulatory processes that modify such rate motifs, which may include canonical and non-canonical ubiquitylation (Kravtsova-Ivantsiv and Ciechanover, 2012; Gilkerson et al., 2015) or other post-translational modifications, such as phosphorylation (Colon-Carmona et al., 2000).

Specific ubiquitylation has been often the rate-limiting step in proteolysis, and E3 ubiquitin-protein ligases typically form an isopeptide bond between the terminal carboxylate group of ubiquitin and the ϵ -amino group of lysine residues within the substrate (Mattioli and Sixma, 2014). Surprisingly, an attempt to identify preferred lysine ubiquitylation sites on rapidly degraded AtAUX/IAA1 concluded that exhaustive lysine-to-arginine substitutions did not considerably stabilize the mutant protein nor impaired its ability to heterodimerize with AtAUX/IAA7 or to interact with TIR1 (Gilkerson et al., 2015). The same study obtained evidence for noncanonical, oxyester-linked ubiquitylation of serine and threonine side-chains on the lysine-free AtAUX/IAA1 variant, and a mixture of both on WT AtAUX/IAA1. The latter observation suggests that ubiquitylation on multiple AUX/IAA sites is a robust process that supports complex AUX/IAA degradation dynamics depending on intrinsic substrate properties (Gilkerson et al., 2015).

Two other known independent auxin receptors include AUXIN BINDING PROTEIN 1 (ABP1) (Hertel et al., 1972; Jones et al., 1998) and S-PHASE KINASE ASSOCIATED PROTEIN 2A (SKP2A) (Jurado et al., 2010). ABP1 was demonstrated to be a cell-surface based auxin receptor and has been shown to mediate a non-transcriptional auxin responses (Chen et al., 2012; Chen et al., 2014; Paque et al., 2014; Xu et al., 2014; Grones and Friml, 2015b). The ABP1 homodimer has high affinity to auxin, which adopts a Germin/Seed storage 7S superfamily fold containing a defined auxin binding pocket (PDB ID: 1LR5, 1LRH) (Woo et al., 2002; Grandits and Oostenbrink, 2014; Grones et al., 2015). Recent discoveries demonstrated its role in several plant cellular and developmental processes (Habets and Offringa, 2015). If ABP1 functions as an auxin receptor or not, is still unclear

(Gao et al., 2015). SKP2A, also known to be a nuclear auxin receptor is involved in regulating cell cycle transcription repressors and contributes to auxin action during cell proliferation (Jurado et al., 2010; Del Pozo and Manzano, 2014). Auxin enhances SKP2A binding to DPB (E2F dimerization partner B) (Jurado et al., 2010). This suggests the presence of other possible auxin signaling pathways, which are yet to be studied in detail.

1.2.3 AUXIN RESPONSE FACTORS

ARF1, the founding member of the *Arabidopsis* ARF family was identified in a yeast one-hybrid screen and shown to bind *in vitro* to distinctly spaced palindromic TGTCTC elements (ER7) (Ulmasov et al., 1997a). Loss-of-function (LOF) mutant of ARFs showed similar phenotypes to *aux/iaa* gain-of-function (GOF) mutants, e.g., GOF of AtAUX/IAA12 (*iaa12/bdl*) and LOF of AtARF5 (*arf5/mp*) showed similar root-less phenotype (Hardtke and Berleth, 1998). Later, it was revealed that ARF dimers bind to duplicate *AuxREs* as direct, inverted or everted repeat and the first four nucleotides of the TGTCTC motif are crucial for binding (Guilfoyle et al., 1998; Ulmasov et al., 1999; Tiwari et al., 2003). It was also shown that all ARFs bind with a specificity on palindromic *AuxREs*; however, robust DNA recognition requires ARF dimerization and the first four nucleotides of the TGTCTC motif (Ulmasov et al., 1999; Tiwari et al., 2003).

1.2.3.1 ARF domain architecture

ARF proteins contain three separate distinctly functioning regions i.e., a conserved N-terminal DBD, a highly variable middle region (MR) and a C-terminal domain. The core region of the DBD of the 22 full-length AtARFs is related to the plant-specific B3 domain (Yamasaki et al., 2013), but flanking residues are necessary for efficient *AuxRE* binding (Ulmasov et al., 1999). MR determines the overall function of the ARF either as an activator or as a repressor, based on high abundance of specific amino acids (Q-rich AtARF5-8 and AtARF19 activators or S, P, L/G-rich ARF repressor) (Finet et al., 2013; Guilfoyle, 2015). The C-terminal domain which is shared between ARF and AUX/IAA families mediates protein-protein interaction between and within family members (Fig. 2) (Guilfoyle and Hagen, 2007; Guilfoyle, 2015).

1.2.3.2 Structural insights of ARF DBD recognition of auxin-responsive DNA elements

ARF proteins contain an N-terminal DBD, which is comprised of three modular structured domains, (i) B3 domain, seven stranded open β -barrel fold binds to sequence specific DNA,

(ii) DD - dimerizing domain, five antiparallel β -strand with novel taco-like fold, which is responsible for homodimerization, and (iii) AD - ancillary domain, five stranded beta barrel-like Tudor domain of unknown function (Fig. 6) (Boer et al., 2014). All AtARF proteins contain a DBD, except AtARF23. Boer et al., (2014) solved the high-resolution co-crystal structures of the AtARF5 activator and the phylogenetically distant AtARF1 repressor, which allowed unprecedented insight into the mechanism of ARF:DNA interaction. ARF DNA binding residues are highly conserved, but each pair has a different optimal spacing between binding sites, thereby giving them the name ‘molecular calipers’. The ARF DBD homo- or heterodimerize to generate co-operative DNA binding *in planta* (Boer et al., 2014). ARF DBD structure also revealed that homo-dimerization between ARF DBDs are mediated by DD. ARF monomers are juxtaposed using helix $\alpha 6$ with centered conserved AtARF1 DBD^{G245} and other interacting residues around it. Additionally, P233-S238 loop’s S235 (S269) fits to the groove of the opposite monomer (Fig. 6B).

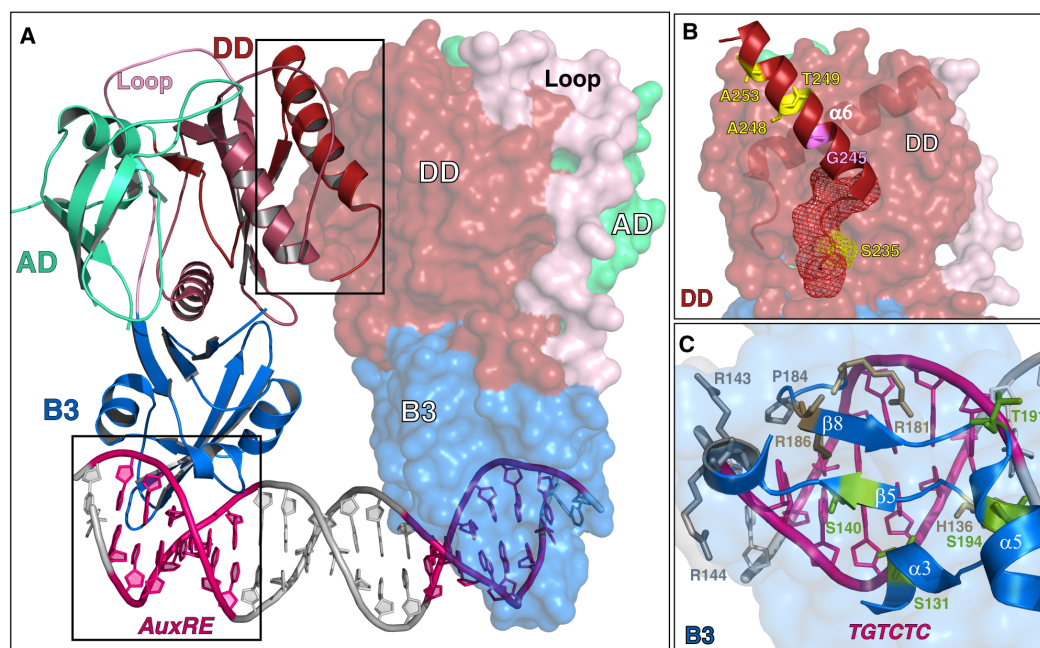


Figure 6: ARF DBD as “molecular calipers” bound to *AuxRE* DNA elements

The ‘molecular caliper’ concept for cooperative recognition of composite *AuxREs* by ARF DBD dimers. (A) The co-crystal structure of the AtARF1 DBD:ER7 complex (PDB ID: 4LDX). The two everted TGTCTC motifs of the ER7 oligonucleotide are highlighted in bright pink and its 7-bp spacer in gray. The two AtARF1 DBD monomers are shown as cartoon (left) and surface (right) presentation. The three subdomains of the DBD are colored: B3-type (B3, blue), dimerization (DD, maroon), ancillary (AD, green), and the variable loop connecting B3 and DD (pale pink). The two boxes frame the protein (DD):protein (DD) and protein (B3):DNA (ER7) interaction interfaces, which are enlarged in panel B and C, respectively. The flexible loop varies among ARF members and is

thought to generate various ‘molecular calipers’ that recognize *AuxREs* of differently spaced TGTCTC elements. (B) Molecular interactions at the AtARF1 DBD dimerization interface. The DD helix 6 ($\alpha 6$) of each monomer is juxtaposed and centered at a conserved glycine residue (G245). Flanking residues at the same face of the helix (A248, T249, A253) make hydrophobic contacts whereas the preceding short loop with a serine residue (S235) at its center fits into a groove of the opposite monomer (Boer et al., 2014). (C) Molecular interactions at the AtARF1 DBD:DNA interface. The AtARF1 B3 subdomain recognizes a single TGTCTC element of the ER7 *AuxRE* mainly at the major groove via nucleobase contacts (olive: R181, R186, H136), backbone interactions (green: S131, S140, T191, S194) and other conserved DNA interacting residues (gray: P184, R143, R144), which are supported by two adjacent β strands ($\beta 5$ and $\beta 8$), helices ($\alpha 3$ and $\alpha 5$) and their connecting loop (Boer et al., 2014).

Therefore, dimers are stabilized by several hydrophobic interactions and a network of hydrogen bonds involving water molecules. *In planta*, mutational studies validated that ARF dimerizes in the absence of its CTD and is essential for its function *in vivo*. Presence of CTDs will give additional stabilization to full-length ARF dimers. The crystal structure of mutant AtARF1 DBD^{G245A} superimposed with WT AtARF1 DBD revealed that mutations in DD interface residue disrupted the symmetry and also displayed impaired biological function of AtARF5 (Boer et al., 2014).

In the early 90’s, *AuxRE* was defined as TGTCTC motif inverted repeats with a seven nucleotides spacer showing efficient binding (Ulmasov et al., 1995; Ulmasov et al., 1997a). The co-crystal structure of AtARF1 DBD with *AuxRE* ER7 DNA reveal how a U shaped dimeric DBD sits on the DNA using the B3 domain on its tip and that DNA adopts a B-DNA conformation and bends by 40°. ARF DBD contains a B3 domain (insertion) whose N- and C-terminal regions fold together into a single second DD subdomain, which was likely a bromodomain/WD40 repeat protein (Boer et al., 2014; Guilfoyle, 2015). The $\alpha 1$ -helix acts as a pivot point on which the B3 domain is balanced, and a highly disordered loop connecting B3 and DD on either side of the helix gives flexibility. Comparing apo- and DNA-bound structures of AtARF1 DBD explain the 25° shift of B3 domain because of the intrinsic flexibility when compared with DD, thereby locking DBD dimer upon binding to DNA. Two adjacent β strands of the B3-type subdomain ($\beta 5$, $\beta 8$), helices ($\alpha 3$ and $\alpha 5$) and their connecting loops bind to the major groove (TGTCTC element), and the identified AtARF1 DBD:DNA contacts were validated by biophysical and genetic experiments. Interestingly, the DNA-binding residues are almost completely conserved within the ARF family. In agreement, an unbiased interrogation of the hexamer space by protein binding microarrays indicated that

both AtARF1 DBD and AtARF5 DBD prefer the same *AuxRE* motif (TGTCGG rather than the canonical TGTCTC element), although the two proteins have different biochemical and biological functions (Guilfoyle and Hagen, 2007; Boer et al., 2014; Franco-Zorrilla et al., 2014). Knowledge-based methods have helped in redesigning of *AuxRE-like* elements and inefficient prediction of auxin response genes (Keilwagen et al., 2011; Mironova et al., 2014; Ponomarenko and Ponomarenko, 2015). The DNA binding mechanism of ARF protein was quite comparable with other available B3 domain protein structures i.e., VRN1 (non-specific DNA binding), RAV1 (specific DNA binding) and At1g16640 (no DNA binding) from plants (Kagaya et al., 1999; Yamasaki et al., 2004; King et al., 2013), (reviewed in Yamasaki et al., 2013). Additionally, restriction endonucleases such as EcoRII (Zhou et al., 2004; Golovenko et al., 2009) and BfiI (Grazulis et al., 2005; Golovenko et al., 2014) also have a similar conserved DNA-binding mechanism.

Their co-operative binding was analyzed using mutant protein binding studies by Surface Plasmon Resonance (SPR) and its sequence specificity was examined by altering the DNA binding site, showing that ARF DBD binds specifically *AuxRE* and always functions as a dimer *in vivo*. The AtARF1 DBD^{G245A} mutation even abrogates co-operative DNA binding explaining the ‘molecular calipers’ mechanism. ARF DBD dimerization provides a means to recognize composite *AuxREs* of uniquely spaced TGTCTC-type elements. Indeed, because the AtARF5 DBD has increased interdomain flexibility, the AtARF1 and AtARF5 DBD homodimers can discriminate between palindromic *AuxREs* of different spacer length. Thus, the various possible ARF dimers are hypothesized to provide an assortment of ‘molecular calipers’ to gauge and recognize uniquely spaced, palindromic TGTCTC-type *AuxRE* elements. Multiple composite *AuxREs* are often found in ARF target genes, including many members of the *AUX/IAA* family (Abel et al., 1996; Chapman and Estelle, 2009; Krogan et al., 2014).

1.2.4 AUXIN/IAA-INDUCIBLE Proteins

AUX/IAA genes are primary response genes, which are induced by auxin (Abel et al., 1995). *AUX/IAA* proteins are transcriptional repressors and interact with itself forming homooligomers. Additionally, *AUX/IAAs* interact with ARF activators, thereby repressing its function (Kim et al., 1997; Guilfoyle et al., 1998). In *Arabidopsis*, first *aux/iaa* gain-of-function (GOF) mutant of *AUX/IAA17* carried mutations in DII, which stabilized the protein

and showed dramatic developmental defects and decreased auxin sensitivity in the mutant plants (Rouse et al., 1998; Ouellet et al., 2001). In a similar fashion several other *aux/iaa* GOF mutants were also discovered and characterized. On the other hand, LOF mutants failed to show any auxin-related phenotype, suggesting that 29 AUX/IAAs are genetically redundant in *Arabidopsis* (Overvoorde et al., 2005), but in tomato (*Solanum lycopersicum*) 26 *SLAUX/IAA* show different spatio-temporal transcript accumulation indicating them as non-redundant (Remington et al., 2004; Okushima et al., 2005; Wu et al., 2012; Salehin et al., 2015).

Pioneering research work on AUX/IAA4 from pea (Pisum sativum)

Since the last 30 years, research from Prof. Athanasios Theologis's and Prof. Steffen Abel's laboratories have made several pioneering contributions related to molecular auxin action. Auxin-induced mRNAs were first discovered in pea plants and their genes were structurally characterized (Theologis and Ray, 1982; Theologis, 1989; Oeller et al., 1993). Later, these newly identified genes were found to be rapidly induced (4-30 min) by auxin and, named *AUX/IAA* genes (auxin/IAA-inducible). The encoded proteins are short-lived and localize to the cell nucleus (Abel et al., 1994; Abel and Theologis, 1995; Koshiba et al., 1995; Oeller and Theologis, 1995). *Ps-IAA4/5*-like cDNA sequences were also prepared from auxin-induced transcripts from *Arabidopsis thaliana*. AUX/IAA proteins (19-36 kDa) contain four conserved sequential domains (DI-DIV) separated by variable spacers (Abel et al., 1995). DIII was predicted to adopt a beta-alpha-alpha ($\beta\alpha\alpha$) fold similar to the beta-sheet DNA-binding domain found in prokaryotic repressors (Abel et al., 1994; Morgan et al., 1999). Therefore, initially it was hypothesized that the AUX/IAA proteins contain a DNA-binding domain and mediate auxin response in plants (Abel et al., 1994; Abel and Theologis, 1996). Transgenic tobacco lines carrying *Ps-IAA4/5* and *Ps-IAA6* suggested that spatio-temporal co-expression of various *Ps-IAA4/5*-like members might be responsible for plant development and cell specific auxin response (Wong et al., 1996). The *Ps-IAA4/5* promoter deletion analysis defined the *auxin response DNA elements (AuxREs)* required for auxin inducibility (Ballas et al., 1993; Ballas et al., 1995). Direct homo- and hetero-typic interaction of AUX/IAA and ARF family members via their homologous C-terminal regions were verified using *in vitro* and *in vivo* experiments (Kim et al., 1997). Post-translational modification of AUX/IAA was first revealed from the study of *in vitro* phosphorylation of PsIAA4 by phytochrome A (Ser/Thr kinase) (Colon-Carmona et al., 2000).

1.2.4.1 AUX/IAA domain architecture

AUX/IAA proteins share four regions of sequence conservation known as domains I-IV (DI-IV) (Overvoorde et al., 2005). The N-terminal DI, containing an ETHYLENE- RESPONSIVE ELEMENT BINDING FACTOR-ASSOCIATED AMPHIPHILIC REPRESSION-LIKE (EAR-like) D/E-L-X-L-X-L motifs (Li et al., 2011a), physically interacts with the C-terminal LISSENCEPHALY HOMOLOGY (CTLH) domain of TPL/TPR co-repressors (Fig. 2) (Tiwari et al., 2004; Long et al., 2006; Szemenyei et al., 2008; Li et al., 2011b; Causier et al., 2012a; Causier et al., 2012b). Transcriptional repression occurs either by TPL/TPRs recruiting HDAC and associated chromatin-modifying enzymes, which leads to a hypoacetylation of histones, resulting in a transcriptionally inactive chromatin state (Haberland et al., 2009; Anzola et al., 2010; Krogan et al., 2012a; Wang et al., 2013a; Wang and Estelle, 2014), or by AUX/IAA sequestering ARF proteins away from target promoters (Farcot et al., 2015). The highly conserved DII containing the degron motif (GWPPV) interacts with TIR1/AFBs and is required for auxin-dependent co-receptor assembly (Tan et al., 2007; Salehin et al., 2015; refer section 1.2.2). The C-terminal region contains conserved domains III/IV, which mediate homo- and hetero-typic interactions within and between AUX/IAAs and ARF family members (Kim et al., 1997; Vernoux et al., 2011).

1.2.4.2 Structural insights into the TPL/TPR co-repressor interaction with AUX/IAA DI

The TPL/TPR (Tup1/Groucho/TLE-like) co-repressor's N-terminal domain (TPD) contain LisH, CTLH and a Zn finger (Fig. 2), and their C-terminus contains two WD40 domains, which are believed to recruit HDAC and associated chromatin-modifying enzymes.

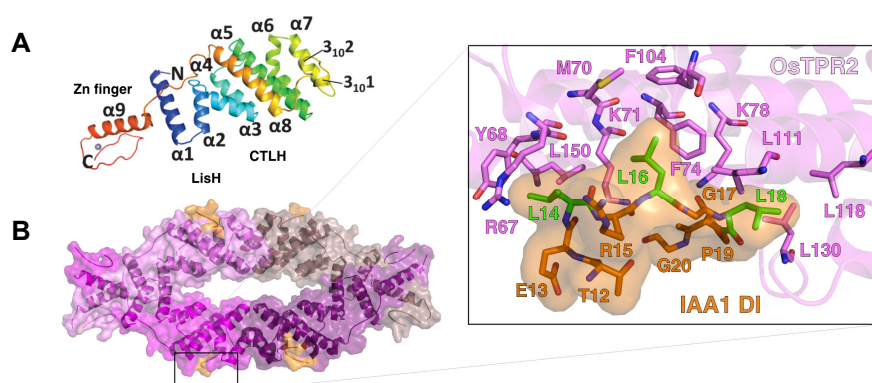


Figure 7: TOPLESS related protein homotetramer binding to AtAUX/IAA DI
 (A) OsTPR2 TPD monomer in rainbow color scheme, displaying N-terminal (violet) LisH (α1 and α2), CTLH (α3 and α5) and a C-terminal (red) Zn-finger domain (Zn ion, gray ball). (B) Structural model of the TPD homotetramer of OsTPR2 (shades of purple)

complexed with four EAR peptides of AtAUX/IAA1 DI (light orange). Zoom in shows the interacting AtAUX/IAA1 and TPR2 residues in stick representation (right), LxLxL motif (green). Adapted from (Ke et al., 2015).

N-terminal DI of most AUX/IAAs bind to TPL/TPR proteins via its EAR-like motif (D/E-L-X-L-X-L), which is the prototypic repressor motif found in many plant transcriptional regulators (Kagale and Rozwadowski, 2011; Causier et al., 2012a).

The recently solved crystal structures of the N-terminal TOPLESS domain (TPD) of rice (*Oryza sativa*) OsTPR2 in complex with the EAR motifs from *Arabidopsis thaliana* AUX/IAA1 and AUX/IAA10 revealed a novel fold of nine helices and a zinc finger domain, which oligomerizes into a donut-like tetramer (Fig. 7) (Ke et al., 2015). The tetrameric complex is formed by the dimer of dimers containing two different interaction interfaces. A shallow groove on each TPD monomer (CTLH motif) binds via hydrophobic and positively charged residues a single EAR motif peptide of extended conformation (Fig. 7 inset). Biophysical studies indicated that a single EAR peptide weakly interacts with OsTPR2 whereas a tetrameric bacterial protein displaying four EAR peptides binds with much higher affinity (>200-fold). Thus, AUX/IAA repressor multimerization likely facilitates synergistic recruitment of TPL/TPR tetramers, which may provide, as for OsTPR2, expanded scaffolds of eight seven-bladed WD40 β -propeller domains for mediating the assembly of chromatin remodeling complexes and the interaction with the transcription preinitiation complex (Ke et al., 2015) (Fig. 7). While TPL/TPR co-repressor complexes are tethered to auxin-responsive promoters via the interaction between AUX/IAA repressors and ARF activators, members of the ARF repressor class, which do not bind AUX/IAAs (Vernoux et al., 2011; Piya et al., 2014), may interact directly with TPL/TPR co-repressors (Causier et al., 2012a).

1.2.4.3 Structural insights into the AUX/IAA DII and its conformational changes

The DII is essential for auxin-dependent AUX/IAA degradation and dominant mutations, foremost in its nearly invariant GWPPV core motif, abolish AUX/IAA binding to TIR1/AFBs and cause auxin-resistant phenotypes (Salehin et al., 2015). Jing et al. (2015) have discovered a novel mechanism that regulates AUX/IAA repressor degradation through post-translational modification of the GWPPV motif, catalyzed by a cyclophilin-type peptidyl-prolyl *cis/trans* isomerase (PPIase) e.g., LATERAL ROOTLESS 2 (LTR2) (Fig. 5A). It directly regulates binding of OsIAA11 to OsTIR1 and thus OsIAA11 stability (Jing et al., 2015). NMR

spectroscopy based ROESY experiment demonstrated that LRT2 efficiently catalyzes the *cis/trans* conformational exchange in the core GWPPV motif of the OsAUX/IAA11 degron peptide (Jing et al., 2015). Notably, the crystal structure of the TIR1:auxin:AUX/IAA7 co-receptor complex revealed that the *cis*-conformation of the first proline residue is necessary for maintaining the coiled binding conformation of the AtAUX/IAA7 degron peptide (Tan et al., 2007) (Fig. 5). Because LRT2-like proteins are conserved in land plants and their functional loss leads to similar auxin-insensitive phenotypes (Oh et al., 2006; Lavy et al., 2012), it has been proposed that the cyclophilin-catalyzed *cis/trans* isomerization of AUX/IAA transcriptional repressors may represent a general mechanism to accelerate their proteolysis (Jing et al., 2015). Mutation of LTR2 homologs in tomato DIAGEOTROPICA (DGT) and moss PpDGT (*Physcomitrella patens*) also displayed auxin-related phenotype (Ivanchenko et al., 2006; Oh et al., 2006; Lavy et al., 2012; Retzer and Luschnig, 2015). Therefore, *cis/trans* isomerization of GWPPV motif stabilize AUX/IAAs and add a further layer of regulation in auxin signaling (Jing et al., 2015).

1.2.4.4 Structural insights into the C-terminal DIII/IV of AUX/IAAs and ARFs

AUX/IAA and ARF family members contain the conserved C-terminal domains DIII and IV, which are required for protein-protein interaction (Kim et al., 1997). The DIII/IV is predicted to adopt a globular ubiquitin-like β grasp fold and is related to an ancient Phox and Bem1p (PB1) domain containing protein (Burroughs et al., 2007; Guilfoyle and Hagen, 2012). The CTD of AUX/IAA and ARF are protein-protein interaction modules, which act as ‘molecular magnets’ allowing homo- and hetero-dimerization between these two major classes of transcription regulators. Recent structural studies of the oligomerization domain (ARFs and AUX/IAAs) (Han et al., 2014; Korasick et al., 2014; Nanao et al., 2014; Dinesh et al., 2015) are extensively discussed in this thesis work.

PB1 domain containing proteins

PB1 domains were named after the first structures, p67^{Phox} - phagocyte oxidase activator Phox and Bem1p - yeast polarity protein (Ito et al., 2001; Ponting et al., 2002). It adopts a typical Ub-like β grasp fold similar to ubiquitin (Fig. 8) and comprises of ~80 AAs. PB1 domains are protein-protein interaction modules conserved in different organisms including plants. They

are found as a module in multi-domain proteins and are involved in various biological processes (Sumimoto et al., 2007).

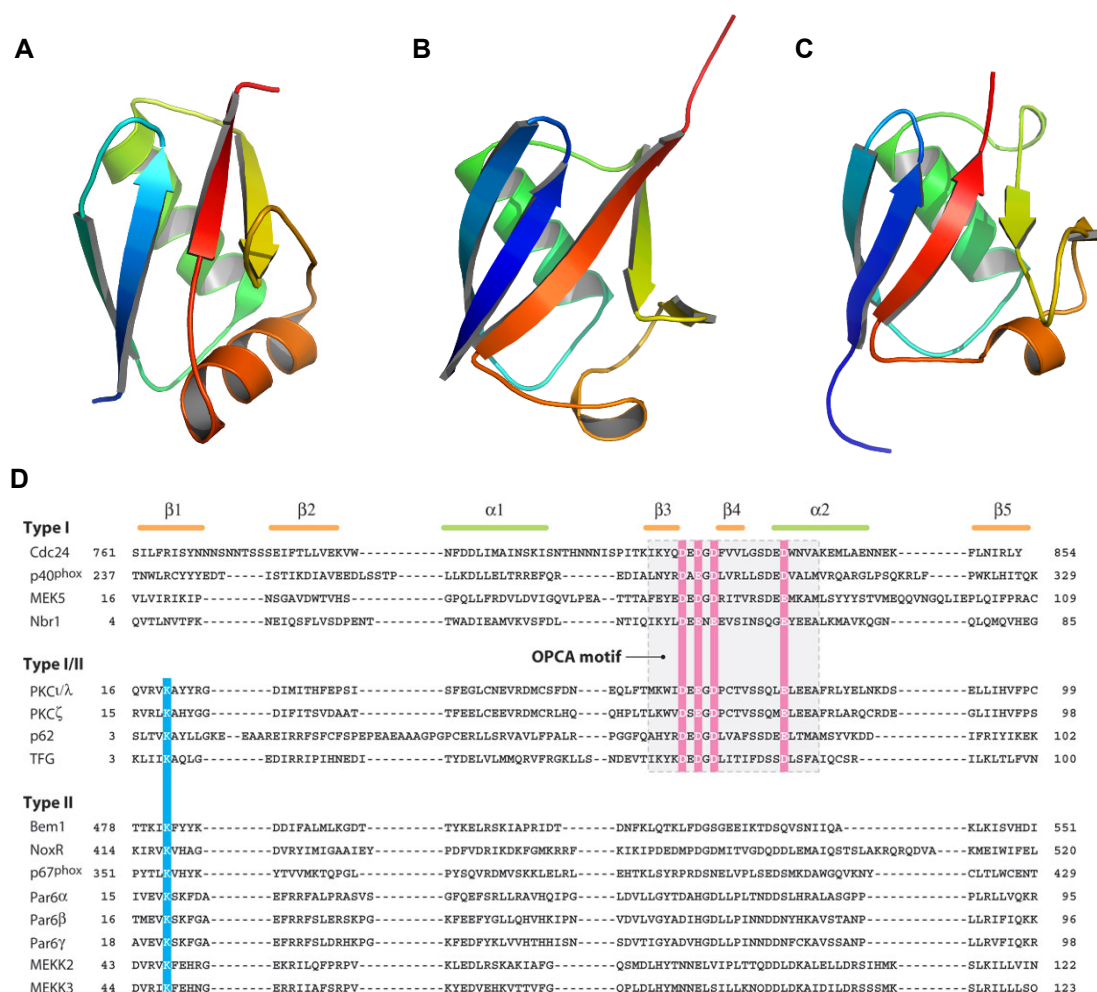


Figure 8: Structure of ubiquitin and Ub-like fold containing proteins, and PB1 domain classification

(A) Ubiquitin (PDB ID: 1AAR) (B) p67^{phox} (PDB ID: 1AAR) and (C) Bem1p (PDB ID: 1AAR). All 3D structures are colored as rainbow color scheme from N- (violet) to C-terminus (red). (D) MSA of PB1 domains from different proteins. Cdc24 and Bem1 are from *Saccharomyces cerevisiae*; NoxR from *Epichloë festucae*; and the others from human. The secondary structural elements are shown above the sequences by green bars (β) and orange bars (α). The OPCA motifs (pink) in type I and type I/II PB1 domains and the Lys residue conserved among type I/II and type II PB1 domains (blue). Conserved acidic residues in the OPCA motif are shown in pink; conserved lysine is indicated in blue, adapted from (Sumimoto et al., 2007).

Canonical PB1 domains are composed of two helices and a mixed five-stranded β sheet. They are classified into three types depending on the conservation and presence of oppositely

charged and oriented surface patches (Sumimoto et al., 2007). PB1 domains may expose a conserved acidic cluster (D-X-D/E-X-D-X_n-D) at the linker between $\beta 3$ and $\beta 4$, known as the octicosapeptide repeat, p40phox, Cdc24p, atypical PKC interaction domain motif (OPCA) (type I) (Ponting et al., 2002), a basic surface patch with an invariant lysine residue on $\beta 1$ as its hallmark (type II), or both characteristic features (type I/II). Electrostatic interactions between the two different faces drive specific PB1 dimer formation between type I and type II PB1 domains, or multimerization by directional front-to-back association of type I/II PB1 monomers (Lamark et al., 2003; Sumimoto et al., 2007). PB1 domains can also interact with proteins lacking canonical PB1 domains. Theoretically, self-interaction between type I/II is possible but it is not true for all. All available structures solved using X-ray and NMR techniques revealed that different types of PB1 domains adopt similar topology, as Ub-like β grasp fold (Table 3). Experimental and *in silico* studies assisted in understanding the interaction code within the family of mammalian PB1 domain containing proteins (Lamark et al., 2003). Recently available cryo-EM structures of p62 PB1 domain homo-oligomers shows flexible helical filaments (Ciuffa et al., 2015). The assembly state of p62/SQSTM1 is affected by multiple post-translational modifications, including phosphorylation by cAMP-dependent protein kinase at a serine residue on the basic face of its PB1 domain, which disrupts homopolymerization or interaction with OPCA motif containing PB1 domains (Christian et al., 2014).

Table 3: List of currently available PB1 domain structures

Protein name	Organism	PDB ID	Experimental method	Reference
PsIAA4 and AtAUX/IAA17	Plant	2M1M, 2MUK	NMR	(Han et al., 2014; Dinesh et al., 2015)
AtARF5 and AtARF7	Plant	4CHK, 4NJ6	X-ray	(Korasick et al., 2014; Nanao et al., 2014)
p62 and oligomers	Human, Rat	4UF8, 4UF9, 2KTR, 2KKC	Cryo EM, X-ray, NMR	(Saio et al., 2009; Saio et al., 2010; Ciuffa et al., 2015)
PKC zeta and p62	Rat	4MJS	X-ray	(Ren et al., 2014)
ERK5	Human	4IC7	X-ray	(Glatz et al., 2013)
Bem1 and Cdc24p, Bem1p	Yeast	2KFK, 2KFJ, 1IP9, 1IPG	NMR	(Terasawa et al., 2001; Ogura et al., 2009)

MEKK2b, MEKK3 and MEK5	Human	2CU1, 2PPH, 2JRH	NMR	(Hu et al., 2007)
NBR1	Human	2G4S, 2BKF	X-ray	(Muller et al., 2006; Mueller-Dieckmann et al., 2007)
p40phox, p40-p67phox	Human	2DYB, 1OEY	X-ray	(Wilson et al., 2003; Honbou et al., 2007)
atypical PKC ι , atypical PKC-Par6 α	Human	1VD2, 1WMH	NMR, X-ray	(Hirano et al., 2004; Hirano et al., 2005)
CDC24P	Yeast	1TZ1, 1PQS, 1Q1O	NMR	n/a, (Yoshinaga et al., 2003; Leitner et al., 2005)
RSGI RUH-024	Human	1WJ6	NMR	n/a
MAP2K5, MAP2K5 with MAP3K3B and MAP3K2; MAP3K3	Mouse, Human	1WI0, 2O2V, 2NPT, 2C60	NMR, X-ray	n/a

Computational analyses of the evolutionary history of Ub superfamily suggested that plant ARF transcriptional regulators might contain Ub-like domain, which emerged from the ancient PB1 family (Burroughs et al., 2007; Burroughs et al., 2012). Recently solved tertiary structures from AUX/IAA and ARF PB1 domain (type I/II) from plants also showed similar overall fold with additional secondary structural elements (Han et al., 2014; Korasick et al., 2014; Nanao et al., 2014; Dinesh et al., 2015). Additionally, few other plant PB1 domain-containing proteins have been recently studied, which include PAL OF QUIRKY (AtPOQ) (Trehin et al., 2013), homolog of mammalian Neighbor of BRCA1 (AtNBR1) (Svenning et al., 2011), MsPBL from *Medicago sativa* (Kovacs et al., 1998), NtJoka2 from *Nicotiana tabacum* (Zientara-Rytter and Sirko, 2014), and Nodule inception (NIN) from *Lotus japonicus* (Suzuki et al., 2013; Chardin et al., 2014).

1.2.5 AUX/IAA:ARF interaction using the CTD

ARF and AUX/IAA family members interact directly via their similar CTD containing DIII and IV (Kim et al., 1997; Ulmasov et al., 1997b). The importance of this interaction for ARF repression was demonstrated in transfection assays with ARF proteins lacking the C-terminal interaction domain, which results in constitutive, high auxin responses (Krogan et al., 2012b; Guilfoyle, 2015). Heterodimeric interaction between specific AUX/IAA and ARF transcription regulators are responsible for unique biological function (Weijers et al., 2005).

AUX/IAA proteins interact physically with transcription factors of the ARF family (Fig. 9) (Kim et al., 1997; Vernoux et al., 2011) bound to *AuxREs* in many auxin regulated genes (Guilfoyle and Hagen, 2007). AtARF3, 13 and 17 lacks DIII/IV. ARFs can be regulated by different AUX/IAAs depending on its localization (Piya et al., 2014) e.g., AtARF7 is regulated by AtAUX/IAA3 in root and AtAUX/IAA19 in hypocotyls (Tatematsu et al., 2004).

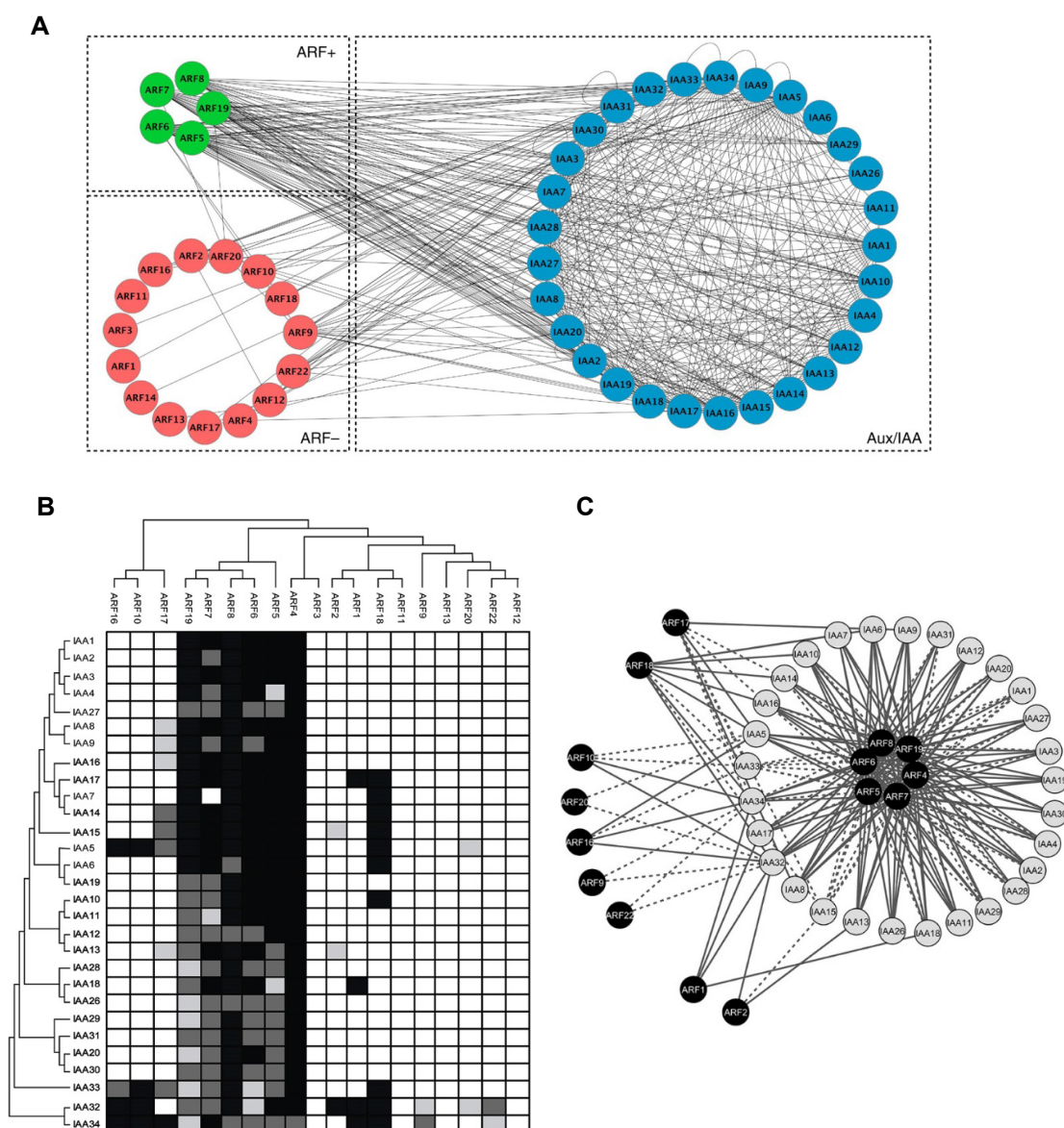


Figure 9: AUX/IAA:ARF interaction and co-expression networks

(A) Visual representation of the AUX/IAA:ARF interactome, adapted from (Vernoux et al., 2011). The proteins are grouped according to their biological identity as indicated. Note the global differences in connectivity of the three biological groups (AUX/IAA, ARF activators: ARF+ and ARF repressors: ARF-) (B) Protein-protein interaction map of *Arabidopsis* ARF and AUX/IAA proteins, adapted from (Piya et al., 2014). Empty boxes indicate no interaction while gray and black boxes indicate the weak and strong interaction, respectively. (C) Gene co-expression network of the interacting ARF-

AUX/IAA proteins, adapted from (Piya et al., 2014). Continuous edges indicate protein pairs with significantly correlated expression profiles in at least one tissue, whereas dotted edges indicate protein pairs without significantly correlated expression profiles.

Several large-scale protein-protein interaction studies have been reported between AUX/IAAs and ARF family proteins (Li et al., 2011c; Vernoux et al., 2011; Piya et al., 2014). Recent studies with full-length proteins by Piya et al., (2014) also showed ARF activators interact with all AUX/IAAs, except AtARF7, which does not interact with AtAUX/IAA7 (Fig. 9). Few AtARF repressors interact preferentially with AtAUX/IAA32 and AtAUX/IAA34 (Piya et al., 2014) and AtARF9 repressor interacts with AtAUX/IAA10 *in vivo* (Rademacher et al., 2012). Additionally, they have reported regions outside DIII/IV are also involved in AUX/IAA:ARF interaction (Shen et al., 2010; Piya et al., 2014). For example, AtARF7 without DIII/IV also interact with AUX/IAAs and truncated AtARF1 with only DIII/IV, that failed to interact with its known interactor AtAUX/IAA17 (Ouellet et al., 2001; Tiwari et al., 2003; Vernoux et al., 2011). ARFs have been also shown to function in absence of DIII/IV (Wang et al., 2013b). Nevertheless, AUX/IAA mediated regulation of ARFs is crucial for auxin response (Krogan et al., 2012b). However, the mechanisms of transcriptional regulation by ARF repressors, and ARF activators, are not well understood.

2 HYPOTHESIS AND OBJECTIVES

Rationale of the study

PsIAA4 is the first AUX/IAA protein to be discovered. Various pioneering studies were performed with PsIAA4 for exploring the nuclear auxin action, showing its high significance (refer section 1.2.4). Therefore, it was selected for detailed structure-function studies in this thesis work. The C-terminal region (domain III/IV) of AUX/IAAs contain a protein-protein interaction domain (Kim et al., 1997). Based on the biochemical and bioinformatics analyses, AUX/IAA domain III was predicted to adopt a $\beta\alpha\alpha$ fold, similar to prokaryotic transcription factors which belong to the Ribbon-Helix-Helix family (Abel et al., 1994; Morgan et al., 1999). If so, AUX/IAA proteins would be the first known eukaryotic members of this family of DNA-binding proteins and regulate auxin-dependent transcription regulation.

Goals

The main aim was to solve the high-resolution 3D solution structure of PsIAA4 DIII/IV and to perform structure-function studies to understand its macromolecular interaction mechanism.

Major objectives

The first step towards the major goal is to recombinantly express PsIAA4 DIII/IV fusion protein in an *E.coli* expression system and to purify it by chromatography techniques. Because of the known aggregating nature and high instability of the AUX/IAA proteins, the buffer conditions have to be optimized for preparing a stable protein sample for biophysical studies. Subsequently, the conformation and molecular state of the protein should be determined using circular dichroism and analytical ultracentrifugation. Finally, the NMR spectroscopic experiments should be performed to solve the high-resolution 3D structure of PsIAA4 DIII/IV. Additionally, *in silico* analyses should be employed to devise the mutants required for abrogating the protein-protein interaction. Systematic alanine scanning mutations are planned to identify the crucial residues involved in the molecular mechanism of interaction by yeast-two-hybrid assays (*in vivo*). NMR based *in vitro* studies will be executed with PsIAA4 DIII/IV variants to further map the interaction interface on the structure.

3 MATERIALS AND METHODS

3.1 MATERIALS

3.1.1 Bacterial and yeast strains

Table 4: Genotype and details of bacterial and yeast strains

Strain	Genotype	Source
<i>E. coli</i> One shot® TOP10	<i>F- mcrA Δ(mrr-hsdRMS-mcrBC) φ80lacZΔM15 ΔlacX74 nupG recA1 araD139 Δ(ara-leu)7697 galE15 galK16 rpsL(Str^R) endA1 λ⁻</i>	Invitrogen, DE
<i>E. coli</i> DH5α	<i>F- endA1 glnV44 thi-1 recA1 relA1 gyrA96 deoR nupG Φ80dlacZΔM15 Δ(lacZYA-argF)U169, hsdR17(rκ⁻ mκ⁺), λ⁻</i>	Promega, USA
<i>E. coli</i> XL1-Blue	<i>endA1 gyrA96(nal^R) thi-1 recA1 relA1 lac glnV44 F'[::Tn10 proAB⁺ lacI^q Δ(lacZ)M15] hsdR17(rκ⁻ mκ⁺)</i>	Stratagene, USA
<i>E. coli</i> XL10-Gold	<i>endA1 glnV44 recA1 thi-1 gyrA96 relA1 lac Hte Δ(mcrA)183 Δ(mcrCB-hsdSMR-mrr)173 tet^R F'[proAB lacI^qZΔM15 Tn10(Tet^R Amy Cm^R)]</i>	Stratagene, USA
<i>E. coli</i> M15 [pREP]	<i>F-, Φ80ΔlacM15, thi, lac-, mtl-, recA+, KmR</i>	Qiagen, DE
<i>S. cerevisiae</i> EGY48	<i>MATa, trp1, his3, ura3, lexAop(x6)-Leu2</i>	(Estojak et al., 1995)
<i>S. cerevisiae</i> YM4271	<i>MATa, ura3-52, his3-200, lys2-801, ade2-101, ade5, trp1-901, leu2-3, 112, tyr1-501, gal4Δ, gal80Δ, ade5::hisG</i>	(Liu et al., 1993)

3.1.2 Bacterial and yeast plasmids

Table 5: List of bacterial and yeast plasmids

Construct	GOI	Features and antibiotic resistance	Source
pQE7-16	PsIAA4 FL and PsIAA4 PB1	C-terminal 6X His-tag, Ampicillin and Kanamycin	(Colon-Carmona et al., 2000)
pQE30	AtAUX/IAA33 FL	N-terminal 6X His-tag, Ampicillin	Qiagen, DE
pDONR221	PsIAA4 FL	Gateway® entry vector, Kanamycin	Invitrogen™
pGlida	PsIAA4 FL	BD-LexA Binding Domain, <i>HIS3</i> , Ampicillin	(Golemis et al., 1996)
pB42AD	PsIAA4 FL	AD-B42 Activation Domain, <i>TRP1</i> , HA epitope tag, Ampicillin	(Gyuris et al., 1993)

3.1.3 Culture media, buffers and solutions

3.1.3.1 Media

Luria Bertani (LB) broth (1 L) (pH 7.5)

Bacto-tryptone 10 g, Yeast extract 5 g, NaCl 10 g, Agar 10 g (optional)

Bacterial glycerol stock: LB medium and 30% (v/v) Glycerol

Double Yeast Tryptone (2YT /dYT) broth (1 L)

2YT (Carl Roth, DE) 31 g dissolved in ddH₂O, or

Bacto-tryptone 16 g, Yeast Extract 10 g, NaCl 5 g

Super Optimal Broth (SOC) medium (1 L)

Tryptone 10 g, Yeast Extract- 2.5 g, 1 M NaCl 5 mL, 1 M KCl 1.2 µL, 1 M MgCl₂ 5mL, 1 M MgSO₄ 5 mL and 1 M Glucose 10 mL

Minimal medium (M9) for isotopic NMR labelling (1 L)

5X M9: Na₂HPO₄·12 H₂O 85 g, KH₂PO₄ 15 g, NaCl 2.5 g, ¹⁵NH₄Cl 5 g

Trace element Solution (TS2): ZnSO₄·7 H₂O 100 mg, MnCl₂·4 H₂O 30 mg, H₃BO₃ 300 mg, CoCl₂·6 H₂O 200 mg, NiCl₂·6 H₂O 20 mg, CuCl₂·2 H₂O 10 mg, Na₂MoO₄·2 H₂O 900 mg, Na₂SeO₃ 20 mg

Vitamin stock: 100X cocktail (BME vitamins, Sigma, DE)

Antibiotics stock: Ampicillin (100 mg/mL), Kanamycin (50 mg/mL)

M9 minimal media (1 L): 5X M9 200 mL, TS2 2 mL, 1 M MgSO₄ 2 mL, 0.1 M CaCl₂ 1 mL, 10 mM Fe(III)-citrate 1 mL, 30% (w/v) Glucose 20 mL (6 g), (¹³C-Glucose 2 g), and ddH₂O 775 mL with BME vitamins 5 mL (1:200) and Ampicillin (50 µg/mL), Kanamycin (50 µg/mL)

All solutions were filter sterilized using syringe filter 0.22 µm (Carl Roth, DE).

Yeast extract-Peptone-Dextrose (YPD) media (1L) (pH 6.5)

Difco peptone 20 g, Yeast extract 10 g, 40% (w/v) Dextrose 50 mL, Agar (optional) 20 g

Synthetically Defined (SD) media (500 mL) (pH 5.8)

SD w/o AA Yeast Nitrogen Base (YNB) 3.35 g, 10X BU salts 50 mL, 40% (w/v) Dextrose (glucose) 25 mL, Agar (optional) 10 g

10X BU salts (pH 7): $\text{NaHPO}_4 \cdot 7\text{H}_2\text{O}$ 70 g, NaH_2PO_4 30 g

X-Gal dissolved in DMF 20 mg/mL

SD restrictive media (SD/-Ura/-His/-Trp): SD media without -U-H-T 0.35 g

SD/Gal/Raf/-Ura/-His/-Trp + X-Gal: SD restrictive media (500 mL), 40% (w/v) Galactose 25 mL, 40% (w/v) Raffinose 12.5 mL, X-Gal 2 mL

3.1.3.2 DNA electrophoresis buffers and solutions

1X TAE DNA running buffer (1 L) (pH 8.0)

Tris base 4.84 g, Acetic acid 1.14 mL, EDTA 0.37 g

6X Orange-G DNA loading buffer (10 mL)

10 mM Tris-HCL, 0.15% (w/v) Orange-G, 60% (v/v) Glycerol, 60 mM EDTA

Non-denaturing DNA-PAGE (60 mL)

10X TAE 6 mL, acrylamide:bisacrylamide (37.5:1, RotiphoreseTM gel 30, Carl Roth, DE) 21 mL, ddH₂O 33 mL, TEMED 90 µL, 10% (v/v) APS 900 µL

3.1.3.3 Protein electrophoresis buffers and solutions

4X SDS- or Tricine-PAGE loading buffer

1 M Tris-HCl 3 mL (pH 6.8), SDS 1.2 g, 10% (w/v) Bromophenol-Blue 600 µL, Glycerol 7.5 mL, 20 % (v/v) β-Mercaptoethanol

10X SDS-PAGE running buffer

250 mM Tris (pH 8.3), 1.92 M Glycine, 1 % (w/v) SDS

Tricine-PAGE running buffer

1X Cathode buffer (pH 8.25): 100 mM Tris, 100 mM Tricine, 0.1% (w/v) SDS

1X Anode buffer (pH 8.9): 100 mM Tris, 22.5 mM HCl

Coomassie staining solution

40% (v/v) Ethanol, 10% (v/v) Acetic acid, 0.1% (w/v) Coomassie Brilliant-Blue R250

Coomassie destaining solution

40% (v/v) Ethanol, 10% (v/v) Acetic acid

Silver Staining solutions (Chevallet et al., 2006)

Fixing solution: 50% (v/v) Ethanol, 10% (v/v) Acetic acid

Rinsing solution: 20% (v/v) Ethanol

Sensitizer*: 0.02% (w/v) Sodium thiosulfate

Silver nitrate solution*: 0.2% (w/v) AgNO_3

Developer solution*: 3% (w/v) Sodium carbonate, 37% (v/v) Formaldehyde,
0.0012% (w/v) Sodium thiosulfate

Stop solution: 4% (w/v) Tris, 2% (v/v) Acetic acid

*freshly prepared

3.1.3.4 Western blotting buffers and solutions**Towbin transfer buffer**

25 mM Tris, 192 mM Glycine, 20% (v/v) Methanol, 1.3 mM SDS

10X PBS buffer (pH 7.4)

1.39 M NaCl, 27 mM KCl, 125 mM $\text{Na}_2\text{HPO}_4 \cdot 2\text{H}_2\text{O}$, 18 mM KH_2PO_4

10X TBS buffer (pH 7.8)

500 mM Tris-HCl, 1.5 M NaCl, 10 mM $\text{MgCl}_2 \cdot 6\text{H}_2\text{O}$

For PBS-T and TBS-T buffers add 0.5% (v/v) Tween-20

Blocking Solution

3-5% (w/v) Milk powder in 1X TBS-T

3.1.3.5 Protein purification buffers**Lyse buffers**

Lyse buffer A (pH 8): 50 mM NaH_2PO_4 , 300 mM NaCl, 2 mM MgCl_2 , 20 mM Imidazole

Lyse buffer B (pH 7 and pH 8): 50 mM HEPES-NaOH, 300 mM NaCl, 20 mM Imidazole

Elution buffer

Elution buffer A (pH 8): 50 mM NaH_2PO_4 , 300 mM NaCl, 2 mM MgCl_2 , 500 mM Imidazole

Elution buffer B (pH 7 and pH8): 50 mM HEPES-NaOH, 300 mM NaCl, 500 mM Imidazole

Gel filtration buffers (pH 8)

50 mM NaH_2PO_4 , 300 mM NaCl and 0.01% (w/v) Sodium azide

Dialysis buffers

Acidic buffer (pH 2.5): 50 mM NaH₂PO₄, 2 mM MgCl₂, 5 mM DTT, 1 mM NaN₃

Citrate buffer (pH 6.25): 50 mM Tri-sodium citrate, 150 mM NaCl₂, 2 mM MgCl₂, 3 mM TCEP

pH scanning buffers

pH 2 : 50 mM Glycine, 500 mM NaCl, 2 mM EDTA, 3 mM TCEP

pH 6.25: 50 mM Tri-sodium citrate, 500 mM NaCl, 2 mM EDTA, 3 mM TCEP

All buffers used for purification were filtered using Steritop™ GP Sterilization Bottle Top Vacuum Filter Unit (Millipore, DE) with 0.22 µm PES (Polyethersulfone) membrane and degassed before using a vacuum pump.

3.1.3.6 Yeast transformation buffers and solutions

10X Lithium acetate (LiAc) solution (pH 7.5): 1 M LiAc

10X TE buffer (pH 8.0): 100 mM Tris-HCl, 10 mM EDTA.

Polyethylene glycol PEG/LiAc solution (10 mL): 50% (w/v) PEG 4000 8 mL, 10X TE buffer 1 mL, 10X LiAc 1 mL

Yeast lysis buffer: 60 mM Tris HCl (pH 6.8), 10% (v/v) Glycerol, 2% (w/v) SDS, 5% (v/v) β-Mercaptoethanol, 0.025% (w/v) Bromophenol Blue, PMSF (1/100), 1mM Benzamidine, Roche cOmplete™ protease inhibitor Cocktail tablet.

3.1.4 FPLC column materials

TALON Superflow™ resin	(Clontech, USA)
TALON HiTrap-TALON® crude (Prepacked 5 mL)	(GE-Healthcare, DE)
Ni-NTA Protino® agarose resin	(Macherey-Nagel, DE)
Protino® Ni-NTA Columns (Prepacked 5 mL)	(Macherey-Nagel, DE)
Gel filtration: HiLoad 16/60 Superdex 200 PG	(GE-Healthcare, DE)

3.1.5 DNA and protein markers

O'Range™ Ruler 100bp DNA ladder, 100-1500 bp	(Thermo Scientific, DE)
1 kb GeneRuler™ DNA ladder, 250-10,000 bp	(Thermo Scientific, DE)
PageRuler™ prestained protein ladder, 10-180 kDa	(Thermo Scientific, DE)
Mark12™ unstained standard, 2.5-200 kDa	(Invitrogen, DE)

3.1.6 Enzymes

Taq polymerases	5 U/ μ L	(New England Biolabs, DE)
DreamTaq™ polymerase	5 U/ μ L	(Thermo Scientific, DE)
Pfu Ultra High-Fidelity polymerase	2.5 U/ μ L	(Stratagene, USA)
AccuPrime™ Pfx DNA polymerase	2.5 U/ μ L	(Life Technologies, DE)
FastDigest™ RE	1 U/ μ L	(Thermo Scientific, DE)
T4 DNA ligase	5 U/ μ L	(Thermo Scientific, DE)
DpnI	10 U/ μ L	(Stratagene, USA)
DNase I	1 U/ μ L	(Sigma-Aldrich, DE)
Lysozyme		(Sigma-Aldrich, DE)

3.1.7 Miscellaneous

DreamTaq™ Green PCR Master Mix (2X)	(Life Technologies, DE)
Protease Inhibitor Cocktail- P2714	(Sigma-Aldrich, DE)

3.1.8 Molecular biology kits

QIAGEN Plasmid mini/maxi prep	(Qiagen, DE)
QIAquick™ PCR purification	(Qiagen, DE)
QIAquick™ Gel extraction	(Qiagen, DE)
Dialysis membranes and cassettes	(Spectrum, USA)
QuikChange™ II Site- Directed Mutagenesis	(Agilent, USA)
ECL western blotting substrate- SuperSignal West Pico	(Life Technologies, DE)
Gateway® LR Clonase II Enzyme mix	(Life Technologies, DE)
Gateway® BP Clonase II Enzyme mix	(Life Technologies, DE)

3.1.9 Instruments

Table 6: List of instruments

Instrument name - model	Manufacturer
ÄKTA - Explorer, Purifier, FPLC and Pure	GE-Healthcare, DE
Autoclave - DX-200 VX-95	Systec, DE
Analytical Ultracentrifuge - Beckman XL-A	Beckman Coulter, USA
BioPhotometer™ Plus	Eppendorf, DE
CD Spectrometer - J-815	Jasco, DE
Centrifuge - bench-top, Avanti J-26 XP/J-301, Sorvall RC5B plus	Eppendorf, Beckman Coulter, Thermo Scientific, DE
DNA gel chamber	Biotech Fischer, DE
DNA Gel Doc - Bioimaging System	Syngene Gene Genius, DE
French Press - EmulsiFlex 05	Avestin, USA
Gel rocker - Duomax 2030	Heidolph, DE
Incubator shaker - Innova 43/40, Unitron	New Brunswicks, Infors, DE
Isothermal titration calorimeter - MicroCal™ iTC200	Malvern, DE
NanoQuant™ Photometer - Infinite M200, M1000	Tecan, DE
NMR Spectrometer - Avance III 600 MHz, 800 MHz	Bruker, DE
pH meter	inoLab, DE
Peristaltic Pump P1	Pharmacia/GE, DE
Protein gel imager - FluorChem® Q	AlphaInnotech, DE
Protein gel electrophoresis chamber - Protean™ Mini	Bio-Rad, DE
Rotator - Mixer	Starlab, DE
Semi-dry blotters - Trans Blot® SD	Bio-Rad, DE
Sonicator - Sonopuls, W-250D Power sonic 450	Bandelin, Branson, DE
Thermomixer/Heat block	Eppendorf, DE
Thermal cycler - PCR Veriti™, Mastercycler Gradient	Applied Biosystem, Eppendorf, DE
Ultrapure water system	Millipore, TKA, DE
UV/VIS spec- V-650, Biophotometer Plus	Jasco, Eppendorf, DE
Vacuum pump	Vacuubrand, DE

3.1.10 Computational software and servers

Table 7: List of software and servers

Name	Source/links	Purpose
ApE	http://biologylabs.utah.edu/jorgensen/wayned/ape/	A Plasmid Editor
CloneManager9	http://www.scied.com/pr_cmpro.htm	Cloning, sequence analysis
CLUSTAL, MAFFT	http://www.clustal.org/ http://mafft.cbrc.jp/alignment/server/	MSA
CorelDraw	www.coreldraw.com/	Image processing
EMBOSS	http://www.ebi.ac.uk/Tools/psa/emboss_needle/	Pairwise alignment
ENDscript	http://esript.ibcp.fr/ESPript/ENDscript/	Structure analysis
GeneDoc 2.7	http://genedoc.software.informer.com/2.7/	MSA editing
GraFit 5	http://www.erithacus.com/grafit/	Data analysis, plotting
HADDOCK	http://haddock.science.uu.nl/services/HADDOCK/	Protein-protein docking
Jalview	http://www.jalview.org/	MSA analyses
NMRpipe	http://spin.niddk.nih.gov/NMRPipe/	NMR data processing and analyses
NMRview	http://www.onemoonscientific.com/	NMR data analysis
Origin7 (ITC)	http://origin.en.softonic.com/	Data analysis
OligoPerfect	http://tools.lifetechnologies.com/	Primer designing
PDBsum Generate	https://www.ebi.ac.uk/thornton-srv/databases/pdbsum/Generate.html	Protein structural analysis
Phyre2 server	http://www.sbg.bio.ic.ac.uk/phyre2/	Protein threading
ProtParam	http://web.expasy.org/protparam/	pI calculate
PyMOL	https://www.pymol.org/	Structure analysis
Primer Design	www.genomics.agilent.com/primerDesignProgram.jsp	SDM primers
QuteMol	http://qutemol.sourceforge.net/	Visualize complexes
Random coil chemical shift	http://spin.niddk.nih.gov/bax/nmrserver/Poulsen_rc_CS/	Chemical shift values calculation
Sigmaplot 10	http://www.sigmaplot.com/products/sigmaplot/	Scientific graphs
SnapGene	http://www.snapgene.com/	Plasmid maps
Spectra Manager	http://www.jascoinc.com/spectroscopy/spectroscopy-software	UV and CD spectral analysis
TALOS	http://spin.niddk.nih.gov/bax/software/TALOS/	Torsion angles prediction
TM align	http://zhanglab.cmb.med.umich.edu/TM-align/	Superimpose proteins
TOPSPIN2.3	https://www.bruker.com/products/mr/nmr/	NMR recording

3.2 METHODS

3.2.1 Molecular biological techniques

3.2.1.1 Plasmid isolation

Plasmids were isolated from 5 mL of o/n bacterial culture using the QIAprep™ Spin Mini or QIAGEN Midiprep kit, according to the manufacturer's instructions. Final plasmid DNA was eluted using 30-50 µL of 1X TE buffer or ddH₂O.

3.2.1.2 Agarose gel electrophoresis

DNA agarose gel (1-3% w/v) was prepared with 1X TAE buffer for separating plasmid DNA, RE digested fragments or PCR product. 0.8 µL of Stain G (DNA Stain G, SERVA, DE) was added to 50 mL of melted agarose before casting to stain nucleic acids. 20-50 µL of DNA samples were prepared in 1X Orange-G DNA loading buffer and loaded onto the gel. Electrophoresis was performed in a horizontal electrophoresis chamber at 100 V for ~1 h. Subsequently, DNA was visualized under an UV transilluminator. The desired DNA marker was used which allowed analysis of the resolved fragments.

3.2.1.3 Quantification of nucleic acids

Plasmid DNA was quantified using NanoQuant™ (TECAN, Infinite M200) with Quad-4 monochromators which can detect DNA concentration as low as 1 ng/µL. 2 µL of control TE buffer/ddH₂O and samples were spotted on NanoQuant Plate™ (quartz) and the absorbance were measured at 260 nm and 280 nm wavelength. Final quantification results were listed in ng/µL, along with the purity factor (~1.8).

3.2.1.4 Polymerase chain reaction

In vitro DNA amplification was done in thermocycler by using gene specific primers. Amplified fragments were analyzed using DNA gel electrophoresis. PCR products were purified and used for traditional and Gateway® cloning. Following protocol was used to set-up a reaction in thermocycler.

PCR reaction (25 µL)

2X Master Mix Green DreamTaq™ 12.5 µL

Forward and reverse primers 1 µL + 1 µL (0.1-1 µM)

Template	1 μ L (10 pg-1 μ g)
ddH ₂ O	up to 25 μ L

PCR set-up condition

Initial Denaturation	95°C; 1-5 min	} 30 cycles
Denaturation	95°C; 1 min	
Annealing	T _m * -5°C, 1 min	
Extension	72°C; 1 min**	
Final extension	72°C; 7 min	

* the annealing temperature was always set 5°C below the calculated melting temperature (T_m) of oligonucleotide primers.

** extension time was calculated depending on the size of the fragment to be amplified and the polymerization rate of the polymerase used (DreamTaq™ polymerase, 1 min/kb, and Pfu polymerases, 2 min/kb).

After cloning, the presence of the GOI was analyzed by colony PCR using a similar set-up, with 5 min of initial denaturation step.

3.2.1.5 Site-directed mutagenesis

SDM was performed to generate mutations by exchanging single or multiple nucleotides at the particular site in the GOI, for functional studies. Template plasmid DNA (50-100 ng/ μ L) was mixed with designed SDM primers (Table 8) and PCR reaction was set-up with the following conditions as below, according to QuikChange™ II Site-Directed Mutagenesis Kit protocol or modified using Pfu ultra HF or Pfx.

SDM-PCR reaction (50 μ L)

10X Buffer	5 μ L
dNTPs	1 μ L
Forward and reverse primers	1 μ L + 1 μ L
Quik™ solution	3 μ L
ddH ₂ O	30 μ L
Template pDNA	1 μ L (~50 ng)
DNA polymerase	0.4-1 μ L
Pfu HF Ultra or Turbo (1 μ L) or AccuPrime Pfx (0.4 μ L)	

SDM-PCR condition

Initial denaturation	95°C; 1 min	
Denaturation	95°C; 50 sec	} 16-18 cycles
Annealing	T _m * -5°C; 50 sec	
Extension	68°C; ** min	
Final extension	72°C; 7 min	

DpnI digestion for 1 h at 37°C or o/n

* annealing temperature was always set at 5°C below the calculated melting temperature (T_m) of oligonucleotide primers.

** time varies based on vector size and enzyme, Pfu Ultra HF or Pfx DNA Pol, 2 min/kb

After final DpnI digestion, PCR product (2-10 µL) was transformed into ultra-competent *E. coli* One shot® TOP10 or XL10-Gold® cells and selected colonies were screened and confirmed by plasmid isolation and subsequent DNA sequencing, respectively.

Table 8: List of oligonucleotides used for SDM of the PsIAA4

K96A	FWD REV	WT	GGTGGGATCTTTGTG <u>G</u> CAGTGAGCATGGATGGTG CACCATCCATGCTCACT <u>TG</u> CCACAAAGATCCCACC
R106A or BM2	FWD REV	WT or K96A	GGATGGTGCCCCCTTACCTT <u>G</u> CAAAGATTGACTTAAGGGTC GACCCCTAAGTCAATCTTT <u>G</u> CAAGGTAAGGGGCACCATCC
BM3	FWD REV	BM2	TGGTGCCCCCTTACCTT <u>G</u> CAGCGATTGACTTAAGGGTCTAT ATAGACCCTTAAGTCAATC <u>G</u> CTGCAAGGTAAGGGGCACCA
D151A	FWD REV	WT	GCACCAACTTATGAAG <u>C</u> CAAGGATGGTGATTGG CCAATCACCATCCTT <u>G</u> GCTTCATAAGTTGGTGC
D153A	FWD REV	WT	CAACTTATGAAGACAAG <u>G</u> CTGGTGATTGGATGTTAGTTG CAACTAACATCCAATCACC <u>A</u> GCCTTGTCTTCATAAGTTG
AM2	FWD REV	D151A	CCAACTTATGAAGCCAAG <u>G</u> CTGGTGATTGGATGTTAGTT AACTAACATCCAATCACC <u>A</u> GCCTTGGCTTCATAAGTTGG
AM3	FWD REV	AM2	TGAAGCCAAGGCTGGT <u>G</u> CTTGGATGTTAGTTGGAG CTCCAACATAACATCCA <u>A</u> GCACCAAGCCTTGGCTTCA
D100N	FWD REV	WT	TTGTGAAAGTGAGCATGA <u>A</u> TGGTGCCCCCTTACCTT AAGGTAAGGGGCACC <u>A</u> TTTCATGCTCACTTTCACAA

The above listed primers were used for SDM to generate mutated PsIAA4 PB1 variants for *in vitro* protein-protein interaction studies and PsIAA4 FL mutants for Y2H analyses.

3.2.1.6 Gateway® directional TOPO cloning

Gateway® BP Reaction

The PsIAA4 FL coding sequence (Kim et al., 1997) was amplified by using Gateway®-cloning compatible primers with *attB1* and *attB2* site (underlined) in forward and reverse primers, respectively. Recombination of purified PCR products into pDONR221 entry vector were performed using the BP Clonase II enzyme mix, according to the manufacturer's instructions.

Table 9: Oligonucleotides used for Gateway® cloning

FW	<u>GGGGACAAGTTTGTACAAAAAAGCAGGCT</u> TCATGGAATTCAAGGCAACTGAGCTTA
RV	<u>GGGGACCACTTTGTACAAGAAAGCTGGGT</u> CTCATAACCCACAACCCAATCCTTTA

Gateway® LR Reaction

pDONR221 Gateway® entry clones with GOI were mobilized into Gateway® destination vectors. pGlida and pB42AD vectors were used to generate DBD and AD fusions respectively, using Gateway® LR Clonase II Enzyme mix, according to the manufacturer's instructions.

3.2.1.7 Chemically competent cells preparation

Chemically competent cells were prepared using CaCl₂. LB broth (200-500 mL) was inoculated with 5 mL of o/n culture of required bacterial strain and incubated at 37°C until the OD₆₀₀ reaches 0.4-0.7. Cells were collected by centrifugation for 15 min at 5000 rpm (4°C), and were resuspended in 50 mL of sterile 0.1 M CaCl₂ ice-cold solution and incubated for 90-120 min on ice. Cells were collected by centrifugation, resuspended in 2 mL of 0.1 M CaCl₂, and incubated for another 90-120 min on ice. 10% (v/v) glycerol was added to the cell suspension. The competent cells were then frozen using liquid N₂ and stored in 100 µL aliquots at -80°C.

3.2.1.8 Bacterial heat-shock transformation

Bacterial transformation was done by adding 5 μ L of plasmid or 1-5 μ L of the ligation reaction to 50-100 μ L chemically competent *E. coli* TOP10, XL1-Blue, XL10-Gold, DH5 α or M15[pREP] cells and incubated on ice for 10 min, followed by heat shock at 42°C for 45 sec without shaking and immediately placed on ice for 2 min. Subsequently, cells were incubated with 200 μ L of SOC media at 37°C and 150 rpm for 1 h. Finally, 200 μ L of the cells were spread plated on LB agar containing selective antibiotics and incubated o/n at 37°C.

3.2.1.9 DNA sequencing

Plasmid DNA samples were adjusted to 50-100 ng/ μ L for sequencing at Eurofins MWG, DE. Sequencing was carried out using universal/customized primers. The results were evaluated using ApE or SnapGene or Clone Manager software, to check the fidelity of an insert or presence of desired mutations (SDM).

3.2.1.10 Recombinant protein expression and optimization

The pQE vector supporting the expression of C-terminal 6X His-tagged PsIAA4 DIII/IV (AA residues 86–189, 12.5 kDa) was described and mobilized into *E. coli* strain M15[pREP] (Qiagen) (Colon-Carmona et al., 2000). Transformed *E. coli* M15 expression strain was initially screened for protein expression in 5 mL cultures and analyzed using PAGE gel electrophoresis. For unlabeled protein preparations, respective bacterial expression constructs containing POI were grown o/n in 25-50 mL 2YT medium with selective antibiotics (50 μ g/mL Ampicillin and 25 μ g/mL Kanamycin), according to the batch size. Large batches of protein over-expression were performed in baffled Erlenmeyer conical flasks (LY98.1, 2000 mL capacity) (Rotilabo, Carl Roth, DE) by seeding o/n bacterial culture with an initial OD (A_{600}) \sim 0.05. Cells were induced for protein over-expression at OD₆₀₀ \sim 0.8-1.0 with 1 mM IPTG and incubated for 4-8 h at 37°C or low temperature expression o/n at 18-20°C. Similarly, uniformly single (¹⁵N) or double (¹³C, ¹⁵N) labeled proteins were prepared by culturing bacterial cells in M9-minimal medium supplemented with 1 g/L ¹⁵NH₄Cl or 1 g/L ¹⁵NH₄Cl and 2 g/L [¹³C] glucose as a sole source of nitrogen and carbon (Cambridge Isotope Laboratories, USA), respectively. Pre-culture (200 mL) was prepared with selected bacterial cells. Large batch M9 media was initially seeded with OD₆₀₀ \sim 0.5 and was induced and expressed similar to unlabeled protein over-expression protocol. Additional unlabeled glucose

was added after IPTG induction to boost the bacterial growth during expression of single labeled sample.

3.2.1.11 Protein purification

After protein expression, the bacterial cells were harvested from liquid (2-6 L) culture by centrifugation at 8000 rpm, 4°C for 15-20 min. Collected pellet was resuspended in respective ice-cold lyse buffer A or B (~50 mL), each supplemented with 500 µL PIC and 1 mg/mL lysozyme. Non-denaturing or native protein purification protocol was used to purify recombinantly over-expressed labeled/unlabeled, WT or variant of PsIAA4 DIII/IV by FPLC using IMAC columns. After incubating resuspended pelleted cells in lyse buffer supplemented with PIC and lysozyme for 1-2 h, cell lysis was performed either by 2-5 passes through a French pressure cell or by sonication at 80% amplitude on ice for 10-15 min. Lysed cells were incubated for 1-2 h with 20 µL DNase I (2 mg/mL). The cell lysate was centrifuged at high speed, $20,000 \times g$ for 30 min at 4°C to remove unwanted bacterial cell components. Prepared lysate were retreated with DNase I incase of high viscosity and centrifuged to remove residual DNA. The supernatant (~50 mL) were loaded onto manually packed or prepacked 5 mL Co^{2+} -TALON column using peristaltic (P1) pump. Column loaded with sample was connected to FPLC instrument and was washed with 2-3 CV of lyse buffer (20 mM Imidazole), followed by an extensive wash step with 10 CV of lyse buffer containing 50-100 mM Imidazole, for removing residual impurities. All steps were monitored at A_{280} with 0.5 mL/min flow rate. Proteins were eluted with elution buffer A or B containing 500 mM Imidazole. Eluted samples were automatically fractionated using fraction collector FRA-950 or F9-C at 4°C. Second-step purification by gel filtration was precluded because of on-column protein aggregation. The purity of the sample was verified by SDS- or Tricine-PAGE and concentration was measured by UV spectroscopy. Protein preparation after optimization of one-step IMAC purification was readily used for all experiments after dialysis. Small batch screening purifications were done using Ni^{2+} -NTA agarose resins and gravity flow columns (Bio-Rad, DE) which were incubated on a rotator-mixer followed by sample elution.

3.2.1.12 Dialysis

Dialysis was the final step in protein purification that allow buffer exchange and removal of impurities. Dialysis tubing (MWCO 500-3000 Da) Spectro/Por (Spectrum, USA) or Slide-A-

Lyzer™ (Thermo Scientific, DE) was prepared by washing with dialysis buffer. Protein sample was loaded in Spectro/Por dialysis bags and clipped or injected in Slide-A-Lyzer™ cassette according to the manufacturer's instructions. Dialysis tubing or cassette containing the sample was transferred to container with 0.5-1 L of respective dialysis buffer and dialyzed at 4°C with gentle stirring. The buffer was replaced every 2-4 h for increasing its efficiency and left o/n. Purified WT PsIAA4 DIII/IV formed homo-oligomers precluding NMR analysis. Therefore, eluted WT PsIAA4 protein samples were dialyzed against acidic buffer (pH 2.5), which prevented protein aggregation, and were later used for AUC and NMR experiments. PsIAA4 DIII/IV variants were dialyzed against citrate buffer for protein sample preparation for AUC, ITC and NMR titration. Final protein samples were analyzed using SDS- or Tricine-PAGE and quantified using a UV spectrophotometer. Samples were concentrated using AMICON Ultra-15 (Millipore, DE), and Vivaspin (Sartorius, FR) with MWCO 3K or 10K concentrators.

3.2.1.13 Polyacrylamide gel electrophoresis

Protein samples were separated in presence of SDS and resolved based on their molecular size during 10% SDS- (Laemmli) or Tricine-PAGE (Schägger and von Jagow) (Schägger, 2006). Protein samples were prepared with 1X SDS- or Tricine-PAGE loading dye supplemented with β -mercaptoethanol and denatured by heating at 95°C, before loading to the gel.

10 % (v/v) Laemmli or Tris-glycine SDS-PAGE (4 gel)

Resolving gel: ddH₂O 8.26 mL, 30% (v/v) acrylamide/bisacrylamide 6.6 mL, 1.5 M Tris-HCl buffer containing 0.4% (w/v) SDS (pH 8.8) 5.0 mL, 10% (w/v) APS 120 μ L, TEMED 13 μ L
Stacking gel: ddH₂O 6 mL, 30% (v/v) acrylamide/bisacrylamide 1.4 mL, 1.5 M Tris-HCl buffer containing 0.4% (w/v) SDS (pH 6.8) 1.25 mL, 10% (v/v) APS 25 μ L, TEMED 20 μ L

10% (v/v) Tricine-SDS-PAGE gel (Schägger, 2006)

Acrylamide-Bisacrylamide (AB-3) stock (100 mL): acrylamide 48 g, bisacrylamide 1.5 g

3X gel buffer (pH 8.45): 3 M Tris, 1 M HCl, 0.3% (w/v) SDS

Resolving gel: AB-3 6 mL, 3X gel buffer 10 mL, glycerol 3 g, 10% (w/v) APS 150 μ L, TEMED 15 μ L

Stacking gel: AB-3 1 mL, 3X gel buffer 3 mL, 10% (w/v) APS 90 μ L, TEMED 9 μ L

Tricine-SDS-PAGE gels are commonly used for resolving small proteins with molecular weight ~10 kDa or less. Electrophoretic separation was performed at initial 100V for 15 min and later 250V for 30-50 min for better separation. Separated proteins after SDS- or tricine-PAGE were stained using either Coomassie Brilliant Blue or silver nitrate staining and destained. Gels were imaged and analyzed using pre-stained protein marker. Protein samples with low concentration were stained using silver nitrate for efficient detection or semi-dry blotted and detected using tag-specific antibodies. Final protein gel or blot was visualized and imaged using gel imager.

3.2.1.14 Protein PAGE gel staining

Protein gels were usually stained using either Coomassie Brilliant Blue or silver staining protocols. Both SDS- and Tricine-PAGE gels can be stained using these methods.

Coomassie Brilliant Blue staining

Protein gels were washed in ddH₂O and transferred to a box containing Coomassie staining solutions and incubated for 1-2 h. Stained gels were washed twice in ddH₂O for 10 min each, and transferred to a box containing destaining solution and destained. Resolved protein gels were imaged.

Silver nitrate staining (Chevallet et al., 2006)

Initially proteins were fixed on SDS- or Tricine-PAGE by incubating in fixing solution for 1 h or o/n, followed by ddH₂O washes at least twice. Fixing solution was replaced with sensitizer and incubated for 45 min, followed by rinse solution and ddH₂O, at least two times. Finally, gels were impregnate in silver nitrate solution for 1 h, transferred to ddH₂O for 10 sec, immediately transferred to a box with the developer and was incubated on rocker (mild shaking) for 2-10 min. Staining can be stopped by transferring into a box containing stopper solution for at least 30 min followed by ddH₂O washes at least twice. Silver stained gels are stable and can be stored in ddH₂O for several months at RT. During incubation periods, protein gels were placed on a gel rocker (Duomax 2030, Heidolph, DE) at RT.

3.2.1.15 Western Blotting

Electrophoretically separated proteins were transferred onto nitrocellulose membrane with pore diameter 0.45 µm (Sartorius, DE) using a TransBlot® semi-dry blotter for 60 to 90 min

at 20V in Towbin transfer buffer, according to the manufacturer's instructions. The western blot technique was used to analyze expression of PsIAA4 fusion proteins from crude total protein extracts prepared from diploid yeast cells, which were used for Y2H analyses.

3.2.1.16 Immunostaining

Immobilized blotted proteins were immunostained with respective antibodies that can bind to their corresponding tag in fusion proteins. The blotted membrane was incubated for 30 min in blocking solution. Post blocking, the membrane was incubated with primary antibodies diluted in fresh blocking solution at 4°C o/n on a gel rocker. The membrane was washed thrice with TBS-T (5 min) and followed by TBS wash (10 min). Blots were then transferred to a box containing freshly prepared corresponding secondary antibodies and incubated for 2 h at RT followed by washing with TBS-T as before. Finally, chemiluminescent substrate from SuperSignal™ West Pico Chemiluminescent Kit was uniformly spread on the surface of the membrane and after few min of incubation, immunostained protein bands were detected using the gel imager.

Table 10: List of primary and secondary antibodies

Fusion Tag	Primary antibodies (1:1000)	Secondary antibodies (1:10,000)	Purpose	Source
HA-tag	Anti-HA, #sc-7392	HRP-conjugated anti-mouse, #31430	Detection of AD-hybrids	Santa Cruz Biotechnology, Thermo Scientific, DE
LexA	Anti-LexA, #ab14553	HRP-conjugated anti-rabbit, #sc-2004	Detection of DBD-hybrids	Abcam, UK and Santa Cruz Biotechnology, DE
His-tag	Anti-His, #sc-803	HRP-conjugated anti-rabbit, #sc-2004	Detection of 6X His-tag	Santa Cruz Biotechnology, DE

3.2.1.17 Quantification of proteins

Purified protein samples were quantified and concentrated to the required concentration before performing any biochemical or biophysical studies. Accurate protein concentration of samples were determined by measuring Tyr and Trp absorption at 280 nm using a UV

spectrometer with 1 cm quartz cuvette (Hellma, DE) and concentration was calculated by Beer-Lambert law (Hammes, 2007) using theoretical extinction coefficients of the WT and PsIAA4 variants with ExPASy ProtParam tool (refer Appendices 7.4 and 7.7) (Gill and von Hippel, 1989).

$$A = \epsilon cl$$

$$c = (A_{280} \times \text{dilution factor}) / (\epsilon \times l) \text{ M}$$

A - Absorbance, ϵ - Extinction co-efficient, c - concentration and l - path length (1 cm)

Protein concentration in mg/mL can be obtained by multiplying by its molecular weight (kDa). PsIAA4 PB1; Molecular weight: 12.5 kDa, extinction co-efficient: 21,430 M⁻¹ cm⁻¹

3.2.2 Biophysical Techniques

3.2.2.1 Circular Dichroism spectroscopy

Far-UV CD spectroscopy measures differences in the absorption of left- vs right-handed circular polarized light, which arise due to structural asymmetry. This method is widely used to analyze the protein conformation and predict secondary structures in solution. Experiments were carried out on a CD spectrometer (JASCO, DE) equipped with a Peltier element PTC-423S/15. CD spectrum (190-260 nm) was recorded at 20-25°C with the protein concentration of 10-50 μ M in desired buffer using a 1 mm path length quartz cuvette with the following parameters (Yang et al., 1986) 100 nm/min scanning rate, 1 sec response time, 0.2 nm data pitch, 1 nm band width, 30 accumulations using continuous scanning mode.

3.2.2.2 Analytical ultracentrifugation

Purified protein preparations (30-200 μ M) were measured by the Beckman XL-A centrifuge with An50Ti rotor, and double sector cells. Sedimentation equilibria were monitored at 14,000 rpm and 20°C (A_{280}). Sedimentation velocities were analyzed by taking scans in every 10 min at 40,000 rpm and 20°C (A_{230} or A_{280}). WT PsIAA4 DIII/IV protein was analyzed at different pH (2.5-7.0), and salt concentrations (0.2-2.0 M NaCl). PsIAA4 truncated variant (pH 6.25) and AtAUX/IAA33 FL (pH 8.0) were analyzed for its molecular state in solution. Data analysis was conducted by using the Sedfit software (Schuck, 2000). All experiments

were performed in cooperation with the Institute for Biochemistry and Biotechnology, Martin Luther University Halle-Wittenberg, DE.

3.2.2.3 Isothermal Titration Calorimetry

Protein-protein interaction studies were performed on MicroCal™ iTC200 micro calorimeter. Both mutant proteins, PsIAA4 PB1^{BM3} (pI 5.55) and PB1^{AM3} (pI 7.05) were dialyzed for 8–12 h against citrate buffer system (pH 6.25). Prepared samples were loaded in the syringe and in the cell (1:10) before titration. Experimental conditions were designed and setup-using software provided with the instrument. The syringe was inserted into the cell manually and the titration was started. After thermal equilibrium at 25°C, initially 0.4 µL of the PsIAA4 PB1^{BM3} (960 µM) was injected. Subsequently 20 injections with 2 µL of the titrant (PsIAA4 PB1^{BM3}) was added to the sample cell (200 µL) containing titrand PsIAA4 PB1^{AM3} (96 µM) at an interval of 150 or 240 s with continuous stirring (1000 rpm) to achieve a final binding isotherm. Similar titration was performed with PsIAA4 PB1^{AM3} as titrant and PsIAA4 PB1^{BM3} as titrand. The heat associated with each titration peak was integrated and plotted against the respective molar ratio of two mutant proteins. The titrant's heat of dilution was calculated using the last few injections after saturation and subtracted to obtain effective heat of binding. ΔG , ΔH , ΔS and $T\Delta S$ values are connected by

$$\Delta G = -RT\ln(K_{eq}) \text{ and } \Delta G = \Delta H - T\Delta S$$

$R = 8.314 \text{ J mol}^{-1} \text{ K}^{-1}$ and T is the temperature on the Kelvin scale.

Data were analyzed by a nonlinear least-squares curve fitting using the standard one-binding site model supplied with ITC-Origin software. The equilibrium dissociation constant (K_D) to quantify affinity is the reciprocal of the equilibrium constant (K_{eq}).

3.2.2.4 NMR spectroscopy

NMR spectroscopy is one of the major experiment for protein structure determination. It is also well suited for studying in solution macromolecule interactions. The isotopically labeled, NMR active samples were prepared and analyzed. The data recorded was used for sequential backbone assignment and three dimensional structure calculations.

Pipeline for NMR based structure calculation of the wild-type PsIAA4 DIII/IV

- (i) **NMR sample preparation**
- (ii) **NMR data acquisition and processing**
- (iii) **NMR data analysis generating restraints**
 - Sequential backbone assignment
 - Side-chain assignment
 - Structural restraints generation
- (iv) **Structure calculation and refinement**
- (v) **Structure validation and**
- (vi) **Deposition of final structure ensemble and NMR restraints**

(i) NMR sample preparation, data acquisition and processing

From the pH scanning experiments (pH 2-4), purified single or double-labeled protein sample (1-1.5 mM) was prepared in NMR compatible buffer at pH 2.5. 450 μ L WT PsIAA4 DIII/IV concentrated protein sample was transferred to a 5 mm NMR tubes (New Era, USA) with 50 μ L D₂O before every measurement. Suites of 2D and 3D NMR spectra were recorded using Bruker Avance III 600 MHz (14.1 Tesla) with QXI probe or 800 MHz (18.59 tesla) spectrometers with Cryogenic TCI probe at 25°C and the raw data was visualized using Bruker TopSpin NMR software.

List of 2D and 3D NMR experiments used for structure calculation:

2D ¹H-¹⁵N-HSQC, 2D ¹H-¹³C-HSQC aliphatic, 2D ¹H-¹³C-HSQC aromatic, 2D ¹H-¹H-NOESY, 3D HNCA, 3D HNCACB, 3D HN(CO)CACB, 3D ¹H-¹⁵N-NOESY, 3D ¹H-¹³C-NOESY aliphatic, 3D ¹H-¹³C-NOESY aromatic, 3D HNCO, 3D HCCH-TOCSY

Two batches of purified samples with identical buffer conditions were used to perform all the required experiments. 2D projection spectra obtained from 3D NOESY data was identical for both the batches of protein samples. Each 3D NMR experiment was performed with initial 2D HSQC spectrum to confirm sample stability. Finally obtained NMR spectra were processed and analyzed using the NMRPipe (Delaglio et al., 1995) and NMRView software. All NMR data acquisition was carried out in cooperation with the Institute for Physics/Biophysics, Martin Luther University Halle-Wittenberg, DE.

(ii) NMR dynamics experiments

The backbone $^1\text{H}\{-^{15}\text{N}\}$ heteronuclear NOE (Kay et al., 1989; Grzesiek and Bax, 1993c) experiment was performed for single labeled WT PsIAA4 DIII/IV using the sensitivity-enhanced pulse schemes. This provides information about the motion of the individual N-H bond of the protein molecule. The experimental data were recorded with proton saturation of 3-5 sec in 600 MHz spectrometer. The $^1\text{H}\text{-}^{15}\text{N}$ -NOE values were calculated from the ratio of cross peak intensities in the two spectra collected with (I_{sat}) and without (I_{eq}) amide proton saturation (Feng et al., 1998). The final data $I_{\text{sat}}/I_{\text{eq}}$ was plotted using GraFit software to distinguish the presence of highly structured and flexible or intrinsically disordered regions.

(iii) Sequential backbone assignment

Processed NMR data of ^{13}C , ^{15}N -labeled WT PsIAA4 DIII/IV were obtained from a set of 2D $^1\text{H}\text{-}^{15}\text{N}$ -HSQC, 3D HNCA, and 3D HNCACB experiments. 3D HNCA and HNCACB spectra were striped and analyzed using NMRView software (Johnson and Blevins, 1994). Different NMR experiments used for the assignment process were first referenced with 2D HSQC spectrum. Each cross peak in $^1\text{H}\text{-}^{15}\text{N}$ -HSQC spectrum connects the chemical shift of N and H present in the protein (backbone amide and side-chain of Arg, Asn, Gln, His, Trp and Lys). All cross peaks were picked and arbitrarily labeled which represented individual amino acid fingerprint. Every single residue shows a unique cross peak in HSQC spectrum. Peak of one corresponding residue in HSQC spectrum is referred as the peak of i (residue). Information of i and its preceding residue, $i-1$ can be obtained from other 3D experiments (HNCA, HNCACB) using its corresponding strip. NMR based sequential backbone resonance assignment for WT PsIAA4 DIII/IV was performed manually. Residues like Gly, Tyr, Ser and Thr in the protein sequence have distinct $\text{C}\alpha$ and $\text{C}\beta$ chemical shifts, which were selected to initiate the sequential backbone assignment. After the prediction of specific residues, strips were sequentially arranged in order to assign the cross peaks using NMRView, as described below in Fig 10. A 2D TOCSY spectrum showing a complete spin system of each amino acid was used for cross peak confirmation. The sequential backbone assignment was completed by performing a similar analysis with HNCACB, which includes an additional cross peak for $\text{C}\beta$ in each strip.

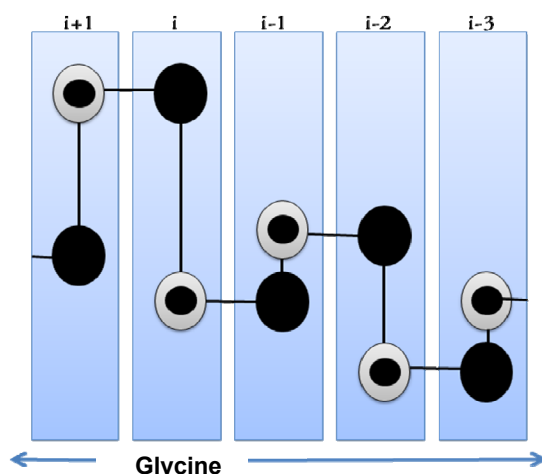


Figure 10: Schematic illustration of sequential walk with HNCA strips plot

HNCA strip plot of Glycine residue with distinct $\text{C}\alpha$ chemical shift represented by bigger cross peak (black circle) was used as a landmark, additionally smaller peak (gray with inner black circle) provides information about the (i-1) residue in the same strip. Smaller peak was further used to identify (i-1)th residue's own peak, by finding bigger peak of corresponding chemical shift value. A similar trend was followed to identify and assign all other sequential residues.

(iv) Experimental secondary structure prediction

Chemical shift information obtained after the backbone assignment was used for the Chemical Shift Index (CSI) and Torsion Angle Likelihood Obtained from Shift and Sequence (TALOS) calculations, to predict secondary structural elements from experimental data.

CSI: It was first introduced in early 90's (Wishart et al., 1992), which explains how the chemical shift information can be used to predict the presence of defined secondary structures (more negative, α -helix or more positive, a β -strand). The difference between the standard available $\text{C}\alpha$ random coil chemical shift and the observed $\text{C}\alpha$ chemical shift is obtained/calculated. Using analyzed and plotted data, we can predict that regions in the sequence containing an alpha helix ($\sim +2.6$ ppm) and a beta strand (~ -1.7 ppm). Usually loops or highly disordered region has a random distribution of data points.

TALOS+: (Shen et al., 2009): TALOS+ analysis was performed to predict the backbone dihedral angles using experimental NMR chemical shift information and distribution of secondary structural elements. Input file was created in either TALOS or BMRB format, which include all the chemical shift data of the $\text{C}\alpha$, $\text{C}\beta$, C , N and HN of each amino acid. TALOS+ is also now available as a part of NMRPipe package or analysis can be performed

by using a formatted input file with an online server. Using input chemical shift data and amino acid type, TALOS+ will predict the region of the Ramachandran plot where the residue is likely to reside in by help of available chemical shift information from already solved 3D structures (200 proteins). Dihedral angle information obtained from TALOS+ analysis was used as structural restraints for NMR structure calculation.

(v) Structure calculation and refinement

Structure calculation was performed in a semi-automated manner using ARIA v2.3. Several restraints were collected for structure calculation from sequential backbone assignments, side-chain assignment and dihedral restraints information from TALOS+ analysis, ambiguous assigned NOEs were used to perform the ARIA structure runs (Ramachandran et al., 1963; Cornilescu et al., 1999; Rieping et al., 2007). First set of restraints was generated from sequential backbone assignment and TALOS. Side-chain assignments were performed using information obtained from H(C)CH-TOCSY spectrum, aliphatic/aromatic 3D NOESY-edited HSQC experiments (120 ms mixing time). ^1H - ^1H -NOESY, ^1H - ^{15}N -NOESY-HSQC, ^1H - ^{13}C -NOESY-HSQC (aliphatic and aromatic signal region were separated) were used to generate NOE restraints. Dihedral angles from TALOS+ and generate NOE restraint information were important structural restraints for NMR structure calculation.

A final ensemble of the 10 NMR structures was used for further structural refinement. The 10 lowest energy structures were finally energy minimized and water refined to generate the high-resolution solution NMR structure of PsIAA4 DIII/IV. Side-chain assignment and NMR structure calculation were done in cooperation with the Institute for Physics/Biophysics, Martin Luther University Halle-Wittenberg, DE.

(vi) Structure validation and deposition

The ARIA calculated 10 lowest energy structure ensembles were validated by performing the Ramachandran analysis using PROCHECK-NMR (Laskowski et al., 1996). Final 3D structure ensembles and restraints were deposited in publicly available protein structure databases (PDB and BMRB). The deposited structural information can be downloaded using its accession IDs. PDB ID: 2M1M and BMRB accession number: 18870. Final deposited chemical shift data include, ^{13}C chemical shifts: 399, ^{15}N chemical shifts: 104 and ^1H chemical shifts: 629 count (Table A15).

3.2.2.5 NMR titration and interface mapping

^{13}C , ^{15}N -labeled PsIAA4 PB1^{BM3} and unlabeled PsIAA4 PB1^{AM3} were expressed, purified, and dialyzed against citrate buffer (pH 6.25). The concentrated labeled PsIAA4 PB1^{BM3} preparation showed a well-dispersed 2D ^1H - ^{15}N -HSQC spectrum, indicating suitability for NMR experiments at pH 6.25. Protein-protein interaction studies were performed by mixing the labeled and unlabeled PsIAA4 PB1 variants containing oppositely charged patches for interaction. ^{13}C , ^{15}N -labeled PsIAA4 PB1^{BM3} (450 μM) in low salt (150 mM NaCl) was used to perform TROSY-based 3D experiments using 600 MHz and 800 MHz spectrometers.

Sequential backbone assignment of PsIAA4 PB1^{BM3}

The 2D ^1H - ^{15}N -HSQC-TROSY spectrum were acquired for labeled PsIAA4 PB1^{BM3} (110 μM) prior to and after the addition of unlabeled PsIAA4 PB1^{AM3} (75 μM) in a molar ratio of 4:1. 2D ^1H - ^{15}N -HSQC-TROSY spectrum of free ^{15}N -labeled PsIAA4 PB1^{BM3} and bound PsIAA4 PB1^{BM3}:PsIAA4 PB1^{AM3} (4:1) was assigned by using TROSY-based 3D HNCA and HNCACB. HNCACO, HN(CO)CACB and HNCO were further used to identify and verify cross peaks containing information only for the (i-1)th residue in selected strips. NMR-based pH scanning experiment for PsIAA4 PB1^{BM3} variant was performed at pH range 4.5-6.25 (Fig. 31) to track the cross peaks which were assigned in 2D HSQC spectrum of WT PsIAA4 PB1 at pH 2.5 that accelerated the assignment process.

NMR based interface mapping

^1H - ^{15}N -HSQC-TROSY spectrum of free ^{15}N -labeled PsIAA4 PB1^{BM3} and bound PsIAA4 PB1^{BM3}:PsIAA4 PB1^{AM3} were overlaid. The chemical shift perturbation ($\Delta\omega$) analysis was performed using the corresponding chemical shift data in the proton and nitrogen dimension from assigned free and bound spectra using a formula below (Grzesiek et al., 1996).

$$\Delta\omega \text{ (ppm)} = [(\Delta\delta_{\text{HN}}^2 + \Delta\delta_{\text{N}}^2/25)/2]^{1/2}$$

$\Delta\delta_{\text{HN}}$ - chemical shift difference between HN (ppm) from free and bound spectra

$\Delta\delta_{\text{N}}$ - chemical shift difference between N (ppm) from free and bound spectra

The calculated data were plotted against its corresponding residue numbers. Residues showing increased CSP (ppm) were mapped over the 3D structure of WT PsIAA4 DIII/IV.

3.2.3 Yeast-two hybrid assays

LexA based Y2H assay was used to validate protein-protein interaction of full length PsIAA4 protein fusion proteins *in vivo*. *Saccharomyces cerevisiae* strains EGY48 (MAT α) carrying the LacZ reporter plasmid pSH18-34 and YM4271 (MAT α) competent cells were prepared according to Clontech Laboratories, Inc. Yeast Protocols Handbook (Protocol #PT3024-1)

3.2.3.1 LiAc yeast transformation

Isolated pGlida and pB42AD harboring GOI with DBD and AD fusion constructs were transformed into competent EGY48/pSH18-34 and YM4271 yeast cells, respectively. 0.1 μ g of plasmid DNA was added to 100 μ L of yeast cell suspension containing 0.1 mg of ssDNA (Salmon sperm DNA). 600 μ L of PEG/LiAc were added to the cells, and the cell suspension was incubated with shaking at 30°C, 200 rpm for 30 min. 70 μ L of DMSO were added and cells were heat-shocked for 15 min at 42°C. Cells were transferred to ice for 1-2 min, collected by centrifugation at 14,000 rpm for 5 sec. Cells were resuspended in 500 μ L of TE buffer. 100 μ L of this suspension were plated on SD restrictive media (-Ura/-His or -Trp) plate and incubated at 28°C for 3 days for selection of transformed plasmid.

3.2.3.2 Protein-protein interaction assays

Resulting haploid yeast cells EGY48 containing pGlida-PsIAA4 and YM4271 containing pB42AD-PsIAA4 were mated by streaking as intersecting lines on YPD media and incubated at 28°C for 1 day. Diploid yeast cells from the intersecting point were restreaked on SD restrictive media (-Ura/-His/-Trp) plate. Selected diploid cells were resuspended in 1X TE buffer and prepared dilutions (0.8-1.0 OD₆₀₀), using TECAN M1000. 5 μ L of the resuspended cells were spotted in duplicates on SD restrictive media containing Gal/Raf +X-Gal and incubated at 30°C for 3 days. Cells were assessed for activation of the β -galactosidase reporter gene (blue color) as a readout of protein-protein interaction. Plates were scanned and imaged 3-4 days after spotting. Growth control plates were prepared by spotting same diploid cells on SD -Ura/-His/-Trp medium.

3.2.3.3 Preparation of yeast protein extract

Selected diploid cells were grown in SD Gal/Raf restrictive liquid medium (3 mL) in an incubator shaker at 30°C and >200 rpm for 2 days. OD₆₀₀ was measured and all cultures were

diluted to similar OD as the lowest one. Cells were grown for another 1-2 h and were collected by centrifugation at 13,000 rpm for 1 min at 4°C. The cell were washed twice by resuspending in 500 µL ice-cold water and transferred to 1.5 mL reaction tubes. The supernatant was discarded and the washing step repeated. Pellets were resuspended in 500 µL of lysis buffer were vortexed with ~250 µL of glass beads at max speed, for 45 sec (five times). Lysed cell debris was separated by centrifugation at 13,000 rpm for 5 min. Supernatant containing yeast protein extract was collected and analyzed for protein expression by western blotting technique.

3.2.4 *In silico* analyses

3.2.4.1 Sequence analyses

MSA of PsIAA4 PB1 along with the all available *Arabidopsis* AUX/IAA and ARF PB1s were performed using MAFFT algorithm for sequence comparison. The generated MSA was visualized and analyzed manually with Jalview or GeneDoc. PsIAA4 PB1 sequence was also aligned with closely related AtAUX/IAA and AtARF PB1

3.2.4.2 Structural analyses

Structural comparison with available *Arabidopsis* AUX/IAA17 PB1, ARF5 and ARF7 were performed using PyMOL and TM-align. Mutations and electrostatics surfaces were generated using PyMOL and analyzed manually. Structure based sequence alignment was performed and the overall structural deviations were analyzed by ENDscript 2.0 server.

3.2.4.3 Protein-protein docking

The data-driven docking was performed using defined active residues derived from experiments (NMR and Y2H), acidic patch (D151, D153, D155, and D161) and basic patch (K96 and R106). The passive surrounding surface residues were selected automatically by HADDOCK (Easy interface) server. Input data were converted in highly ambiguous intermolecular restraints to drive docking with the PsIAA4 PB1 monomer ensemble (10 lowest energy structures) to allow more flexibility. Resulting docked structures were manually visualized and analyzed using PDBsum Generate.

4 RESULTS

4.1 Structural characterization of PsIAA4 C-terminal domains

AUX/IAA transcriptional repressors comprise four conserved sequential domains, unstructured N-terminal domains I, II and structured C-terminal domains III and IV (DIII/IV). Earlier, domain III was predicted to adopt a $\beta\alpha\alpha$ fold similar to the bacterial Ribbon-Helix-Helix transcription factor family (Abel et al., 1994; Morgan et al., 1999). Bioinformatics analyses suggested that DIII/IV present at the C-terminus of AUX/IAAs and ARFs might fold together to form a single globular domain. In the here presented study, the C-terminal domains of AUX/IAA protein PsIAA4 from *Pisum sativum* comprising residues 86-189, termed PsIAA4 DIII/IV, was selected for structural elucidation using NMR spectroscopy. To reveal the high-resolution atomic structure of PsIAA4 DIII/IV, recombinantly over-expressed, isotopically labeled, purified protein samples were prepared for biophysical studies.

4.1.1 Recombinant protein expression and purification of PsIAA4 DIII/IV

Full-length (FL) and truncated variants of AUX/IAA1 and AUX/IAA3 from *Arabidopsis thaliana*, and AUX/IAA4 from *Pisum sativum* in a pQE vector system containing a C-terminal 6X His-tag were heterologously expressed using an *E. coli* M15 expression system. All constructs were purified using the Ni^{2+} -IMAC gravity columns and analyzed by SDS-PAGE gel (Fig. A1). The PsIAA4 DIII/IV protein was selected from the large batch purification of several AUX/IAA protein variants, because of its high significance (see 1.2.4) and high yield (Fig. A2). Both unlabeled and isotopically labeled PsIAA4 DIII/IV containing the entire C-terminal structured region was purified using one-step IMAC native purification protocol (refer Materials and Methods). The one-step IMAC purification was optimized by extending the washing step with gradient of 50-100 mM imidazole in lysis buffer, which resulted in the removal of all impurities and a highly pure protein sample was obtained (Fig. 11). Purified PsIAA4 DIII/IV protein was dialyzed against the final buffer system required for further biophysical studies.

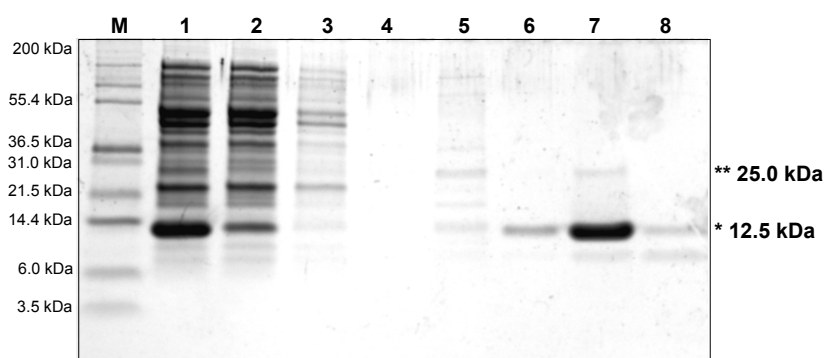


Figure 11: Purified PsIAA4 DIII/IV using IMAC

12% Tricine-PAGE gel, lane descriptions: M- protein marker (Mark12™ unstained standard, 2.5 to 200 kDa), 1- cell lysate input, 2- flow through, 3- 20 mM Imidazole wash fraction 1, 4- 20 mM Imidazole wash fraction 2, 5- 50 mM Imidazole wash, 6- 100 mM Imidazole wash, 7- 250 mM Imidazole elute and 8- 500 mM Imidazole elute. Asterisk (*) represents a monomer and double (**) for a dimer POI.

4.1.2 Structural analyses of the PsIAA4 DIII/IV

Recombinantly expressed and purified PsIAA4 DIII/IV protein was concentrated and quantified for preliminary structural analyses, i.e. verification of folded protein, oligomerization state and secondary structure contributions using biophysical methods.

4.1.2.1 Circular Dichroism spectroscopy showed that PsIAA4 DIII/IV contains mixed secondary structures

The far-UV CD spectrum was recorded for a purified and dialyzed low concentrated (~50 μ M) PsIAA4 DIII/IV sample at neutral pH using the CD spectrometer. The spectrum displayed a double minima of mean residual ellipticity (MRE) at 208 nm and 222 nm and indicates the presence of mixed secondary structural elements compared to the standard spectrum (Fig. 12). The standard CD spectrum displays the presence of two minima at 208 nm and 222 nm for α helices, minima at 217 nm for β strands and minima below 200 nm for random coils. The recorded CD spectrum of PsIAA4 DIII/IV showed a characteristic feature demonstrating that the purified protein was folded, and contained mixed secondary structural elements (Fig. 12).

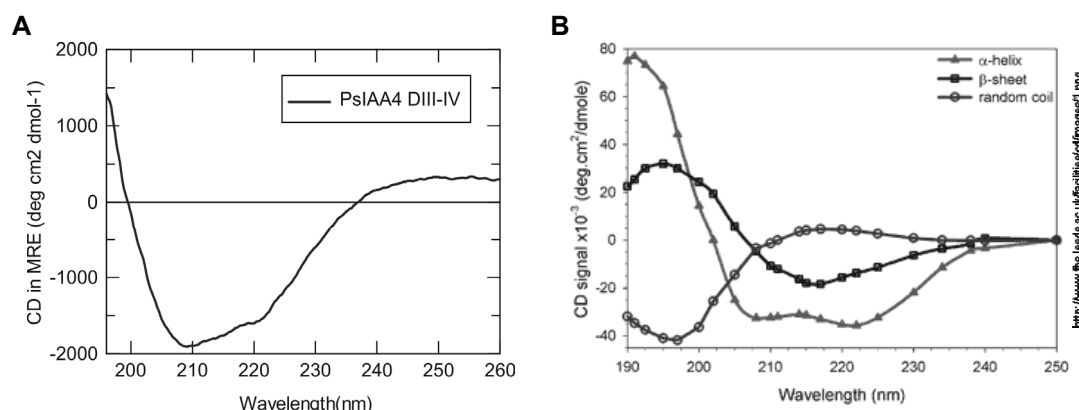


Figure 12: Far-UV CD spectrum of the PsIAA4 DIII/IV

(A) CD spectrum (190-260 nm) of the PsIAA4 DIII/IV confirms the presence of mixed secondary structural elements. (B) A standard spectra of proteins containing only specific secondary structures and unstructured random coil.

4.1.2.2 PsIAA4 DIII/IV is monomeric in a high salt or an acidic buffer system

Dialyzing and concentrating the purified protein resulted in visible aggregates above pH 5.0. Aggregation was reported over a broader pH range for several AUX/IAA proteins and truncated variants *in vitro* (Kim et al., 1997; Morgan et al., 1999). To identify the native state of PsIAA4 DIII/IV, sedimentation equilibrium experiments were performed using the analytical ultracentrifugation (AUC), which calculates the approximate theoretical molecular mass. The sedimentation equilibrium analysis confirmed that PsIAA4 DIII/IV is monomeric and in a homogeneous state at low pH (pH 3.0) compared to neutral pH condition (Fig. 13). At low pH, the protein sample did not denature, it rather improved the protein stability. Although high salt concentrations (>1 M NaCl) prevented the protein aggregation (monomeric) (Fig. A4), but it is not suitable for NMR experiments. In order to increase the NMR sensitivity and obtain a well-dispersed spectrum, sample buffer pH and ionic strength conditions were further optimized. Notably, acidic pH conditions assisted in concentrating the sample, which is a prerequisite for performing the required NMR experiments for sequential assignment and structure calculation.

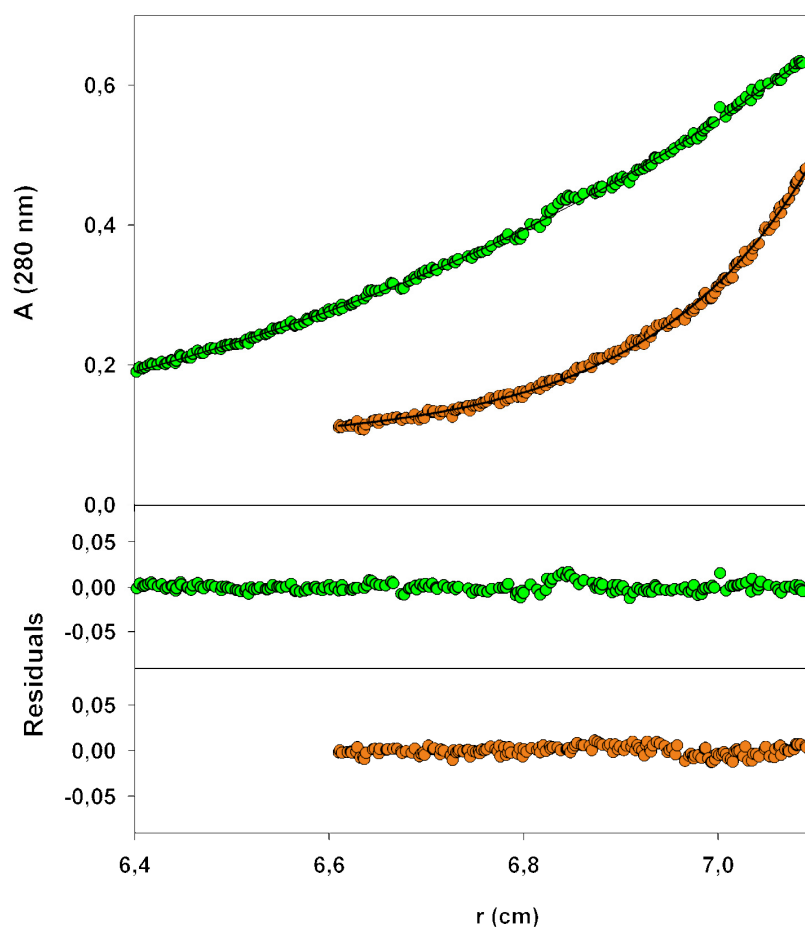


Figure 13: Sedimentation equilibrium analysis of the PsIAA4 DIII/IV

Average molecular mass determination of the PsIAA4 DIII/IV by sedimentation equilibrium experiment using AUC. Upper panel shows the experimental data, and the lower panel shows the residuals of the fit (i.e. the magnitudes of deviation of the model from the data). PsIAA4 DIII/IV exists as a monomeric species (~15 kDa) at pH 3.0 (green), whereas oligomeric species (~45 kDa) dominate at pH 8.0 (orange).

4.1.2.3 ^1H NMR spectral analysis confirmed that the PsIAA4 DIII/IV is folded

The folded state of the protein sample was verified using the 1D NMR experiment. ^1H NMR spectrum was measured for labeled protein sample at low pH (pH 3.0) buffer condition. The recorded spectrum displayed narrow and sharp resonances with good dispersion (-1 to 10 ppm) (Fig. 14). This confirms the folded state of PsIAA4 DIII/IV under NMR buffer condition.

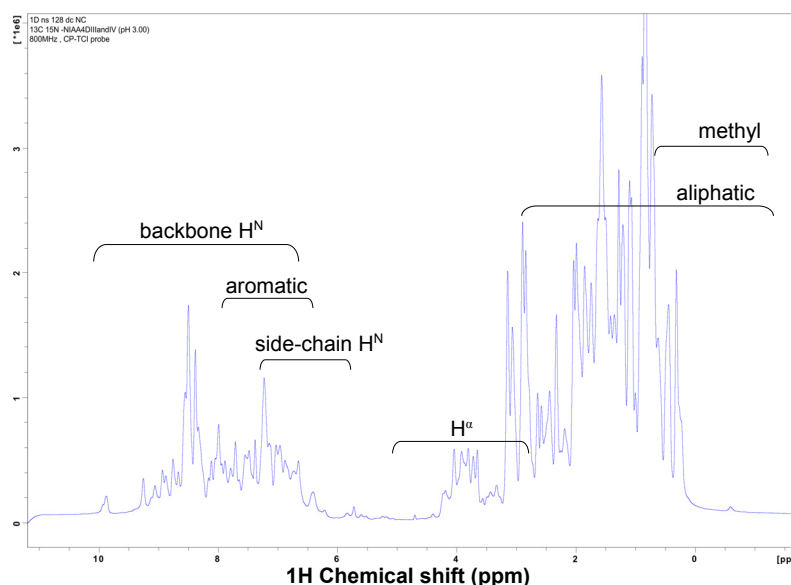


Figure 14: 1D NMR spectrum of the PsIAA4 DIII/IV at low pH

^1H -NMR spectrum of PsIAA4 DIII/IV recorded at pH 3.0, 25°C using a 600 MHz NMR spectrometer showed well dispersed peaks between 10 ppm and in the negative ppm range. Labels display proton peaks arising from different regions of the protein.

4.1.3 Three-dimensional structure determination of the PsIAA4 DIII/IV

To elucidate the tertiary structure, PsIAA4 DIII/IV protein expression was scaled-up (3-6 L) and optimized for a maximum yield. For heteronuclear NMR spectroscopy, an isotopically labeled protein sample was prepared using M9 minimal liquid media. A low temperature (18°C) o/n expression and 1 mM IPTG induction at ~ 1.0 OD₆₀₀ allowed to significantly increase the protein yield (^{15}N -labeled, 41 mg/L and ^{13}C - ^{15}N -labeled, 17 mg/L). To increase spectrum quality, NMR based pH scanning experiments were performed with an fully ^{15}N -labeled sample in a low pH range (2.0-2.5-3.0). ^1H - ^{15}N -HSQC spectrum at pH 2.5 showed a well dispersed and uniform intensity for all cross peaks (Fig. 15). Well-dispersed cross peaks re-confirmed the presence of a folded protein at these acidic pH buffer condition. Strikingly, at this experimental conditions (pH 2.5), the protein was not forming a molten globular or fully unfolded state. Therefore, all the required NMR experiments were performed with samples prepared at pH 2.5 using a buffer system compatible for NMR spectroscopy.

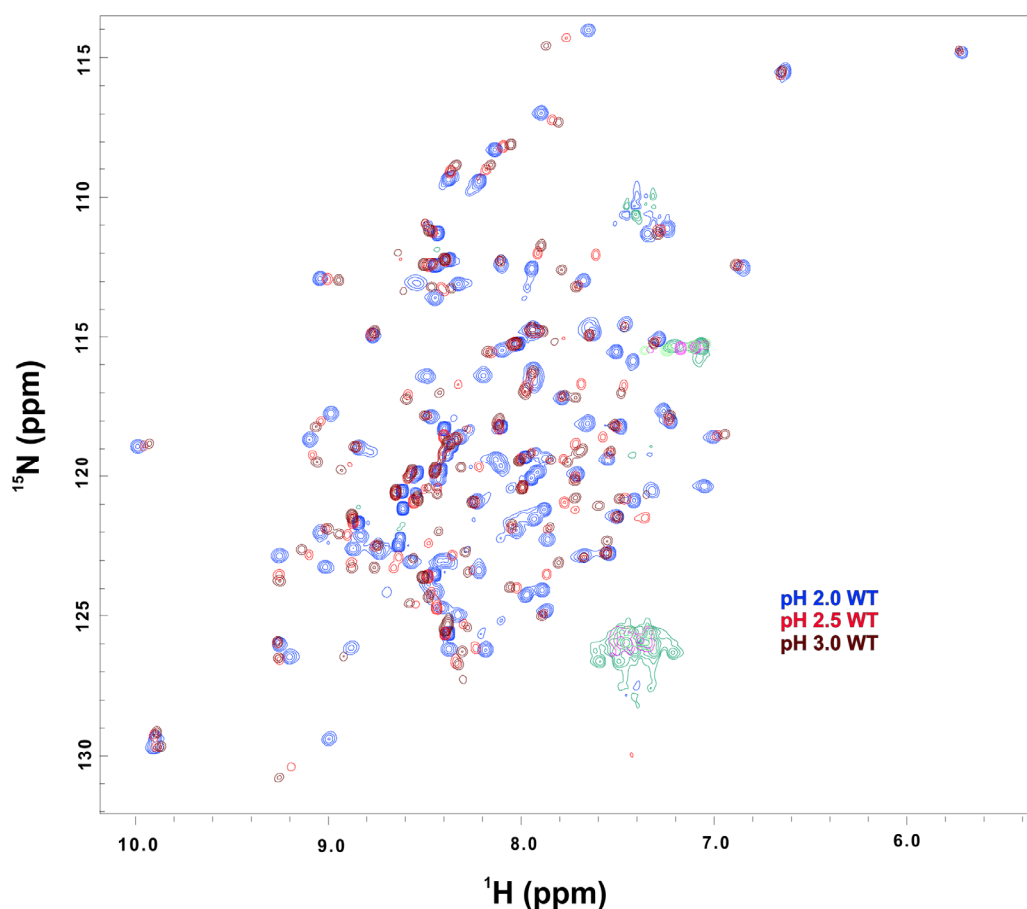


Figure 15: 2D HSQC spectral overlay of the PsIAA4 DIII/IV at low pH

^1H - ^{15}N -HSQC spectrum of PsIAA4 DIII/IV measured at pH 2.0 (blue), pH 2.5 (red) and pH 3.0 (brown), at 25°C using a 600 MHz NMR spectrometer.

4.1.3.1 NMR based sequential backbone assignment and secondary structure prediction

The sequential backbone assignment is the first step and a key requirement in the NMR protein structure calculation. A suite of triple-resonance NMR spectra of 3D HNCA, 3D HNCACB, 3D ^{15}N -TOCSY-HSQC, and ^{15}N -NOESY-HSQC were processed with the NMRPipe and used for the complete backbone assignment of the PsIAA4 DIII/IV. All the NMR spectra showed a single set of resonances for the monomeric protein, which displayed the characteristics of a stably folded polypeptide chain. Each of the 3D experiments were striped and analyzed manually using the NMRView software. Fig. 16 and Fig. A5 shows a region of sequential walk from assigned 3D HNCACB and 3DHNCA strips for residues D68 - V74 respectively, as an illustration. ^{13}C strip plots generated from 3D HNCACB contain $\text{C}\alpha$ (black) and $\text{C}\beta$ (red) cross peaks of its own (i) and preceding (i-1) residue, which can be used

as a reference to annotate the preceding (i-1) and succeeding (i+1) residues. In a similar fashion, more than 95% of the residues detected in the 2D ^1H - ^{15}N HSQC spectrum recorded for ^{15}N -labeled PsIAA4 DIII/IV (Fig. 16).

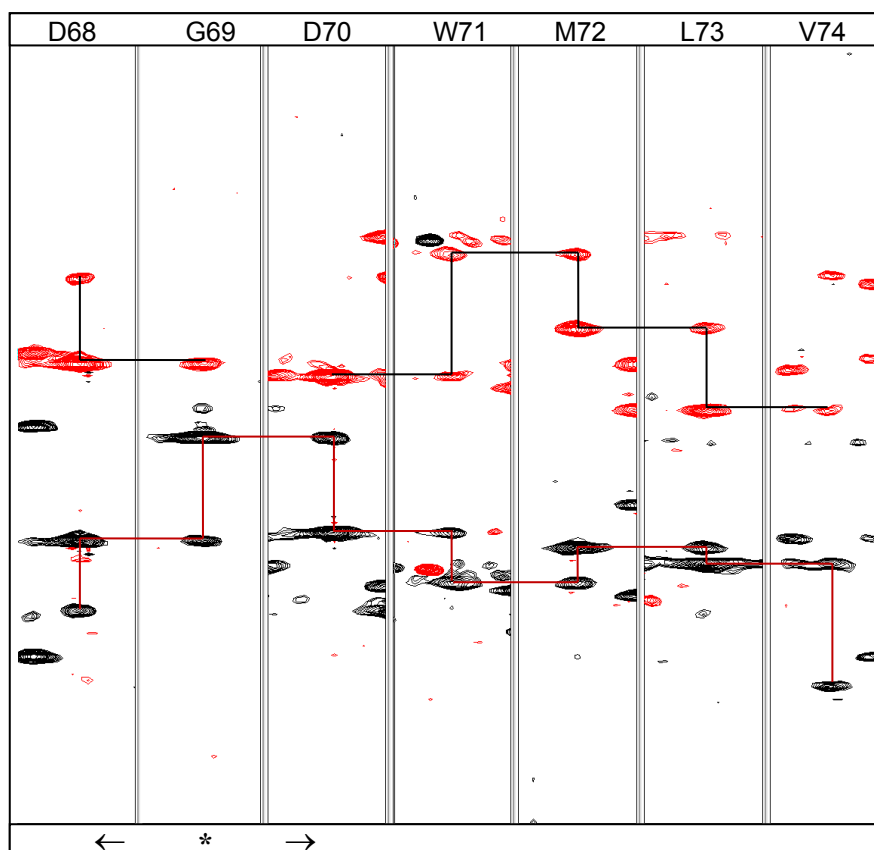


Figure 16: ^{13}C strip-plot of 3D HNCACB ($\text{C}\alpha$ and $\text{C}\beta$) of PsIAA4 DIII/IV

Strip-plot showing $\text{C}\alpha$ (black) and $\text{C}\beta$ (red) cross peaks of its own (i) and preceding (i-1) residue. Sequential connectivities were obtained by connecting i, i-1 and i+1 residue signals. The G69 (*) strip was used as a landmark for a sequential walk on either side (black and red lines).

Subsequently, individual cross peaks were labeled with a single letter amino acid code followed by its residue number, based on the information obtained from the sequential backbone assignment analysis (Fig. 17). The resulting backbone and $\text{C}\beta$ assignments were used as basis for the secondary structure prediction, and the side-chain assignment.

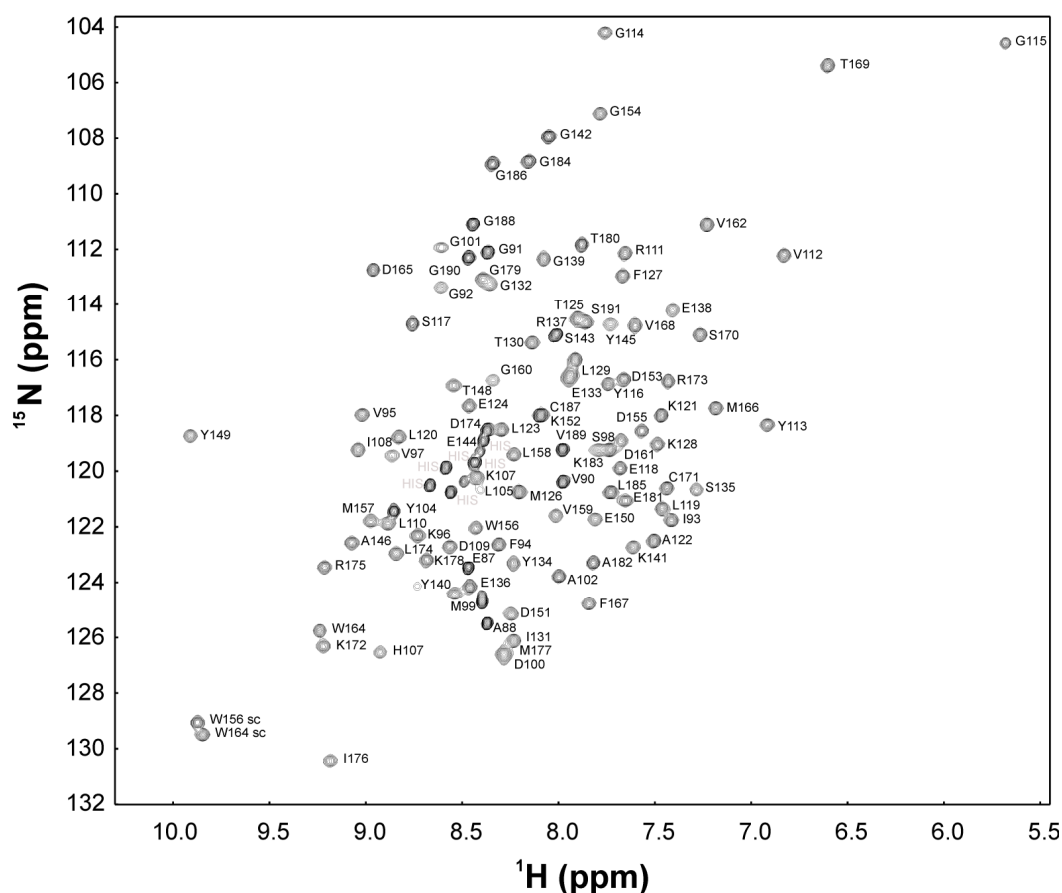


Figure 17: Complete sequential backbone assignment of the PsIAA4 DIII/IV

The ^1H - ^{15}N -HSQC spectrum (positive contours) of PsIAA4 DIII/IV was measured at 800 MHz, 25°C and pH 2.5. Each cross peak corresponding to the backbone chemical shift information of an individual amino acid residue is labeled by the one-letter code followed by residue number. The cross peaks arose from the 6X His-tag residues were labeled in gray.

4.1.3.2 NMR based analyses revealed the boundaries of PsIAA4 DIII/IV structured regions

The steady-state heteronuclear NOE (hNOE) analysis (dynamics on a ns-ps timescale) demonstrated the presence of two rigid regions (DIII and DIV) separated by a central loop and unstructured C- and N-terminal ends that clearly match to the later described NMR structure of PsIAA4 DIII/IV (Fig. 18) with increased backbone dynamics indicated by negative or near zero hNOE values. The CSI plot displayed chemical shift (δ) differences between the observed and standard random coil chemical shift values. The grouping of $\text{C}\alpha$ chemical shift differences of $\sim +2.6$ ppm represents the helical regions and ~ -1.7 ppm represents the beta sheet regions. The resulting CSI plot showed the presence of mixed secondary structural elements and its boundaries (β , β , α , β , β , α) (Fig. 19).

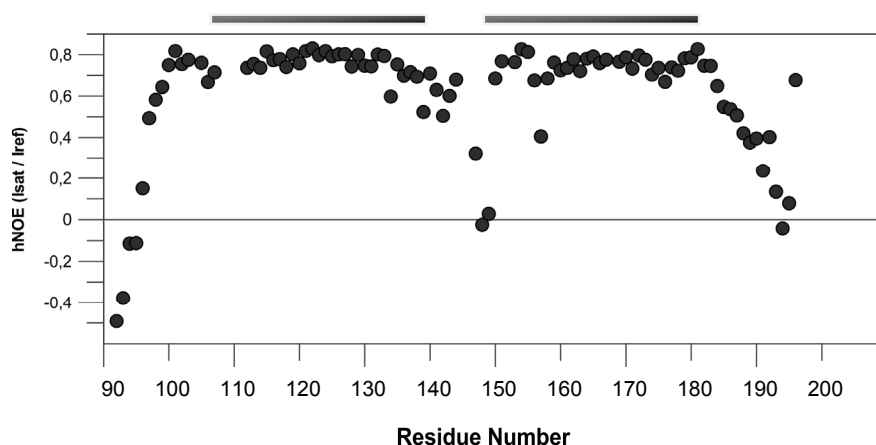


Figure 18: NMR based steady-state hNOE data revealed the flexible regions of PsIAA4 DIII/IV

$^1\text{H}\{-^{15}\text{N}\}$ -hNOE data of PsIAA4 DIII/IV at 600 MHz NMR spectrometer plotted against the residue number. Solid horizontal bars above represent the structured regions.

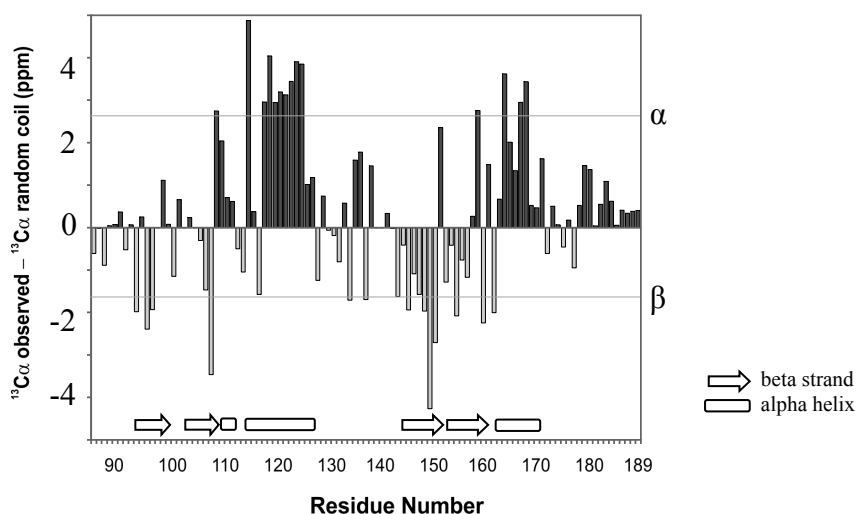


Figure 19: CSI plot of the PsIAA4 DIII/IV displays the Ca chemical shift differences

The chemical shift differences between the observed Ca and standard random coil values (Table A19) were plotted against the residue number. Black and gray bars represent positive and negative chemical shift differences, respectively. The shown arrow and rectangle at the bottom of the plot represent the predicted alpha helix and beta strands, respectively.

4.1.3.3 Solution structure of the PsIAA4 oligomerization domain

The isotopically ^{13}C , ^{15}N double labeled wild-type PsIAA4 DIII/IV with the C-terminal 6X His-tagged protein was used for the NMR structure determination. An optimized acidic buffer system (pH 2.5) facilitated to concentrate the labeled NMR sample to 1.5 mM (18 mg/mL), which was beneficial for 3D NMR experiments for the structure calculation.

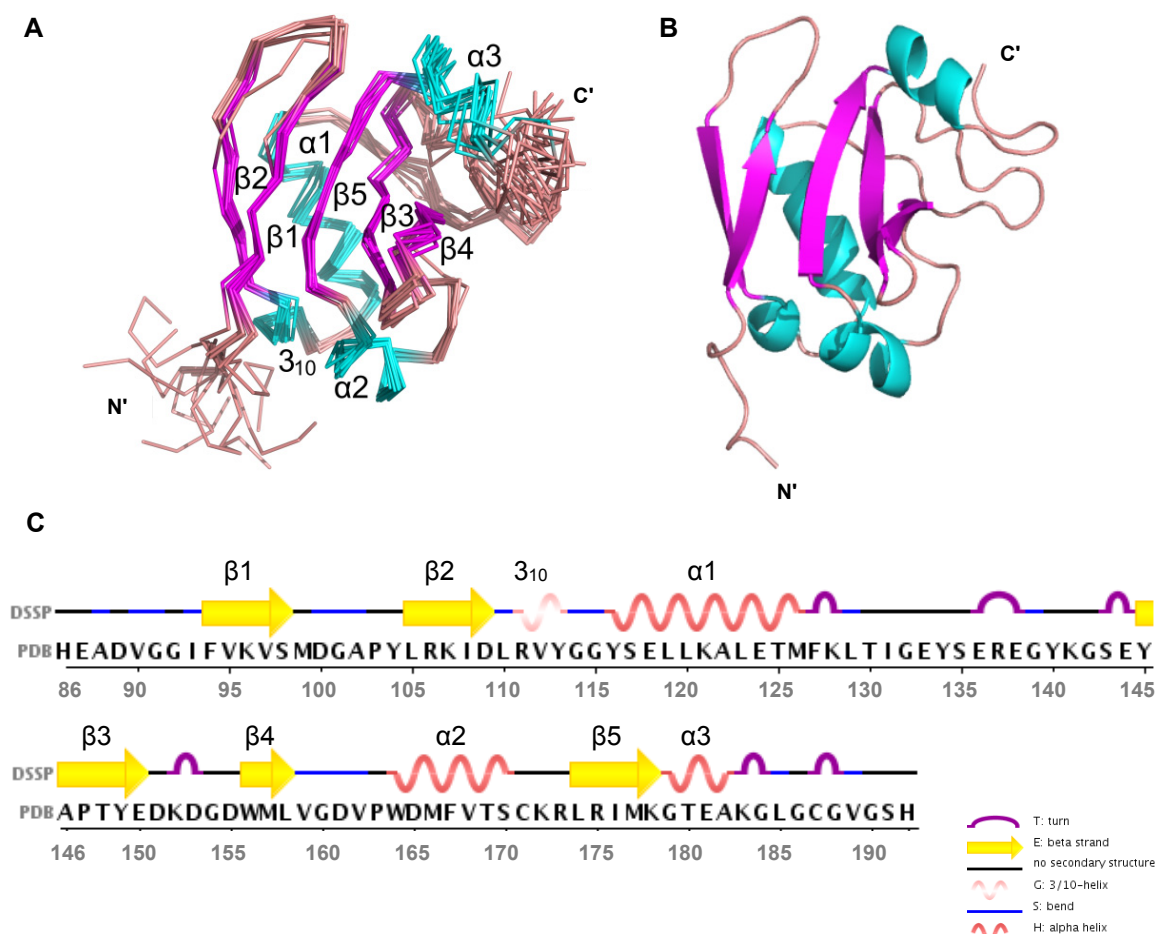


Figure 20: NMR structure of the PsIAA4 DIII/IV

(A) Backbone representation of the 10 lowest energy NMR structure ensembles. Structural elements are highlighted in color: helices ($\alpha 1$ - $\alpha 3$, 3_{10} helices, cyan), β -strands ($\beta 1$ - $\beta 5$, magenta), and loops (salmon). (B) Cartoon representation of the lowest energy structure. (C) Secondary structure boundaries of PsIAA4 DIII/IV generated using DSSP.

Longterm stability of the ^{15}N -single labeled sample was checked over several weeks (3-4) before performing 3D NMR experiments.

The NMR structure of the PsIAA4 DIII/IV monomer was calculated with the program ARIA version 2.3 (Rieping et al., 2007) by using the NOE and dihedral angle constraints listed in

Table 11. The 10 lowest-energy water-refined structure ensemble of the PsIAA4 DIII/IV converges with a backbone r.m.s.d. of 0.66 ± 0.07 Å (Fig. 20A). The well superimposing residues in the structure ensemble clearly reveal the canonical topology of a globular ubiquitin (Ub)-like β -grasp fold. Conserved DIII and DIV correspond to subdomains $\beta 1$ - $\alpha 1$ and $\beta 3$ - $\alpha 3$ of the PsIAA4 globular fold, respectively. The lowest energy structure illustrates the presence of three alpha helices, one 3^{10} helix and five beta strands and their connecting loops. The structure also displayed the twisted mixed beta sheet grasping a long alpha helix (Fig. 20B and Fig. 21). Secondary structural elements were calculated for a solved NMR structure using Define Secondary Structure of Proteins (DSSP) algorithm, that showed the position of the alpha helices, beta strands and loops over the protein sequence (Fig. 20C). Experimental constraints and NMR structure statistics of PsIAA4 DIII/IV are summarized in Table 11 and the distribution of NOE data in Fig. 22.

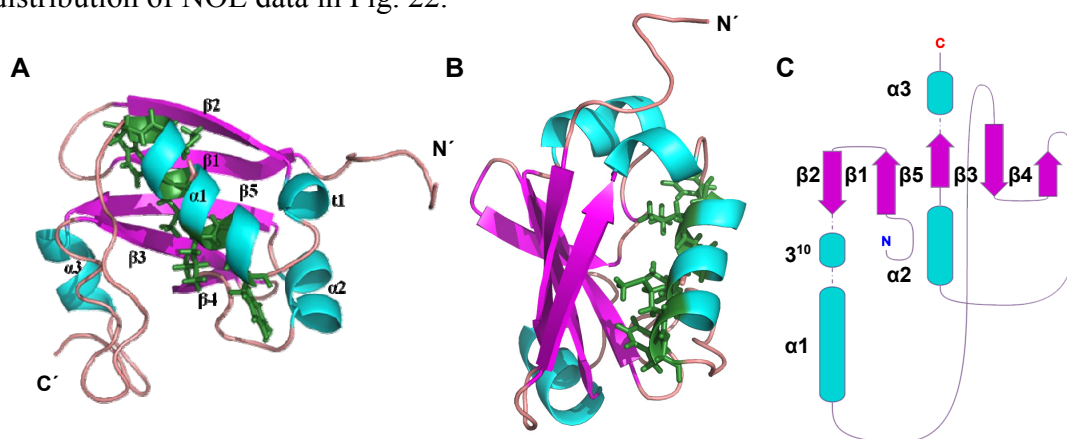


Figure 21: PsIAA4 DIII/IV illustrating twisted β -sheet grasping the $\alpha 1$ helix

(A and B) Different orientations of PsIAA4 DIII/IV displaying twisted 5 stranded β -sheet (magenta) grasp the long amphipathic $\alpha 1$ helix showing hydrophobic residues (green, sticks) in the inner surface of the helix. (C) Topology diagram of the PsIAA4 DIII/IV displaying the position of various secondary structural elements from N- to C-terminal.

The N-terminal DIII include an anti-parallel $\beta 1$ and $\beta 2$ followed by a short 3^{10} helix and a long $\alpha 1$ helix. The C-terminal DIV region include three anti-parallel beta strands and two alpha helices. The beta sheet comprises an N-terminal $\beta 2$ - $\beta 1$ and C-terminal $\beta 5$ - $\beta 3$ - $\beta 4$ forming a mixed and curved single beta sheet ($\beta 2$ - $\beta 1$ - $\beta 5$ - $\beta 3$ - $\beta 4$) which is decorated by amphipathic helices forming an hydrophobic core buried in the globular fold (Fig. 21C). Domain III and IV of the PsIAA4 are connected by a long loop ($\alpha 1$ - $\beta 3$) which is of a variable length in other AtAUX/IAA family members. The PsIAA4 DIII/IV has a minimal loop length, which is comparable with the selected AtAUX/IAAs and all AtARFs (Fig. 36).

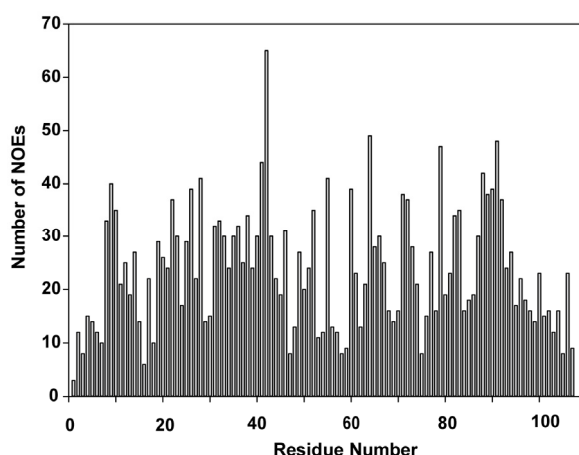


Figure 22: The bar diagram of NOE data of the PsIAA4 DIII/IV

The NOE data plotted against the amino acid residue in PsIAA4 DIII/IV showing the data quality used for NMR structure calculation.

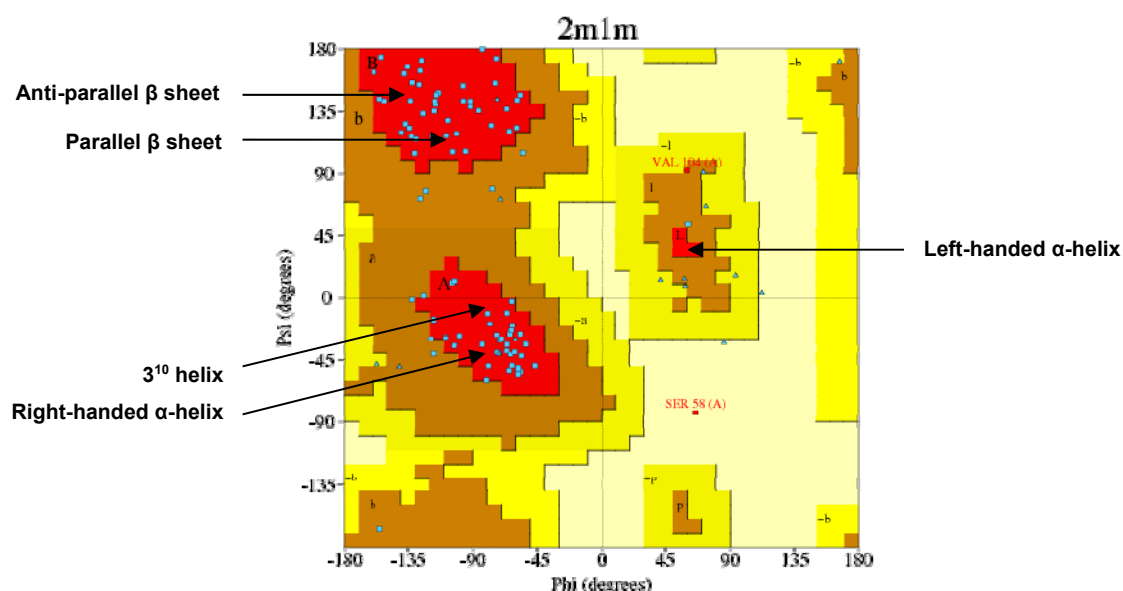


Figure 23: The Ramachandran plot analysis of the PsIAA4 DIII/IV

Structure validation using the Ramachandran plot of the solved NMR structure. The distribution of dihedral angles from the calculated PsIAA4 DIII/IV NMR structure were plotted in the Ramachandran plot as small triangles representing glycine and squares representing all other residues except glycine in blue (allowed) and red (disallowed). The background colors correspond to the allowed regions with no steric clashes (red), with slightly shorter van der Waals radii (brown) and disallowed regions (shades of yellow).

The Ramachandran plot analysis of final 10 lowest-energy structure ensemble was performed using the PROCHECK-NMR program, indicating >98% residues located in the allowed region (Fig. 23 and Table 11). This indicates the good stereo chemical quality of the final calculated NMR structure ensemble.

Table 11: NMR structure constraints and refinement statistics for PsIAA4 DIII/IV

NMR DISTANCE AND DIHEDRAL CONSTRAINTS	
Distance constraints	1,927
Total unambiguous NOE	1,424
Intra-residue	606
Inter-residue	
Sequential ($ i - j = 1$)	351
Medium-range ($ i - j < 4$)	187
Long-range ($ i - j > 5$)	280
Total ambiguous NOE	503
Intermolecular	0
Hydrogen bonds	0
Total dihedral angle restraints	174
phi Φ	87
psi Ψ	87
STRUCTURE STATISTICS	
Violations (mean and s.d.)	
Distance constraints (Å)	0.024 ± 0.001
Dihedral angle constraints (°)	2.0 ± 0.1
Max. dihedral angle violation (°)	6.0
Max. distance constraint violation (Å)	2.1
Ramachandran analysis	
Most favored	86.1 %
Additionally allowed	11.7 %
Generously allowed	0.7 %
Disallowed	1.5 %
Deviations from idealized geometry	
Bond lengths (Å)	0.001
Bond angles (°)	0.32
Impropers (°)	0.21
Average pairwise r.m.s.d.** (Å)	
Heavy	0.98 ± 0.06
Backbone	0.66 ± 0.07

*Pairwise r.m.s.d. was calculated among 10 refined structures of PsIAA4 DIII/IV (86–189 AAs) along with three additional residues (Gly-Ser-His) at its C-terminus without the 6X His-tag. Detailed TALOS+ results (Φ and Ψ angles) are shown in Table A15

After validating the PsIAA4 DIII/IV NMR structure ensemble, its atomic coordinates, chemical shifts and the structure restraints were deposited in the Protein Data Bank (PDB ID: 2M1M), and in the Biological Magnetic Resonance Data Bank (BMRB accession no. 18870).

4.2 Functional studies of the PsIAA4 DIII/IV

The PsIAA4 DIII/IV adopts an Ub-like β grasp fold similar to the Phox and Bem1p (PB1) domain. Sequence and structural analyses of AUX/IAAs and ARFs family members revealed that most of the PB1 domains belong to the type I/II, containing a conserved basic invariant K patch in DIII and an acidic OPCA motif in DIV (Fig. 24). These conserved residues are on the either sides of the protein surface (Fig. 25) and are responsible for the homo- and hetero-oligomerization within and between the members of both families. Such conserved residues of type I/II PB1 domain containing proteins from various organisms were shown to be involved in ‘front-to-back’ or ‘head-to-tail’ mode of interaction.

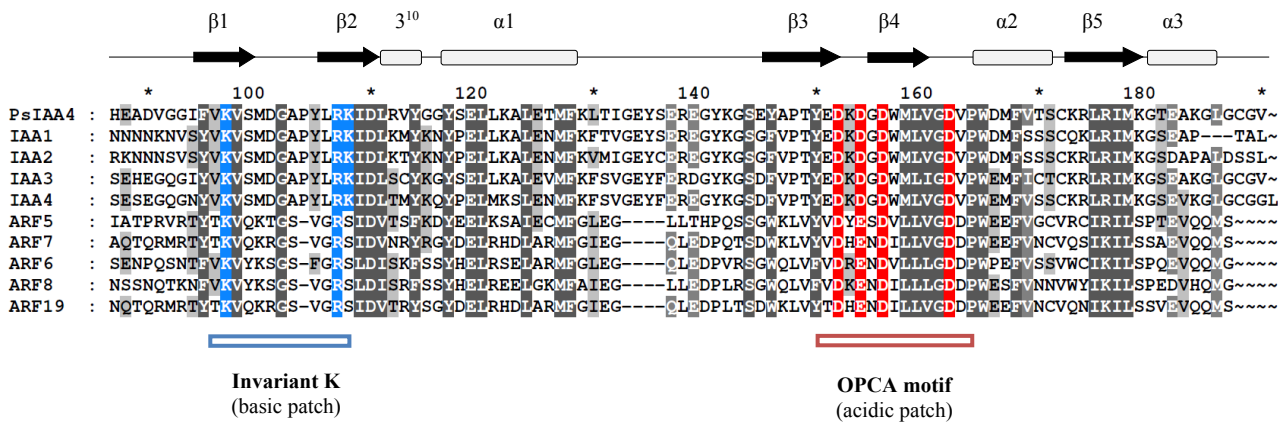


Figure 24: Conserved basic and acidic patch residues of PsIAA4 DIII/IV are highlighted in the MSA

The sequence alignment of PsIAA4 DIII/IV, *Arabidopsis* AUX/IAA1-4 and ARF activator DIII/IV were aligned using ClustalW. Gray shades show similar and identical residues conserved between both family members. Invariant lysine (blue) residue and OPCA motif (red) are highlighted along with other conserved residues forming the charged acidic and basic patches.

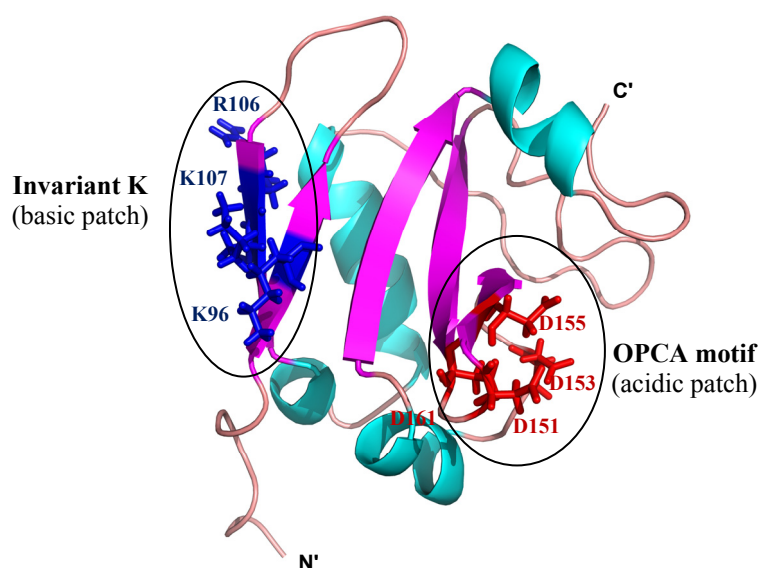


Figure 25: NMR structure highlighting basic and acidic patch residues

Conserved basic patch displaying invariant K along with other conserved basic residues and acidic patch showing OPCA motif residues of the canonical type I/II PB1 features are presented as blue (basic) and red (acidic) sticks, respectively.

A systematic mutational study was performed for the functional characterization of the PsIAA4 using Y2H assays with WT PsIAA4 FL and mutant proteins. Subsequently, the recombinantly purified PsIAA4 DIII/IV truncated variants were further analyzed biophysically using NMR and ITC.

4.2.1 Structural comparison confirms the presence of PB1 fold in the PsIAA4 DIII/IV

The DaliLite v3 server (Holm and Park, 2000) was used to identify the closest structural homologs of PsIAA4 DIII/IV NMR structure from the publicly available protein structures in the PDB. The NEXT TO BREAST CANCER 1 (NBR1) PB1 domain (PDB ID: 2BKF) shared the highest structural homolog (Z-score 6.3), aligned with PsIAA4 DIII/IV showing overall r.m.s.d 2.79 Å over a length of 77 residues (Fig. 26) and the overall sequence identity was < 30%. The PsIAA4 DIII/IV is highly comparable with PB1 domain of NBR1, but contains an additional $\alpha 3$ helix at its C-terminal end (Burroughs et al., 2007). The structural similarity with other PB1 family members demonstrates that the NMR structure of the wild-type PsIAA4 DIII/IV monomer, solved at pH 2.5, represents the native architecture in solution (Fig. 26). PsIAA4 DIII/IV is hereafter referred as the PsIAA4 PB1 domain.

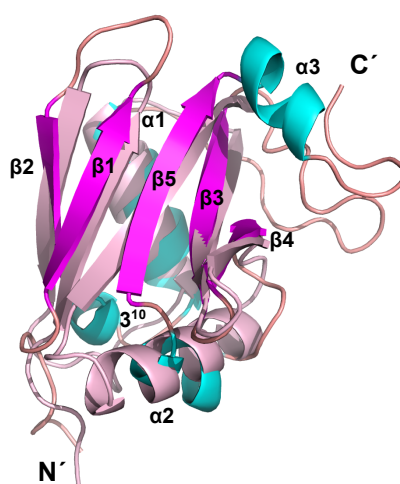


Figure 26: Structural alignment between PB1 domains of NBR1 and PsIAA4

The structures of the closest homolog, NBR1 PB1 domain (pink) and PsIAA4 DIII/IV (magenta and cyan) were superimposed using TM align algorithm.

4.2.2 Mutations of typeI/II conserved residues disturb the PsIAA4 PB1 surface charges

The PB1 fold contains the invariant K patch and the OPCA motif on opposite faces of the PsIAA4 PB1 structure (Fig. 27). The mutation of highly conserved residues, either in the basic or acidic patches abolished homo-oligomerization between PB1 domain containing proteins (Sumimoto et al., 2007). *In silico* PsIAA4 PB1 variants were generated by replacing charged residues on the basic (K96A, R106A, K107A) or the acidic (D151A, D153A, D155A) patches, resulted in a disrupted contiguous charged patches (Fig. 27). Electrostatic surface potentials of the WT and PsIAA4 PB1 variants demonstrated that replacing two or more charged patch residues to alanine would disturb the surface charged patches. The basic patch includes residues with K96 at its center, which is flanked by R106, K107, and K128, as well as by K172 and R173 (Fig. 27). These basic residues are highly conserved in AUX/IAA family proteins (Fig. 36), and the latter two (K172 and R173) were functionally identified as a nuclear localization signal (NLS) of PsIAA4 (Abel and Theologis, 1995). The acidic patch contains three conserved aspartic acid residues of the OPCA motif (D151 X D153 X D155) forming an acidic bulge that is a part of an extended acidic patch complemented by conserved D161 and E136 (Fig. 27). The double and triple mutants of PsIAA4 FL and truncated variants will be designated as BM2 (K96A/R106A), AM2 (D151A/D153A), BM3 (K96A/R106A/K107A), and AM3 (D151A/D153A/D155A).

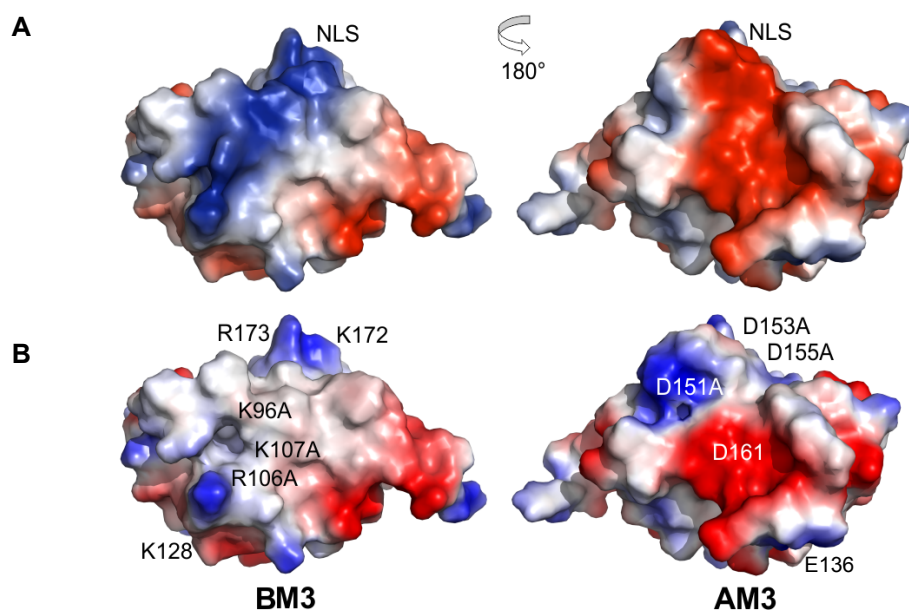


Figure 27: Electrostatic charged surfaces of the WT and mutant PsIAA4 PB1

(A) Electrostatic surface potential of the WT PsIAA4 PB1 revealed extended basic (blue) and acidic (red) patches on the protein surface, containing (see B for residue labeling) invariant K96 and the OPCA motif (D151, D153, D155, and D161). K96 is flanked by R106, K107, and K128 and by K172 and R173 of the NLS. (B) *In silico* generated mutant PsIAA4 PB1 (BM3 and AM3) displaying disrupted contiguous charged patches.

4.2.3 PsIAA4 FL mutations abolish homotypic interaction *in vivo*

The generated single and double PsIAA4 FL variants with mutated charged patches, and WT PsIAA4 FL constructs were analyzed using LexA based Y2H to establish the mechanism of interaction between AUX/IAA PB1 domains through their conserved charge residues. A systematic site-directed mutagenesis of one or two central amino acid residues on the basic (K96A/R106A, BM2) or acidic (D151A/D153A, AM2) patch of the PsIAA4 PB1 domain was performed and generated an Y2H protein-protein interaction matrix (Fig. 28). The results showed that the WT PsIAA4 FL as AD or DBD fusion interacted with itself or with each of the mutant. Y2H analyses suggested that a single charged surface is sufficient for homotypic PsIAA4 interaction. Likewise, mutations of the basic PB1 face (PsIAA4^{K96A}, PsIAA4^{R106A}, or PsIAA4^{BM2}) did not prevent PsIAA4 dimerization when paired with mutations of the acidic PB1 face (PsIAA4^{D151A}, PsIAA4^{D153A}, or PsIAA4^{AM2}), and vice versa. Both PsIAA4^{AM2} and the PsIAA4^{BM2} variants failed to interact with itself in Y2H assays, suggesting that the presence of both negative and positive surface is necessary for homotypic PsIAA4 interaction *in vivo*.

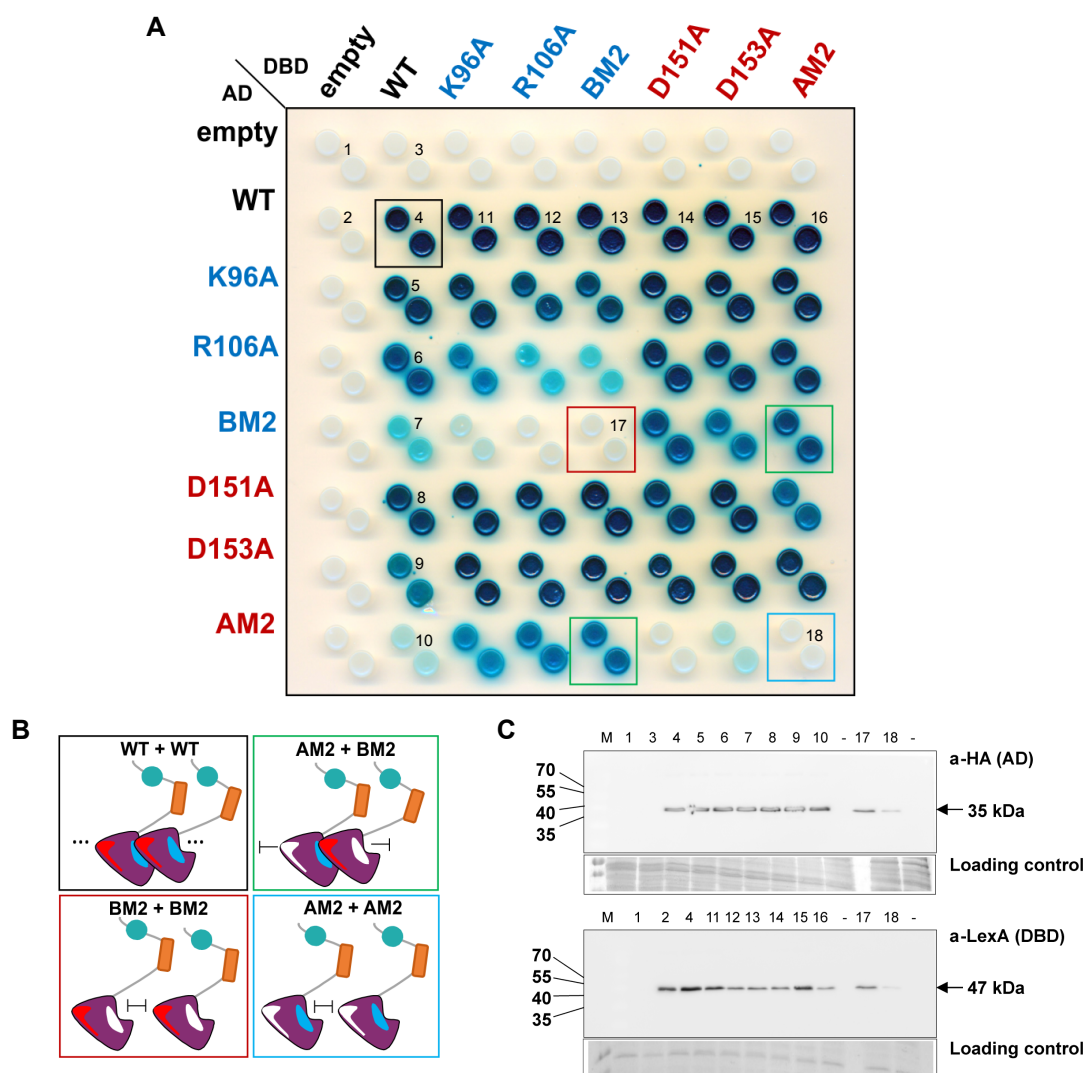


Figure 28: Y2H assays confirm type I/II PB1-mediated homotypic interaction of the PsIAA4 FL

(A) Interaction matrix of the WT and mutant PsIAA4 FL protein with single or double residue change in the basic or acidic PB1 interface. Diploids expressing WT and mutant DBD–PsIAA4 and AD–PsIAA4 protein fusions were generated and spotted on selective induction medium (Gal/Raf/–Ura/–Trp/–His/+X-Gal). β -galactosidase expression, reporting protein–protein interaction (blue colonies) shown here are 4 days after spotting. PsIAA4^{BM2} interacted with PsIAA4^{AM2} in either vector configuration (green boxes). Each double mutant failed to interact with itself, PsIAA4^{BM2} (red box), and PsIAA4^{AM2} (blue box). The WT PsIAA4 control is shown in a black box. DBD, DNA-binding domain; AD, activation domain. (B) Schematic model of WT and mutant PsIAA4 interactions from Y2H assays, explaining different scenarios in above Y2H matrix (colored boxes correspond to A). (C) Immunoblot analysis revealed that PsIAA4 protein variants accumulate in all selected diploid yeast cells (lanes numbered as in A).

Selected diploid cells were checked on western blot for protein expression. DBD LexA fusion adds ~25 kDa, and AD (B42AD + HA tag + NLS) fusion tag adds ~14 kDa. HA-tag in AD

hybrids and LexA tag in DBD hybrids were immunoblotted with anti-HA and anti-LexA antibodies respectively, on extracts prepared from diploids expressing WT and mutant PsIAA4, lanes are labeled as in Fig. 28A. Silver-stained non-specific bands are shown as a loading control of yeast total protein extract. Immunoblot analysis confirmed expression of PsIAA4 protein fusions in yeast cells (Fig. 28C). Thus, the Y2H study validates the mode of PsIAA4 dimerization via ‘front-to-back’ interaction of its PB1 domain.

4.2.4 Mutations suppress homotypic interaction at neutral pH

PsIAA4 PB1 double and triple mutants were expressed and purified (Fig. 29) for *in vitro* functional studies to identify the crucial residues involved in electrostatic interaction for oligomerization. PsIAA4 PB1 variants were purified using a similar strategy as WT and subsequently, buffer conditions were optimized to prepare monomeric sample around physiological pH (Fig. 29). Citrate buffer system (pH 6.25) with a low salt concentration (150 mM NaCl) and TCEP was used during interaction studies.

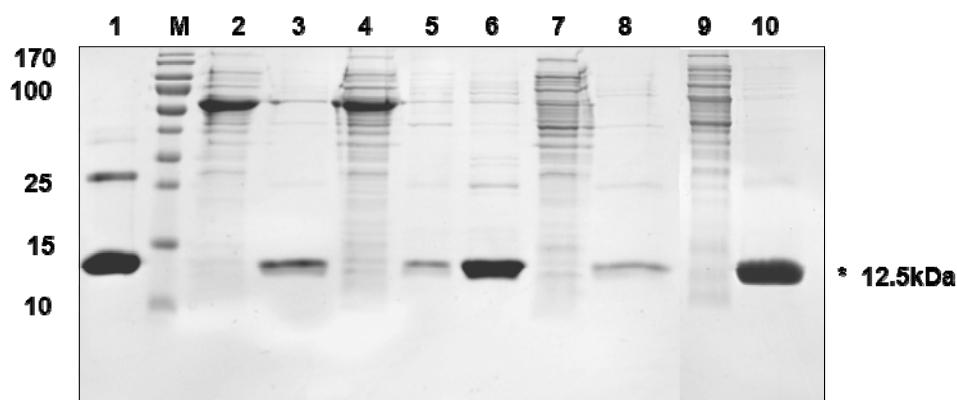


Figure 29: Protein purification of PsIAA4 PB1 double and triple mutants

12% SDS-PAGE gel: 1- WT PsIAA4 PB1, M- PageRuler Prestained Protein Ladder (10 to 180 kDa), 2- PsIAA4 PB1AM2 input, 3- PsIAA4 PB1AM2 elute, 4- PsIAA4 PB1AM3 input, 5- PsIAA4 PB1BM2 elute1, 6- PsIAA4 PB1BM2 elute2, 7- PsIAA4 PB1 BM2 input, 8- PsIAA4 PB1BM2 elute, 9- PsIAA4 PB1BM3 input, 10- PsIAA4 PB1BM3 elute. Astrick (*) marks the POI.

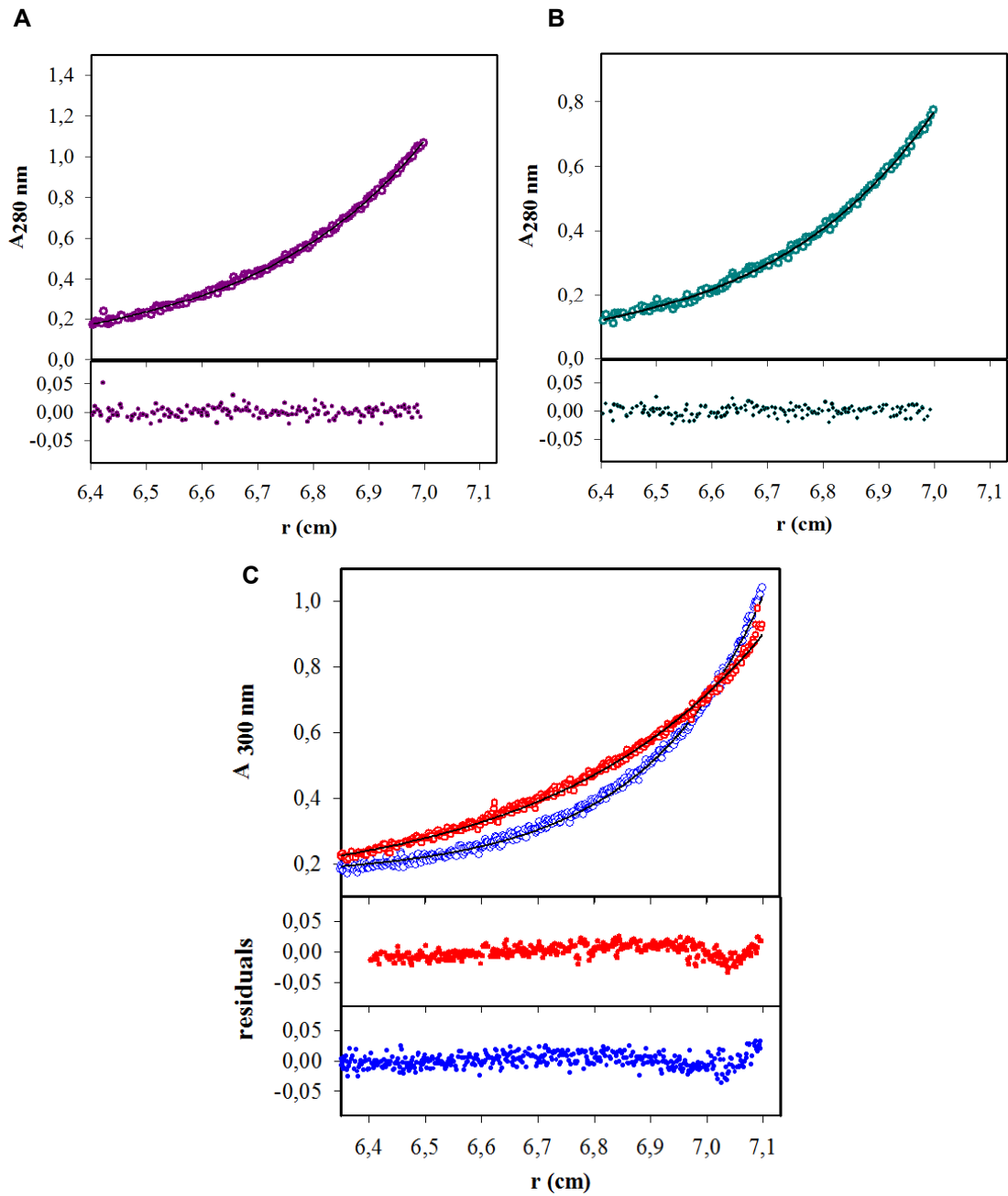


Figure 30: Sedimentation equilibrium analysis of PsIAA4 PB1 double and triple mutants

(A) Average molecular mass determination of PsIAA4 PB1^{BM3} (violet curve) and (B) PsIAA4 PB1^{AM3} (cyan curve) exist as a monomeric species (~12 kDa) around neutral pH. (C) PsIAA4 PB1^{BM3} (red curve) and PsIAA4 PB1^{AM3} (blue curve) at pH 6.25 in similar buffer condition indicates the presence of homogeneous monomer species (~12 kDa). The upper panel shows the experimental data and fits, and the lower panel shows the residuals.

To determine the structural requirements for PsIAA4 PB1 dimerization or oligomerization (Kim et al., 1997) *in vitro*, systematic mutation in basic and acidic surface residues on the type I/II PB1 domain were introduced. Solubility of the double and triple amino acid substituted mutants of PsIAA4 PB1 around neutral pH (pH 6.25) considerably improved, as indicated by sedimentation equilibrium AUC analysis of PsIAA4 PB1 in conserved patches, i.e. PsIAA4 PB1^{BM2}, PsIAA4 PB1^{BM3}, PsIAA4 PB1^{AM2} and PsIAA4 PB1^{AM3} (Fig. 30). Thus, suppression of protein aggregation and the resulting monomeric state of mutant PsIAA4 PB1 polypeptides with disrupted type I/II charged surface residues at near-neutral pH is consistent with homotypic front-to-back dimerization. Additionally, *in vitro* analysis by AUC, showed that higher order mutants were mostly monomeric in optimized buffer conditions. PsIAA4 PB1 triple mutants were used for further biophysical studies.

4.2.5 NMR based pH scanning and sequential backbone assignment of the PsIAA4 PB1^{BM3} variant

NMR based pH scanning experiments were performed using ¹⁵N-labeled mutant PsIAA4 PB1^{BM3} protein to obtain 2D HSQC spectra over the pH range 4.0-6.25 to track the movement of cross peaks (Fig. 31). This assisted in the sequential backbone assignment process along with available assigned 2D HSQC spectrum of WT PsIAA4 PB1 recorded at pH 2.5 (Fig. 17). PsIAA4 PB1^{BM3} having theoretical pI 5.5 was scanned only at pH 4.0, 4.5 and 6.25, and aggregation behavior was observed below pH 4.0 (Fig. A8). 2D HSQC spectral overlay of PsIAA4^{BM3} displayed mostly a linear shift and WT PsIAA4 PB1 was overlaid as a reference. The data were used for the sequential backbone assignment of PsIAA4 PB1^{BM3} mutant.

Further, all standard TROSY based triple-resonance NMR experiments were performed with ¹³C-¹⁵N-labeled PsIAA4 PB1^{BM3} mutant for the sequential backbone assignment. 2D HSQC-TROSY spectrum of PsIAA4 PB1^{BM3} were assigned to near completeness using the 3D HNCA, HNCACB, HNCO and HN(CO)CACB experiments (Fig. 32).

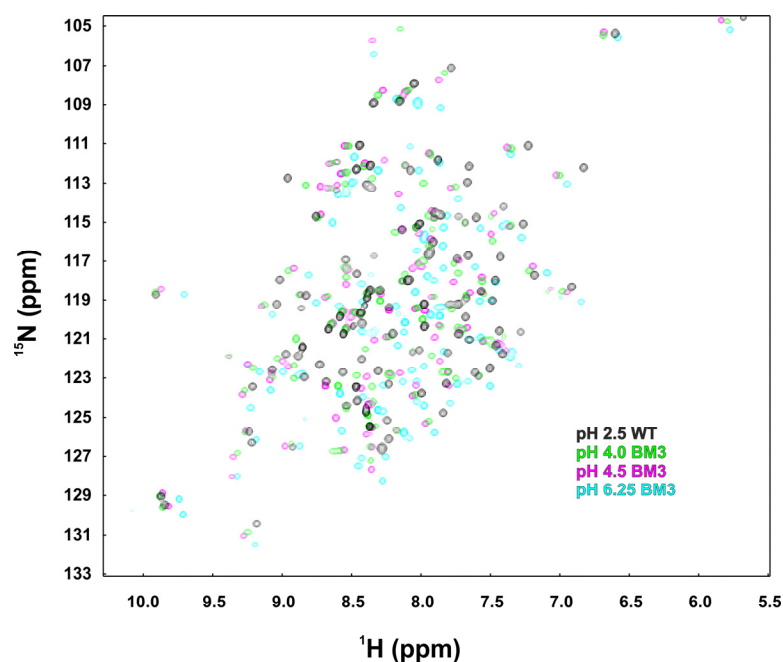


Figure 31: NMR-based pH scanning of the PsIAA4 PB1^{BM3} mutant protein

Overlay of ^1H - ^{15}N -HSQC spectra of the WT PsIAA4 PB1 at pH 2.5 (black) and the PsIAA4 PB1^{BM3} mutant were recorded at pH 4.0 (green), pH 4.5 (magenta), and pH 6.25 (cyan).

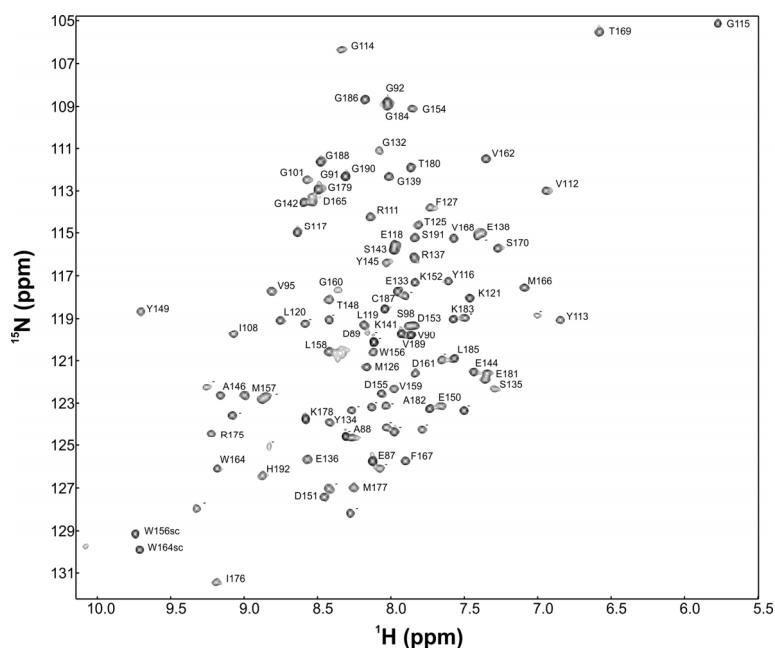


Figure 32: Sequential backbone assignment of 2D HSQC-TROSY spectrum of the PsIAA4 PB1^{BM3} mutant

The ^1H - ^{15}N -HSQC-TROSY spectrum of PsIAA4 PB1^{BM3} was measured at 800 MHz, 25°C and pH 6.25. Each cross peak corresponds to the backbone chemical shift of an individual amino acid residue, and is labeled by the one-letter code, followed by residue number. (-) represents the ambiguous/unassigned cross peaks.

4.2.6 Mapping the acidic interface of the PsIAA4 PB1 dimer

PsIAA4 PB1^{BM3} basic and PsIAA4 PB1^{AM3} acidic patch variants assisted in understanding the homotypic ‘front-to-back’ interaction of PsIAA4 PB1 using the NMR spectroscopy. Over-expressed and purified, isotopically ¹⁵N-labeled PsIAA4 PB1^{BM3} and unlabeled PB1^{AM3} proteins were used for the NMR titration experiment. Both PsIAA4 PB1^{BM3} and PsIAA4 PB1^{AM3} mutants remained monomeric and stable in solution at a high protein concentration (0.5 mM) under the physiological condition (pH 6.25). Each mutant comprises a single undisturbed electrostatic face, thereby retaining one charged interacting surface.

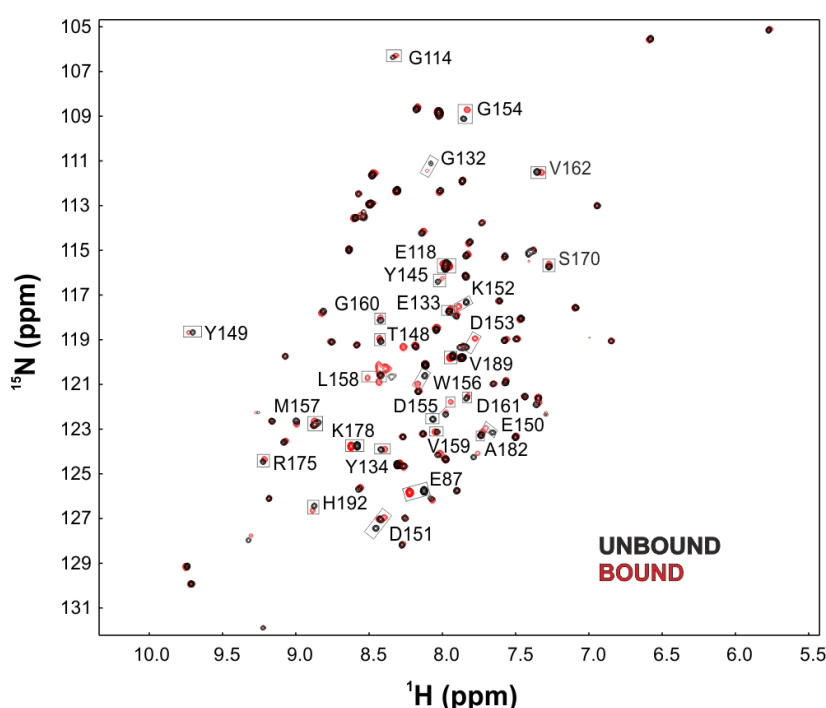


Figure 33: Acidic dimer interface analysis of the PsIAA4 PB1 mutant

¹H-¹⁵N-HSQC spectral superimposition of unbound ¹⁵N-labeled PsIAA4 PB1^{BM3} monomer (black cross peaks) and the bound complex of ¹⁵N-labeled PsIAA4 PB1^{BM3} with unlabeled PsIAA4 PB1^{AM3} (4:1 ratio; red cross peaks), which revealed specific chemical shift changes indicating the molecular interaction of both monomers.

Mixing of labeled PsIAA4 PB1^{BM3} and unlabeled PsIAA4 PB1^{AM3} mutant variant samples resulted in dimer formation followed by ¹H-¹⁵N-HSQC spectra. Complex association and dissociation is fast on the chemical shift time-scale, which allowed to track the shifting crosspeaks upon complex formation. Overlay of the ¹H-¹⁵N-HSQC spectra of free and bound PsIAA4 PB1^{BM3} revealed major and minor chemical shift perturbations.

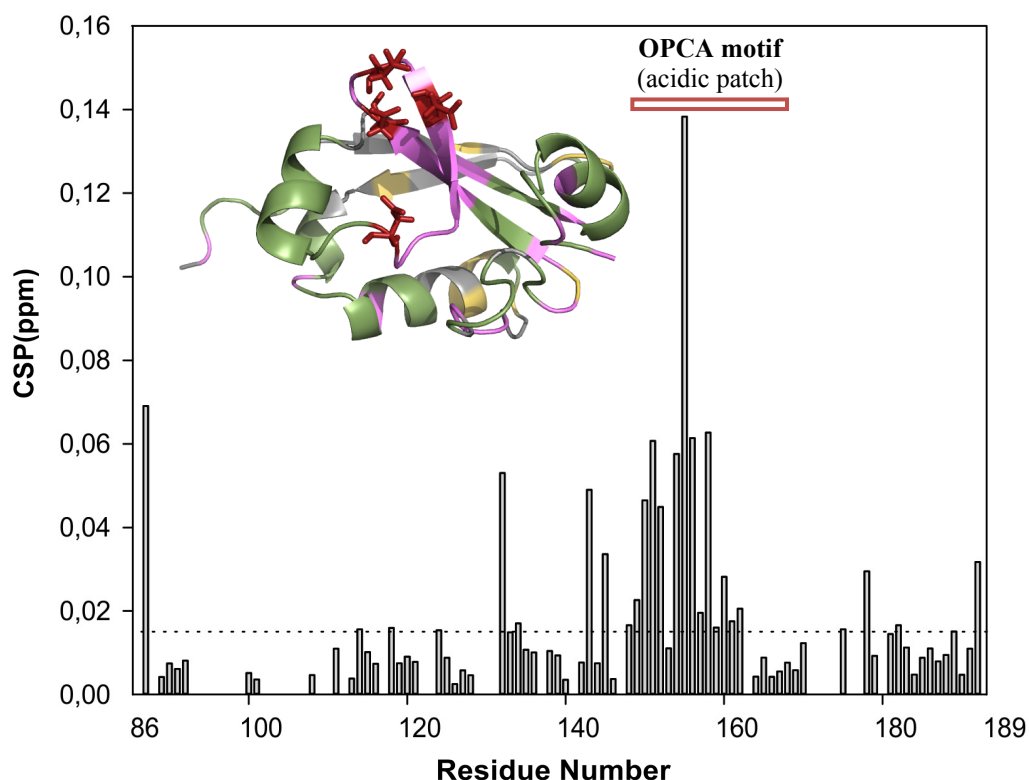


Figure 34: NMR based interface mapping of the PsIAA4 PB1

NMR chemical shift perturbations (CSP) from interaction between PsIAA4 PB1^{BM3} and PsIAA4 PB1^{AM3}. (Inset) Structural mapping of interacting residues of PsIAA4 PB1^{BM3} with PsIAA4 PB1^{AM3} as derived by backbone chemical shift perturbation (as indicated by gray boxes in the NMR spectra in Fig. 33). Mapped residues include the OPCA motif (red) and additional interface residues (pink). Colored regions of the structure correspond to unambiguously assigned residues (red, pink, and green); residues with spectral overlap (yellow); and unassigned residues (gray).

Cross peaks with high and low chemical shift perturbations of the backbone amide ¹H and ¹⁵N resonances between free and bound states of PsIAA4 PB1^{BM3} mutants were calculated and mapped onto the WT PsIAA4 PB1 structure and are shown in gray boxes in the HSQC spectra (Fig. 33). The acidic dimer interaction interface are highlighted in pink and red (Fig. 34 inset). Chemical shift changes mapped on the structure of PsIAA4 PB1 reveals a significant perturbation around the OPCA motif containing acidic residues as well as additional residues surrounding the acidic surface patch. As expected, amino acid residues at the opposite side of PsIAA4 PB1^{BM3}, including the mutated basic patch, showed no or only minor perturbations upon titration (Fig. 34). Thus, the NMR mapping analyses revealed that

the interaction between AUX/IAA PB1 is possibly mediated by electrostatic head-to-tail mode of interaction similar to the other PB1 domain containing proteins.

4.2.7 Thermodynamic analysis of PsIAA4 PB1 homo-dimerization by ITC

The binding affinity and thermodynamic parameters of PsIAA4 PB1^{BM3}:PsIAA4 PB1^{AM3} homotypic interaction was investigated by Isothermal Titration Calorimetry (ITC) (Fig. 35) (refer Materials and Methods).

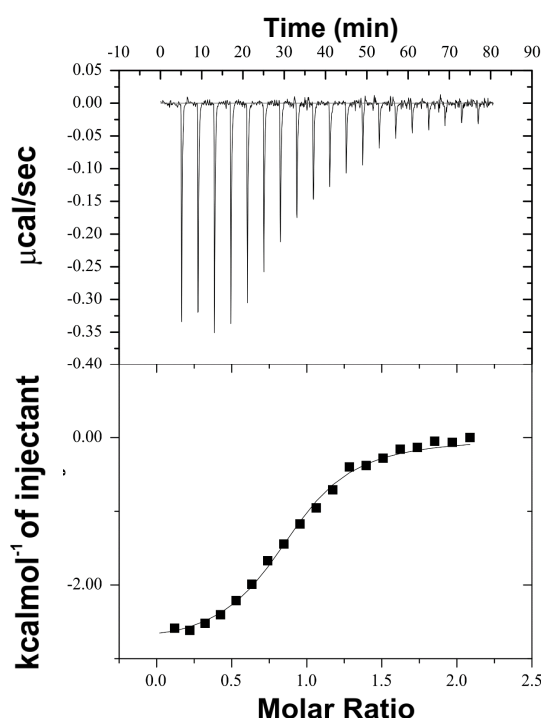


Figure 35: Thermodynamic analysis of the PsIAA4 PB1 homodimerization

ITC thermogram (upper) and binding isotherm (lower) correspond to the binding of PsIAA4 PB1^{BM3} with PsIAA4 PB1^{AM3}, at pH 6.25 and 25°C. A single binding site model was fitted to the data using Origin v7.0 software provided with the iTC200 calorimeter.

Interaction analysis indicated the dimer formation (1:1 stoichiometry) with an equilibrium dissociation constant (K_D) of $6.4 \pm 0.9 \mu\text{M}$ (Fig. 35). Formation of arrested PsIAA4 PB1 mutant dimer is driven by favorable enthalpy and entropy changes ($\Delta H = -2.815 \text{ kcal/mol}$, $\Delta S = 14.3 \text{ cal/mol per K}$, $T\Delta S = 4.261 \text{ kcal/mol}$ and $\Delta G = -7.47 \text{ kcal/mol}$).

4.3 *In silico* analyses

In silico analyses were performed to compare the sequence and structure of PsIAA4 PB1 with AtAUX/IAA and AtARF PB1 domains.

4.3.1 Sequence comparison of PsIAA4 PB1 with AtAUX/IAA and AtARF PB1s

The PsIAA4 PB1 sequence is closely related to *Arabidopsis* AUX/IAA1-4 (Fig. 36). In domain III, the basic patch residues in β 1- β 2 strands are highly conserved in PsIAA4 with a basic K-X₃-D/E-X₅-R-K motif similar to most of the AtAUX/IAAs, except AtAUX/IAA33 (refer experimental details in Appendix 7.12). But AtARF PB1s contain the K-X₈₋₉-R motif, most of which lack the conserved D/E in the basic motif, except AtARF10 and AtARF16. Only AtARF activators contain additional basic residues in the K-X₈₋₉-R motif (Fig. 36). The α 1 helix following the basic motif is quite similar within AtAUX/IAA family members, whereas ARFs contain more residues that are charged. In PsIAA4, the loop connecting the sequential domain III-IV is shorter (16 AAs) similar to a subset of AtAUX/IAAs and is highly variable for the other AtAUX/IAAs and ARFs (~5-30 AAs). In domain IV, the acidic OPCA motif is different from the AtAUX/IAA and AtARF family members. AtAUX/IAAs contain mostly an E-D-K-D/E-G-D motif similar to other PB1 domain containing proteins. AtARFs contain a D-X-E/D-X-D motif without the initial acidic residue and missing the characteristic G residue in OPCA motif (Fig. 36). Few AtARFs (AtARF10, -13, -14, -15, -16, -20 and -21) contain a disturbed OPCA motif (Fig. 36). Usually, the OPCA motif is followed by a G-D-V-P or G-D-D-P motif in AtAUX/IAAs and AtARFs (except AtARF16), respectively (Fig. 36). AtARFs contain additional acidic residues after the G-D-D-P motif. In AtAUX/IAAs, β 5 contain a K/R-R-X-K/R-X₂-K/R motif, a putative NLS sequence that is absent in ARFs. AtARFs activators contain a highly conserved K/R-I-L-S motif. The final α 3 helix size and sequence are variable. The loop at the end of PB1 domains are of variable lengths in PsIAA4, AtAUX/IAAs and AtARFs. Therefore, differences in and around the charged surface patches might be responsible for its specificity.

Other prominent differences between AtARF activators and repressors include an aromatic residue (Y/F), before β 1 in ARF activators, which is similar to PsIAA4 and AtAUX/IAAs. AtARF activators lack a single amino acid in the loop between β 1 and β 2. The loop-connecting domain III and IV contain an E-X₃-E-D motif, except in AtARF5. AtARF

activator's $\alpha 1$ residues lack two conserved acidic residues and an additional conserved basic residue, which makes it different from other AtARF proteins.

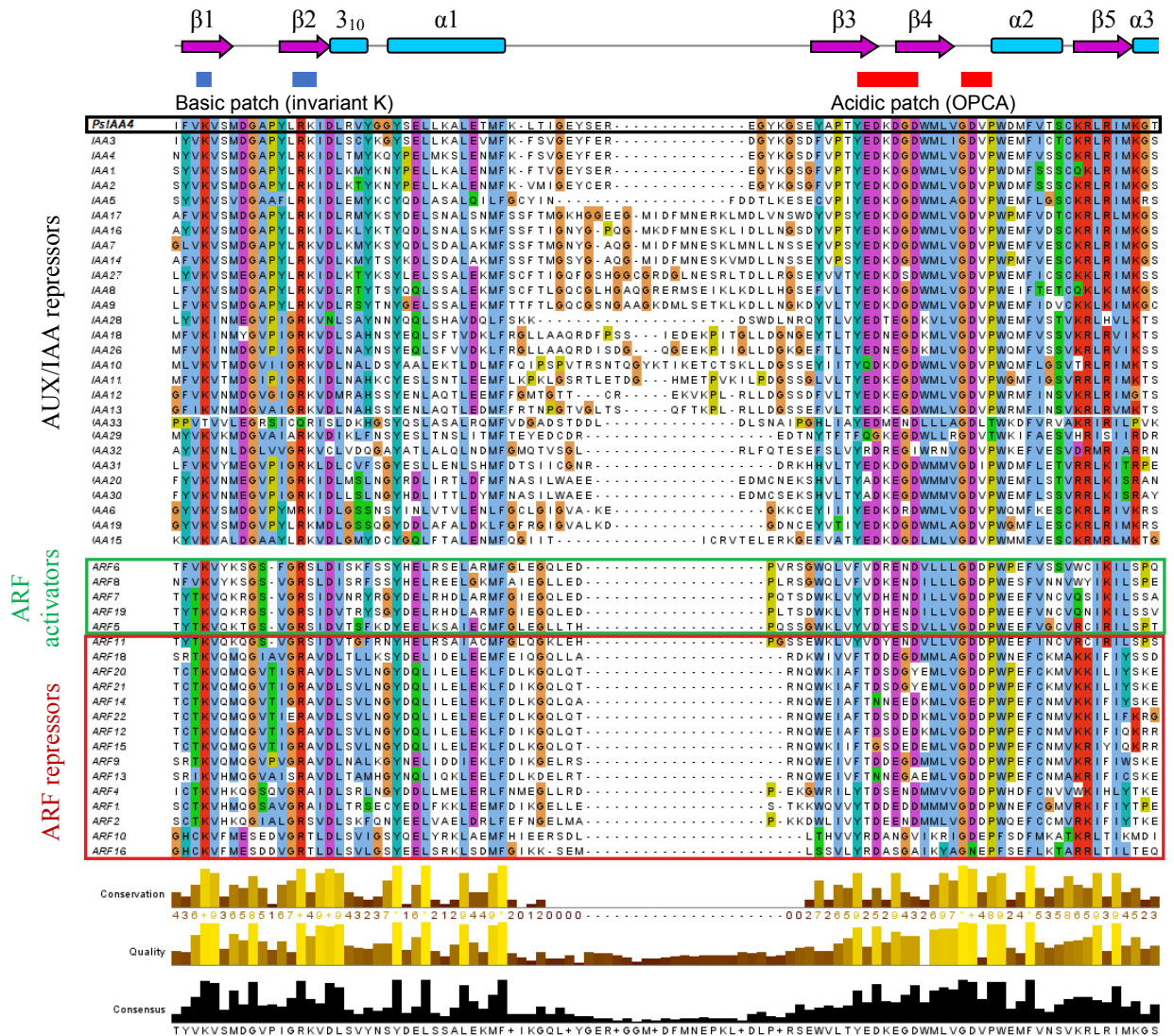


Figure 36: MSA of the PB1 domains of PsIAA4, AtAUX/IAA and AtARFs

The canonical features of type I/II PB1, the invariant K residue and OPCA motif, are marked as blue (basic patch) and red (acidic patch) bars on the top, respectively. The PsIAA4 PB1 sequence is shown in the black box. AtARF activators and repressors are shown in green and red box, respectively. Secondary structural elements are shown as magenta arrows for β -strand and cyan rectangles for α -helix. Conservation and consensus sequence are shown below the MSA generated and visualized using Jalview. Aligned residues are colored based on ClustalX format for differentiating conserved and non-conserved residues.

The overall distribution of charged residues and other special sequence signatures in AtARF activators further enhances its interaction with AtAUX/IAA repressors.

presence of a similar PB1 domain architecture, although the three polypeptides share low sequence identity (~26%). (C) Superimposed structures of PsIAA4 PB1 with AtAUX/IAA17 PB1 (pale gray; the insertion helix $\alpha 1'$ in olive green) show an additional alpha helix in the loop between DIII and DIV. (D) Superimposed C α trace of PsIAA4, AtAUX/IAA17, AtARF5 and AtARF7 PB1 domains are represented as an ENDscript sausage model, where the radius is proportional to the deviation of r.m.s between C α pairs per residue between structures. The coloring is based on the structure conservation, low (white) to high (red).

Superimposed solution structure of the PsIAA4 PB1 (PDB ID: 2M1M) on the crystal structures of AtARF5 PB1 (4CHK) and AtARF7 PB1 (4NJ6) show r.m.s.d values of 1.02 Å and 1.19 Å, respectively for the structured regions (Fig. 37A). The structural comparison of PB1 domains of available AUX/IAAs showed that AtAUX/IAA17 (PDB ID: 2MUK) has a loop connecting DIII and DIV, which contains an insertion of 13 residues (olive green in Fig. 37C), which folds into an additional α -helix ($\alpha 1'$) (Han et al., 2014), which is absent in PsIAA4 PB1 domain (Fig. 37C). Although the C-terminal $\alpha 3$ helix of AtAUX/IAA17 PB1 is oriented toward the $\alpha 1'$ helix, the typical β -grasp fold is not affected; thus, both AUX/IAA PB1 domains can be well superimposed (r.m.s.d. of 1.65 Å) (Fig. 37C). The overall r.m.s comparison of all available AtAUX/IAA and AtARF PB1 domain structures were performed using ENDscript server (Robert and Gouet, 2014). The r.m.s seems to be conserved in most of the regions of the structure, except a slight variation in the C-terminal $\beta 3$ and $\beta 4$ strands and are highly variable in loop connecting DIII and IV, and end loops (Fig. 37D).

The K96-centered motif of PsIAA4 forms a prominent ridge; the corresponding K114-centered patch on AtAUX/IAA17 is less compact, although it also includes part of the NLS conserved in AUX/IAAs (Fig. 38). This topologic difference, and a possible contribution of non-bonded contacts, may explain why replacement of more than one basic residue in PsIAA4 PB1 is required to abolish homotypic monomer interactions *in vivo* (Fig. 28) and *in vitro* (Fig. 30). Conversely, the density and distribution of negative charges (OPCA motif) are similar for both AUX/IAA PB1 domains. However, for AtAUX/IAA17 the acidic surface is considerably expanded and incorporates residue D118 (Fig. 38). Interestingly, the D118N mutation suppresses growth phenotypes caused by AtAUX/IAA17 protein stabilization, and Y2H analysis indicated that D118 is necessary for AtAUX/IAA17 homotypic and heterotypic (AtAUX/IAA3, AtARF5, and AtARF7) interactions (Rouse et al., 1998; Ouellet et al., 2001). As expected from the different PsIAA4 PB1 topology (Fig. 38), the corresponding PsIAA4 mutation (D100N) does not prevent homodimerization in yeast (Fig. A10), suggesting that the

AtAUX/IAA17 PB1 interaction face differs from PsIAA4 and closely related AtAUX/IAA1-4 PB1 domains (Dinesh et al., 2015).

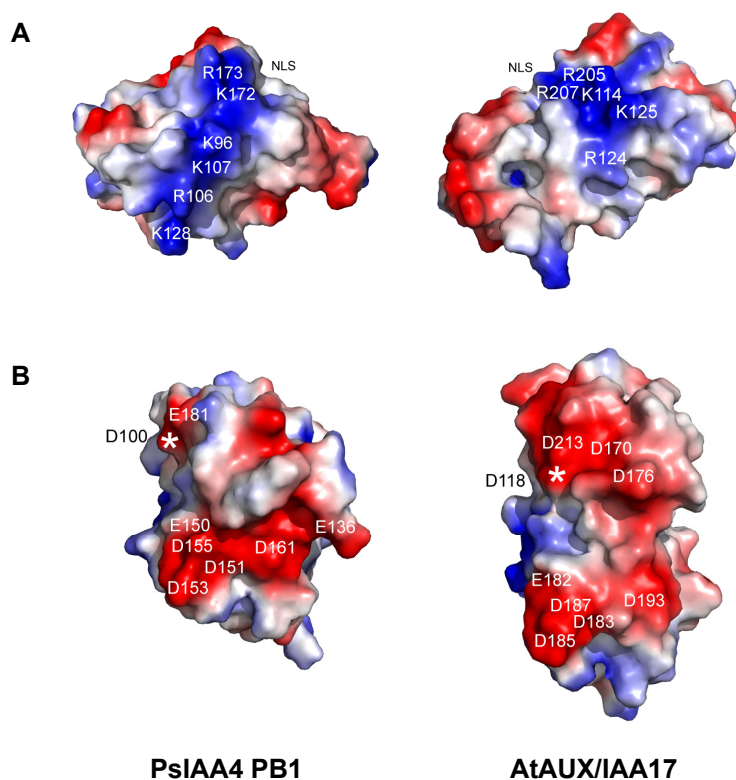


Figure 38: Comparison of PsIAA4 and AtAUX/IAA17 PB1 domains surface electrostatics

Overall electrostatic surface charges of the basic (A) and acidic (B) patches of PsIAA4 and AtAUX/IAA17 PB1 domains. Note that WT amino acid residues were reintroduced *in silico* into the NMR structure of the mutant AtAUX/IAA17 PB1 domain (Han et al., 2014). Amino acid residues K172/R173 (PsIAA4 PB1) and R205/R207 (AtAUX/IAA17 PB1) are the part of NLS, which are conserved in AUX/IAA proteins. The amino acid residues D118/D213, together with helix $\alpha 3$ (D170/D176), extends the acidic OPCA surface on AtAUX/IAA17 PB1 domain. The mutation of D118N (marked as asterisk in Fig. 38B) prevents homo-dimerization and hetero-dimerization of AtAUX/IAA17 in yeast (Ouellet et al., 2001).

4.3.3 Data-driven homodimer docking of PsIAA4 PB1

NMR-based mapping was used only to map the acidic interface between PsIAA4 PB1 homodimer. High Ambiguity Driven protein–protein DOCKing (HADDOCK) is one of the powerful tools for generating the protein structure complexes using experimental information. Using experimentally derived data from *in vitro* NMR mapping (Fig. 34) and *in vivo* Y2H analysis (Fig. 28) as ambiguous restraints, the PsIAA4 PB1 homodimer model was generated

from directed docking between two monomeric NMR structure ensembles (10 models). Later, interface residues were analyzed further and compared with other PB1 domain containing protein dimers. Data-driven protein–protein docking analyses were performed by using the HADDOCK server (Dominguez et al., 2003) for the refined modeling of the either interaction interfaces.

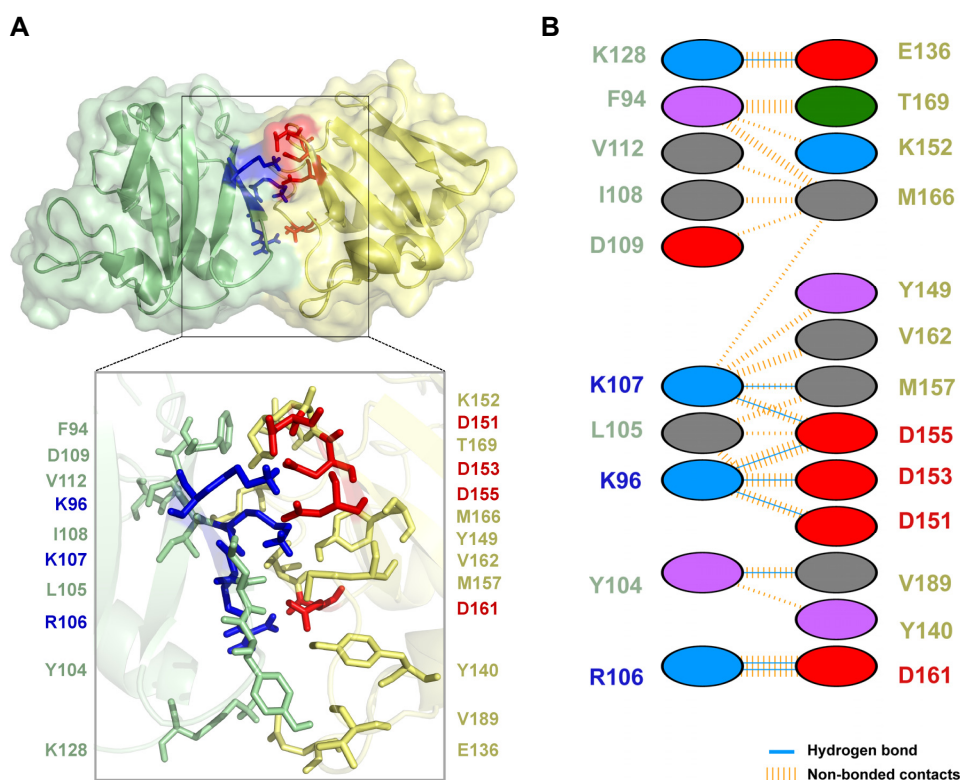


Figure 39: PsIAA4 PB1 HADDOCK dimer model and interface analysis

(A) A protein–protein docked model of the PsIAA4 PB1 homodimer was generated by HADDOCK using data from NMR acidic interface mapping and Y2H analysis. The model highlights canonical electrostatic interactions between the monomers (box). Conserved basic (blue) and acidic (red) residues are shown as sticks. The box below shows all interface residues (sticks) that interact via hydrogen bonds (blue and red) and nonbonded contacts (light green and yellow) (B) PsIAA4 PB1 homodimer model was analyzed by using PDBsum Generate, which was used to display additional interface residues and their interactions (hydrogen bonds and nonbonded contacts). These are depicted in a cartoon diagram together with the basic (K96, R106, and K107) and acidic (D151, D153, D155, and D161) amino acid residues of the canonical PB1 features. The thickness of nonbonded contacts is proportional to the number of atomic contacts.

HADDOCKing resulted in 11 clusters of 164 structures, which represent 82% of the generated water-refined model. The top 10 clusters with lowest Z-scores were used for selecting the four best structures from each for the detailed analysis of PsIAA4 PB1 homodimer models by using PDBsum Generate server (Laskowski et al., 1997). The best

PsIAA4 PB1 homodimer pose (Fig. 39A) resembles the closest available PB1 dimeric protein structures, including the AtARF5 PB1 homodimer, despite different sets of interface residues.

Further analysis pointed to an expanded interaction interface of the K96-centered (698 Å²) and OPCA (644 Å²) motifs. All together 23 interacting residues may engage in 9 hydrogen bonds and ~70 nonbonded contacts (Table 12). Notably, the center of either electrostatic surface ridge is intersected at a similar angle (~70°) by a stretch of hydrophobic and polar residues that are likely to be involved in nonbonded contacts, which thus, contribute to complementary surfaces for asymmetric homodimer formation (Fig. 39). Docking results provided a complete model about the PB1 complex and a detailed overview about the interaction interfaces.

4.3.4 Comparison of homodimer interfaces of PsIAA4 and AtARF5 PB1

The PB1 domain sequences of PsIAA4 and closely related *Arabidopsis* AUX/IAA proteins (Abel et al., 1995), and AtARF activators (Guilfoyle and Hagen, 2007) were aligned and analyzed. The MSA displayed a highly conserved invariant K residue (K96) in β 1, R residue in β 2 and the canonical acidic OPCA motif (D151, D153, D155, D161) at both flanks of β 4 (Fig. 40) found in both protein families. *In silico* generated homodimers of PsIAA4 PB1 were compared with the interaction interface of the crystal structure of AtARF5 PB1 dimer.

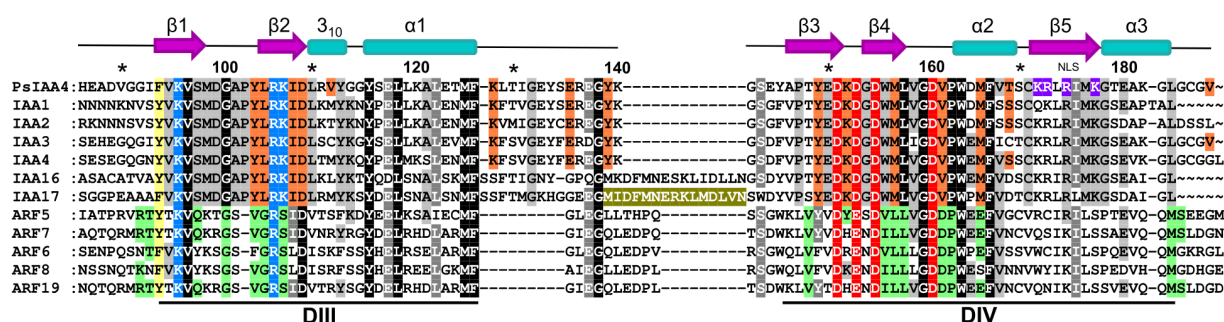


Figure 40: The MSA of PsIAA4 PB1, selected AtAUX/IAA and ARF PB1 domains

The PB1 domains sequence of PsIAA4, aligned with its closely related *Arabidopsis* AUX/IAAs (AtAUX/IAA1-4, AtAUX/IAA16 and AtAUX/IAA17), and ARF activators. The canonical features of type I/II PB1 are highlighted that includes basic (blue) and acidic OPCA motifs (red). The insertion helix α 1' of AtAUX/IAA17 is highlighted in olive green. Additional residues of the homodimeric interface of PsIAA4 PB1 (HADDOCK) and AtARF5 PB1 (X-ray structure) are indicated in orange and green, respectively. The

common aromatic interface residue in both groups are highlighted in yellow. Other conserved positions are highlighted in gray shades, if not part of the interaction face. The conserved C-terminal SV40-type NLS of PsIAA4 PB1 is shown in purple.

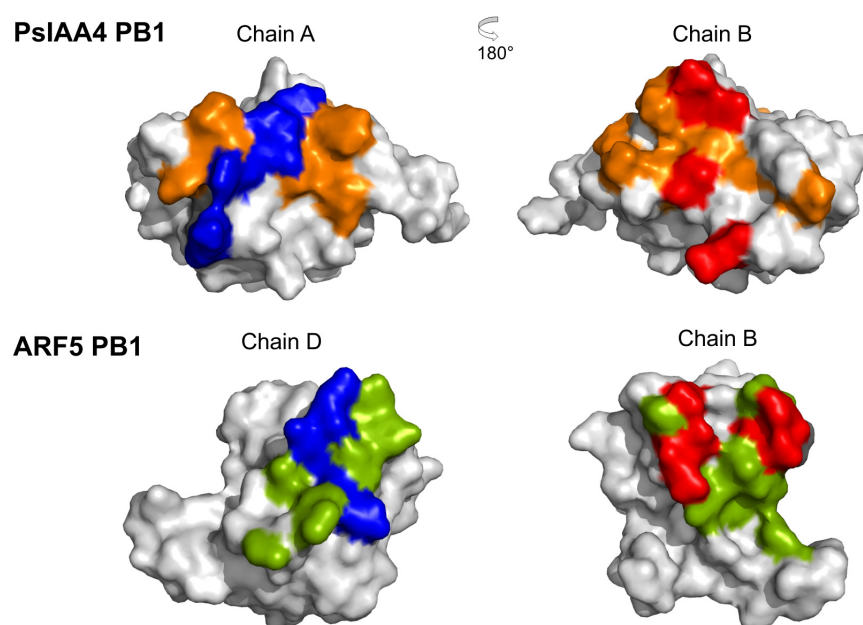


Figure 41: Interaction surfaces of the PsIAA4 and AtARF5 PB1 homodimers

Juxtaposed faces of the two monomeric structures (chains A and B) of PsIAA4 PB1 homodimer (upper panel) compared with its corresponding interfaces from the experimental AtARF5 PB1 domain (chains D and B) shown in lower panel. The basic and acidic surfaces contain residues which interact via hydrogen bonds are labeled in blue and red, respectively. Hydrophobic and polar residues forming nonbonded contacts are labeled in orange (PsIAA4 PB1) or green (AtARF5 PB1).

Interaction interface comparison of the experimentally determined AtARF5 PB1 and experimental data-driven *in silico* generated PsIAA4 PB1 homodimer illustrates that even though they possess the highly conserved charged residues, the other interacting residues are highly variable (Fig. 40 and Fig. 41). The list of interface statistics for PsIAA4 PB1 and AtARF5 PB1 were calculated using PDBsum Generate server summarized in Table 12 (Dinesh et al., 2015).

Table 12: Interface statistics for PsIAA4 PB1 and AtARF5 PB1

Structure (Method)	Chain	No. of residues	Area (Å ²)	Salt-bridge	S-S	H-bonds	Non-bonded contacts
PsIAA4 PB1 (NMR and HADDOCK)	A	10	698	-	-	9	~70
	B	13	644				
AtARF5 PB1 (X-ray)	D	14	567	-	-	12	81
	B	11	630				

Although electrostatic contacts and hydrogen bonds are critical for PB1 oligomerization, additional (non-bonded) contacts are likely responsible for the reported high specificity and affinity of modular interactions of PB1 domain proteins (Sumimoto et al., 2007; Dinesh et al., 2015), which may also confer specificity to intrafamily and interfamily interactions between AUX/IAA and ARF members.

5 DISCUSSION

In recent past, structural biology has gained enormous momentum and has become increasingly clear that the key players of nuclear auxin action are embedded in complex molecular networks. Furthermore, our current findings provide detailed structural insights into the nuclear auxin action. The current model of nuclear auxin action with all available structural models is shown in Fig. 42.

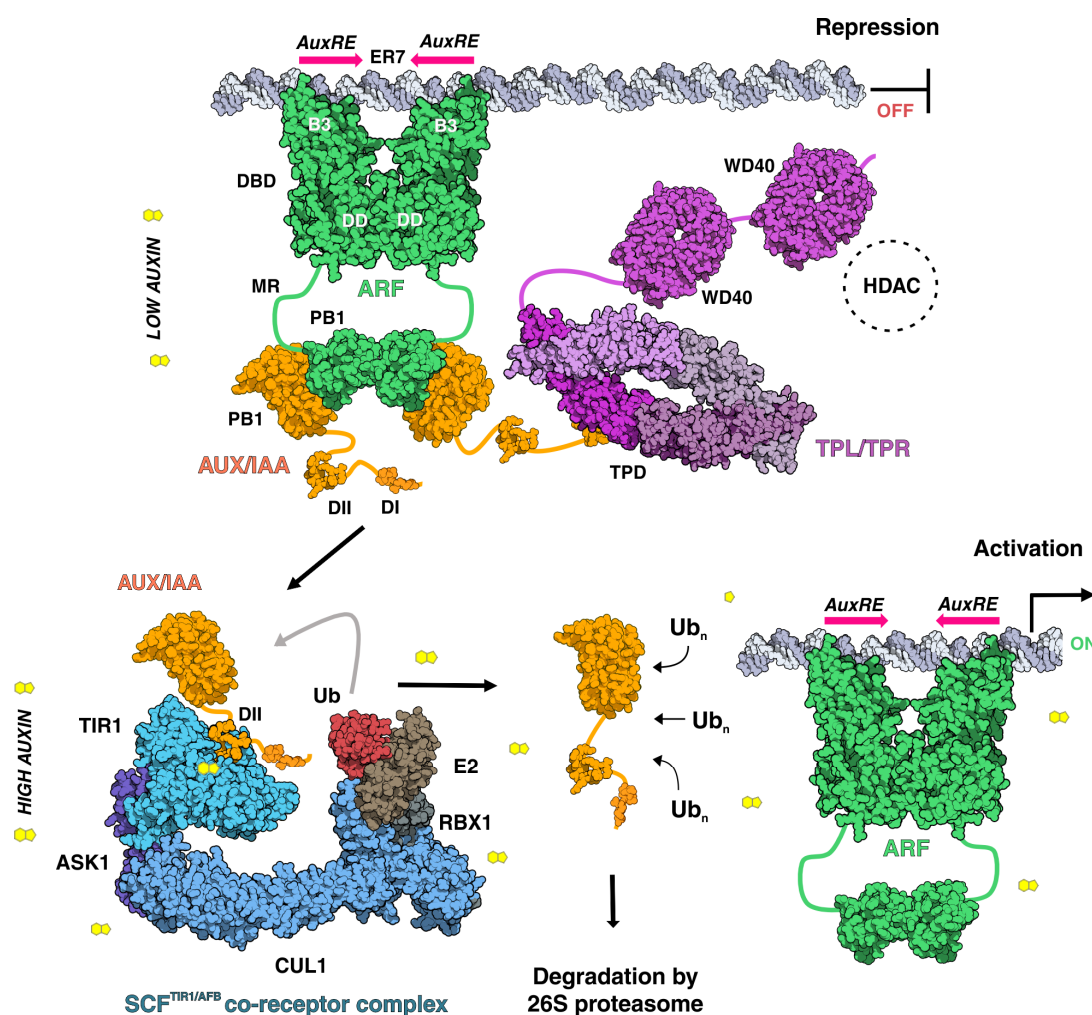


Figure 42: The current model of nuclear auxin response core module

(A) Under the low-auxin scenario, transcription of primary auxin genes is actively repressed by inactivation of promoter-bound ARF activators. In the composite model, the AtARF5 dimer (green) binds two everted TGTCTC motifs (*AuxRE*) separated by 7-bp (ER7 oligonucleotide) via its B3-type subdomains (Korasick et al., 2015b). Dimerization of the N-terminal AtARF5 DBD is mediated by the DD subdomain, and the C-terminal AtARF5 PB1 domain may further stabilize ARF5 dimerization (Boer et al., 2014). The ARF PB1 domain is also thought to mediate ARF oligomerization by directional

interactions (not shown) and ARF heteromerization with AUX/IAA repressors (orange) via the AUX/IAA PB1 domain (shown for AtAUX/IAA17 (Nanao et al., 2014)). The structure of the AtARF5 MR remains to be determined (green line). The AUX/IAA model also shows the fold of the AtAUX/IAA7 degron peptide (DII) (Ke et al., 2015) and the extended conformation of the AtAUX/IAA1 EAR motif (DI) (Tan et al., 2007). The structure of the connecting loop is not known (orange lines).

The PsIAA4 protein is encoded by a primary auxin response gene, which have long been a conceptual model for discovering the early auxin action in plants (Theologis, 1989; Abel and Theologis, 1996). Structural studies of these proteins had been hampered by its low solubility and formation of aggregates. In the current work, the PsIAA4 DIII/IV protein was heterologously expressed, purified and the high-resolution NMR structure was solved by protonation of charged surface patches at low pH. PsIAA4 DIII/IV adopts the ubiquitin-like β -grasp fold, which minimally deviates from the canonical type I/II PB1 protein-protein interaction domain (Dinesh et al., 2015). Following the release of the PsIAA4 DIII/IV NMR structure in PDB (2M1M), several other homologous structures from *Arabidopsis* ARF5, ARF7, and AUX/IAA17 C-terminal DIII/IV were deposited in PDB (Han et al., 2014; Nanao et al., 2014; Korasick et al., 2015a). These *Arabidopsis* structures also revealed similar canonical type I/II PB1 domain features forming charged surface patches on opposite faces mediating electrostatic front-to-back interaction of monomers resulting in an oligomer (Han et al., 2014; Nanao et al., 2014; Dinesh et al., 2015; Guilfoyle, 2015; Korasick et al., 2015a).

5.1 Structural comparison of AUX/IAA and ARF PB1 domains

The solution structure of the WT PsIAA4 DIII/IV monomer was determined at pH 2.5, which suppresses homo-oligomerization *in vitro*. Even at this low pH, PsIAA4 DIII/IV displays the topology of a globular ubiquitin-like β -grasp fold that closely matches the structure of PB1 domain containing proteins, NBR1 (Muller et al., 2006) and recently solved WT AtARF5 PB1 structures (Fig. 26 and Fig. 37) (Nanao et al., 2014). Additionally, structures of the charge-neutralized mutant of AtARF7 PB1 and AtAUX/IAA17 PB1 also displayed similar topology (Fig. 37) (Korasick et al., 2014; Han et al., 2014). The overall structure of AtAUX/IAA and AtARF PB1 domains are comparable to the PB1 domain structure found in other organisms (Sumimoto et al., 2007), with an additional α 3-helix at the C-terminal end or α 1'-helix between domain III and IV. The function of both helices (α 1' and α 3) are unknown; however, they obstruct neither the canonical PB1 fold nor its propensity for protein-protein

interaction (Han et al., 2014). The characteristic features of the well-defined type I/II PB1 domain of PsIAA4 contains a distinct basic (invariant K96) and an acidic (D-X-D/E-X-D-X₄-G-D or OPCA) motifs which are displayed as a surface patch on the structure. These features mediate directional self-assembly *in vitro*, which is disrupted either by protonation of OPCA residues (pH 2.5) or by introducing mutations on any of the charged patches rendering the protein stable at neutral pH (Fig. 13 and Fig. 30). Similarly, the structure-function studies of *Arabidopsis* ARF5, ARF7 and AUX/IAA17 PB1 domains from other laboratories also revealed the presence of both the acidic and basic charged faces (type I/II), which mediate homotypic as well as heterotypic front-to-back interactions (Han et al., 2014; Korasick et al., 2014; Nanao et al., 2014). The presence of type I/II PB1 domain is a typical feature in most of the *Arabidopsis* AUX/IAA and ARF proteins with an exception in few cases, for e.g., AtAUX/IAA33-type I (refer experimental details in Appendix 7.12) and AtARF10, 13, 16-type II, in which either one of the charged patches is absent or disturbed. The mutation of at least two residues from the charged patches of PsIAA4 PB1 domain abolished the homo-oligomerization as revealed by *in vivo* Y2H assays (Fig. 28), supporting the importance of the front-to-back mode of interaction in the PsIAA4 FL protein. Even though, there are four structures of PB1 domains in AUX/IAA and ARF family currently studied, the major residues involved in conferring the specificity of interaction between them are not well understood.

5.2 Comparison of AUX/IAA and ARF homo- and heterotypic interactions

The C-terminal PB1 domain containing region of AUX/IAAs and ARFs is responsible for homo- and hetero-oligomerization using conserved charged residues and unique conserved surface residues (Ogura et al., 2009). The specificity of these versatile combinations is likely determined by additional contacts surrounding the core set of electrostatic interactions to fine-tune auxin response (Dinesh et al., 2015; Korasick et al., 2015). This is suggested by the broad range of PB1 domain affinities determined for AtAUX/IAA17 and PsIAA4 self-interaction (each $K_D \sim 6.5 \mu\text{M}$), AtARF5 and AtARF7 homodimerization ($K_D \sim 0.2\text{-}0.9 \mu\text{M}$), and AtARF5:AtAUX/IAA17 heterodimerization ($K_D \sim 0.07 \mu\text{M}$), which cover almost two orders of magnitude (Han et al., 2014; Korasick et al., 2015). Interestingly, the reported binding constants for AtAUX/IAA17 and PsIAA4 PB1 self-interaction are remarkably similar, yet enthalpy and entropy changes are quite different for each association, which is likely a consequence of clear topologic differences between either AUX/IAA PB1 interface

(Han et al., 2014; Dinesh et al., 2015). A refined thermodynamic and structural analysis of the AtARF7 PB1 interface showed that electrostatic force drives AtARF7 PB1 dimerization between the invariant K and the main cluster of acidic residues in the OPCA motif. Furthermore, it is also driven by electrostatic interactions of a second set of charged residues, which include a conserved R on the basic face and a minor cluster of conserved acidic residues on the OPCA face (Korasick et al., 2015) (Fig. 39, Fig. 43 and Fig. 44). Residues of these two PB1 dimer-stabilizing “electrostatic prongs” (Korasick et al., 2015), which are also evident in the PsIAA4 and AtARF5 PB1 dimerization interface (Nanao et al., 2014; Dinesh et al., 2015), are conserved in AtARF and AtAUX/IAA PB1 domains and thought to facilitate intra- and interfamilial protein-protein interactions of *Arabidopsis* ARF and AUX/IAA members (Korasick et al., 2015). The type I/II PB1 interaction modus was further validated *in vivo* by yeast two-hybrid assays (Korasick et al., 2014; Nanao et al., 2014; Dinesh et al., 2015) and *in planta* showing the importance of PB1 mediated multimerization for the control of ARF function in auxin signaling (Nanao et al., 2014; Korasick et al., 2014). A systematic Y2H analysis of the AtAUX/IAA PB1 and AtARF PB1 interactome indicated very limited AtARF PB1 dimerization, frequent AtAUX/IAA PB1 homo- and heterodimerization, and preferential interaction of AUX/IAAs with ARF activators (Fig. 9A) (Vernoux et al., 2011a). The latter observation was also confirmed by interrogating full-length AtARF and AtAUX/IAA proteins in yeast (Fig. 9B and Fig. 9C) (Piya et al., 2014). The high affinity and complexity of PB1 domain multimerization highlights the need for post-translational control of ARF:AUX/IAA interactions to fine-tune auxin responses.

The PB1 domains of some AUX/IAA and ARF proteins may be classified as type I or type II and could thus terminate multimerization if incorporated as a capping subunit into a growing chain (Overvoorde et al., 2005). These scaffold-like complexes may acquire additional subunits via noncanonical PB1 interactions for enabling specificity and fidelity in signal transduction (Sumimoto et al., 2007). An interesting feature of type I/II PB1 domains is their intrinsic potential to form helical filaments by polymerization with significant curvature and pitch variation. This ability was recently reported in mammals for the PB1-containing, signaling scaffold protein p62/SQSTM1 (Ciuffa et al., 2015) or for the PB1-like domain protein Par-3 (Feng et al., 2007; Zhang et al., 2013). Therefore, it can be speculated that long helical polymers composed of various ARF and AUX/IAA proteins provide rotationally

shifted ‘molecular caliper’ arrangements for recognizing multiple and more distantly positioned composite *AuxREs* in auxin-regulated promoters.

5.3 Comparison of interaction interfaces of AtAUX/IAA and AtARF PB1s

Interface mapping of the arrested PsIAA4 PB1 dimer by NMR titration followed by data-driven homodimer docking indicated that hydrophobic and polar residues, which contribute to directional PB1 interactions (Fig. 39), possibly expanding both interaction interfaces. Interestingly, the PsIAA4 PB1 homodimer interface is comparable with the experimentally determined interface of the WT AtARF5 PB1 homodimer (Nanao et al., 2014) (Fig. 41 and Table 12).

The homodimeric interfaces of AtAUX/IAA17 and AtARF5 PB1 are unique in charge density and distribution. Because the AtAUX/IAA17 PB1 interface is not significantly altered upon interaction with AtARF5 PB1, optimal combinations of complementary bonded and non-bonded contacts are presumably major specificity determinants of AtAUX/IAA and AtARF PB1 domain interactions (Han et al., 2014). This finding suggests that, in addition to electrostatic interactions between the basic K96 and acidic OPCA motifs, other types of contact contribute to the PsIAA4 PB1 homodimerization (Dinesh et al., 2015).

The interface residues conferring specificity likely vary between phylogenetic clades of both families (Fig. 36) and may thus determine combinatorial specificity of AUX/IAA-ARF interactions. For example, in Y2H assays, the 29 AtAUX/IAA proteins often homodimerize and heterodimerize and interact preferentially with the 5 AtARF activators, whereas the 15 PB1 domain-containing AtARF repressors show no or very limited interactions within this network (Vernoux et al., 2011; Piya et al., 2014). Sequence logos generated for all *Arabidopsis* AUX/IAAs and ARFs together illustrate the core and family-specific residues on both acidic and basic interfaces (Fig. 43 and Fig. 44). The highly conserved charged and other interface residues on the surface of PsIAA4 PB1 structure was comprehensively compared with the corresponding homologous structures of *Arabidopsis* AUX/IAA17 and ARF5 and ARF7 (Fig. 43 and Fig. 44). Even though, they contain highly conserved core residues between the families, they also contain family specific residues, which might be responsible for its specificity.

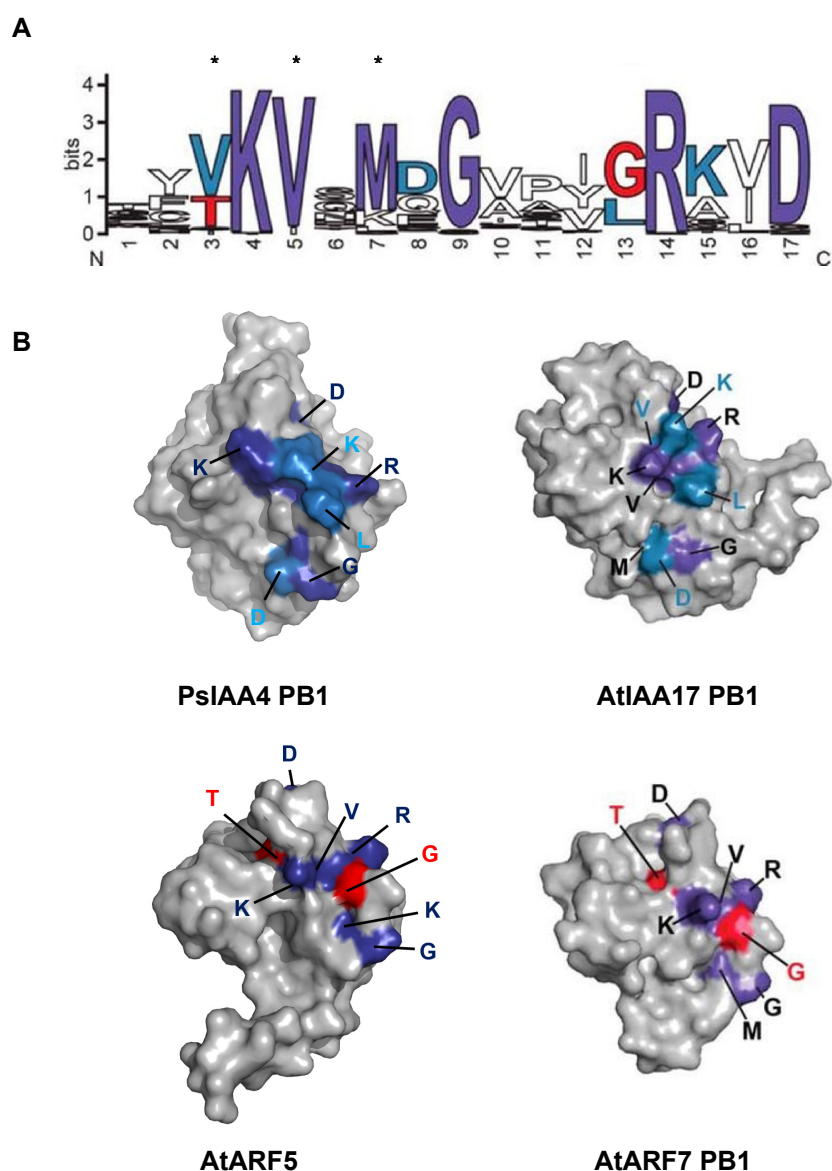


Figure 43: AUX/IAAs and ARFs core and family-specific residues at the basic interface

The NMR solution structure of PsIAA4 PB1 (PDB ID: 2M1M) and AtAUX/IAA17 PB1 (PDB ID: 2MUK) in comparison with the X-ray structure of AtARF5 PB1 (PDB ID: 4CHK) and AtARF7 PB1 (PDB ID: 4NJ6) are represented as surface models with highlighted areas of sequence conservation. Residues conserved in ARF (red), AUX/IAA (light blue), and in both ARF and AUX/IAA (purple) are shaded as indicated. (A) Amino acid sequence logo showing conservation of residues on the ARF and AUX/IAA PB1 domain basic faces. (B) Surface view of the PsIAA4, AtAUX/IAA17, AtARF5, AtARF7 PB1 basic face. AtARF5, AtAUX/IAA17 PB1 structural representations and sequence logos were adapted from (Korasick et al., 2015). Astericks (*) denotes residues missing on the surface of PsIAA4 PB1.

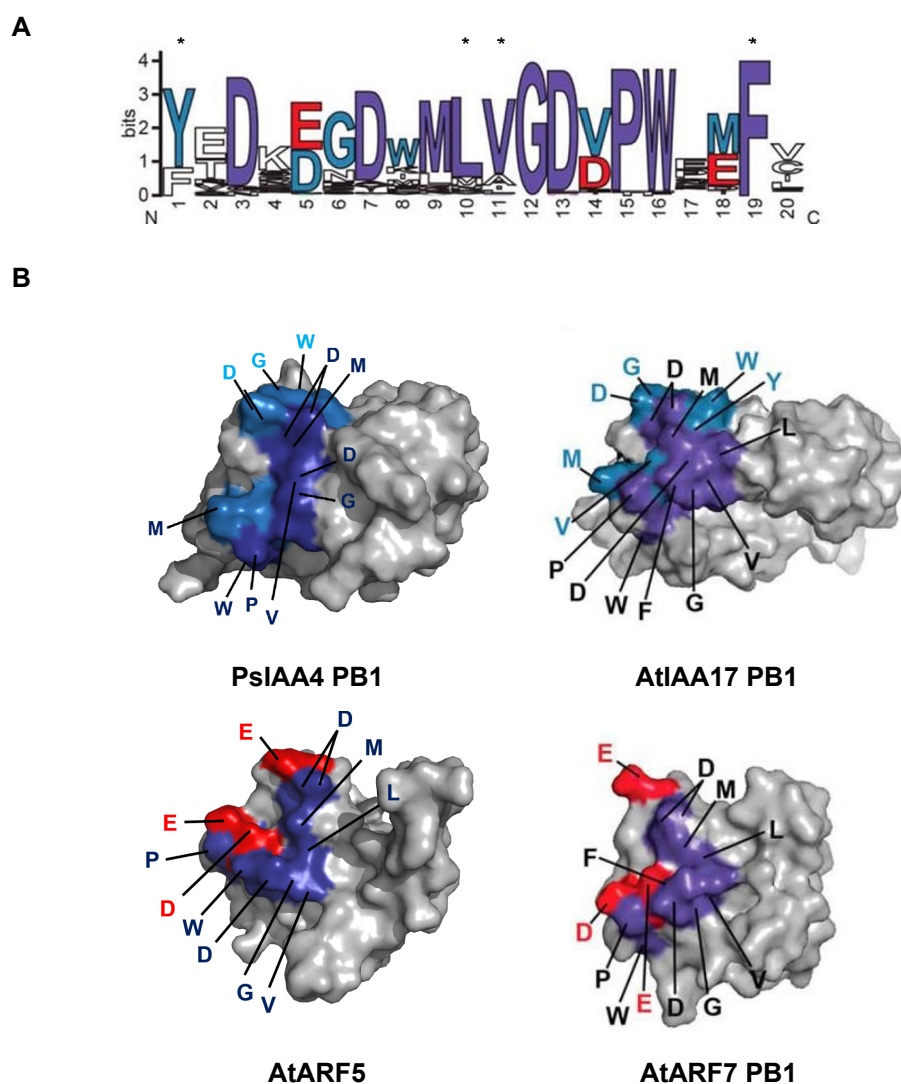


Figure 44: AUX/IAAs and ARFs core and family-specific residues at the acidic interface

The NMR solution structure of PsIAA4 PB1 (PDB ID: 2M1M) and AtAUX/IAA17 PB1 (PDB ID: 2MUK) in comparison with the X-ray structure of AtARF5 PB1 (PDB ID: 4CHK) and AtARF7 PB1 (PDB ID: 4NJ6) are represented as surface models with highlighted areas of sequence conservation. Residues conserved in ARF (red), AUX/IAA (light blue), and in both ARF and AUX/IAA (purple) are shaded as indicated. (A) Amino acid sequence logo showing conservation of residues on the ARF and AUX/IAA PB1 domain acidic faces. (B) Surface view of the PsIAA4, AtAUX/IAA17, AtARF5, AtARF7 PB1 acidic face. AtARF5 PB1, AtAUX/IAA17 PB1 structural representations and sequence logos were adapted from (Korasick et al., 2015). Asterisks (*) denotes residues missing on the surface of PsIAA4 PB1.

5.4 AUX/IAA and ARF PB1 domain interacts with other proteins

The assembly state of p62/SQSTM1 is affected and likely regulated by multiple post-translational modifications, including phosphorylation by cAMP-dependent protein kinase at a serine residue on the basic face of its PB1 domain, which disrupts homopolymerization and p62 interaction with OPCA motif-containing PB1 domains (Christian et al., 2014). A recent study showed that the brassinosteroid-regulated GSK3-like kinase BRASSINOSTEROID-INSENSITIVE2 (BIN2) phosphorylates AtARF7 and AtARF19 activators, which suppresses their interaction with AUX/IAAs, facilitates AUX/IAA degradation, and enhances ARF DNA binding and target gene activation (Cho et al., 2014). BIN2 phosphorylates two serine residues in the Q-rich middle region of AtARF7; however, it is not clear how this modification disrupts AtARF7 interaction with AtAUX/IAAs. BIN2 also phosphorylates AtARF2, which inhibits the repressor activity of AtARF2 by preventing its binding to *AuxREs* presumably in competition with ARF activators (Vert et al., 2008). Thus, BIN2-dependent phosphorylation of ARF activators and repressors potentiates auxin response and provides a node for signal integration (Hill, 2015). Evidence for AUX/IAA phosphorylation and its relevance is very limited (Colon-Carmona et al., 2000). However, it is of note that clades of *Arabidopsis* ARF and AUX/IAA proteins feature conserved T or S residues near the invariant K of the basic PB1 face. The high affinity and complexity of PB1 domain multimerization highlights the need for post-translational control of ARF:AUX/IAA interactions to fine-tune auxin responses. In addition to the canonical PB1 domain-mediated interactions of ARF and AUX/IAA proteins, members of both families can recruit other transcription factors. For example, at least some ARFs have been reported or implicated to specifically interact with members of the MYB family (MYB77) (Shin et al., 2007), the bHLH family (BIGPETAL, PIF4) (Varaud et al., 2011; Oh et al., 2014), the bZIP family (bZIP11) (Weiste and Droge-Laser, 2014) or with plant-specific transcriptional regulators such as BZR1/BZR2 (Walcher and Nemhauser, 2012; Oh et al., 2014) or BRX (Scacchi et al., 2010). Sunflower (*Helianthus annuus*) HaIAA27 interacts with heat-shock TF HaHSF9 protein during seed development. Domains III/IV or the middle region of ARFs is required for these interactions, which often support co-operative recognition of promoter elements and likely integrate auxin response with other signaling pathways, as best understood for the auxin-brassinosteroid crosstalk (Hill 2015).

Therefore, the modular PB1 domain is well suited to assemble assorted protein complexes via directional (hetero)oligomerization (type I/II) and chain termination (type I or type II). These scaffold-like complexes may acquire additional subunits by noncanonical PB1 interactions for enabling specificity and fidelity of signal transduction pathways (Sumimoto et al., 2007). It is of note that DIII/IV of certain AUX/IAA and ARF proteins has been reported to interact with other transcription factors (Guilfoyle and Hagen, 2012) and that AUX/IAA multimerization with ARF activators is likely necessary for repressor function *in planta*, possibly by disrupting the cooperative binding of ARF oligomers to *AuxREs* (Boer et al., 2014; Korasick et al., 2014; Nanao et al., 2014).

6 CONCLUSION

This research work reports the high-resolution NMR structure of wild-type domain III/IV of PsIAA4 from pea (*Pisum sativum*), a pioneering experimental system for exploring AUX/IAA function in auxin action. Moreover, mutational studies identified the amino acid residues that engage in directional interaction of monomers, largely via hydrogen bonds between conserved basic and acidic surface patches. Protein-protein interaction interfaces of PsIAA4 PB1 homodimer were identified by NMR mapping (acidic interface) and subsequent *in silico* docking studies using experimental data revealed basic interface of the other interacting monomer. Thus, the solution structure of wild-type PsIAA4 PB1 (Dinesh et al., 2015), together with the recently solved *Arabidopsis* ARF and AUX/IAA PB1 structures (Han et al., 2014; Korasick et al., 2014; Nanao et al., 2014), provide a framework for elucidating the structural rules of intricate interactions between members of the two central families of transcription factors in early auxin action.

Open questions:

What are the precise structural determinants that promote selective interactions between ARF activators and AUX/IAA repressors via their PB1 domains?

What is the extent (composition, stoichiometry) and *in vivo* significance of PB1-mediated multimerization of ARFs and AUX/IAAs?

Are helical PB1 scaffolds formed for distant *AuxRE* recognition, which further integrate other PB1 domain-containing proteins?

How the formation of ARF:AUX/IAA complexes is regulated by post-translational modifications, such as phosphorylation or ubiquitylation?

Recent advances in the field of auxin research along with the combination of molecular and structural biology techniques will definitely pave a way to unravel the foresaid questions in the near future.

7 APPENDICES

7.1 Selection of an AUX/IAA protein for the structure-function studies

The C-terminally 6X His-tagged AtAUX/IAA1 DIII (63-122), AtAUX/IAA3 DIII (80-133), PsIAA4 DIII/IV (86-189) and PsIAA4 full length (FL) proteins in pQE expression system were initially expressed and purified in small (3 mL) batches (Fig. A1). The PsIAA4 DIII/IV truncated protein which contains the complete C-terminal structured region (based on Phyre2 prediction) was selected from the expression and purification screening.

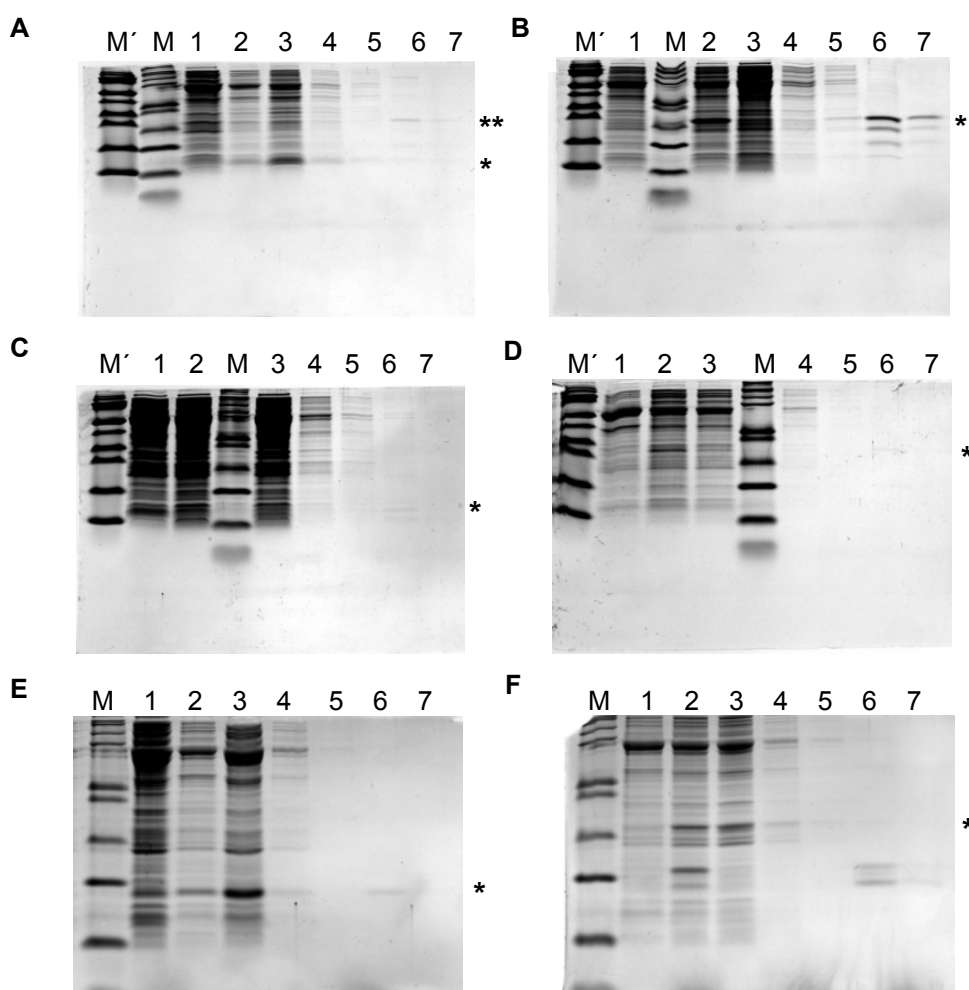


Figure A1: Expression and purification analyses of selected AUX/IAAs

Small batches (3 mL) of protein expression and purification analyzed in SDS-PAGE (A) AtAUX/IAA1 DIII, (B) AtAUX/IAA1 FL (C) AtAUX/IAA3 DIII, (D) AtAUX/IAA3 FL, (E) PsIAA4 DIII/IV and (F) PsIAA4 FL. Lanes, 1: before induction, 2: after induction, 3: Flow through, 4: Wash 100mM Imidazole, 6 and 7: Elution fractions. Single asterisks (*) represents a monomer and double (**) for a dimer. Protein markers, M: Mark12™ Unstained ladder, 2.5 to 200 kDa and M'- PageRuler Prestained, 10 to 180 kDa.

7.2 Large scale purification of selected IAAs

Selected AtAUX/IAA1 DIII, AtAUX/IAA1 FL, PsIAA4 DIII/IV and PsIAA4 FL protein were expressed and purified using IMAC. Both truncated and FL AtAUX/IAA3 showed dimerization behavior, even in a denaturing SDS-PAGE. AtAUX/IAA3 FL exhibit increased degradation compared to truncated ones. Finally, PsIAA4 DIII/IV (AAs 86-189, 12.5 kDa) was selected for the structure-function studies. PsIAA4 FL was also highly unstable, which usually dimerize and degrade (Fig. A2).

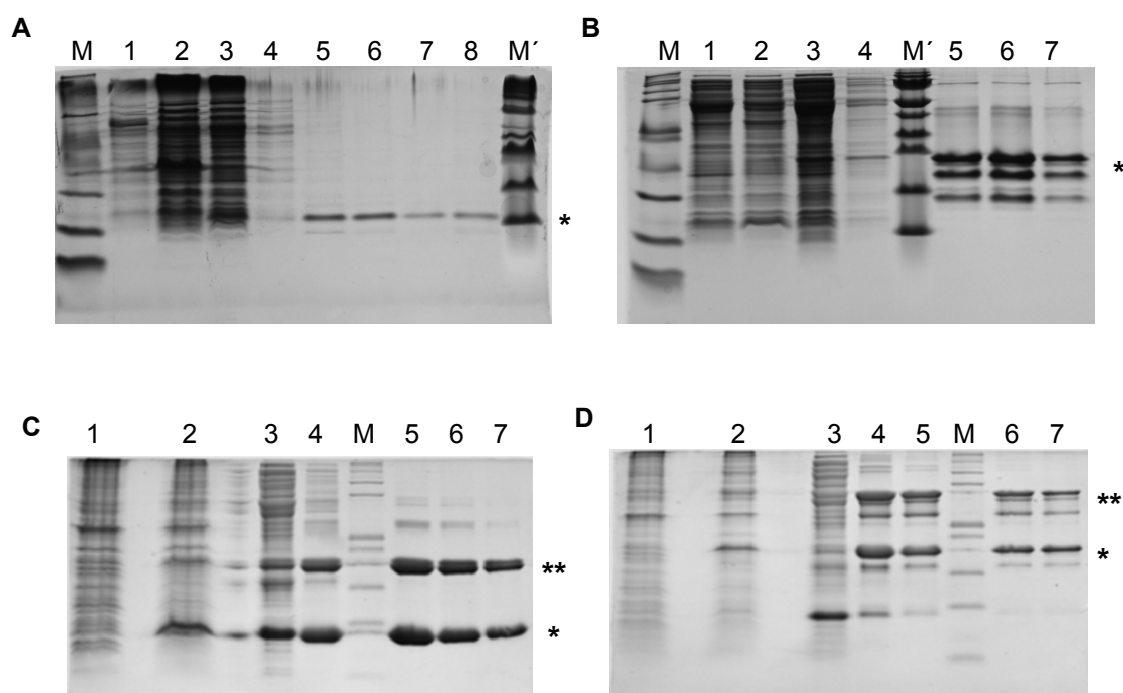


Figure A2: Large scale batch purification and optimization of AUX/IAAs

12% SDS-PAGE gel: expression and purification (1 L) of (A) AtAUX/IAA1 DIII, (B) AtAUX/IAA1 FL, (C) PsIAA4 DIII/IV, and (D) PsIAA4 FL. Lanes, 1: before induction, 2: after induction, 3: Flow through, 4: Wash 100mM Imidazole, 5, 6, 7 (8): Elution fractions. Protein markers: M : Mark12™ unstained standard, 2.5 to 200 kDa, prestained marker and M' : PageRuler prestained protein ladder, 10 to 180 kDa.

7.3 CD spectral comparison of AtAUX/IAA1 DIII and PsIAA4 DIII/IV

CD spectra were recorded for AtAUX/IAA3 DIII and PsIAA4 DIII/IV proteins at low concentration and around neutral pH conditions. Spectral comparison of PsIAA4 DIII/IV (maroon) and AtAUX/IAA1 DIII (blue) showed the presence of the mixed secondary structural elements. PsIAA4 DIII/IV spectrum displayed a deeper dip for the minima at 208 nm because of presence of more secondary structural elements in DIV (Fig. A3).

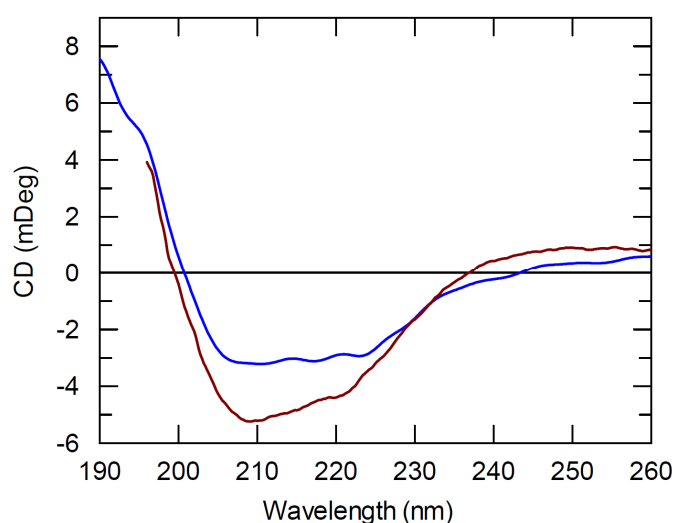


Figure A3: CD spectra of AtAUX/IAA1 DIII and PsIAA4 DIII/IV

Overlaid spectra of AtAUX/IAA1 DIII (blue) and PsIAA4 DIII/IV (maroon). Measured millidegrees were plotted against the wavelength (190-260 nm).

7.4 Sequence information of the WT PsIAA4 DIII/IV fusion protein

```

  90      100      110      120      130      140
HEADVGGIFV KVSMDGAPYL RKIDLRVYGG YSELLKALET MFKLTIGEYS EREGYKGSEY
 150      160      170      180      190
APTYEDKDGD WMLVGDVPWD MFVTSCKRLR IMKGTEAKGL GCGVGSHHHH HH

```

Number of AAs: 112

Molecular weight: 12608.3

Theoretical pI: 6.15

Extinction coefficient = 21430 ($\text{M}^{-1} \text{cm}^{-1}$, at 280 nm measured in water)

Absorbance 0.1% (=1 g/l) 1.700, assuming all Cys residues are reduced

Table A1: The residue number and a three-letter AA code of the PsIAA4 DIII/IV

86	HIS	104	TYR	122	ALA	140	TYR	158	LEU	176	ILE
87	GLU	105	LEU	123	LEU	141	LYS	159	VAL	177	MET
88	ALA	106	ARG	124	GLU	142	GLY	160	GLY	178	LYS
89	ASP	107	LYS	125	THR	143	SER	161	ASP	179	GLY
90	VAL	108	ILE	126	MET	144	GLU	162	VAL	180	THR
91	GLY	109	ASP	127	PHE	145	TYR	163	PRO	181	GLU
92	GLY	110	LEU	128	LYS	146	ALA	164	TRP	182	ALA
93	ILE	111	ARG	129	LEU	147	PRO	165	ASP	183	LYS
94	PHE	112	VAL	130	THR	148	THR	166	MET	184	GLY
95	VAL	113	TYR	131	ILE	149	TYR	167	PHE	185	LEU
96	LYS	114	GLY	132	GLY	150	GLU	168	VAL	186	GLY
97	VAL	115	GLY	133	GLU	151	ASP	169	THR	187	CYS
98	SER	116	TYR	134	TYR	152	LYS	170	SER	188	GLY
99	MET	117	SER	135	SER	153	ASP	171	CYS	189	VAL
100	ASP	118	GLU	136	GLU	154	GLY	172	LYS	190	GLY
101	GLY	119	LEU	137	ARG	155	ASP	173	ARG	191	SER
102	ALA	120	LEU	138	GLU	156	TRP	174	LEU	192	HIS
103	PRO	121	LYS	139	GLY	157	MET	175	ARG		

Table A2: Total amino acid composition of the PsIAA4 DIII/IV

A	ALA	5	4.5%	M	MET	5	4.5%
C	CYS	2	1.8%	N	ASN	0	0.0%
D	ASP	8	7.1%	P	PRO	3	2.7%
E	GLU	9	8.0%	Q	GLN	0	0.0%
F	PHE	3	2.7%	R	ARG	5	4.5%
G	GLY	15	13.4%	S	SER	6	5.4%
H	HIS	7	6.2%	T	THR	5	4.5%
I	ILE	4	3.6%	V	VAL	8	7.1%
K	LYS	9	8.0%	W	TRP	2	1.8%
L	LEU	9	8.0%	Y	TYR	7	6.2%

7.5 The high salt analyses of the PsIAA4 DIII/IV at neutral pH

The PsIAA4 DIII/IV remained as a monomeric species at very high salt concentration, which explains that the major interaction between monomers are electrostatics. Average molecular mass of PsIAA4 DIII/IV was determined by sedimentation equilibrium. Analytical ultracentrifugation studies of purified PsIAA4 DIII/IV protein were carried out at 20°C, and data were collected at a rotor speed of 14,000 rpm (refer Materials and Methods).

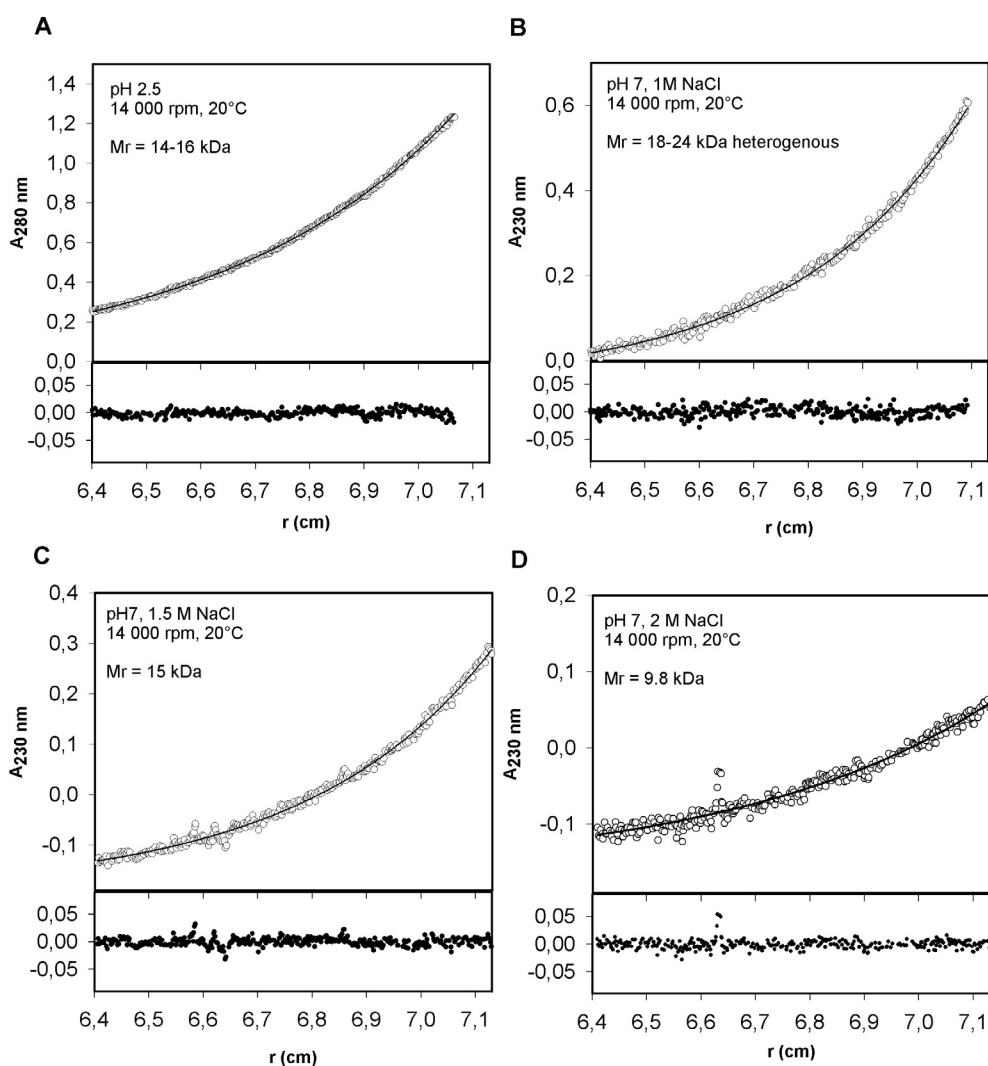


Figure A4: Comparison of sedimentation analysis of the PsIAA4 DIII/IV

(A) PsIAA4 DIII/IV exists as a monomeric species (14-16 kDa) at pH 2.5 and (B-D) PsIAA4 DIII/IV also exists as a monomeric species at pH 7 with very high salt concentration (1.0-2.0 M). Upper panel shows the experimental data, and lower panel shows the residuals.

7.6 Sequential walk on 3D HNCA strips of the PsIAA4 DIII/IV

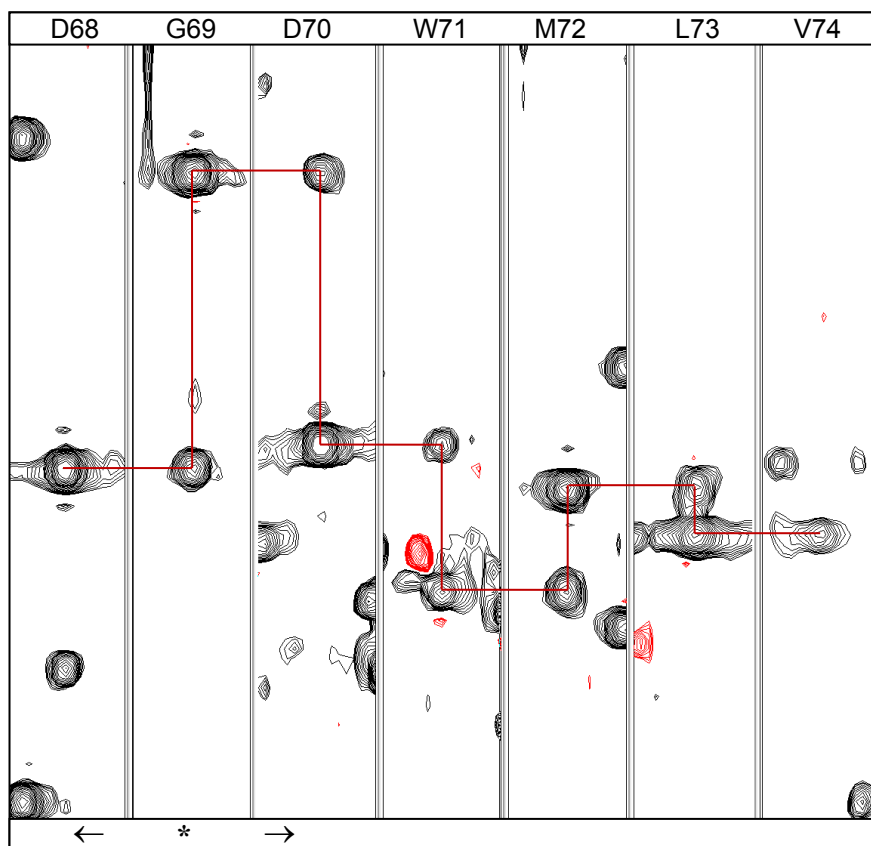


Figure A5: ^{13}C strip-plot of the 3D HNCA ($\text{C}\alpha$) from PsIAA4 DIII/IV

Strip-plot showed $\text{C}\alpha$ (black) cross peaks of its own (i) and preceding (i-1) residue. Sequential connectivities were obtained by connecting i, i-1 and i+1 residue signals. G69 (*) strip was used as a landmark for a sequential walk on either side (arrows).

Table A3: TALOS+ torsion angle restraints

NO.	RES	PHI	PSI	DPHI	DPSI	DIST	S2	COUNT	CLASS
86	H	0	0	0.000	0.000	0.000	0.062	0	None
87	E	-114.000	144.000	52.000	21.000	58.170	0.105	10	Dyn
88	A	-78.340	145.712	47.912	37.813	35.261	0.174	10	Dyn
89	D	-110.569	116.743	69.933	31.645	35.515	0.274	8	Dyn
90	V	-75.400	161.227	60.762	49.573	42.327	0.359	6	Dyn
91	G	-178.552	176.136	87.307	32.083	45.013	0.475	7	Dyn
92	G	88.000	-3.000	12.000	16.000	46.950	0.612	5	Warn
93	I	-105.000	142.000	29.000	34.000	41.510	0.749	10	Good
94	F	-101.000	148.000	23.000	11.000	37.040	0.829	10	Good
95	V	-136.000	157.000	13.000	11.000	37.210	0.884	10	Good
96	K	-121.000	143.000	27.000	11.000	41.900	0.886	10	Good
97	V	-130.000	147.000	13.000	17.000	40.720	0.891	10	Good
98	S	-118.000	157.000	28.000	19.000	80.650	0.885	10	Good
99	M	-115.000	149.000	71.000	23.000	95.090	0.882	10	Good
100	D	-80.000	130.000	23.000	13.000	86.890	0.851	10	Good
101	G	77.000	7.000	9.000	11.000	80.440	0.806	10	Good
102	A	-92.000	152.000	25.000	26.000	94.570	0.813	10	Good
103	P	-63.000	-18.000	16.000	12.000	118.720	0.851	10	Good
104	Y	-90.000	-15.000	21.000	32.000	130.090	0.917	10	Good
105	L	-89.000	7.000	12.000	13.000	126.440	0.926	9	Good
106	R	61.000	40.000	8.000	5.000	83.080	0.912	6	Warn
107	K	-131.000	144.000	16.000	15.000	68.190	0.888	10	Good
108	I	-132.000	147.000	15.000	13.000	40.500	0.869	10	Good
109	D	-124.000	156.000	47.000	30.000	47.750	0.857	10	Good
110	L	-62.000	-29.000	8.000	14.000	45.320	0.850	10	Good
111	R	-62.000	-28.000	12.000	10.000	39.240	0.837	10	Good
112	V	-79.000	-24.000	26.000	18.000	41.730	0.798	10	Good
113	Y	-97.000	-4.000	16.000	14.000	60.640	0.765	10	Good
114	G	65.000	37.000	14.000	10.000	74.100	0.773	10	Good
115	G	-133.000	155.000	53.000	32.000	71.680	0.800	10	Good
116	Y	-55.000	-32.000	12.000	14.000	55.130	0.826	10	Good
117	S	-71.000	-21.000	14.000	16.000	38.750	0.803	10	Good
118	E	-98.000	8.000	18.000	24.000	37.250	0.818	10	Good
119	L	-66.000	-39.000	17.000	20.000	35.940	0.844	10	Good
120	L	-60.000	-42.000	5.000	5.000	29.350	0.889	10	Good
121	K	-64.000	-42.000	4.000	3.000	28.180	0.896	10	Good
122	A	-64.000	-45.000	6.000	5.000	27.220	0.898	10	Good
123	L	-63.000	-40.000	5.000	9.000	27.030	0.898	10	Good
124	E	-63.000	-41.000	6.000	4.000	28.140	0.904	10	Good
125	T	-65.000	-41.000	8.000	5.000	30.910	0.892	10	Good
126	M	-64.000	-44.000	9.000	7.000	35.540	0.867	10	Good

127	F	-97.000	3.000	11.000	7.000	46.560	0.834	10	Good
128	K	56.000	46.000	4.000	8.000	45.910	0.813	10	Good
129	L	-123.000	150.000	19.000	16.000	40.410	0.807	9	Good
130	T	-106.000	140.000	30.000	17.000	40.790	0.788	10	Good
131	I	-119.000	126.000	11.000	15.000	44.770	0.756	10	Good
132	G	149.000	-174.000	77.000	26.000	44.820	0.700	8	Warn
133	E	-97.000	142.000	22.000	29.000	41.260	0.672	10	Warn
134	Y	-73.000	132.000	58.000	26.000	45.480	0.694	10	Good
135	S	-101.000	144.000	27.000	18.000	43.690	0.760	10	Good
136	E	-61.000	-28.000	4.000	9.000	53.780	0.828	10	Good
137	R	-65.000	-33.000	11.000	11.000	41.740	0.842	10	Good
138	E	-92.000	-9.000	17.000	12.000	56.730	0.851	10	Good
139	G	65.000	36.000	14.000	20.000	117.800	0.871	10	Warn
140	Y	-93.000	6.000	15.000	15.000	106.570	0.892	10	Good
141	K	61.000	36.000	8.000	8.000	99.040	0.855	8	Warn
142	G	83.000	11.000	12.000	17.000	92.080	0.665	10	Good
143	S	-90.000	-28.000	22.000	25.000	43.530	0.642	5	Warn
144	E	-94.000	-7.000	14.000	13.000	40.930	0.660	6	Warn
145	Y	-141.000	153.000	20.000	15.000	41.330	0.835	10	Good
146	A	-126.000	136.000	22.000	30.000	73.070	0.868	10	Good
147	P	-68.000	142.000	10.000	12.000	72.560	0.882	10	Good
148	T	-130.000	160.000	21.000	15.000	67.320	0.895	10	Good
149	Y	-131.000	147.000	16.000	9.000	46.490	0.903	10	Good
150	E	-111.000	122.000	9.000	12.000	48.280	0.895	10	Good
151	D	-94.000	178.000	23.000	9.000	47.710	0.870	10	Good
152	K	-64.000	-20.000	8.000	16.000	40.680	0.833	10	Good
153	D	-87.000	2.000	10.000	10.000	46.750	0.765	10	Good
154	G	81.000	9.000	17.000	21.000	46.010	0.700	10	Good
155	D	-66.000	140.000	52.000	16.000	40.410	0.692	10	Good
156	W	-79.000	127.000	60.000	18.000	39.440	0.726	10	Good
157	M	-126.000	161.000	21.000	16.000	36.120	0.791	10	Good
158	L	-82.000	142.000	24.000	16.000	44.440	0.795	10	Good
159	V	-65.000	135.000	10.000	8.000	43.550	0.806	10	Good
160	G	-100.000	145.000	37.000	34.000	45.270	0.817	6	Warn
161	D	-82.000	-28.000	13.000	16.000	54.200	0.848	10	Good
162	V	-126.000	165.000	19.000	12.000	82.360	0.865	10	Good
163	P	-62.000	145.000	6.000	6.000	82.560	0.880	10	Good
164	W	-49.000	-45.000	11.000	10.000	56.640	0.890	10	Good
165	D	-62.000	-28.000	13.000	15.000	42.680	0.895	10	Good
166	M	-70.000	-36.000	12.000	12.000	43.670	0.881	10	Good
167	F	-61.000	-42.000	3.000	7.000	36.600	0.870	10	Good
168	V	-68.000	-30.000	14.000	12.000	38.330	0.840	10	Good
169	T	-77.000	-26.000	18.000	13.000	39.840	0.764	10	Good
170	S	-95.000	-12.000	18.000	16.000	48.510	0.757	10	Good

171	C	-98.000	118.000	35.000	21.000	47.150	0.780	10	Good
172	K	-128.000	161.000	17.000	11.000	53.110	0.875	10	Good
173	R	-140.000	149.000	24.000	7.000	50.780	0.894	10	Good
174	L	-135.000	138.000	11.000	12.000	40.820	0.898	10	Good
175	R	-126.000	128.000	11.000	8.000	45.520	0.889	10	Good
176	I	-101.000	125.000	18.000	14.000	44.990	0.869	10	Good
177	M	-128.000	142.000	18.000	15.000	41.480	0.830	10	Good
178	K	-81.000	126.000	21.000	14.000	42.660	0.778	10	Good
179	G	-65.000	-25.000	10.000	16.000	42.840	0.756	10	Good
180	T	-70.000	-22.000	16.000	13.000	48.040	0.724	10	Good
181	E	-68.248	-32.965	12.038	14.296	47.224	0.703	10	Good
182	A	-66.722	-34.447	4.601	12.030	45.943	0.666	10	Good
183	K	-70.047	-26.415	9.766	15.458	38.728	0.649	10	Good
184	G	-64.839	-36.881	6.941	12.072	37.959	0.643	8	Warn
185	L	-79.373	-17.697	19.046	23.698	42.832	0.626	9	Warn
186	G	-63.816	-36.261	5.817	13.163	38.026	0.612	6	Warn
187	C	-95.665	-3.267	12.708	12.476	42.761	0.524	6	Warn
188	G	87.795	5.388	13.509	18.754	38.598	0.451	5	Dyn
189	V	-98.407	104.997	26.195	31.852	44.581	0.379	6	Dyn
190	G	80.013	15.140	9.280	15.394	39.020	0.339	9	Dyn
191	S	0	0	0.000	0.000	0.000	0.321	0	None

HN, N, CA and CB chemical shifts (in ppm) were used for TALOS prediction calculation.

Table A4: All amino acid residues and its side-chain atoms

A	C	D	E	F	G	H	I	K	L
H	H	H	H	H	H	H	H	H	H
HA	HA	HA	HA	HA	HA2	HA	HA	HA	HA
HB1	HB2	HB2	HB2	HB2	HA3	HB2	HB	HB2	HB2
HB2	HB3	HB3	HB3	HB3	C	HB3	HG13	HB3	HB3
HB3	C	C	C	HD1	CA	HD2	HG21	HG2	HG
C	CA	CA	CA	HD2	N	HE1	HG22	HG3	HD11
CA	CB	CB	CB	HE1		CA	HG23	HD2	HD12
CB	N	N	N	HE2		N	HD11	HD3	HD13
N				HZ			HD12	HE2	HD21
				C			HD13	HE3	HD22
				CA			CA	C	HD23
				CB			CB	CA	C
				CD2			CG1	CB	CA
				CE2			CG2	CG	CB
				CZ			CD1	CD	CG
				N			N	CE	CD1
								N	CD2
									N

M	N	P	Q	R	S	T	V	W	Y
H	H	-	H	H	H	H	H	H	H
HA	HA	HA	HB2	HA	HA	HA	HA	HA	HA
HB2	HB2	HB2	HB3	HB2	HB2	HB2	HB	HB2	HB2
HB3	HB3	HB3	HG2	HB3	HB3	HB3	HG11	HB3	HB3
HG2	HD21	HG2	HG3	HG2	C	HD1	HG12	HD1	HD1
HG3	HD22	HG3	HD2	HG3	CA	HE1	HG13	HE1	HD2
HE1	CA	HD2	HD3	HD2	CB	HE3	HG21	HE3	HE1
HE2	CB	HD3	HE21	HD3	N	HZ2	HG22	HZ2	HE2
HE3	N	CA	HE22	C		HZ3	HG23	HZ3	C
C	ND	CB	CA	CA		C	C	C	CA
CA		CG	CB	CB		CA	CA	CA	CB
CB		CD	CG	CG		CB	CB	CB	CD1
CG			N	CD		CD1	CG1	CD1	CE1
CE			NE2	N		CE3	CG2	CE3	N
N						CZ2	N	CZ2	
						CZ3		CZ3	
						N		N	
						NE1		NE1	

Table A5: Complete assignment of the wild-type PsIAA4 PB1 domain (AA 86-189)

AA	Atom	CS/ppm	AA	Atom	CS/ppm	AA	Atom	CS/ppm	AA	Atom	CS/ppm
86	C	173.793	91	H	8.37	94	N	122.628	97	CB	34.87
87	H	8.472	91	HA2	3.843	95	H	9.019	97	CG1	21.208
87	HA	3.791	91	HA3	3.991	95	HA	4.503	97	CG2	22.448
87	HB2	2.418	91	C	172.689	95	HB	1.847	97	N	119.483
87	HB3	2.193	91	CA	45.49	95	HG11	0.667	98	H	7.787
87	HG2	2.748	91	N	112.118	95	HG12	0.667	98	HA	4.851
87	HG3	2.209	92	H	8.61	95	HG13	0.667	98	HB2	3.906
87	C	175.368	92	HA2	3.632	95	HG21	0.665	98	HB3	3.598
87	CA	55.97	92	HA3	4.025	95	HG22	0.665	98	CA	56.36
87	CB	29.31	92	C	173.159	95	HG23	0.665	98	CB	67.28
87	CG	35.121	92	CA	45.53	95	C	174.574	98	N	119.247
87	N	123.507	92	N	113.38	95	CA	59.99	99	H	7.996
88	H	8.371	93	H	7.417	95	CB	35.85	99	HE1	1.534
88	HA	4.133	93	HA	4.004	95	CG1	20.147	99	HE2	1.534
88	HB1	1.227	93	HB	1.434	95	CG2	20.133	99	HE3	1.534
88	HB2	1.227	93	HG13	0.837	95	N	117.99	99	CE	18.202
88	HB3	1.227	93	HG21	0.559	96	H	8.729	100	H	8.279
88	C	177.266	93	HG22	0.559	96	HA	4.921	100	HA	4.183
88	CA	52.7	93	HG23	0.559	96	HB2	1.755	100	HB2	2.701
88	CB	19.44	93	HD11	0.638	96	HB3	1.69	100	HB3	2.59
88	N	125.5	93	HD12	0.638	96	HG2	1.507	100	C	176.123
89	H	8.371	93	HD13	0.638	96	HG3	1.255	100	CA	55.91
89	HA	4.549	93	C	174.587	96	HD2	1.757	100	CB	39.95
89	HB2	2.63	93	CA	60.67	96	HD3	1.696	100	N	126.692
89	HB3	2.739	93	CB	39.33	96	HE2	2.825	101	H	8.611
89	C	175.427	93	CG1	27.088	96	HE3	2.825	101	HA2	3.548
89	CA	53.38	93	CG2	13.385	96	C	175.62	101	HA3	4.092
89	CB	38.91	93	CD1	17.778	96	CA	56.43	101	C	173.173
89	N	118.51	93	N	121.756	96	CB	34.59	101	CA	45.43
90	H	7.977	94	H	8.308	96	CG	26.551	101	N	111.972
90	HA	3.975	94	HA	5.18	96	CD	34.74	102	H	7.997
90	HB	1.951	94	HB2	2.799	96	CE	42.543	102	HA	4.813
90	HG11	0.779	94	HB3	2.575	96	N	122.336	102	HB1	1.3
90	HG12	0.779	94	HD1	6.931	97	H	8.864	102	HB2	1.3
90	HG13	0.779	94	HD2	6.931	97	HA	5.141	102	HB3	1.3
90	HG21	0.779	94	HE1	7.226	97	HB	1.894	102	CA	49.58
90	HG22	0.779	94	HE2	7.226	97	HG11	0.882	102	CB	20.38
90	HG23	0.779	94	HZ	7.225	97	HG12	0.882	102	N	123.763
90	C	176.608	94	C	176.711	97	HG13	0.882	103	HA	4.405
90	CA	62.73	94	CA	57.37	97	HG21	0.843	103	HB2	1.972
90	CB	32.77	94	CB	41.11	97	HG22	0.843	103	HB3	1.789
90	CG1	20.551	94	CD2	128.852	97	HG23	0.843	103	HG2	1.881
90	CG2	21.428	94	CE2	128.898	97	C	173.266	103	HG3	1.508
90	N	120.377	94	CZ	127.512	97	CA	60.01	103	HD2	3.582

AA	Atom	CS/ppm	AA	Atom	CS/ppm	AA	Atom	CS/ppm	AA	Atom	CS/ppm
103	HD3	3.393	108	HA	4.686	111	HB2	1.743	115	HA2	1.908
103	CA	63.978	108	HB	1.761	111	HB3	1.643	115	HA3	3.289
103	CB	31.879	108	HG13	0.979	111	HG2	1.571	115	C	172.226
103	CG	27.073	108	HG21	0.731	111	HG3	1.48	115	CA	44.08
103	CD	50.859	108	HG22	0.731	111	HD2	3.016	115	N	104.622
104	H	8.856	108	HG23	0.731	111	HD3	3.015	116	H	7.74
104	C	174.416	108	HD11	0.634	111	HE	7.157	116	HA	3.85
104	N	121.487	108	HD12	0.634	111	C	177.696	116	HB2	2.872
105	H	8.406	108	HD13	0.634	111	CA	58.19	116	HB3	2.623
105	HA	4.803	108	C	172.55	111	CB	30.26	116	C	177.997
105	HB2	1.549	108	CA	59.9	111	CG	27.902	116	CA	62.76
105	HB3	1.548	108	CB	42.78	111	CD	43.491	116	CB	38.39
105	HG	1.542	108	CG1	27.493	111	N	112.147	116	N	116.872
105	HD11	0.778	108	CG2	17.772	111	NE	84.22	117	H	8.755
105	HD12	0.778	108	CD1	14.704	112	H	6.833	117	HA	4.21
105	HD13	0.778	108	N	119.237	112	HA	3.69	117	HB2	3.617
105	HD21	0.829	109	H	8.562	112	HB	1.659	117	HB3	3.649
105	HD22	0.829	109	HA	4.735	112	HG11	0.379	117	C	177.443
105	HD23	0.829	109	HB2	1.906	112	HG12	0.379	117	CA	58.73
105	CA	55.127	109	HB3	2.697	112	HG13	0.379	117	CB	64.07
105	CB	44.726	109	C	176.503	112	HG21	0.416	117	N	114.746
105	CG	27.769	109	CA	50.8	112	HG22	0.416	118	H	7.683
105	CD1	25.437	109	CB	39.37	112	HG23	0.416	118	HA	4.578
105	CD2	25.313	109	N	122.747	112	C	175.813	118	HB2	2.101
105	N	120.662	110	H	8.884	112	CA	63.07	118	HB3	1.972
106	C	174.484	110	HA	4.128	112	CB	31.58	118	C	178.792
107	H	8.424	110	HB2	1.559	112	CG1	19.934	118	CA	55.27
107	HA	5.187	110	HB3	1.403	112	CG2	20.98	118	CB	28.62
107	HB2	1.522	110	HG	1.685	112	N	112.243	118	N	119.877
107	HB3	1.521	110	HD11	0.791	113	H	6.912	119	H	7.458
107	HG2	1.287	110	HD12	0.791	113	HA	4.348	119	HA	3.212
107	HG3	1.225	110	HD13	0.791	113	HB2	3.028	119	HB2	1.958
107	HD2	1.145	110	HD21	0.436	113	HB3	2.872	119	HB3	1.354
107	HD3	1.144	110	HD22	0.436	113	C	175.676	119	HG	1.308
107	HE2	2.463	110	HD23	0.436	113	CA	58.42	119	HD11	0.589
107	HE3	2.463	110	C	178.175	113	CB	40.39	119	HD12	0.589
107	C	175.369	110	CA	58	113	N	118.366	119	HD13	0.589
107	CA	55.84	110	CB	43.01	114	H	7.762	119	HD21	1.044
107	CB	35.56	110	CG	27.199	114	HA2	3.365	119	HD22	1.044
107	CG	29.826	110	CD1	23.935	114	HA3	3.774	119	HD23	1.044
107	CD	25.157	110	CD2	26.538	114	C	172.385	119	C	177.565
107	CE	41.974	110	N	121.881	114	CA	44.93	119	CA	58.18
107	N	120.246	111	H	7.657	114	N	104.242	119	CB	41.94
108	H	9.045	111	HA	4.007	115	H	5.678	119	CG	28.066

AA	Atom	CS/ppm	AA	Atom	CS/ppm	AA	Atom	CS/ppm	AA	Atom	CS/ppm
19	CD1	23.948	123	HD22	0.806	126	CE	17.081	129	N	116.643
119	CD2	27.509	123	HD23	0.806	126	N	120.752	130	H	8.137
119	N	121.365	123	C	178.779	127	H	7.667	130	HA	4.366
120	H	8.828	123	CA	58.47	127	HA	4.329	130	HB	3.915
120	HA	3.668	123	CB	41.97	127	HB2	3.026	130	HG21	1.047
120	HB2	1.781	123	CG	26.491	127	HB3	2.838	130	HG22	1.047
120	HB3	1.403	123	CD1	25.537	127	C	173.355	130	HG23	1.047
120	HG	1.731	123	CD2	23.358	127	CA	58.67	130	C	173.508
120	HD11	0.831	123	N	118.509	127	CB	39.88	130	CA	62.47
120	HD12	0.831	124	H	8.461	127	N	112.993	130	CB	70.34
120	HD13	0.831	124	HA	3.78	128	H	7.483	130	CG2	22.023
120	HD21	0.747	124	HB2	2.42	128	HA	3.849	130	N	115.375
120	HD22	0.747	124	HB3	2.199	128	HB2	1.898	131	H	8.232
120	HD23	0.747	124	HG2	2.749	128	HB3	1.702	131	HA	4.094
120	C	179.057	124	HG3	2.211	128	HG2	1.188	131	HB	1.424
120	CA	59.15	124	C	173.834	128	HG3	1.187	131	HG13	0.588
120	CB	40.61	124	CA	60.05	128	HD2	1.543	131	HG21	0.887
120	CG	28.855	124	CB	29.34	128	HD3	1.542	131	HG22	0.887
120	CD1	24.931	124	CG	35.15	128	HE2	2.861	131	HG23	0.887
120	CD2	23.83	124	N	117.636	128	HE3	2.861	131	HD11	0.524
120	N	118.748	125	H	7.901	128	C	174.55	131	HD12	0.524
121	H	7.468	125	HA	3.925	128	CA	57.19	131	HD13	0.524
121	C	179.267	125	HB	4.167	128	CB	29.01	131	C	175.255
121	CA	59.23	125	HG21	1.137	128	CG	25.272	131	CA	61.2
121	CB	32.32	125	HG22	1.137	128	CD	29.584	131	CB	40.85
121	N	117.997	125	HG23	1.137	128	CE	42.756	131	CG1	28.47
122	H	7.506	125	C	176.475	128	N	119.006	131	CG2	18.456
122	HA	4.104	125	CA	66.06	129	H	7.934	131	CD1	13.858
122	HB1	1.363	125	CB	69.37	129	HA	4.627	131	N	126.127
122	HB2	1.363	125	CG2	21.911	129	HB2	1.287	132	H	8.384
122	HB3	1.363	125	N	114.494	129	HB3	1.228	132	C	172.244
122	C	180.991	126	H	8.206	129	HG	1.181	132	CA	45.05
122	CA	55.55	126	HA	3.746	129	HD11	0.153	132	N	113.138
122	CB	18.48	126	HB2	1.902	129	HD12	0.153	133	H	7.969
122	N	122.5	126	HB3	1.469	129	HD13	0.153	133	C	176.004
123	H	8.295	126	HG2	2.199	129	HD21	0.244	133	CA	56.02
123	HA	4.006	126	HG3	1.758	129	HD22	0.244	133	CB	29.38
123	HB2	1.971	126	HE1	1.812	129	HD23	0.244	133	N	116.754
123	HB3	1.111	126	HE2	1.812	129	C	176.135	134	H	8.266
123	HG	1.919	126	HE3	1.812	129	CA	54.01	134	C	175.358
123	HD11	0.636	126	C	177.087	129	CB	44.92	134	CA	58.42
123	HD12	0.636	126	CA	59.43	129	CG	26.295	134	CB	39.37
123	HD13	0.636	126	CB	34.79	129	CD1	25.699	134	N	123.188
123	HD21	0.806	126	CG	31.96	129	CD2	25.307	135	H	7.347

AA	Atom	CS/ppm	AA	Atom	CS/ppm	AA	Atom	CS/ppm	AA	Atom	CS/ppm
135	HA	4.154	143	H	8.016	147	CB	30.8	153	HA	4.559
135	HB2	3.437	143	HA	4.209	147	CG	28.069	153	HB2	2.826
135	HB3	3.674	143	HB2	3.651	147	CD	49.69	153	HB3	2.609
135	C	173.787	143	HB3	3.614	148	H	8.545	153	C	175.211
135	CA	56.51	143	C	174.582	148	HA	5.546	153	CA	53.52
135	CB	64.8	143	CA	58.73	148	HB	4.278	153	CB	39.04
135	N	120.449	143	CB	64.07	148	HG21	1.072	153	N	116.739
136	H	8.46	143	N	115.126	148	HG22	1.072	154	H	7.786
136	C	174.579	144	H	8.435	148	HG23	1.072	154	HA2	3.636
136	CA	58.4	144	C	175.837	148	C	172.855	154	HA3	4.017
136	CB	27.93	144	CA	55.27	148	CA	60.48	154	C	173.494
136	N	124.126	144	CB	28.62	148	CB	73.42	154	CA	45.18
137	H	7.913	144	N	119.746	148	CG2	22.789	154	N	107.127
137	HA	4.009	145	H	7.732	148	N	116.92	155	H	7.57
137	HB2	1.609	145	HA	4.928	149	H	9.909	155	HA	4.687
137	HB3	1.608	145	HB2	2.443	149	C	170.694	155	HB2	2.453
137	HG2	1.491	145	HB3	2.358	149	CA	55.79	155	HB3	2.612
137	HG3	1.429	145	HD1	6.84	149	CB	42.61	155	C	173.815
137	HD2	3.03	145	HD2	6.84	149	N	118.754	155	CA	52.94
137	HD3	3.029	145	HE1	6.651	150	H	7.812	155	CB	40.24
137	HE	7.064	145	HE2	6.651	150	HA	4.053	155	N	118.511
137	C	177.247	145	C	174.264	150	HB2	0.921	156	H	8.422
137	CA	58	145	CA	57.13	150	HB3	-0.647	156	HA	5.013
137	CB	31.33	145	CB	42.45	150	HG2	2.095	156	HB2	2.794
137	CG	27.894	145	CD1	130.668	150	HG3	0.673	156	HB3	2.793
137	CD	43.459	145	CE1	115.763	150	C	175.823	156	HD1	7.153
137	N	115.993	145	N	114.738	150	CA	52.31	156	HE1	9.881
137	NE	84.104	146	H	9.07	150	CB	30.23	156	HE3	6.627
138	H	7.406	146	HA	4.554	150	CG	31.994	156	HZ2	7.139
138	C	176.233	146	HB1	0.956	150	N	121.754	156	C	176.124
138	CA	55.34	146	HB2	0.956	151	H	8.245	156	CA	56.78
138	N	114.247	146	HB3	0.956	151	HA	5.112	156	CB	30.35
139	H	8.078	146	CA	48.17	151	HB2	2.521	156	CD1	124.93
139	HA2	3.342	146	CB	21.26	151	HB3	3.262	156	CE3	119.866
139	HA3	3.669	146	N	122.622	151	C	177.262	156	CZ2	111.755
139	CA	46.77	147	HA	4.565	151	CA	51.85	156	N	122.005
139	N	112.373	147	HB2	1.626	151	CB	40.69	156	NE1	129.041
141	C	174.269	147	HB3	1.494	151	N	125.138	157	H	8.971
142	H	8.053	147	HG2	2.163	152	H	8.102	157	HA	4.606
142	HA2	3.14	147	HG3	1.555	152	C	176.46	157	HB2	1.982
142	HA3	3.733	147	HD2	2.975	152	CA	58.97	157	HB3	1.038
142	C	174.196	147	HD3	2.449	152	CB	32.29	157	HG2	2.107
142	CA	45.6	147	C	174.112	152	N	117.94	157	HG3	2.106
142	N	107.999	147	CA	62.27	153	H	7.66	157	HE1	1.727

AA	Atom	CS/ppm	AA	Atom	CS/ppm	AA	Atom	CS/ppm	AA	Atom	CS/ppm
157	HE2	1.727	160	C	173.65	164	HZ2	7.549	167	CA	60.5
157	HE3	1.727	160	CA	43.02	164	HZ3	6.183	167	CB	40.44
157	C	175.077	160	N	116.749	164	C	176.301	167	CD2	129.89
157	CA	54.08	161	H	7.673	164	CA	61.007	167	CE2	128.2
157	CB	36.31	161	HA	4.315	164	CB	30.04	167	CZ	125.5
157	CG	32.728	161	HB2	2.839	164	CD1	124.494	167	N	124.743
157	CE	17.598	161	HB3	2.838	164	CE3	119.62	168	H	7.598
157	N	121.761	161	C	174.609	164	CZ2	112.984	168	HA	2.663
158	H	8.232	161	CA	55.67	164	CZ3	118.543	168	HB	1.358
158	HA	4.476	161	CB	40.16	164	N	125.757	168	HG11	0.266
158	HB2	1.812	161	N	118.899	164	NE1	129.504	168	HG12	0.266
158	HB3	1.409	162	H	7.228	165	H	8.958	168	HG13	0.266
158	HG	1.768	162	HA	4.886	165	HA	3.996	168	HG21	0.22
158	HD11	1.012	162	HB	2.339	165	HB2	2.721	168	HG22	0.22
158	HD12	1.012	162	HG11	0.866	165	HB3	2.771	168	HG23	0.22
158	HD13	1.012	162	HG12	0.866	165	C	177.23	168	C	176.42
158	HD21	0.868	162	HG13	0.866	165	CA	56.47	168	CA	65.57
158	HD22	0.868	162	HG21	0.779	165	CB	37.68	168	CB	31.36
158	HD23	0.868	162	HG22	0.779	165	N	112.754	168	CG1	21.912
158	C	177.423	162	HG23	0.779	166	H	7.184	168	CG2	21.523
158	CA	55.43	162	C	176.924	166	HA	4.148	168	N	114.749
158	CB	42.99	162	CA	58.41	166	HB2	2.017	169	H	6.605
158	CG	27.279	162	CB	33.272	166	HB3	1.963	169	HA	3.992
158	CD1	26.567	162	CG1	21.677	166	HG2	2.469	169	HB	4.144
158	CD2	23.948	162	CG2	18.2	166	HG3	2.382	169	HG21	1.007
158	N	119.378	162	N	111.126	166	HE1	1.983	169	HG22	1.007
159	H	8.015	163	HA	4.585	166	HE2	1.983	169	HG23	1.007
159	HA	3.416	163	HB2	2.497	166	HE3	1.983	169	C	175.046
159	HB	1.691	163	HB3	1.861	166	C	177.854	169	CA	62.5
159	HG11	0.802	163	HG2	2.093	166	CA	57.07	169	CB	69.36
159	HG12	0.802	163	HG3	1.972	166	CB	32.96	169	CG2	22.342
159	HG13	0.802	163	HD2	3.859	166	CG	32.52	169	N	105.375
159	HG21	0.379	163	HD3	3.623	166	CE	17.43	170	H	7.266
159	HG22	0.379	163	CA	64.063	166	N	117.746	170	HA	4.357
159	HG23	0.379	163	CB	32.834	167	H	7.838	170	HB2	3.746
159	C	175.199	163	CG	28.596	167	HA	3.635	170	HB3	3.823
159	CA	65.25	163	CD	51.724	167	HB2	2.859	170	C	173.634
159	CB	31.93	164	H	9.236	167	HB3	2.726	170	CA	58.96
159	CG1	24.387	164	HA	3.917	167	HD1	5.791	170	CB	65.82
159	CG2	22.344	164	HB2	3.02	167	HD2	5.791	170	N	115.125
159	N	121.624	164	HB3	2.903	167	HE1	6.301	171	H	7.431
160	H	8.337	164	HD1	6.936	167	HE2	6.301	171	HA	3.971
160	HA2	1.628	164	HE1	9.852	167	HZ	6.696	171	HB2	1.804
160	HA3	3.241	164	HE3	6.827	167	C	176.468	171	HB3	1.418

AA	Atom	CS/ppm	AA	Atom	CS/ppm	AA	Atom	CS/ppm	AA	Atom
171	C	174.204	174	HD13	1.006	177	HB3	1.713	180	CG2
171	CA	60.17	174	HD21	0.842	177	HG2	2.217	180	N
171	CB	26.89	174	HD22	0.842	177	HG3	1.884	181	H
171	N	120.627	174	HD23	0.842	177	HE1	1.609	181	HA
172	H	9.219	174	C	175.719	177	HE2	1.609	181	HB2
172	HA	4.388	174	CA	55.24	177	HE3	1.609	181	HB3
172	HB2	1.533	174	CB	47.88	177	C	175.662	181	C
172	HB3	1.279	174	CG	28.744	177	CA	54.35	181	CA
172	HG2	1.146	174	CD1	26.559	177	CB	36.07	181	CB
172	HG3	1.145	174	CD2	27.801	177	CG	31.878	181	N
172	HD2	1.533	174	N	122.992	177	CE	16.701	182	H
172	HD3	1.279	175	H	9.211	177	N	126.564	182	HA
172	HE2	2.741	175	HA	5.186	178	H	8.687	182	HB1
172	HE3	2.741	175	HB2	1.528	178	HA	4.15	182	HB2
172	C	176.304	175	HB3	1.527	178	HB2	1.693	182	HB3
172	CA	56.04	175	HG2	1.289	178	HB3	1.498	182	C
172	CB	34.23	175	HG3	1.222	178	HG2	1.183	182	CA
172	CG	24.389	175	HD2	2.472	178	HG3	1.182	182	CB
172	CD	34.23	175	HD3	2.471	178	HD2	1.439	182	N
172	CE	43.499	175	C	175.355	178	HD3	1.438	183	H
172	N	126.351	175	CA	55.47	178	HE2	2.786	183	HA
173	H	7.431	175	CB	35.42	178	HE3	2.786	183	HB2
173	HA	4.463	175	CG	29.838	178	C	177.854	183	HB3
173	HB2	1.837	175	CD	41.967	178	CA	57.13	183	HG2
173	HB3	1.836	175	N	123.476	178	CB	33.26	183	HG3
173	HG2	1.538	176	H	9.184	178	CG	25.838	183	HD2
173	HG3	1.537	176	HA	4.199	178	CD	29.592	183	HD3
173	HD2	3.264	176	HB	1.459	178	CE	42.356	183	HE2
173	HD3	3.123	176	HG13	0.524	178	N	123.239	183	HE3
173	HE	7.323	176	HG21	0.439	179	H	8.391	183	C
173	C	173.271	176	HG22	0.439	179	HA2	3.56	183	CA
173	CA	56.52	176	HG23	0.439	179	HA3	3.773	183	CB
173	CB	33.65	176	HD11	0.252	179	C	175.089	183	CG
173	CG	27.493	176	HD12	0.252	179	CA	46.75	183	CD
173	CD	43.895	176	HD13	0.252	179	N	113.128	183	CE
173	N	116.76	176	CA	61.22	180	H	7.876	183	N
173	NE	84.133	176	CB	36.86	180	HA	3.991	184	H
174	H	8.842	176	CG1	27.622	180	HB	4.053	184	HA2
174	HA	5.474	176	CG2	19.009	180	HG21	1.054	184	HA3
174	HB2	1.741	176	CD1	13.514	180	HG22	1.054	184	C
174	HB3	1.471	176	N	130.458	180	HG23	1.054	184	CA
174	HG	1.624	177	H	8.292	180	C	175.576	184	N
174	HD11	1.006	177	HA	4.533	180	CA	63.55	185	H
174	HD12	1.006	177	HB2	1.853	180	CB	69.14	185	HA

AA	Atom	CS/ppm	AA	Atom	CS/ppm
185	HB2	1.637	189	HG23	0.783
185	HB3	1.577	189	C	176.919
185	HG	1.495	189	CA	62.97
185	HD11	0.674	189	CB	32.77
185	HD12	0.674	189	CG1	21.446
185	HD13	0.674	189	CG2	20.652
185	HD21	0.7	189	N	119.247
185	HD22	0.7	190	H	8.468
185	HD23	0.7	190	HA2	3.854
185	C	178.026	190	HA3	3.965
185	CA	55.59	190	C	173.942
185	CB	42.39	190	CA	45.57
185	CG	27.319	190	N	112.295
185	CD1	23.648	191	H	7.861
185	CD2	25.57	191	HA	4.474
185	N	120.75	191	HB2	3.868
186	H	8.344	191	HB3	4.008
186	HA2	3.89	191	CA	57.73
186	HA3	3.891	191	CB	65.1
186	C	174.239	191	N	114.624
186	CA	45.8	192	H	8.925
186	N	108.889	192	HA	3.921
187	H	8.117	192	HB2	1.918
187	HA	4.428	192	HB3	1.800
187	HB2	2.788	192	HD2	7.725
187	HB3	2.787	192	HE1	6.828
187	C	175.049	192	CA	58.154
187	CA	58.97	192	N	126.528
187	CB	28.5			
187	N	117.967			
188	H	8.446			
188	HA2	3.886			
188	HA3	3.887			
188	C	174.261			
188	CA	45.71			
188	N	111.119			
189	H	7.977			
189	HA	3.975			
189	HB	1.955			
189	HG11	0.783			
189	HG12	0.783			
189	HG13	0.783			
189	HG21	0.783			
189	HG22	0.783			

7.7 Sequence information for PsIAA4 PB1 double and triple mutants

PsIAA4 PB1 mutants sequence, molecular weight and theoretical pI details. ProtParam calculated theoretical pIs were used later for optimizing buffer conditions.

PsIAA4 PB1^{BM2}

<u>90</u>	<u>100</u>	<u>110</u>	<u>120</u>	<u>130</u>	<u>140</u>
HEADVGGIFV	AVSMDGAPYL	AKIDLRVYGG	YSELLKALET	MFKLTIGEYS	EREGYKGSEY
<u>150</u>	<u>160</u>	<u>170</u>	<u>180</u>	<u>190</u>	
APTYEDKDGD	WMLVGDPVPD	MFVTSCKRLR	IMKGTEAKGL	GCGVGSHHHH	HH

Molecular weight: 12466.1

Theoretical pI: 5.75

PsIAA4 PB1^{BM3}

<u>90</u>	<u>100</u>	<u>110</u>	<u>120</u>	<u>130</u>	<u>140</u>
HEADVGGIFV	AVSMDGAPYL	AAIDLRVYGG	YSELLKALET	MFKLTIGEYS	EREGYKGSEY
<u>150</u>	<u>160</u>	<u>170</u>	<u>180</u>	<u>190</u>	
APTYEDKDGD	WMLVGDPVPD	MFVTSCKRLR	IMKGTEAKGL	GCGVGSHHHH	HH

Molecular weight: 12409.0

Theoretical pI: 5.55

PsIAA4 PB1^{AM2}

<u>90</u>	<u>100</u>	<u>110</u>	<u>120</u>	<u>130</u>	<u>140</u>
HEADVGGIFV	AVSMDGAPYL	AKIDLRVYGG	YSELLKALET	MFKLTIGEYS	EREGYKGSEY
<u>150</u>	<u>160</u>	<u>170</u>	<u>180</u>	<u>190</u>	
APTYEAKAGD	WMLVGDPVPD	MFVTSCKRLR	IMKGTEAKGL	GCGVGSHHHH	HH

Molecular weight: 12520.3

Theoretical pI: 6.71

PsIAA4 PB1^{AM3}

<u>90</u>	<u>100</u>	<u>110</u>	<u>120</u>	<u>130</u>	<u>140</u>
HEADVGGIFV	AVSMDGAPYL	AKIDLRVYGG	YSELLKALET	MFKLTIGEYS	EREGYKGSEY
<u>150</u>	<u>160</u>	<u>170</u>	<u>180</u>	<u>190</u>	
APTYEAKAGA	WMLVGDPVPD	MFVTSCKRLR	IMKGTEAKGL	GCGVGSHHHH	HH

Molecular weight: 12476.3

Theoretical pI: 7.22

7.8 Expression analyses of PsIAA4 PB1 variants

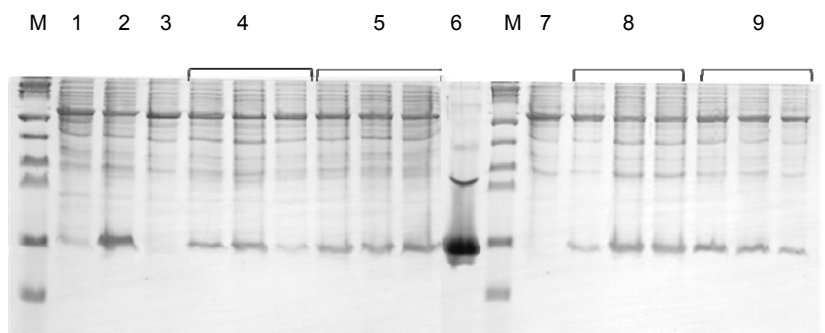


Figure A6: PsIAA4 PB1 mutant protein expression analysis

12% SDS-PAGE gel: M: Mark12™ unstained protein marker, 2.5 to 200 kDa range, 1: WT PsIAA4 PB1 before induction, 2: WT PsIAA4 PB1 after induction, 3: PsIAA4 PB1^{AM2} before induction, 4: PsIAA4 PB1^{AM2} after induction, 5: PsIAA4 PB1^{AM3} after induction, 6: WT PsIAA4 PB1 IMAC purified, 7: PsIAA4 PB1^{BM2} before induction, 8: PsIAA4 PB1^{BM2} before induction, 9: PsIAA4 PB1^{BM2} before induction.

7.9 NMR based pH scanning of the PsIAA4 PB1^{BM3} at a low pH

The PsIAA4 PB1^{BM3} mutants were not stable at a low pH and therefore the resulting spectra had only few cross peaks compared to spectra measured above pH 4.0.

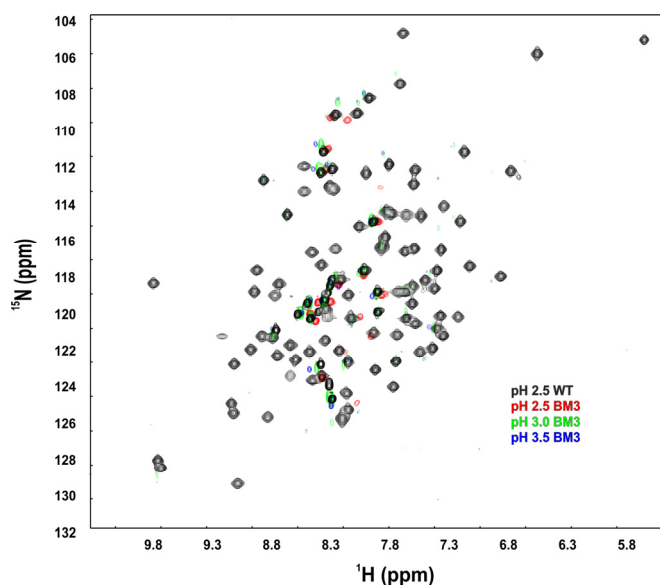


Figure A7: Low pH HSQC spectral overlay of WT PsIAA4 PB1 and PsIAA4 PB1^{BM3}

¹H-¹⁵N-HSQC spectrum of WT PsIAA4 PB1 at pH 2.5 (black), and PsIAA4 PB1^{BM3} pH 2.5 (red) and pH 3.0 (green), pH 3.5 (blue), measured at 25°C on 600/800 MHz NMR spectrometer.

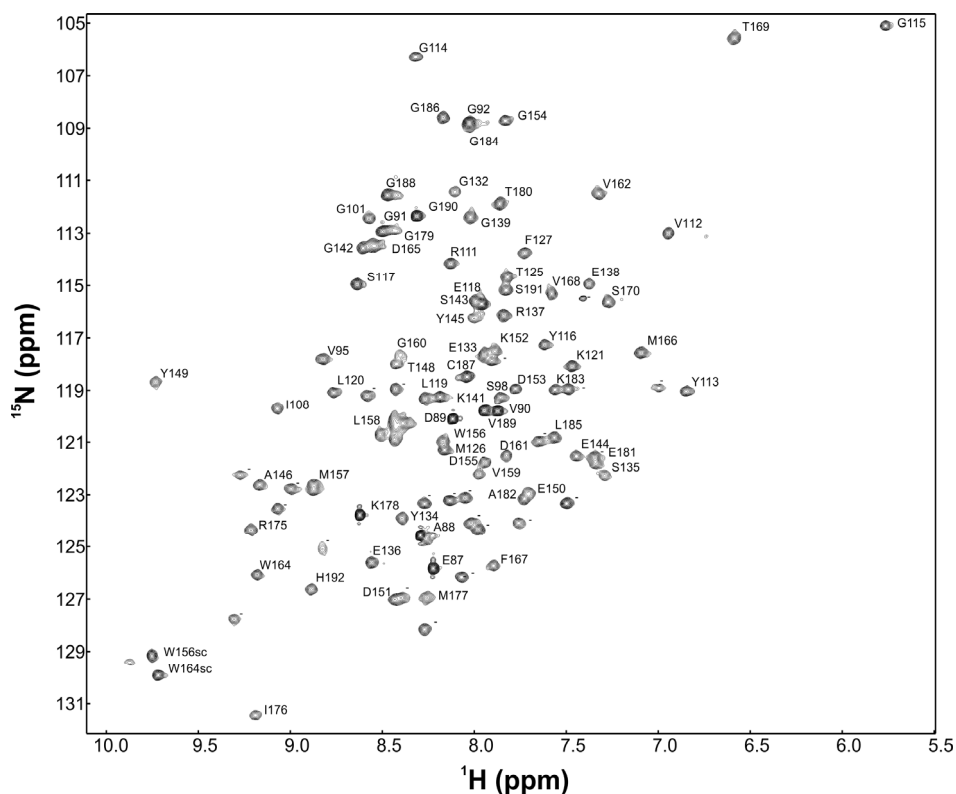


Figure A8: Sequential backbone assignment of bound PsIAA4 PB1^{BM3} and PsIAA4 PB1^{AM3}

The ^1H - ^{15}N -HSQC-TROSY spectrum of bound PsIAA4 PB1^{BM3} and PsIAA4 PB1^{AM3} was measured at 800 MHz, 25°C, and pH 6.25. Each cross peak corresponding to the backbone chemical shift information of an individual amino acid residue is labeled by the one-letter code of amino acids followed by residue number. (-) labeled cross peaks are ambiguous/unassigned.

Table A6: Sequential backbone assignment of the PsIAA4 PB1^{BM3}

PEAK	pH scan	HNCA	ASSIGN	AA	CSP	PEAK	pH scan	HNCA	ASSIGN	AA	CSP
			1	86		50			43	128	
101			2	87					44	129	
94	A3		3	88					45	130	
55			4	89					46	131	
61	V5		5	90		8	T95		47	132	
11	G6		6	91		39			48	133	
5	G57		7	92		84			49	134	
			8	93		74			50	135	
			9	94		100	E51		51	136	
			10	95		31	R52		52	137	
	A		11	96		26	E53		53	138	
	V12		12	97		12	G54		54	139	
			13	98		92	Y55		55	140	
			14	99		53	M41		56	141	
108			15	100		16	G94		57	142	
10	V10		16	101		29	L44		58	143	
			17	102		71			59	144	
			18	103		30	L44		60	145	
			19	104		76			61	146	
			20	105					62	147	
	A		21	106		38	E39		63	148	
	A		22	107		32	Y64		64	149	
44	I23		23	108		89	E65		65	150	
			24	109		107			66	151	
			25	110		35			67	152	
20			26	111		60			68	153	
14	V27		27	112		6	G69		69	154	
43	Y28		28	113		80			70	155	
2	G29		29	114		56			71	156	
0	G30		30	115		79			72	157	
36			31	116		63			73	158	
19	S32		32	117		81	V74		74	159	
69			33	118		34			75	160	
72			34	119		68			76	161	
45	L35		35	120		9	V77		77	162	
41			36	121					78	163	
			37	122		98	W79		79	164	
			38	123		18	D80		80	165	
47			39	124		37	M81		81	166	
22			40	125		103	F82		82	167	
58			41	126		24	V83		83	168	
21	F42		42	127		1	T84		84	169	

PEAK	pH scan	hnca	ASSIGN	AA	CSP
27	S85		85	170	
			86	171	
			87	172	
			88	173	
			89	174	
91	R90		90	175	
112	I91		91	176	
106	M92		92	177	
82	K93		93	178	
17	D80		94	179	
13	T95		95	180	
73			96	181	
88	A97		97	182	
49			98	183	
4	G99		99	184	
70	L100		100	185	
3	G101		101	186	
48	C102		102	187	
7	G103		103	188	
59	V104		104	189	
15	G94		105	190	
23	V84		106	191	
99	H107		107	192	
	W79sc				
	K87sc				

pH scan confirmed & no 3D data

UNASSIGNED

PROLINE

ASSIGNED AND CONFIRMED

HNCA assigned

PEAK SHIFT

NO SHIFT

Table A7: CSP calculated from free/unbound and bound spectra

87	0,06909	133	0,01487	161	0,01752
88	0	134	0,01701	162	0,02054
89	0,00418	135	0,01069	164	0,00428
90	0,00745	136	0,01007	165	0,00883
91	0,00611	137	0	166	0,00422
92	0,00809	138	0,01043	167	0,00548
100	0,00512	139	0,00933	168	0,00759
101	0,00357	140	0,00349	169	0,00581
108	0,00465	142	0,00766	170	0,01227
111	0,01094	143	0,04902	175	0,0156
112	0	144	0,00748	177	0
113	0,00383	145	0,0336	178	0,0295
114	0,01559	146	0,00367	179	0,00924
115	0,01013	148	0,01653	180	0
116	0,00736	149	0,02262	181	0,01449
117	0	150	0,04651	182	0,01657
118	0,01591	151	0,0607	183	0,01123
119	0,00746	152	0,0449	184	0,00478
120	0,00905	153	0,01102	185	0,00879
121	0,0078	154	0,05759	186	0,01099
124	0,01538	155	0,13828	187	0,00792
125	0,00879	156	0,06139	188	0,00945
126	0,00251	157	0,01951	189	0,01504
127	0,00574	158	0,06269	190	0,00474
128	0,00458	159	0,01603	191	0,01093
132	0,05304	160	0,02816	192	0,03173

7.10 Y2H controls

All diploid cells were respotting on to a control plate containing SD restrictive media but lacking sugars and X-Gal.

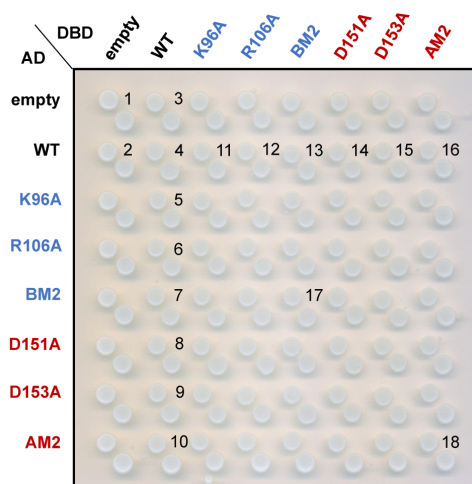


Figure A9: Controls for Y2H assays of homotypic PsIAA4 interaction

Growth controls of PsIAA4 diploids on a selective medium (SD/-Ura/-His/-Trp). All diploid yeast cells were spotted as in Fig. 28.

7.11 PsIAA4^{D100N} and PsIAA4^{E181A} mutational studies

PsIAA4 were mutated at D100 conserved position was shown to be crucial and abolished interaction between AtAUX/IAA17 and, other AUX/IAAs and ARFs family members. Similar mutations in PsIAA4 did not showed any effect and the corresponding D100/E181 patch is separated from the OPCA motif that is believed to be involved in protein-protein interaction (Fig. A10).

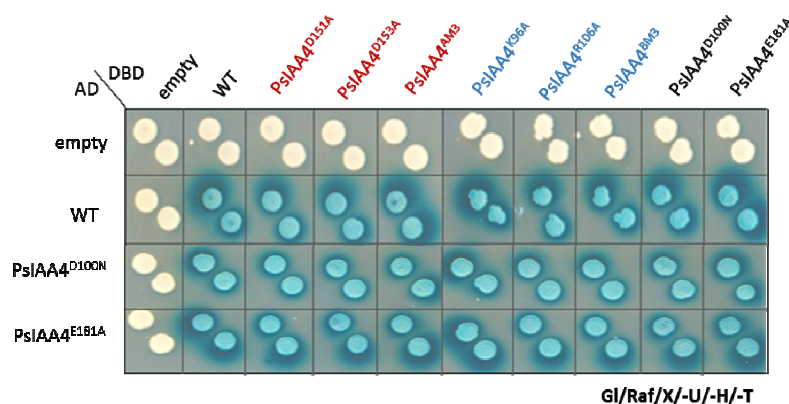


Figure A10: Y2H analysis of PsIAA4^{D100N} and PsIAA4^{E181A} mutants

Interaction matrix of WT and mutant PsIAA4^{D100N} and PsIAA4^{E181A} protein with itself

and single or double residue change in the basic or acidic PB1 interface. Diploids expressing WT and mutant DBD–PsIAA4 and AD–PsIAA4 protein fusions were generated and spotted on selective induction medium (Gal/Raf/–Ura/–Trp/–His/+X-Gal). β -galactosidase expression, reporting protein–protein interaction (blue colonies) is shown 4 days after spotting.

7.12 Cloning and *in vitro* analysis of the non-canonical AtAUX/IAA33

Sequence and phylogenetic analysis of *Arabidopsis thaliana* AUX/IAA showed that AtAUX/IAA33 (At5g57420) are non-canonical, compared to others by having an incomplete DIII/IV with several missing conserved residues (cDNA CDS-516 bp and 171 AA, pUNI51-IAA33 was ordered from ABRC-stock C105341). AtAUX/IAA33 was cloned by traditional cloning method using HindIII and BamHI, cloned in pQE30 vector (N-terminal 6X His-tag, Ampicillin resistance)

AtAUX/IAA33 with an N-terminal 6X His-tag

```

      10      20      30      40      50      60
MRGSHHHHHH GSMNSFEPQS QDSLQRRFHQ DNSTTQQPRD TTPFIPKPA SKNHNNNSNS
      70      80      90     100     110     120
SGAAGRSFQG FGLNVEDDLV SSVVPPVTVV LEGRSICQRI SLDKHGSYQS LASALRQMFV
     130     140     150     160     170     180
DGADSTDDL D LSNAIPGHLI AYEDMENDLL LAGDLTWKDF VRVAKRIRIL PVKGNTQRQVK

```

RNE

Number of amino acids: 183

Molecular weight: 20340.5

Theoretical pI: 6.79

7.12.1 Traditional Cloning of AtAUX/IAA33

The AtAUX/IAA33 sequence was amplified using newly designed primers with BamHI and HindIII restriction sites and were cloned into the pQE30 expression vector.

Table A8: Oligonucleotides used for the traditional AtAUX/IAA33 cloning

Forward primer	GGATCGGGATCCATGAATAGTTTCGAGCCACAAAG
Reverse primer	CTAATTAAGCTTTCCTCGTTTCTTTAACTTGTC

PCR reaction (50 μ L)

10X PCR Buffer	5 μ L
10mM dNTPs	1 μ L
Forward and reverse primers	2 μ L + 2 μ L (0.1-1 μ M)
DNA template (pUNI51-IAA33)	2 μ L (10 pg-1 μ g)
DreamTaq	1 μ L
ddH ₂ O	up to 50 μ L

PCR set-up condition

Initial Denaturation	95°C; 3 min	
Denaturation	95°C; 30 sec	} 30 cycles
Annealing	67°C 30 sec	
Extension	72°C; 1 min 20 sec	
Final extension	72°C; 7 min	

Amplified fragments were gel extracted and purified using the PCR purification kit.

Traditional cloning into pQE30 expression vectors was accomplished by the restriction and ligation reaction as described below.

RE digestion of PCR product

PCR product	25 μ L
10X Buffer2 NEB	5 μ L
BSA	5 μ L
BamH1 and HindIII	1 μ L + 1 μ L
ddH ₂ O	13 μ L

RE digestion of pQE30 empty vector digestion (20 μ L)

pQE30 empty vector (360 ng/ μ L)	2 μ L
Buffer 2 (NEB)	2 μ L
BamH1 and HindIII	1 μ L + 1 μ L
BSA 10X	2 μ L
H ₂ O	12 μ L

and restriction mix was incubated for 1 hr at 37°C

Both digested fragment and plasmids were gel extracted and used for ligation reaction (refer Materials and Methods).

Ligation reaction

2 μ L pQE30,

6 μ L AtAUX/IAA33 digested DNA,

10 μ L 2X Ligation buffer (NEB),

1 μ L DNA Ligase and

1 μ L ddH₂O

10 μ L of the ligation reaction mixture was transformed into *E. coli* DH5 α and confirmed the presence of the insert by sequencing (refer Materials and Methods).

7.12.2 Protein over-expression and AUC analysis of the AtAUX/IAA33

The non-canonical AtAUX/IAA33 fusion protein with an N-terminal 6X His-tag was expressed using *E. coli* M15 cells in 2YT media (1 L) supplemented with selective antibiotics (Ampicillin). Cells were centrifuged and resuspended in a lyse buffer (50 mM NaH₂PO₄, 300 mM NaCl and 10mM Imidazole, pH 8.0) and eluted using similar buffer with 100-200 mM Imidazole.

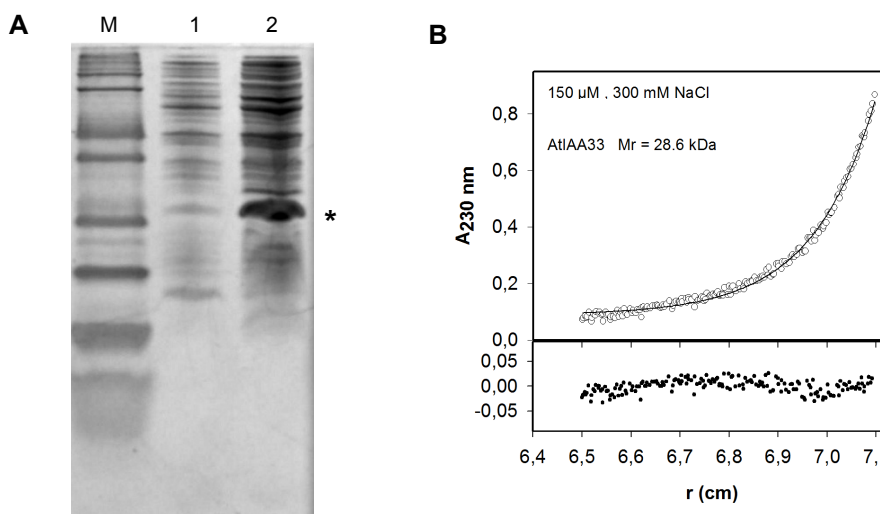


Figure A11: Protein expression and AUC analysis of AtAUX/IAA33

(A) AtAUX/IAA33 FL (*) expression analyzed using SDS-PAGE gel. Lanes: M-Mark12™ unstained protein marker, 2.5 to 200 kDa range, 1- before induction and 2- after induction (B) Average molecular mass determination of WT AtAUX/IAA33 FL by sedimentation equilibrium carried out at 20°C, and data were collected at a rotor speed of 14,000 rpm (refer Materials and methods). Upper panel shows the experimental data, and lower panel shows the residuals.

BIBLIOGRAPHY

- Abel, S. (2007). Auxin is surfacing. *ACS chemical biology* **2**, 380-384.
- Abel, S., and Theologis, A. (1995). A polymorphic bipartite motif signals nuclear targeting of early auxin-inducible proteins related to PS-IAA4 from pea (*Pisum sativum*). *The Plant Journal* **8**, 87-96.
- Abel, S., and Theologis, A. (1996). Early genes and auxin action. *Plant Physiology* **111**, 9-17.
- Abel, S., and Theologis, A. (2010). Odyssey of auxin. *Cold Spring Harbor Perspectives in Biology* **2**, a004572.
- Abel, S., Oeller, P.W., and Theologis, A. (1994). Early auxin-induced genes encode short-lived nuclear proteins. *Proceedings of the National Academy of Sciences* **91**, 326-330.
- Abel, S., Nguyen, M.D., and Theologis, A. (1995). The *PS-IAA4/5*-like family of early auxin-inducible mRNAs in *Arabidopsis thaliana*. *Journal of Molecular Biology* **251**, 533-549.
- Abel, S., Ballas, N., Wong, L.M., and Theologis, A. (1996). DNA elements responsive to auxin. *BioEssays: news and reviews in molecular, cellular and developmental biology* **18**, 647-654.
- Anzola, J.M., Sieberer, T., Ortbauer, M., Butt, H., Korbei, B., Weinhofer, I., Müllner, A.E., and Luschnig, C. (2010). Putative *Arabidopsis* transcriptional adaptor protein (PROPORZ1) is required to modulate histone acetylation in response to auxin. *Proceedings of the National Academy of Sciences* **107**, 10308-10313.
- Ballas, N., Wong, L.M., and Theologis, A. (1993). Identification of the auxin-responsive element, *AuxRE*, in the primary indoleacetic acid-inducible gene, *PS-IAA4/5*, of pea (*Pisum sativum*). *Journal of Molecular Biology* **233**, 580-596.
- Ballas, N., Wong, L.-M., Ke, M., and Theologis, A. (1995). Two auxin-responsive domains interact positively to induce expression of the early indoleacetic acid-inducible gene *PS-IAA4/5*. *Proceedings of the National Academy of Sciences* **92**, 3483-3487.
- Bargmann, B.O., Vanneste, S., Krouk, G., Nawy, T., Efroni, I., Shani, E., Choe, G., Friml, J., Bergmann, D.C., Estelle, M., and Birnbaum, K.D. (2013). A map of cell type-specific auxin responses. *Molecular Systems Biology* **9**, 688.
- Bishopp, A., Mähönen, A.P., and Helariutta, Y. (2006). Signs of change: hormone receptors that regulate plant development. *Development* **133**, 1857-1869.
- Bitto, E., Bingman, C.A., Bittova, L., Houston, N.L., Boston, R.S., Fox, B.G., and Phillips, G.N., Jr. (2009). X-ray structure of ILL2, an auxin-conjugate amidohydrolase from *Arabidopsis thaliana*. *Proteins* **74**, 61-71.
- Boer, D.R., Freire-Rios, A., van den Berg, W.A., Saaki, T., Manfield, I.W., Kepinski, S., Lopez-Vidrieo, I., Franco-Zorrilla, J.M., de Vries, S.C., Solano, R., Weijers, D., and Coll, M. (2014). Structural basis for DNA binding specificity by the auxin-dependent ARF transcription factors. *Cell* **156**, 577-589.
- Brunoud, G., Wells, D.M., Oliva, M., Larrieu, A., Mirabet, V., Burrow, A.H., Beeckman, T., Kepinski, S., Traas, J., Bennett, M.J., and Vernoux, T. (2012). A novel sensor to map auxin response and distribution at high spatio-temporal resolution. *Nature* **482**, 103-106.
- Burroughs, A.M., Iyer, L.M., and Aravind, L. (2012). The natural history of ubiquitin and ubiquitin-related domains. *Frontiers in Bioscience* **17**, 1433-1460.
- Burroughs, A.M., Balaji, S., Iyer, L.M., and Aravind, L. (2007). Small but versatile: the extraordinary functional and structural diversity of the beta-grasp fold. *Biology Direct* **2**, 18.
- Calderon-Villalobos, L.I., Tan, X., Zheng, N., and Estelle, M. (2010). Auxin perception-structural insights. *Cold Spring Harbor Perspectives in Biology* **2**, a005546.
- Calderon-Villalobos, L.I., Lee, S., De Oliveira, C., Ivetac, A., Brandt, W., Armitage, L., Sheard, L.B., Tan, X., Parry, G., Mao, H., Zheng, N., Napier, R., Kepinski, S., and Estelle, M. (2012). A combinatorial TIR1/AFB-Aux/IAA co-receptor system for differential sensing of auxin. *Nature Chemical Biology* **8**, 477-485.
- Carranco, R., Espinosa, J.M., Prieto-Dapena, P., Almoguera, C., and Jordano, J. (2010). Repression by an auxin/indole acetic acid protein connects auxin signaling with heat shock factor-mediated seed longevity. *Proceedings of the National Academy of Sciences of the United States of America* **107**, 21908-21913.
- Causier, B., Ashworth, M., Guo, W., and Davies, B. (2012a). The TOPLESS interactome: a framework for gene repression in *Arabidopsis*. *Plant Physiology* **158**, 423-438.
- Causier, B., Lloyd, J., Stevens, L., and Davies, B. (2012b). TOPLESS co-repressor interactions and their evolutionary conservation in plants. *Plant Signaling and Behavior* **7**, 325-328.
- Chamberlain, P.P., Lopez-Girona, A., Miller, K., Carmel, G., Pagarigan, B., Chie-Leon, B., Rychak, E., Corral, L.G., Ren, Y.J., Wang, M., Riley, M., Delker, S.L., Ito, T., Ando, H., Mori, T., Hirano, Y.,

- Handa, H., Hakoshima, T., Daniel, T.O., and Cathers, B.E.** (2014). Structure of the human Cereblon-DDB1-lenalidomide complex reveals basis for responsiveness to thalidomide analogs. *Nature Structural and Molecular Biology* **21**, 803-809.
- Chapman, E.J., and Estelle, M.** (2009). Mechanism of auxin-regulated gene expression in plants. *Annual Review of Genetics* **43**, 265-285.
- Chardin, C., Girin, T., Roudier, F., Meyer, C., and Krapp, A.** (2014). The plant RWP-RK transcription factors: key regulators of nitrogen responses and of gametophyte development. *Journal of Experimental Botany* **65**, 5577-5587.
- Chen, X., Naramoto, S., Robert, S., Tejos, R., Löfke, C., Lin, D., Yang, Z., and Friml, J.** (2012). ABP1 and ROP6 GTPase signaling regulate clathrin-mediated endocytosis in *Arabidopsis* roots. *Current Biology* **22**, 1326-1332.
- Chen, X., Grandont, L., Li, H., Hauschild, R., Paque, S., Abuzeineh, A., Rakusová, H., Benkova, E., Perrot-Rechenmann, C., and Friml, J.** (2014). Inhibition of cell expansion by rapid ABP1-mediated auxin effect on microtubules. *Nature* **516**, 90-93.
- Chevallet, M., Lucbe, S., and Rabilloud, T.** (2006). Silver staining of proteins in polyacrylamide gels. *Nature Protocols* **1**, 1852-1858.
- Cho, H., Ryu, H., Rho, S., Hill, K., Smith, S., Audenaert, D., Park, J., Han, S., Beeckman, T., and Bennett, M.J.** (2014). A secreted peptide acts on BIN2-mediated phosphorylation of ARFs to potentiate auxin response during lateral root development. *Nature Cell Biology* **16**, 66-76.
- Christian, F., Krause, E., Houslay, M.D., and Baillie, G.S.** (2014). PKA phosphorylation of p62/SQSTM1 regulates PB1 domain interaction partner binding. *Biochimica et Biophysica Acta* **1843**, 2765-2774.
- Ciesielski, T.** (1871). Untersuchung über die Abwärtskrümmung der Wurzel (Dissertation, Breslau).
- Ciuffa, R., Lamark, T., Tarafder, A.K., Guesdon, A., Rybina, S., Hagen, W.J., Johansen, T., and Sachse, C.** (2015). The selective autophagy receptor p62 forms a flexible filamentous helical scaffold. *Cell reports* **11**, 748-758.
- Colon-Carmona, A., Chen, D.L., Yeh, K.C., and Abel, S.** (2000). Aux/IAA proteins are phosphorylated by phytochrome *in vitro*. *Plant Physiology* **124**, 1728-1738.
- Cornilescu, G., Delaglio, F., and Bax, A.** (1999). Protein backbone angle restraints from searching a database for chemical shift and sequence homology. *Journal of Biomolecular NMR* **13**, 289-302.
- Darwin, C., and Darwin, F.** (1880). The power of movement in plants. (John Murray).
- De Rybel, B., Audenaert, D., Beeckman, T., and Kepinski, S.** (2009). The past, present, and future of chemical biology in auxin research. *ACS Chemical Biology* **4**, 987-998.
- De Smet, I., Voß, U., Lau, S., Wilson, M., Shao, N., Timme, R.E., Swarup, R., Kerr, I., Hodgman, C., and Bock, R.** (2011). Unraveling the evolution of auxin signaling. *Plant Physiology* **155**, 209-221.
- Del Pozo, J.C., and Manzano, C.** (2014). Auxin and the ubiquitin pathway. Two players-one target: the cell cycle in action. *Journal of Experimental Botany* **65**, 2617-2632.
- Delaglio, F., Grzesiek, S., Vuister, G.W., Zhu, G., Pfeifer, J., and Bax, A.** (1995). NMRPipe: a multidimensional spectral processing system based on UNIX pipes. *Journal of Biomolecular NMR* **6**, 277-293.
- Dharmasiri, N., Dharmasiri, S., and Estelle, M.** (2005a). The F-box protein TIR1 is an auxin receptor. *Nature* **435**, 441-445.
- Dharmasiri, N., Dharmasiri, S., Jones, A.M., and Estelle, M.** (2003). Auxin action in a cell-free system. *Current Biology* : CB **13**, 1418-1422.
- Dharmasiri, N., Dharmasiri, S., Weijers, D., Lechner, E., Yamada, M., Hobbie, L., Ehrismann, J.S., Jurgens, G., and Estelle, M.** (2005b). Plant development is regulated by a family of auxin receptor F box proteins. *Developmental Cell* **9**, 109-119.
- Di, D.-W., Zhang, C., and Guo, G.-Q.** (2015a). Involvement of secondary messengers and small organic molecules in auxin perception and signaling. *Plant Cell Reports* **34**, 895-904.
- Di, D.-W., Zhang, C., Luo, P., An, C.-W., and Guo, G.-Q.** (2015b). The biosynthesis of auxin: how many paths truly lead to IAA? *Plant Growth Regulation*, 1-11.
- Dinesh, D.C., Kovermann, M., Gopalswamy, M., Hellmuth, A., Calderon-Villalobos, L.I., Lilie, H., Balbach, J., and Abel, S.** (2015). Solution structure of the PsIAA4 oligomerization domain reveals interaction modes for transcription factors in early auxin response. *Proceedings of the National Academy of Sciences of the United States of America* **112**, 6230-6235.
- Dominguez, C., Boelens, R., and Bonvin, A.M.** (2003). HADDOCK: a protein-protein docking approach based on biochemical or biophysical information. *Journal of the American Chemical Society* **125**, 1731-1737.
- dos Santos Maraschin, F., Memelink, J., and Offringa, R.** (2009). Auxin-induced, SCF(TIR1)-mediated poly-ubiquitination marks AUX/IAA proteins for degradation. *The Plant Journal* **59**, 100-109.

- Dreher, K.A., Brown, J., Saw, R.E., and Callis, J. (2006). The *Arabidopsis* Aux/IAA protein family has diversified in degradation and auxin responsiveness. *The Plant Cell* **18**, 699-714.
- Enders, T.A., and Strader, L.C. (2015). Auxin activity: Past, present, and future. *American Journal of Botany* **102**, 180-196.
- Estojak, J., Brent, R., and Golemis, E.A. (1995). Correlation of two-hybrid affinity data with *in vitro* measurements. *Molecular and Cellular Biology* **15**, 5820-5829.
- Farcot, E., Lavedrine, C., and Vernoux, T. (2015). A modular analysis of the auxin signalling network. *PLoS One* **10**, e0122231.
- Feng, W., Tejero, R., Zimmerman, D.E., Inouye, M., and Montelione, G.T. (1998). Solution NMR structure and backbone dynamics of the major cold-shock protein (CspA) from *Escherichia coli*: evidence for conformational dynamics in the single-stranded RNA-binding site. *Biochemistry* **37**, 10881-10896.
- Feng, W., Wu, H., Chan, L.N., and Zhang, M. (2007). The Par-3 NTD adopts a PB1-like structure required for Par-3 oligomerization and membrane localization. *The EMBO Journal* **26**, 2786-2796.
- Finet, C., and Jaillais, Y. (2012). Auxology: when auxin meets plant evo-devo. *Developmental Biology* **369**, 19-31.
- Finet, C., Berne-Dedieu, A., Scutt, C.P., and Marletaz, F. (2013). Evolution of the ARF gene family in land plants: old domains, new tricks. *Molecular Biology and Evolution* **30**, 45-56.
- Fischer, E.S., Bohm, K., Lydeard, J.R., Yang, H., Stadler, M.B., Cavadini, S., Nagel, J., Serluca, F., Acker, V., Lingaraju, G.M., Tichkule, R.B., Schebesta, M., Forrester, W.C., Schirle, M., Hassiepen, U., Ottl, J., Hild, M., Beckwith, R.E., Harper, J.W., Jenkins, J.L., and Thoma, N.H. (2014). Structure of the DDB1-CRBN E3 ubiquitin ligase in complex with thalidomide. *Nature* **512**, 49-53.
- Flores-Sandoval, E., Eklund, D.M., and Bowman, J.L. (2015). A simple auxin transcriptional response system regulates multiple morphogenetic processes in the liverwort *Marchantia polymorpha*. *PLoS Genetics* **11**, e1005207.
- Franco-Zorrilla, J.M., Lopez-Vidriero, I., Carrasco, J.L., Godoy, M., Vera, P., and Solano, R. (2014). DNA-binding specificities of plant transcription factors and their potential to define target genes. *Proceedings of the National Academy of Sciences of the United States of America* **111**, 2367-2372.
- Gagne, J.M., Downes, B.P., Shiu, S.H., Durski, A.M., and Vierstra, R.D. (2002). The F-box subunit of the SCF E3 complex is encoded by a diverse superfamily of genes in *Arabidopsis*. *Proceedings of the National Academy of Sciences of the United States of America* **99**, 11519-11524.
- Gao, Y., Zhang, Y., Zhang, D., Dai, X., Estelle, M., and Zhao, Y. (2015). Auxin binding protein 1 (ABP1) is not required for either auxin signaling or *Arabidopsis* development. *Proceedings of the National Academy of Sciences of the United States of America* **112**, 2275-2280.
- Gilkerson, J., Kelley, D.R., Tam, R., Estelle, M., and Callis, J. (2015). Lysine residues are not required for proteasome-mediated proteolysis of the auxin/indole acidic acid protein IAA1. *Plant Physiology* **168**, 708-720.
- Gill, S.C., and von Hippel, P.H. (1989). Calculation of protein extinction coefficients from amino acid sequence data. *Analytical Biochemistry* **182**, 319-326.
- Glatz, G., Gogl, G., Alexa, A., and Remenyi, A. (2013). Structural mechanism for the specific assembly and activation of the extracellular signal regulated kinase 5 (ERK5) module. *The Journal of Biological Chemistry* **288**, 8596-8609.
- Golemis, E.A., Serebriiskii, I., Finley, R.L., Kolonin, M.G., Gyuris, J., and Brent, R. (1996). Interaction trap/two-hybrid system to identify interacting proteins. *Current Protocols in Cell Biology*, 17.13. 11-17.13. 42.
- Golovenko, D., Manakova, E., Tamulaitiene, G., Grazulis, S., and Siksnys, V. (2009). Structural mechanisms for the 5'-CCWGG sequence recognition by the N- and C-terminal domains of EcoRII. *Nucleic Acids Research* **37**, 6613-6624.
- Golovenko, D., Manakova, E., Zakrys, L., Zaremba, M., Sasnauskas, G., Grazulis, S., and Siksnys, V. (2014). Structural insight into the specificity of the B3 DNA-binding domains provided by the co-crystal structure of the C-terminal fragment of BfiI restriction enzyme. *Nucleic Acids Research* **42**, 4113-4122.
- Grandits, M., and Oostenbrink, C. (2014). Molecular dynamics simulations of the auxin-binding protein 1 in complex with indole-3-acetic acid and naphthalen-1-acetic acid. *Proteins* **82**, 2744-2755.
- Gray, W.M., Kepinski, S., Rouse, D., Leyser, O., and Estelle, M. (2001). Auxin regulates SCF(TIR1)-dependent degradation of AUX/IAA proteins. *Nature* **414**, 271-276.
- Gray, W.M., del Pozo, J.C., Walker, L., Hobbie, L., Risseuw, E., Banks, T., Crosby, W.L., Yang, M., Ma, H., and Estelle, M. (1999). Identification of an SCF ubiquitin-ligase complex required for auxin response in *Arabidopsis thaliana*. *Genes and Development* **13**, 1678-1691.

- Grazulis, S., Manakova, E., Roessle, M., Bochtler, M., Tamulaitiene, G., Huber, R., and Siksnys, V. (2005). Structure of the metal-independent restriction enzyme BfiI reveals fusion of a specific DNA-binding domain with a nonspecific nuclease. *Proceedings of the National Academy of Sciences of the United States of America* **102**, 15797-15802.
- Grones, P., and Friml, J. (2015a). Auxin transporters and binding proteins at a glance. *Journal of Cell Science* **128**, 1-7.
- Grones, P., and Friml, J. (2015b). ABP1: finally docking. *Molecular Plant* **8**, 356-358.
- Grones, P., Chen, X., Simon, S., Kaufmann, W.A., De Rycke, R., Nodzynski, T., Zazimalova, E., and Friml, J. (2015). Auxin-binding pocket of ABP1 is crucial for its gain-of-function cellular and developmental roles. *Journal of Experimental Botany*.
- Grzesiek, S., and Bax, A. (1993). The importance of not saturating water in protein NMR. Application to sensitivity enhancement and NOE measurements. *Journal of the American Chemical Society* **115**, 12593-12594.
- Grzesiek, S., Stahl, S.J., Wingfield, P.T., and Bax, A. (1996). The CD4 determinant for downregulation by HIV-1 Nef directly binds to Nef. Mapping of the Nef binding surface by NMR. *Biochemistry* **35**, 10256-10261.
- Guilfoyle, T., Ulmasov, T., and Hagen, G. (1998). The ARF family of transcription factors and their role in plant hormone-responsive transcription. *Cellular and Molecular Life Sciences CMLS* **54**, 619-627.
- Guilfoyle, T.J. (2015). The PB1 domain in auxin response factor and Aux/IAA proteins: a versatile protein interaction module in the auxin response. *The Plant Cell* **27**, 33-43.
- Guilfoyle, T.J., and Hagen, G. (2007). Auxin response factors. *Current Opinion in Plant Biology* **10**, 453-460.
- Guilfoyle, T.J., and Hagen, G. (2012). Getting a grasp on domain III/IV responsible for Auxin Response Factor-IAA protein interactions. *Plant Science* **190**, 82-88.
- Guseman, J.M., Hellmuth, A., Lancot, A., Feldman, T.P., Moss, B.L., Klavins, E., Calderon-Villalobos, L.I., and Nemhauser, J.L. (2015). Auxin-induced degradation dynamics set the pace for lateral root development. *Development* **142**, 905-909.
- Gyuris, J., Golemis, E., Chertkov, H., and Brent, R. (1993). Cdi1, a human G1 and S phase protein phosphatase that associates with Cdk2. *Cell* **75**, 791-803.
- Haberland, M., Montgomery, R.L., and Olson, E.N. (2009). The many roles of histone deacetylases in development and physiology: implications for disease and therapy. *Nature Reviews Genetics* **10**, 32-42.
- Habets, M.E., and Offringa, R. (2015). Auxin Binding Protein 1: a red herring after all? *Molecular Plant* **8**, 1131-1134.
- Hagen, G., and Guilfoyle, T. (2002). Auxin-responsive gene expression: genes, promoters and regulatory factors. *Plant Molecular Biology* **49**, 373-385.
- Hammes, G.G. (2007). Physical chemistry for the biological sciences. *Methods of Biochemical Analysis* **50**, 3-345.
- Han, M., Park, Y., Kim, I., Kim, E.H., Yu, T.K., Rhee, S., and Suh, J.Y. (2014). Structural basis for the auxin-induced transcriptional regulation by Aux/IAA17. *Proceedings of the National Academy of Sciences of the United States of America* **111**, 18613-18618.
- Hardtke, C.S., and Berleth, T. (1998). The *Arabidopsis* gene MONOPTEROS encodes a transcription factor mediating embryo axis formation and vascular development. *The EMBO Journal* **17**, 1405-1411.
- Havens, K.A., Guseman, J.M., Jang, S.S., Pierre-Jerome, E., Bolten, N., Klavins, E., and Nemhauser, J.L. (2012). A synthetic approach reveals extensive tunability of auxin signaling. *Plant Physiology* **160**, 135-142.
- Hayashi, K., Tan, X., Zheng, N., Hatate, T., Kimura, Y., Kepinski, S., and Nozaki, H. (2008). Small-molecule agonists and antagonists of F-box protein-substrate interactions in auxin perception and signaling. *Proceedings of the National Academy of Sciences of the United States of America* **105**, 5632-5637.
- Hayashi, K., Neve, J., Hirose, M., Kuboki, A., Shimada, Y., Kepinski, S., and Nozaki, H. (2012). Rational design of an auxin antagonist of the SCF(TIR1) auxin receptor complex. *ACS Chemical Biology* **7**, 590-598.
- Hertel, R., Thomson, K.-S., and Russo, V. (1972). *In-vitro* auxin binding to particulate cell fractions from corn coleoptiles. *Planta* **107**, 325-340.
- Hill, K. (2015). Post-translational modifications of hormone-responsive transcription factors: the next level of regulation. *Journal of Experimental Botany* **66**, 4933-4945.
- Hirano, Y., Yoshinaga, S., Ogura, K., Yokochi, M., Noda, Y., Sumimoto, H., and Inagaki, F. (2004). Solution structure of atypical protein kinase C PB1 domain and its mode of interaction with ZIP/p62 and MEK5. *The Journal of Biological Chemistry* **279**, 31883-31890.

- Hirano, Y., Yoshinaga, S., Takeya, R., Suzuki, N.N., Horiuchi, M., Kohjima, M., Sumimoto, H., and Inagaki, F. (2005). Structure of a cell polarity regulator, a complex between atypical PKC and Par6 PB1 domains. *The Journal of Biological Chemistry* **280**, 9653-9661.
- Hobbie, L., and Estelle, M. (1994). Genetic approaches to auxin action. *Plant, Cell and Environment* **17**, 525-540.
- Hobbie, L.J. (1998). Auxin: molecular genetic approaches in *Arabidopsis*. *Plant Physiology and Biochemistry* **36**, 91-102.
- Holm, L., and Park, J. (2000). DaliLite workbench for protein structure comparison. *Bioinformatics* **16**, 566-567.
- Honbou, K., Minakami, R., Yuzawa, S., Takeya, R., Suzuki, N.N., Kamakura, S., Sumimoto, H., and Inagaki, F. (2007). Full-length p40phox structure suggests a basis for regulation mechanism of its membrane binding. *EMBO Journal* **26**, 1176-1186.
- Hu, Q., Shen, W., Huang, H., Liu, J., Zhang, J., Huang, X., Wu, J., and Shi, Y. (2007). Insight into the binding properties of MEKK3 PB1 to MEK5 PB1 from its solution structure. *Biochemistry* **46**, 13478-13489.
- Huang, J., Yue, J., and Hu, X. (2014). Origin of plant auxin biosynthesis in charophyte algae: a reply to Wang et al. *Trends in Plant Science* **19**, 743.
- Ito, T., Matsui, Y., Ago, T., Ota, K., and Sumimoto, H. (2001). Novel modular domain PB1 recognizes PC motif to mediate functional protein-protein interactions. *The EMBO Journal* **20**, 3938-3946.
- Ivanchenko, M.G., Coffeen, W.C., Lomax, T.L., and Dubrovsky, J.G. (2006). Mutations in the Diageotropica (Dgt) gene uncouple patterned cell division during lateral root initiation from proliferative cell division in the pericycle. *The Plant Journal* **46**, 436-447.
- Jaillais, Y., and Chory, J. (2010). Unraveling the paradoxes of plant hormone signaling integration. *Nature Structural and Molecular Biology* **17**, 642-645.
- Jing, H., Yang, X., Zhang, J., Liu, X., Zheng, H., Dong, G., Nian, J., Feng, J., Xia, B., Qian, Q., Li, J., and Zuo, J. (2015). Peptidyl-prolyl isomerization targets rice Aux/IAAs for proteasomal degradation during auxin signalling. *Nature Communications* **6**, 7395.
- Johnson, B.A., and Blevins, R.A. (1994). NMRView - a computer-program for the visualization and analysis of NMR Data. *Journal of Biomolecular NMR* **4**, 603-614.
- Jones, A.M., Im, K.-H., Savka, M.A., Wu, M.-J., DeWitt, N.G., Shillito, R., and Binns, A.N. (1998). Auxin-dependent cell expansion mediated by overexpressed auxin-binding protein 1. *Science* **282**, 1114-1117.
- Jun, J., Fiume, E., and Fletcher, J. (2008). The CLE family of plant polypeptide signaling molecules. *Cellular and Molecular Life Sciences* **65**, 743-755.
- Jurado, S., Abraham, Z., Manzano, C., Lopez-Torres, G., Pacios, L.F., and Del Pozo, J.C. (2010). The *Arabidopsis* cell cycle F-box protein SKP2A binds to auxin. *The Plant Cell* **22**, 3891-3904.
- Kagale, S., and Rozwadowski, K. (2011). EAR motif-mediated transcriptional repression in plants: an underlying mechanism for epigenetic regulation of gene expression. *Epigenetics* **6**, 141-146.
- Kagaya, Y., Ohmiya, K., and Hattori, T. (1999). RAV1, a novel DNA-binding protein, binds to bipartite recognition sequence through two distinct DNA-binding domains uniquely found in higher plants. *Nucleic Acids Research* **27**, 470-478.
- Kato, H., Ishizaki, K., Kouno, M., Shirakawa, M., Bowman, J.L., Nishihama, R., and Kohchi, T. (2015). Auxin-mediated transcriptional system with a minimal set of components is critical for morphogenesis through the life cycle in *Marchantia polymorpha*. *PLoS Genetics* **11**, e1005084.
- Kay, L.E., Torchia, D.A., and Bax, A. (1989). Backbone dynamics of proteins as studied by ¹⁵N inverse detected heteronuclear NMR spectroscopy: application to Staphylococcal nuclease. *Biochemistry* **28**, 8972-8979.
- Kazan, K. (2013). Auxin and the integration of environmental signals into plant root development. *Annals of Botany* **112**, 1655-1665.
- Ke, J., Ma, H., Gu, X., Thelen, A., Brunzelle, J., Li, J., Xu, H.E., and Melcher, K. (2015). Structural basis for recognition of diverse transcriptional repressors by the TOPLESS family of corepressors. *Science Advances* **1**:e1500107.
- Keilwagen, J., Grau, J., Paponov, I.A., Posch, S., Strickert, M., and Grosse, I. (2011). De-novo discovery of differentially abundant transcription factor binding sites including their positional preference. *PLoS Computational Biology* **7**, e1001070.
- Kepinski, S., and Leyser, O. (2005). The *Arabidopsis* F-box protein TIR1 is an auxin receptor. *Nature* **435**, 446-451.
- Kim, J., Harter, K., and Theologis, A. (1997). Protein-protein interactions among the Aux/IAA proteins. *Proceedings of the National Academy of Sciences of the United States of America* **94**, 11786-11791.

- King, G.J., Chanson, A.H., McCallum, E.J., Ohme-Takagi, M., Byriel, K., Hill, J.M., Martin, J.L., and Mylne, J.S. (2013). The *Arabidopsis* B3 domain protein VERNALIZATION1 (VRN1) is involved in processes essential for development, with structural and mutational studies revealing its DNA-binding surface. *The Journal of Biological Chemistry* **288**, 3198-3207.
- Kögl, F., and Smit, A.J.H. (1931). Über die Chemie des Wuchsstoffs.
- Korasick, D.A., Enders, T.A., and Strader, L.C. (2013). Auxin biosynthesis and storage forms. *Journal of Experimental Botany* **64**, 2541-2555.
- Korasick, D.A., Jez, J.M., and Strader, L.C. (2015a). Refining the nuclear auxin response pathway through structural biology. *Current Opinion in Plant Biology* **27**, 22-28.
- Korasick, D.A., Westfall, C.S., Lee, S.G., Nanao, M.H., Dumas, R., Hagen, G., Guilfoyle, T.J., Jez, J.M., and Strader, L.C. (2014). Molecular basis for AUXIN RESPONSE FACTOR protein interaction and the control of auxin response repression. *Proceedings of the National Academy of Sciences of the United States of America* **111**, 5427-5432.
- Korasick, D.A., Chatterjee, S., Tonelli, M., Dashti, H., Lee, S.G., Westfall, C.S., Fulton, D.B., Andreotti, A.H., Amarasinghe, G.K., Strader, L.C., and Jez, J.M. (2015b). Defining a two-pronged structural model for PB1 (Phox/Bem1p) domain interaction in plant auxin responses. *The Journal of Biological Chemistry* **290**, 12868-12878.
- Koshiba, T., Ballas, N., Wong, L.-M., and Theologis, A. (1995). Transcriptional regulation of *PS-IAA4/5* and *PS-IAA6* early gene expression by indoleacetic acid and protein synthesis inhibitors in pea (*Pisum sativum*). *Journal of Molecular Biology* **253**, 396-413.
- Kovacs, I., Ayaydin, F., Oberschall, A., Ipacs, I., Bottka, S., Pongor, S., Dudits, D., and Toth, E.C. (1998). Immunolocalization of a novel annexin-like protein encoded by a stress and abscisic acid responsive gene in alfalfa. *The Plant Journal* **15**, 185-197.
- Kravtsova-Ivantsiv, Y., and Ciechanover, A. (2012). Non-canonical ubiquitin-based signals for proteasomal degradation. *Journal of Cell Science* **125**, 539-548.
- Krogan, N.T., Hogan, K., and Long, J.A. (2012a). APETALA2 negatively regulates multiple floral organ identity genes in *Arabidopsis* by recruiting the co-repressor TOPLESS and the histone deacetylase HDA19. *Development* **139**, 4180-4190.
- Krogan, N.T., Yin, X.J., Ckurshumova, W., and Berleth, T. (2014). Distinct subclades of Aux/IAA genes are direct targets of ARF5/MP transcriptional regulation. *New Phytologist* **204**, 474-483.
- Krogan, N.T., Ckurshumova, W., Marcos, D., Caragea, A.E., and Berleth, T. (2012b). Deletion of MP/ARF5 domains III and IV reveals a requirement for Aux/IAA regulation in *Arabidopsis* leaf vascular patterning. *The New Phytologist* **194**, 391-401.
- Kumari, S., and van der Hoorn, R.A. (2011). A structural biology perspective on bioactive small molecules and their plant targets. *Current Opinion in Plant Biology* **14**, 480-488.
- Laha, D., Johnen, P., Azevedo, C., Dynowski, M., Weiss, M., Capolicchio, S., Mao, H., Iven, T., Steenbergen, M., Freyer, M., Gaugler, P., de Campos, M.K., Zheng, N., Feussner, I., Jessen, H.J., Van Wees, S.C., Saiardi, A., and Schaaf, G. (2015). VIH2 Regulates the Synthesis of Inositol Pyrophosphate InsP8 and Jasmonate-Dependent Defenses in *Arabidopsis*. *The Plant Cell* **27**, 1082-1097.
- Lamark, T., Perander, M., Outzen, H., Kristiansen, K., Overvatn, A., Michaelsen, E., Bjorkoy, G., and Johansen, T. (2003). Interaction codes within the family of mammalian Phox and Bem1p domain-containing proteins. *The Journal of Biological Chemistry* **278**, 34568-34581.
- Lam, H.K., McAdam, S.A., McAdam, E.L., and Ross, J.J. (2015). Evidence That Chlorinated Auxin Is Restricted to the Fabaceae But Not to the Fabeae. *Plant physiology* **168**, 798-803.
- Laskowski, R.A., Rullmann, J.A.C., MacArthur, M.W., Kaptein, R., and Thornton, J.M. (1996). AQUA and PROCHECK-NMR: programs for checking the quality of protein structures solved by NMR. *Journal of Biomolecular NMR* **8**, 477-486.
- Laskowski, R.A., Hutchinson, E.G., Michie, A.D., Wallace, A.C., Jones, M.L., and Thornton, J.M. (1997). PDBsum: a Web-based database of summaries and analyses of all PDB structures. *Trends in Biochemical Sciences* **22**, 488-490.
- Lau, S., Shao, N., Bock, R., Jürgens, G., and De Smet, I. (2009). Auxin signaling in algal lineages: fact or myth? *Trends in Plant Science* **14**, 182-188.
- Lavy, M., Prigge, M.J., Tigyi, K., and Estelle, M. (2012). The cyclophilin DIAGEOTROPICA has a conserved role in auxin signaling. *Development* **139**, 1115-1124.
- Lee, S., Sundaram, S., Armitage, L., Evans, J.P., Hawkes, T., Kepinski, S., Ferro, N., and Napier, R.M. (2014). Defining binding efficiency and specificity of auxins for SCF(TIR1/AFB)-Aux/IAA co-receptor complex formation. *ACS Chemical Biology* **9**, 673-682.

- Leitner, D., Wahl, M., Labudde, D., Krause, G., Diehl, A., Schmieder, P., Pires, J.R., Fossi, M., Wiedemann, U., Leidert, M., and Oschkinat, H. (2005). The solution structure of an N-terminally truncated version of the yeast CDC24p PB1 domain shows a different beta-sheet topology. *FEBS Letters* **579**, 3534-3538.
- Levin, E.J., Kondrashov, D.A., Wesenberg, G.E., and Phillips, G.N., Jr. (2007). Ensemble refinement of protein crystal structures: validation and application. *Structure* **15**, 1040-1052.
- Li, H., Hagen, G., and Guilfoyle, T.J. (2011a). Do some IAA proteins have two repression domains? *Plant Signaling and Behavior* **6**, 858-860.
- Li, H., Tiwari, S.B., Hagen, G., and Guilfoyle, T.J. (2011b). Identical amino acid substitutions in the repression domain of auxin/indole-3-acetic acid proteins have contrasting effects on auxin signaling. *Plant Physiology* **155**, 1252-1263.
- Li, J.F., Bush, J., Xiong, Y., Li, L., and McCormack, M. (2011c). Large-scale protein-protein interaction analysis in *Arabidopsis* mesophyll protoplasts by split firefly luciferase complementation. *PloS One* **6**, e27364.
- Lindsey, K., Casson, S., and Chilley, P. (2002). Peptides: new signalling molecules in plants. *Trends in Plant Science* **7**, 78-83.
- Liu, J., Wilson, T.E., Milbrandt, J., and Johnston, M. (1993). Identifying DNA-binding sites and analyzing DNA-binding domains using a yeast selection system. *Methods* **5**, 125-137.
- Ljung, K. (2013). Auxin metabolism and homeostasis during plant development. *Development* **140**, 943-950.
- Long, J.A., Ohno, C., Smith, Z.R., and Meyerowitz, E.M. (2006). TOPLESS regulates apical embryonic fate in *Arabidopsis*. *Science* **312**, 1520-1523.
- Maraschin Fdos, S., Memelink, J., and Offringa, R. (2009). Auxin-induced, SCF(TIR1)-mediated poly-ubiquitination marks AUX/IAA proteins for degradation. *The Plant Journal* **59**, 100-109.
- Matsubayashi, Y. (2011). Small post-translationally modified peptide signals in *Arabidopsis*. *The Arabidopsis book/American Society of Plant Biologists* **9**, e0150.
- Mattioli, F., and Sixma, T.K. (2014). Lysine-targeting specificity in ubiquitin and ubiquitin-like modification pathways. *Nature Structural and Molecular Biology* **21**, 308-316.
- Mironova, V.V., Omelyanchuk, N.A., Wiebe, D.S., and Levitsky, V.G. (2014). Computational analysis of auxin responsive elements in the *Arabidopsis thaliana* L. genome. *BMC Genomics* **15 Suppl 12**, S4.
- Mockaitis, K., and Estelle, M. (2008). Auxin receptors and plant development: a new signaling paradigm. *Annual Review of Cell and Developmental Biology* **24**, 55-80.
- Morgan, K.E., Zarembinski, T.I., Theologis, A., and Abel, S. (1999). Biochemical characterization of recombinant polypeptides corresponding to the predicted beta-alpha-alpha fold in Aux/IAA proteins. *FEBS Letters* **454**, 283-287.
- Moss, B.L., Mao, H., Guseman, J.M., Hinds, T.R., Hellmuth, A., Kovenock, M., Noorassa, A., Lanctot, A., Calderon-Villalobos, L.I., Zheng, N., and Nemhauser, J.L. (2015). Rate motifs tune Aux/IAA degradation dynamics. *Plant Physiology* (Preview)
- Mueller-Dieckmann, C., Panjekar, S., Schmidt, A., Mueller, S., Kuper, J., Geerloff, A., Wilmanns, M., Singh, R.K., Tucker, P.A., and Weiss, M.S. (2007). On the routine use of soft X-rays in macromolecular crystallography. Part IV. Efficient determination of anomalous substructures in biomacromolecules using longer X-ray wavelengths. *Acta Crystallographica D Biological Crystallography* **63**, 366-380.
- Muller, S., Kursula, I., Zou, P., and Wilmanns, M. (2006). Crystal structure of the PB1 domain of NBR1. *FEBS Letters* **580**, 341-344.
- Nanao, M.H., Vinos-Poyo, T., Brunoud, G., Thevenon, E., Mazzoleni, M., Mast, D., Laine, S., Wang, S., Hagen, G., Li, H., Guilfoyle, T.J., Parcy, F., Vernoux, T., and Dumas, R. (2014). Structural basis for oligomerization of auxin transcriptional regulators. *Nature Communications* **5**, 3617.
- Oeller, P.W., and Theologis, A. (1995). Induction kinetics of the nuclear proteins encoded by the early indoleacetic acid-inducible genes, *PS-IAA4/5* and *PS-IAA6*, in pea (*Pisum sativum* L.). *The Plant Journal* **7**, 37-48.
- Oeller, P.W., Keller, J.A., Parks, J.E., Silbert, J.E., and Theologis, A. (1993). Structural characterization of the early indoleacetic acid-inducible genes, *PS-IAA4/5* and *PS-IAA6*, of pea (*Pisum sativum* L.). *Journal of Molecular Biology* **233**, 789-798.
- Ogura, K., Tandai, T., Yoshinaga, S., Kobashigawa, Y., Kumeta, H., Ito, T., Sumimoto, H., and Inagaki, F. (2009). NMR structure of the heterodimer of Bem1 and Cdc24 PB1 domains from *Saccharomyces cerevisiae*. *Journal of Biochemistry* **146**, 317-325.

- Oh, E., Zhu, J.-Y., Bai, M.-Y., Arenhart, R.A., Sun, Y., and Wang, Z.-Y. (2014). Cell elongation is regulated through a central circuit of interacting transcription factors in the *Arabidopsis* hypocotyl. *eLife* **3**, e03031.
- Oh, K., Ivanchenko, M.G., White, T.J., and Lomax, T.L. (2006). The diageotropica gene of tomato encodes a cyclophilin: a novel player in auxin signaling. *Planta* **224**, 133-144.
- Okushima, Y., Overvoorde, P.J., Arima, K., Alonso, J.M., Chan, A., Chang, C., Ecker, J.R., Hughes, B., Lui, A., and Nguyen, D. (2005). Functional genomic analysis of the AUXIN RESPONSE FACTOR gene family members in *Arabidopsis thaliana*: unique and overlapping functions of ARF7 and ARF19. *The Plant Cell* **17**, 444-463.
- Ouellet, F., Overvoorde, P.J., and Theologis, A. (2001). IAA17/AXR3: biochemical insight into an auxin mutant phenotype. *The Plant Cell* **13**, 829-841.
- Overvoorde, P.J., Okushima, Y., Alonso, J.M., Chan, A., Chang, C., Ecker, J.R., Hughes, B., Liu, A., Onodera, C., Quach, H., Smith, A., Yu, G., and Theologis, A. (2005). Functional genomic analysis of the AUXIN/INDOLE-3-ACETIC ACID gene family members in *Arabidopsis thaliana*. *The Plant Cell* **17**, 3282-3300.
- Paponov, I.A., Teale, W., Lang, D., Paponov, M., Reski, R., Rensing, S.A., and Palme, K. (2009). The evolution of nuclear auxin signalling. *BMC Evolutionary Biology* **9**, 126.
- Paque, S., Mouille, G., Grandont, L., Alabadi, D., Gaertner, C., Goyallon, A., Muller, P., Primard-Brisset, C., Sormani, R., and Blázquez, M.A. (2014). AUXIN BINDING PROTEIN1 links cell wall remodeling, auxin signaling, and cell expansion in *Arabidopsis*. *The Plant Cell* **26**, 280-295.
- Parry, G., Calderon-Villalobos, L.I., Prigge, M., Peret, B., Dharmasiri, S., Itoh, H., Lechner, E., Gray, W.M., Bennett, M., and Estelle, M. (2009). Complex regulation of the TIR1/AFB family of auxin receptors. *Proceedings of the National Academy of Sciences of the United States of America* **106**, 22540-22545.
- Peat, T.S., Bottcher, C., Newman, J., Lucent, D., Cowieson, N., and Davies, C. (2012). Crystal structure of an indole-3-acetic acid amido synthetase from grapevine involved in auxin homeostasis. *The Plant cell* **24**, 4525-4538.
- Pennazio, S. (2002). The discovery of the chemical nature of the plant hormone auxin. *Rivista di Biologia* **95**, 289-308.
- Perez, A.C., and Goossens, A. (2013). Jasmonate signalling: a copycat of auxin signalling? *Plant, Cell and Environment* **36**, 2071-2084.
- Pierre-Jerome, E., Jang, S.S., Havens, K.A., Nemhauser, J.L., and Klavins, E. (2014). Recapitulation of the forward nuclear auxin response pathway in yeast. *Proceedings of the National Academy of Sciences of the United States of America* **111**, 9407-9412.
- Piya, S., Shrestha, S.K., Binder, B., Stewart, C.N., Jr., and Hewezi, T. (2014). Protein-protein interaction and gene co-expression maps of ARFs and Aux/IAAs in *Arabidopsis*. *Frontiers in Plant Science* **5**, 744.
- Ponomarenko, P.M., and Ponomarenko, M.P. (2015). Sequence-based prediction of transcription upregulation by auxin in plants. *Journal of Bioinformatics and Computational Biology* **13**, 1540009.
- Ponting, C.P., Ito, T., Moscat, J., Diaz-Meco, M.T., Inagaki, F., and Sumimoto, H. (2002). OPR, PC and AID: all in the PB1 family. *Trends in Biochemical Sciences* **27**, 10.
- Porter, W.L., and Thimann, K.V. (1965). Molecular requirements for auxin action-I: Halogenated indoles and indoleacetic acid. *Phytochemistry* **4**, 229-243.
- Rademacher, E.H., Moller, B., Lokerse, A.S., Llavata-Peris, C.I., van den Berg, W., and Weijers, D. (2011). A cellular expression map of the *Arabidopsis* AUXIN RESPONSE FACTOR gene family. *The Plant Journal* **68**, 597-606.
- Rademacher, E.H., Lokerse, A.S., Schlereth, A., Llavata-Peris, C.I., Bayer, M., Kientz, M., Rios, A.F., Borst, J.W., Lukowitz, W., and Jürgens, G. (2012). Different auxin response machineries control distinct cell fates in the early plant embryo. *Developmental Cell* **22**, 211-222.
- Ramachandran, G., Ramakrishnan, C., and Sasisekharan, V. (1963). Stereochemistry of polypeptide chain configurations. *Journal of Molecular Biology* **7**, 95-99.
- Ramos, J.A., Zenser, N., Leyser, O., and Callis, J. (2001). Rapid degradation of auxin/indoleacetic acid proteins requires conserved amino acids of domain II and is proteasome dependent. *The Plant Cell* **13**, 2349-2360.
- Reed, J.W. (2001). Roles and activities of Aux/IAA proteins in *Arabidopsis*. *Trends in Plant Science* **6**, 420-425.
- Reinecke, D.M. (1999). 4-chloroindole-3-acetic acid and plant growth. *Plant Growth Regulation* **27**, 3-13.
- Remington, D.L., Vision, T.J., Guilfoyle, T.J., and Reed, J.W. (2004). Contrasting modes of diversification in the Aux/IAA and ARF gene families. *Plant Physiology* **135**, 1738-1752.

- Ren, J., Wang, J., Wang, Z., and Wu, J. (2014). Structural and biochemical insights into the homotypic PB1-PB1 complex between PKC ζ and p62. *Science China. Life Sciences* **57**, 69-80.
- Retzer, K., and Luschnig, C. (2015). DIAGEOTROPICA: news from the auxin swamp. *Trends in Plant Science* **6**, 328-329.
- Rieping, W., Habeck, M., Bardiaux, B., Bernard, A., Malliavin, T.E., and Nilges, M. (2007). ARIA2: automated NOE assignment and data integration in NMR structure calculation. *Bioinformatics* **23**, 381-382.
- Rigal, A., Ma, Q., and Robert, S. (2014). Unraveling plant hormone signaling through the use of small molecules. *Frontiers in Plant Science* **5**, 373.
- Robert, X., and Gouet, P. (2014). Deciphering key features in protein structures with the new ENDscript server. *Nucleic Acids Research* **42**, W320-W324.
- Rouse, D., Mackay, P., Stirnberg, P., Estelle, M., and Leyser, O. (1998). Changes in auxin response from mutations in an AUX/IAA gene. *Science* **279**, 1371-1373.
- Ruegger, M., Dewey, E., Gray, W.M., Hobbie, L., Turner, J., and Estelle, M. (1998). The TIR1 protein of *Arabidopsis* functions in auxin response and is related to human SKP2 and yeast grr1p. *Genes and Development* **12**, 198-207.
- Rymen, B., and Sugimoto, K. (2012). Tuning growth to the environmental demands. *Current Opinion in Plant Biology* **15**, 683-690.
- Saio, T., Yokochi, M., and Inagaki, F. (2009). The NMR structure of the p62 PB1 domain, a key protein in autophagy and NF-kappaB signaling pathway. *Journal of Biomolecular NMR* **45**, 335-341.
- Saio, T., Yokochi, M., Kumeta, H., and Inagaki, F. (2010). PCS-based structure determination of protein-protein complexes. *Journal of Biomolecular NMR* **46**, 271-280.
- Salehin, M., Bagchi, R., and Estelle, M. (2015). SCF TIR1/AFB-based auxin perception: mechanism and role in plant growth and development. *The Plant Cell* **27**, 9-19.
- Santner, A., Calderon-Villalobos, L.I., and Estelle, M. (2009). Plant hormones are versatile chemical regulators of plant growth. *Nature Chemical Biology* **5**, 301-307.
- Sato, A., and Yamamoto, K.T. (2008). Overexpression of the non-canonical Aux/IAA genes causes auxin-related aberrant phenotypes in *Arabidopsis*. *Physiologia Plantarum* **133**, 397-405.
- Sauer, M., Robert, S., and Kleine-Vehn, J. (2013). Auxin: simply complicated. *Journal of Experimental Botany* **64**, 2565-2577.
- Scacchi, E., Salinas, P., Gujas, B., Santuari, L., Krogan, N., Ragni, L., Berleth, T., and Hardtke, C.S. (2010). Spatio-temporal sequence of cross-regulatory events in root meristem growth. *Proceedings of the National Academy of Sciences of the United States of America* **107**, 22734-22739.
- Schägger, H. (2006). Tricine-SDS-PAGE. *Nature Protocols* **1**, 16-22.
- Schuck, P. (2000). Size-distribution analysis of macromolecules by sedimentation velocity ultracentrifugation and lamm equation modeling. *Biophysical Journal* **78**, 1606-1619.
- Shan, X., Yan, J., and Xie, D. (2012). Comparison of phytohormone signaling mechanisms. *Current Opinion in Plant Biology* **15**, 84-91.
- Sheard, L.B., Tan, X., Mao, H., Withers, J., Ben-Nissan, G., Hinds, T.R., Kobayashi, Y., Hsu, F.F., Sharon, M., Browse, J., He, S.Y., Rizo, J., Howe, G.A., and Zheng, N. (2010). Jasmonate perception by inositol-phosphate-potentiated COI1-JAZ co-receptor. *Nature* **468**, 400-405.
- Shen, C., Wang, S., Bai, Y., Wu, Y., Zhang, S., Chen, M., Guilfoyle, T.J., Wu, P., and Qi, Y. (2010). Functional analysis of the structural domain of ARF proteins in rice (*Oryza sativa* L.). *Journal of Experimental Botany* **61**, 3971-3981.
- Shen, Y., Delaglio, F., Cornilescu, G., and Bax, A. (2009). TALOS+: a hybrid method for predicting protein backbone torsion angles from NMR chemical shifts. *Journal of Biomolecular NMR* **44**, 213-223.
- Shin, R., Burch, A.Y., Huppert, K.A., Tiwari, S.B., Murphy, A.S., Guilfoyle, T.J., and Schachtman, D.P. (2007). The *Arabidopsis* transcription factor MYB77 modulates auxin signal transduction. *The Plant Cell* **19**, 2440-2453.
- Shimizu-Mitao, Y., and Kakimoto, T. (2014). Auxin sensitivities of all *Arabidopsis* Aux/IAAs for degradation in the presence of every TIR1/AFB. *Plant and Cell Physiology* **55**, 1450-1459.
- Sugawara, S., Mashiguchi, K., Tanaka, K., Hishiyama, S., Sakai, T., Hanada, K., Kinoshita-Tsujimura, K., Yu, H., Dai, X., and Takebayashi, Y. (2015). Distinct characteristics of indole-3-acetic acid and phenylacetic acid, two common auxins in plants. *Plant and Cell Physiology*, **56**, 1641-1654.
- Sumimoto, H., Kamakura, S., and Ito, T. (2007). Structure and function of the PB1 domain, a protein interaction module conserved in animals, fungi, amoebas, and plants. *Science Signalling*, **401**, re6.

- Suzuki, W., Konishi, M., and Yanagisawa, S.** (2013). The evolutionary events necessary for the emergence of symbiotic nitrogen fixation in legumes may involve a loss of nitrate responsiveness of the NIN transcription factor. *Plant Signaling and Behavior* **8**, e25975.
- Svenning, S., Lamark, T., Krause, K., and Johansen, T.** (2011). Plant NBR1 is a selective autophagy substrate and a functional hybrid of the mammalian autophagic adapters NBR1 and p62/SQSTM1. *Autophagy* **7**, 993-1010.
- Szemenyei, H., Hannon, M., and Long, J.A.** (2008). TOPLESS mediates auxin-dependent transcriptional repression during *Arabidopsis* embryogenesis. *Science* **319**, 1384-1386.
- Tan, X., Calderon-Villalobos, L.I., Sharon, M., Zheng, C., Robinson, C.V., Estelle, M., and Zheng, N.** (2007). Mechanism of auxin perception by the TIR1 ubiquitin ligase. *Nature* **446**, 640-645.
- Tao, Y., Ferrer, J.L., Ljung, K., Pojer, F., Hong, F., Long, J.A., Li, L., Moreno, J.E., Bowman, M.E., Ivans, L.J., Cheng, Y., Lim, J., Zhao, Y., Ballare, C.L., Sandberg, G., Noel, J.P., and Chory, J.** (2008). Rapid synthesis of auxin via a new tryptophan-dependent pathway is required for shade avoidance in plants. *Cell* **133**, 164-176.
- Tatematsu, K., Kumagai, S., Muto, H., Sato, A., Watahiki, M.K., Harper, R.M., Liscum, E., and Yamamoto, K.T.** (2004). MASSUGU2 encodes Aux/IAA19, an auxin-regulated protein that functions together with the transcriptional activator NPH4/ARF7 to regulate differential growth responses of hypocotyl and formation of lateral roots in *Arabidopsis thaliana*. *The Plant Cell* **16**, 379-393.
- Terasawa, H., Noda, Y., Ito, T., Hatanaka, H., Ichikawa, S., Ogura, K., Sumimoto, H., and Inagaki, F.** (2001). Structure and ligand recognition of the PB1 domain: a novel protein module binding to the PC motif. *EMBO Journal* **20**, 3947-3956.
- Theologis, A.** (1986). Rapid gene regulation by auxin. *Annual review of plant physiology* **37**, 407-438.
- Theologis, A.** (1989). Auxin-regulated gene expression in plants. *Biotechnology* **12**, 229-243.
- Theologis, A., and Ray, P.M.** (1982). Early auxin-regulated polyadenylated mRNA sequences in pea stem tissue. *Proceedings of the National Academy of Sciences of the United States of America* **79**, 418-421.
- Theologis, A., Huynh, T.V., and Davis, R.W.** (1985). Rapid induction of specific mRNAs by auxin in pea epicotyl tissue. *Journal of Molecular Biology* **183**, 53-68.
- Tivendale, N.D., and Cohen, J.D.** (2015). Analytical History of Auxin. *Journal of Plant Growth Regulation*, 1-15.
- Tivendale, N.D., Ross, J.J., and Cohen, J.D.** (2014). The shifting paradigms of auxin biosynthesis. *Trends in Plant Science* **19**, 44-51.
- Tiwari, S.B., Hagen, G., and Guilfoyle, T.** (2003). The roles of auxin response factor domains in auxin-responsive transcription. *The Plant Cell* **15**, 533-543.
- Tiwari, S.B., Hagen, G., and Guilfoyle, T.J.** (2004). Aux/IAA proteins contain a potent transcriptional repression domain. *The Plant Cell* **16**, 533-543.
- Trehin, C., Schrempp, S., Chauvet, A., Berne-Dedieu, A., Thierry, A.M., Faure, J.E., Negrutiu, I., and Morel, P.** (2013). QUIRKY interacts with STRUBBELIG and PAL OF QUIRKY to regulate cell growth anisotropy during *Arabidopsis* gynoecium development. *Development* **140**, 4807-4817.
- Ulmasov, T., Hagen, G., and Guilfoyle, T.J.** (1997a). ARF1, a transcription factor that binds to auxin response elements. *Science* **276**, 1865-1868.
- Ulmasov, T., Hagen, G., and Guilfoyle, T.J.** (1999). Dimerization and DNA binding of auxin response factors. *The Plant Journal* **19**, 309-319.
- Ulmasov, T., Liu, Z.B., Hagen, G., and Guilfoyle, T.J.** (1995). Composite structure of auxin response elements. *The Plant Cell* **7**, 1611-1623.
- Ulmasov, T., Murfett, J., Hagen, G., and Guilfoyle, T.J.** (1997b). Aux/IAA proteins repress expression of reporter genes containing natural and highly active synthetic auxin response elements. *The Plant Cell* **9**, 1963-1971.
- Varaud, E., Brioudes, F., Szécsi, J., Leroux, J., Brown, S., Perrot-Rechenmann, C., and Bendahmane, M.** (2011). AUXIN RESPONSE FACTOR8 regulates *Arabidopsis* petal growth by interacting with the bHLH transcription factor BIGPETALp. *The Plant Cell* **23**, 973-983.
- Vernoux, T., Brunoud, G., Farcot, E., Morin, V., Van den Daele, H., Legrand, J., Oliva, M., Das, P., Larrieu, A., Wells, D., Guedon, Y., Armitage, L., Picard, F., Guyomarc'h, S., Cellier, C., Parry, G., Koumproglou, R., Doonan, J.H., Estelle, M., Godin, C., Kepinski, S., Bennett, M., De Veylder, L., and Traas, J.** (2011). The auxin signalling network translates dynamic input into robust patterning at the shoot apex. *Molecular Systems Biology* **7**, 508.
- Vert, G., Walcher, C.L., Chory, J., and Nemhauser, J.L.** (2008). Integration of auxin and brassinosteroid pathways by Auxin Response Factor 2. *Proceedings of the National Academy of Sciences of the United States of America* **105**, 9829-9834.

- Vierstra, R.D. (2009). The ubiquitin-26S proteasome system at the nexus of plant biology. *Nature Reviews. Molecular Cell Biology* **10**, 385-397.
- Walcher, C.L., and Nemhauser, J.L. (2012). Bipartite promoter element required for auxin response. *Plant Physiology* **158**, 273-282.
- Wang, B., Chu, J., Yu, T., Xu, Q., Sun, X., Yuan, J., Xiong, G., Wang, G., Wang, Y., and Li, J. (2015a). Tryptophan-independent auxin biosynthesis contributes to early embryogenesis in Arabidopsis. *Proceedings of the National Academy of Sciences of the United States of America* **112**, 4821-4826.
- Wang, C., Liu, Y., Li, S.S., and Han, G.Z. (2014). Origin of plant auxin biosynthesis in charophyte algae. *Trends in Plant Science* **19**, 741-743.
- Wang, C., Liu, Y., Li, S.S., and Han, G.Z. (2015b). Insights into the origin and evolution of the plant hormone signaling machinery. *Plant Physiology* **167**, 872-886.
- Wang, L., Kim, J., and Somers, D.E. (2013a). Transcriptional corepressor TOPLESS complexes with pseudoresponse regulator proteins and histone deacetylases to regulate circadian transcription. *Proceedings of the National Academy of Sciences of the United States of America* **110**, 761-766.
- Wang, R., and Estelle, M. (2014). Diversity and specificity: auxin perception and signaling through the TIR1/AFB pathway. *Current Opinion in Plant Biology* **21**, 51-58.
- Wang, S., Hagen, G., and Guilfoyle, T.J. (2013b). ARF-Aux/IAA interactions through domain III/IV are not strictly required for auxin-responsive gene expression. *Plant Signaling and Behavior* **8**, e24526.
- Weijers, D., Benkova, E., Jager, K.E., Schlereth, A., Hamann, T., Kientz, M., Wilmoth, J.C., Reed, J.W., and Jurgens, G. (2005). Developmental specificity of auxin response by pairs of ARF and Aux/IAA transcriptional regulators. *The EMBO Journal* **24**, 1874-1885.
- Weiste, C., and Dröge-Laser, W. (2014). The *Arabidopsis* transcription factor bZIP11 activates auxin-mediated transcription by recruiting the histone acetylation machinery. *Nature Communications* **5**.
- Westfall, C.S., Muehler, A.M., and Jez, J.M. (2013). Enzyme action in the regulation of plant hormone responses. *The Journal of Biological Chemistry* **288**, 19304-19311.
- Wilson, M.I., Gill, D.J., Perisic, O., Quinn, M.T., and Williams, R.L. (2003). PB1 domain-mediated heterodimerization in NADPH oxidase and signaling complexes of atypical protein kinase C with Par6 and p62. *Molecular Cell* **12**, 39-50.
- Wishart, D.S., Sykes, B.D., and Richards, F.M. (1992). The chemical shift index: a fast and simple method for the assignment of protein secondary structure through NMR spectroscopy. *Biochemistry* **31**, 1647-1651.
- Wong, L.M., Abel, S., Shen, N., Foata, M., Mall, Y., and Theologis, A. (1996). Differential activation of the primary auxin response genes, *PS-IAA4/5* and *PS-IAA6*, during early plant development. *The Plant Journal* **9**, 587-599.
- Woo, E.J., Marshall, J., Baully, J., Chen, J.G., Venis, M., Napier, R.M., and Pickersgill, R.W. (2002). Crystal structure of auxin-binding protein 1 in complex with auxin. *The EMBO Journal* **21**, 2877-2885.
- Wright, A.D., Sampson, M.B., Neuffer, M.G., Michalczyk, L., Slovin, J.P., and Cohen, J.D. (1991). Indole-3-acetic acid biosynthesis in the mutant maize orange pericarp, a tryptophan auxotroph. *Science* **254**, 998-1000.
- Wu, J., Peng, Z., Liu, S., He, Y., Cheng, L., Kong, F., Wang, J., and Lu, G. (2012). Genome-wide analysis of Aux/IAA gene family in Solanaceae species using tomato as a model. *Molecular Genetics and Genomics* **287**, 295-311.
- Xu, T., Dai, N., Chen, J., Nagawa, S., Cao, M., Li, H., Zhou, Z., Chen, X., De Rycke, R., and Rakusová, H. (2014). Cell surface ABP1-TMK auxin-sensing complex activates ROP GTPase signaling. *Science* **343**, 1025-1028.
- Yamasaki, K., Kigawa, T., Seki, M., Shinozaki, K., and Yokoyama, S. (2013). DNA-binding domains of plant-specific transcription factors: structure, function, and evolution. *Trends in Plant Science* **18**, 267-276.
- Yamasaki, K., Kigawa, T., Inoue, M., Tateno, M., Yamasaki, T., Yabuki, T., Aoki, M., Seki, E., Matsuda, T., Tomo, Y., Hayami, N., Terada, T., Shirouzu, M., Osanai, T., Tanaka, A., Seki, M., Shinozaki, K., and Yokoyama, S. (2004). Solution structure of the B3 DNA binding domain of the *Arabidopsis* cold-responsive transcription factor RAV1. *The Plant Cell* **16**, 3448-3459.
- Yang, J.T., Wu, C.S., and Martinez, H.M. (1986). Calculation of protein conformation from circular dichroism. *Methods Enzymology* **130**, 208-269.
- Yoshinaga, S., Kohjima, M., Ogura, K., Yokochi, M., Takeya, R., Ito, T., Sumimoto, H., and Inagaki, F. (2003). The PB1 domain and the PC motif-containing region are structurally similar protein binding modules. *The EMBO Journal* **22**, 4888-4897.

- Yu, H., Moss, B.L., Jang, S.S., Prigge, M., Klavins, E., Nemhauser, J.L., and Estelle, M.** (2013). Mutations in the TIR1 auxin receptor that increase affinity for auxin/indole-3-acetic acid proteins result in auxin hypersensitivity. *Plant Physiology* **162**, 295-303.
- Yu, H., Zhang, Y., Moss, B.L., Bargmann, B.O., Wang, R., Prigge, M., Nemhauser, J.L., and Estelle, M.** (2015). Untethering the TIR1 auxin receptor from the SCF complex increases its stability and inhibits auxin response. *Nature Plants* **1**.
- Yue, J., Hu, X., and Huang, J.** (2014). Origin of plant auxin biosynthesis. *Trends in Plant Science* **19**, 764-770.
- Zažímalová, E., Petrasek, J., and Benková, E.** (2014). Auxin and its role in plant development. (Springer) ISBN: 978-3-7091-1526-8 (online).
- Zenser, N., Ellsmore, A., Leasure, C., and Callis, J.** (2001). Auxin modulates the degradation rate of Aux/IAA proteins. *Proceedings of the National Academy of Sciences of the United States of America* **98**, 11795-11800.
- Zhang, Y., Wang, W., Chen, J., Zhang, K., Gao, F., Gao, B., Zhang, S., Dong, M., Besenbacher, F., Gong, W., Zhang, M., Sun, F., and Feng, W.** (2013). Structural insights into the intrinsic self-assembly of Par-3 N-terminal domain. *Structure* **21**, 997-1006.
- Zhao, Y.** (2010). Auxin biosynthesis and its role in plant development. *Annual Review of Plant Biology* **61**, 49-64.
- Zhou, X.E., Wang, Y., Reuter, M., Mucke, M., Kruger, D.H., Meehan, E.J., and Chen, L.** (2004). Crystal structure of type IIE restriction endonuclease EcoRII reveals an autoinhibition mechanism by a novel effector-binding fold. *Journal of Molecular Biology* **335**, 307-319.
- Zientara-Rytter, K., and Sirko, A.** (2014). Significant role of PB1 and UBA domains in multimerization of Joka2, a selective autophagy cargo receptor from tobacco. *Frontiers in Plant Science* **5**, 13.

CURRICULUM VITAE

Personal Data

Name **Dinesh, Dhurvas Chandrasekaran**

Date and place of birth **27-07-1985, Pondicherry, India**

Education and research background

Since 2010 **Doctoral degree in Biochemistry (Ph.D.)**

- pursuing *DFG- Graduate Research Training School (GRK 1026)*

Prof. Dr. Steffen Abel and Dr. Luz Irina A. Calderón Villalobos's Lab,
Leibniz Institute of Plant Biochemistry (IPB), Halle (Saale), DE
Prof. Dr. Jochen Balbach's Lab, Institute of Physics/Biophysics,
Martin Luther University Halle-Wittenberg, DE

2008 - 2010 **Junior Research Fellow**

Prof. Dr. Narayanaswamy Srinivasan's Lab, Molecular Biophysics Unit,
Indian Institute of Science (IISc), Bangalore, IN

Aug - **Internship**

Oct 2009 Prof. Dr. U. Benjamin Kaupp's Lab, Centre of Advanced European Studies and
Research (caesar), Research Centre for Neurosciences (MPI), Bonn, DE.

2007 - 2008 **Advanced Diploma in Bioinformatics (A.D.B.I)**

Prof. Sankaran Krishnaswamy's Lab, Madurai Kamaraj University, Madurai, IN

2005 - 2007 **Masters in Biotechnology, (M.Sc.)**

Dr. Fathima Benazir, School of Biotech, Dr. G. R. Damodaran College of Sc.,
Bharathiar University, Coimbatore, IN

2002 - 2005 **Bachelors in Microbiology (B.Sc.)**

St. Joseph's College of Arts and Science, University of Madras, IN

Academic grants and teaching experience

Since 2010 Member of **Deutsche Forschungsgemeinschaft Graduiertenkolleg 1026**, "Conformational transitions in macromolecular interactions", MLU, DE

2014 **DAAD-STIBET and PhD Finalization Grant**

International Office, Martin Luther University Halle-Wittenberg, DE

2012 - 2013 **DAAD-Research Internships in Science and Engineering (RISE)**

Mentoring Program, Deutscher Akademischer Austauschdienst, DE

July - September 2013, Ana Valinhas, University of Lisbon, Portugal

June - August 2012, Marisol Martinez, The Ohio State University, USA.

PUBLICATIONS

Trends in Plant Science 2015 (manuscript accepted)

Dinesh, D.C., Calderón Villalobos, L.I.A., and Abel, S.

Structural biology of nuclear auxin action.

Proceedings of the National Academy of Sciences (USA) 2015, May 12; 112(19), 6230-35

Dinesh, D.C., Kovermann, M., Gopalswamy, M., Hellmuth, A., Calderón Villalobos, L.I.A., Lilie, H., Balbach, J., and Abel, S.

Solution structure of the oligomerization domain PsIAA4 reveals interaction modes for transcription factors in early auxin response.

Solution NMR Structure: PBD ID: **2M1M** and BMRB number: **18870**

Deposition date: 03 Dec, 2012 and Release date: 11 Dec, 2013

OTHER CO-AUTHOR PUBLICATIONS

Developmental Cell 2015 Apr 20; 33, 216-30.

Müller J., Toev, T., Heisters, M., Teller, J., Moore, K.L., Hause, G., Dinesh, D.C., Bürstenbinder, K., and Abel, S.

Iron-dependent callose deposition adjusts root meristem maintenance to phosphate availability.

Contribution: *In silico* protein 3D structure modeling and structure-function analysis.

The Journal of Biological Chemistry, 2013 Jan 18; 288(3):1871-82.

Bürstenbinder, K., Savchenko, T., Müller, J., Adamson, A.W., Stamm, G., Kwong, R., Zipp, B.J. & Dinesh, D.C. and Abel, S.

Arabidopsis calmodulin-binding IQD1 localizes to microtubules and interacts with Kinesin Light Chain-Related Protein-1.

Contribution: *In silico* protein 3D structure modeling and sequence based motif analysis.

CONFERENCES AND WORKSHOPS

Poster Presentation

- 4 - 6 Nov., 2013, "Structure-function studies on the pea IAA4 dimerization domain provide insights into auxin dependent transcriptional regulation -an update"
3rd International Meeting "Conformational transition in macromolecular interaction", Leopoldina (The German Academy of Natural Scientists), Halle, DE
- 28 - 31 May, 2013, "Structure-function studies of the pea IAA4 dimerization domain provide insights into auxin dependent transcriptional regulation"
9th Plant Science Student Conference (PSSC) * Best Poster Award
Leibniz Institute of Plant Biochemistry, Halle (Saale), and IPK, Gatterseben, DE
- 22 - 27 May, 2011, "Structural studies of AUX/IAA transcriptional regulators using CD and NMR spectroscopy", **Gordon Research Conf.: Computational Aspects-Biomolecular NMR**
Il Ciocco, Hotel and Resort, Lucca (Barga), IT
- 14 - 17 June, 2011, "The Art and Science Behind the making of the World famous South Indian Pathamadaï Silk Mats" (M.Sc., dissertation work)
7th Plant Science Student Conference (PSSC), Leibniz Institute of Plant Biochemistry, Halle, and IPK, Gatterseben, DE
- 3 - 5 Mar., 2011, "Structural studies of AUX/IAA transcriptional regulators using CD and NMR spectroscopy", **2nd International Meeting "Conformational transition in macromolecular interactions"**, Martin Luther University Halle-Wittenberg, Halle (Saale), DE
- 3 - 6 Sep., 2010, "Structural studies of Aux/IAA transcription factors from *Arabidopsis thaliana* and *Pisum sativum* using NMR spectroscopy"**Annual Meeting of the German Biophysical Society**, Ruhr university, DE

Other Conferences Attended

- 8 - 11 January, 2013, **International Conference on Biomolecular forms and functions, A celebration of 50 yrs of the Ramachandran Map**
Indian Institute of Science, Bangalore, India (IN)
- 24 - 26 February, 2011, **4th Halle Conference on Recombinant Protein Production**
Martin Luther University Halle-Wittenberg, Halle (Saale), DE

Workshops Attended

Structure Club (X-ray crystallography and Nuclear Magnetic Resonance Spectroscopy), Cryo-Electron Microscopy, Analytical Ultra Centrifugation (AUC), Fluorescence Cross-Correlation Spectroscopy, Protein-protein interaction techniques.

DFG-GRK 1026, Martin Luther University Halle-Wittenberg, Halle (Saale), DE.

Oral Presentations (2010 - 2014)

Biannual Retreats of DFG-Graduate Research Training School (GRK 1026)

- 22 - 23 February, 2013, "High-resolution NMR structure of the dimerisation domain of AUX/IAA transcription factor PsIAA4 from pea (*Pisum sativum*) ", **Spring Meeting**, Meißen, DE.
- 01 - 03 October, 2012, "NMR structure and functional studies of AUX/IAA transcription factors", **Fall Meeting**, Naumburg, DE.
- 23 - 25 February, 2012, "Structure and DNA binding studies of AUX/IAA: a putative transcription factor", **Spring Meeting**, Eisenach, DE.
- 29 November - 01 October, 2011, "Towards the solution structure of AUX/IAA transcription factor", **Fall Meeting**, Leuna, DE.
- 30 November - 02 October, 2010, "Structural studies and post-translational regulation of AUX/IAA transcription factors in the integration of auxin and light signaling", **Fall Meeting**, Blankenburg, DE.
- 18 - 20 March, 2010, "Characterization of conformational patterns in active and inactive states of kinases using Protein Blocks approach", **Spring Meeting**, Halle, DE.

Department of Molecular Signal Processing (MSV), IPB Retreats/Workshops

- 22 - 24 October, 2014, "Solution structure and functional studies of PsIAA4 C'terminal domain", Schloss Oppurg, Thuringia, DE
- 20 - 22 March, 2013, "Structure-Function studies of AUX/IAA transcription factor PsIAA4 from *Pisum sativum*", Schloss Wendgraeben, Saxony-Anhalt, DE
- 13 - 14 October, 2011, "Towards the solution structure of AUX/IAA transcription factor", Schloss Wendgraeben, Saxony-Anhalt, DE.

DECLARATIONS

DECLARATION BY THE CANDIDATE

I, Dinesh Dhurvas Chandrasekaran, hereby declare that the research work described and presented in this dissertation, entitled “**High-resolution NMR structure and functional studies of the oligomerization domain of PsIAA4, an auxin-inducible transcriptional repressor from pea (*Pisum sativum*)**”, are my own and were conducted under the guidance of Prof. Dr. Steffen Abel and Dr. Luz Irina A. Calderón Villalobos, Signal Integration Group, Department of Molecular Signal Processing, Leibniz Institute of Plant Biochemistry and Prof. Jochen Balbach, Institute of Physics/Biophysics, Martin Luther University, Halle (Saale), Germany.

In addition, I confirm that no part of this dissertation will be used in a submission in my name, for any other degree at another university or research institute.

Date: 30.09.2015

Halle (Saale), Germany

Dinesh Dhurvas Chandrasekaran.

DECLARATION BY THE SUPERVISOR

I, Prof. Dr. Steffen Abel, certify that the above statements made by the candidate are true to the best of my knowledge.

Date: 30.09.2015

Halle (Saale), Germany

Prof. Dr. Steffen Abel.

ACKNOWLEDGEMENTS

The completion of my Ph.D. project and the thesis has been a long journey. I have finished, but not alone, and am elated. My Ph.D. thesis appears in its current form by the invaluable support and the guidance of several individuals. I would therefore like to offer my sincere thanks to all of them. To this select group, I'd like to convey my cordial thanks, first and foremost to my supervisor **Prof. Dr. Steffen Abel** for his thoughtful guidance. It has been an honor to be his PhD student. I appreciate all his contributions of time, ideas, and support to make my Ph.D. experience productive, stimulating and memorable. His advice on both research as well as on my career have been priceless. I have been extremely lucky to have him as my supervisor who cared so much about my work, and who responded to my questions and queries so promptly. The joy and enthusiasm he have for research was contagious and motivational for me, even during tough times in my Ph.D. pursuit. I am very fortunate to follow up the research work from **Prof. Dr. Athanasios Theologis** (Sakis) Laboratory, USA, pioneer in identifying the PsIAA4. Thank you for the insightful discussion and blessings which accelerated my work towards publication during his visit to Halle.

Secondly, I would like to express special appreciation and thanks to my co-supervisor, **Prof. Dr. Jochen Balbach** for providing me NMR and other biophysical instrumentation facilities in his group in the Institute of Physics/Biophysics at MLU to accomplish my work successfully. I would thank him for the patient guidance, encouragement and advice he has provided, and showering all his positive thoughts throughout my time as his student. I am particularly indebted to **Mohanraj G** for introducing me to biophysical techniques and NMR data analysis. I am especially grateful to **Dr. Michael Kovermann** for performing side chain assignments and ARIA structure runs thereby speeding up the structure calculation processes. I cannot forget Andi for helping me in performing NMR titration experiments; Amit and Rica for setting up few of the NMR experiments; Tobias and all other members of Biophysics for scientific discussions. I am thankful to all of them.

I very much appreciate **Dr. Hauke Lilie** from the Institute of Biochemistry and Biotechnology, MLU for his enthusiasm, intensity, and willingness to perform Analytical Ultra-centrifugation runs and analyzing the data. I want to express my deep thanks to him for his insightful discussion, offering valuable advice and for his support during the whole period of the study.

I would like to thank **Dr. Luz Irina A. Calderón Villalobos** for providing a friendly working environment in the lab and helping me in designing my experiments, talks, discussion and useful suggestions. I also thank her and Ub-nexus group for organizing journal clubs which helped me in gaining recent updates in our field. My gratitude is also extended to all the members of Signal integration group who has been a source of friendships as well as fruitful discussion. I am thankful to **Antje** for performing Y2H experiment and for the stimulating discussions, motivating me during my hard times and all the fun we had during my stay in the lab. Thanks to Martin for sharing ideas and making the lab-life lively, 24x7. Of course I cannot forget celebrating birthdays and farewell parties together with AG Calderón. Thanks to Verona for her excellent technical assistance in the lab and all other members.

I am very grateful and would like to give heartfelt, special thanks to all the members of my dissertation committee for their time, interest, and insightful comments and encouragement.

I am grateful for IPB for providing me the platform to carry out my research and supporting me financially during my last year of my PhD. My special gratitude to all the members of department of molecular signal processing (**MSV**) for their academic support and input, and personal cheering are greatly appreciated. Special thanks to Jacob for his tips and tricks during my initial experiments and all the group leaders and Post-Docs for their valuable comments. My deep thanks to senior **Prof. Dr. Claus Waternack** for his moral support and blessing. I would like to acknowledge all the IPB administrative members, especially **Alexandra** for always helping me with all the administrative work related to professional or personal life, and translating Deutsch letter.

Finally, I would like to thank the GRK1026 not only for providing the funding which allowed me to undertake the research with successful collaborations and also for giving me the opportunity to attend conferences. Special thanks to **Prof. Dr. Milton Stubbs** and other GRK members for conducting workshops and for their critical comments during research talks. I cannot forget GRK coordinators **Wahle, Martina** and **Uli** for their constant support throughout my stay.

Special thanks to **Anshu** for helping me during NMR analysis, helping me out in all my hard times. I would like to thank her for comments and willingness to proofread my thesis countless times. Thanks to Marisol and Ana for being my summer interns and Susan for preliminary insilico analysis. And also thanks Antje, Romel, Tamil, Waran and all other friends for final proofreading of my thesis. My heartfelt thanks to my friends- Sabi, Siji, Yamuna, Aravind, Kannan, Senthil, Balaji, Balu, Rajeshwaran, Sudha, Gandhimathi, Thirulog, Kali, Jag, Subroto, Bobby, Suraj, Dilip, Praveen,

Chandrasbose, IISc friends and endless list; for being the wonderful friends and making my stay in the city an enjoyable experience. I would also like to acknowledge all other seniors and friends for their help, motivation and lively discussion over a sip of coffee. Although we have lived far away from our homes but communication with you all provided emotional atmosphere for me. Hereby I would like to thank Halle Indians for all the get togethers and cultural events during Indian festivals.

No words in the world can explain how indebted to my teachers, Prof. Dr. Srinivasan N., Dr. Fathima Benazir J, Dr. Rafi Z.A. (late), Prof. Krishnaswamy S. and Pandian sir. They constantly motivated me to reach out for my dreams and excel in whatever I do in life.

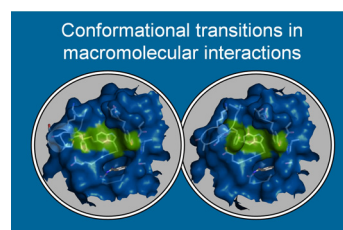
Of course no acknowledgments would be complete without giving thanks to my parents. Both have instilled many admirable qualities in me and given me a good foundation with which to meet life. They've taught me about hard work and self-respect, about persistence and about how to be independent. Both have always expressed how proud they are of me. I am grateful for them both and for the 'smart genes' they passed on to me. My sincere apology to my parents, **D.R. Chandrasekaran** (bho), **D.C. Shanthi** (ambo) and my sister **D.C. Poorni** (mai) for being away for such a long time and their patience, who experienced all the ups and downs of my research life. Words cannot express how grateful I am to them for all of the sacrifices that they have made. I also thank my uncle **D.P Raghavan** (DP bho) and all my relatives who prayed for me throughout the time of my research. Your prayer for me was what sustained me thus far.

I am thankful to the almighty for always showering his choicest blessings upon me.

Many Thanks/Vielen Dank !

Deutsche
Forschungsgemeinschaft

DFG



GRK1026

